University of Kentucky
UKnowledge

Theses and Dissertations--Chemistry

Chemistry

2013

DOXORUBICIN-INDUCED, TNF-α-MEDIATED BRAIN OXIDATIVE STRESS, NEUROCHEMICAL ALTERATIONS, AND COGNITIVE DECLINE: INSIGHTS INTO MECHANISMS OF CHEMOTHERAPY INDUCED COGNITIVE IMPAIRMENT AND ITS PREVENTION

Jeriel T. Keeney
University of Kentucky, jtke224@uky.edu

Right click to open a feedback form in a new tab to let us know how this document benefits you.

Recommended Citation

Keeney, Jeriel T., "DOXORUBICIN-INDUCED, TNF-α-MEDIATED BRAIN OXIDATIVE STRESS, NEUROCHEMICAL ALTERATIONS, AND COGNITIVE DECLINE: INSIGHTS INTO MECHANISMS OF CHEMOTHERAPY INDUCED COGNITIVE IMPAIRMENT AND ITS PREVENTION" (2013). *Theses and Dissertations--Chemistry*. 27.
https://uknowledge.uky.edu/chemistry_etds/27

This Doctoral Dissertation is brought to you for free and open access by the Chemistry at UKnowledge. It has been accepted for inclusion in Theses and Dissertations--Chemistry by an authorized administrator of UKnowledge. For more information, please contact UKnowledge@lsv.uky.edu.

STUDENT AGREEMENT:

I represent that my thesis or dissertation and abstract are my original work. Proper attribution has been given to all outside sources. I understand that I am solely responsible for obtaining any needed copyright permissions. I have obtained and attached hereto needed written permission statements(s) from the owner(s) of each third-party copyrighted matter to be included in my work, allowing electronic distribution (if such use is not permitted by the fair use doctrine).

I hereby grant to The University of Kentucky and its agents the non-exclusive license to archive and make accessible my work in whole or in part in all forms of media, now or hereafter known. I agree that the document mentioned above may be made available immediately for worldwide access unless a preapproved embargo applies.

I retain all other ownership rights to the copyright of my work. I also retain the right to use in future works (such as articles or books) all or part of my work. I understand that I am free to register the copyright to my work.

REVIEW, APPROVAL AND ACCEPTANCE

The document mentioned above has been reviewed and accepted by the student's advisor, on behalf of the advisory committee, and by the Director of Graduate Studies (DGS), on behalf of the program; we verify that this is the final, approved version of the student's dissertation including all changes required by the advisory committee. The undersigned agree to abide by the statements above.

Jeriel T. Keeney, Student

Dr. D. Allan Butterfield, Major Professor

Dr. Dong-Sheng Yang, Director of Graduate Studies

DOXORUBICIN-INDUCED, TNF-α-MEDIATED BRAIN OXIDATIVE STRESS, NEUROCHEMICAL ALTERATIONS, AND COGNITIVE DECLINE: INSIGHTS INTO MECHANISMS OF CHEMOTHERAPY INDUCED COGNITIVE IMPAIRMENT AND ITS PREVENTION

DISSERTATION

This dissertation is in partial fulfillment of requirements for the degree of
Doctor of Philosophy in the college of Arts and Sciences,
University of Kentucky

By
Jeriel Thomas Richard Keeney

Lexington, KY

Director: Dr. D. Allan Butterfield, Professor of Chemistry

University of Kentucky

Lexington, KY

2013

Copyright © Jeriel T. R. Keeney, 2013

ABSTRACT OF DISSERTATION

DOXORUBICIN-INDUCED, TNF-α -MEDIATED BRAIN OXIDATIVE STRESS, NEUROCHEMICAL ALTERATIONS, AND COGNITIVE DECLINE: INSIGHTS INTO MECHANISMS OF CHEMOTHERAPY INDUCED COGNITIVE IMPAIRMENT AND ITS PREVENTION

The works presented in this dissertation provide insights into the mechanisms of chemotherapy-induced cognitive impairment (CICI or “ChemoBrain”) and take steps toward outlining a preventive strategy. CICI is now widely recognized as a complication of cancer chemotherapy experienced by a large percentage of cancer survivors. Approximately fifty percent of existing FDA-approved anti-cancer drugs generate reactive oxygen species (ROS). Doxorubicin (Dox), a prototypical ROS-generating chemotherapeutic agent, produces the reactive superoxide radical anion (O_2^{-}•) *in vivo.* Dox treatment results in oxidation of plasma proteins, including ApoA-I, leading to TNF-α-mediated oxidative stress in plasma and brain. TNF-α elevation in brain leads to further central nervous system toxicity including mitochondrial dysfunction, neuronal death, and cognitive impairment. Co-administration of the antioxidant drug, 2-mercaptoethane sulfonate sodium (MESNA), prevents Dox-induced protein oxidation and subsequent TNF-α elevation in plasma without interfering with the cancer-killing ability of Dox.

In studies presented in this dissertation, we measured oxidative stress in both brain and plasma of Dox-treated mice both with and without MESNA. MESNA ameliorated Dox-induced oxidative protein damage in plasma, confirming our prior studies, and in a new finding led to decreased oxidative stress in brain. Using novel object recognition (NOR), we demonstrated the Dox administration resulted in memory deficits. Using hydrogen magnetic resonance imaging spectroscopy (H^1-MRS) techniques, we demonstrated that Dox administration led to a dramatic decrease in choline(phosphocholine)/creatine (Cho/Cr) ratios in mouse hippocampus. The activities of both phosphatidylcholine-specific phospholipase C (PC-PLC) and phospholipase D(PLD) were severely diminished

following Dox administration. The activity of PC-PLC was preserved when MESNA was co-administered with Dox. In the absence of TNF-α, MRS-indexed Cho/Cr ratio, PLD activity, and mitochondrial oxygen consumption are preserved in brain, and markers of oxidative stress are reduced.

Together with results from our previous studies, these results provide strong evidence that TNF-α is strongly associated, if not responsible for CICI. We also tested the notion that O_2^{-}• is responsible for Dox-induced plasma protein oxidation and TNF-α release. O_2^{-}• resulted in increased oxidative damage to proteins when added to plasma and increased levels of TNF-α in macrophage culture, providing strong evidence that O_2^{-}• is responsible for these Dox-induced toxicities.

Keywords: Chemotherapy-induced cognitive impairment, Doxorubicin, MESNA, tumor necrosis factor-alpha, superoxide.

Jeriel T.R. Keeney

December 5, 2013

DOXORUBICIN-INDUCED, TNF-α -MEDIATED BRAIN OXIDATIVE STRESS, NEUROCHEMICAL ALTERATIONS, AND COGNITIVE DECLINE: INSIGHTS INTO MECHANISMS OF CHEMOTHERAPY INDUCED COGNITIVE IMPAIRMENT AND ITS PREVENTION

By

Jeriel T. R. Keeney

Dr. D. Allan Butterfield

Director of Dissertation

Dr. Dong-Sheng Yang

Director of Graduate Studies

December 5, 2013

Date

To my wife, Sarah, and my son, Max

ACKNOWLEDGEMENTS

I would like to extend my deepest thanks to my Ph.D. advisor, Professor Dr. D. Allan Butterfield, for his acceptance, time, attention, guidance, mentorship, and support. I entered the Ph.D. program at the University of Kentucky, Department of Chemistry as a non-traditional student. Dr. Butterfield gave me a chance, provided strong guidance, leadership, and experience. He was both my hardest critic and biggest advocate. I needed both. I would also like to offer special thanks to research faculty Dr. Rukhsana Sultana for all of the things that she taught me, both how to be a better scientist and a better person. My sincerest thanks go out to the members of my Ph.D. advisory committee (Dr. Yinan Wei, Dr. Jim Geddes, and Dr. David Atwood) for their time, guidance, expertise, understanding, compassion, and patience.

I am grateful to former and current group members for advice, a helping hand, friendship, and company. My peers, Josh, Chris, Miranda, Sarita, Aaron, Jessica, Zhaoshu, Judy, Xiaojia, Eugenio, and Sarah enriched my life at UK with their scientific knowledge and friendships. Mollie Fraim has been always ready with a helping hand, a kind word, and a smiling face. This research group truly feels like family. I have made lasting friendships with so many fellow graduate students, undergraduates, post-docs, collaborators, and staff. Particularly, I cherish close friends that I have made at UK, Josh, Austin, Melissa.

I am thankful to the many research collaborators and their lab members who helped make many of my research endeavors go more smoothly. Specifically, I

would like to acknowledge Teresa, Dr. D. St.Clair, Dr. K. Saatman, Dr. D. Powell, Dr. L. Brewer, Dr. N. Porter, Dr. M. Vore, and Dr. J. Moscow for the direct collaborations with them and members of their laboratories to help me extend the scientific knowledge presented here far beyond what I could have accomplished on my own. Thanks also to the UK chemistry department chairs, past and present (Dr. S. Yates and Dr. M. Meier), past and present directors of graduate study (Dr. R. Grossman, Dr. J. Anthony, and Dr. D. Yang), and all of the chemistry department faculty and staff who work tirelessly to help us achieve our goals.

Most importantly, my deepest love and gratitude go out to my family and friends who supported me and believed in me along the long road to achieve this dream. My mother and grandmother helped me get a great start, without which, I would not have believed in myself. My son, Max, was my inspiration to return to school after so many years to finish what I started. My wife, Sarah, continues to provide unwavering love and support through all of the long hours and indefinite end to this endeavor. I cherish her greatly.

TABLE OF CONTENTS

ACKNOWLEDGEMENTS iii
LIST OF TABLES x
LIST OF FIGURES xi
CHAPTER 1: INTRODUCTION 1
CHAPTER 2: BACKGROUND 4
2.1 Cancer: Incidence, mortality, and treatments 4
2.2 Chemotherapy-induced cognitive impairment (CICI, “Chemobrain”) 5
2.2.1 CICI, definition and prevalence 5
2.2.2 Gray and white matter changes in CICI 5
2.2.3 Potential reasons for varied patient outcomes 6
2.2.4 Clinical presentation of and current treatments for CICI 7
2.2.5 Our model of CICI 7
2.3 Doxorubicin (Dox) 8
2.4 Apolipoprotein A-I (ApoA-I) 11
2.4.1 Cholesterol and Its Transport 12
2.4.2 HNE modification of ApoA-I 15
2.4.3 ApoA-I and ABCA1 interaction and subsequent signaling 16
2.4.4 ApoA-I and chemotherapy-induced cognitive impairment 20
2.5 Tumor necrosis factor-alpha (TNF-α) 23
2.5.1 Overview of TNF-α and CICI 23
2.5.2 TNF-α signaling, inflammation, and apoptosis 24
2.6 MESNA 28
2.7 Oxidative Stress 30
2.7.1 Reactive oxygen and reactive nitrogen species 31
2.7.2 Mitochondria as a source of ROS 31
2.7.3 Free radicals and lipid peroxidation 32
2.7.4 NO and tyrosine nitration 35
2.7.5 Protein carbonyl formation 39
2.7.6 Oxidation of DNA and RNA 39
CHAPTER 3: MATERIALS AND METHODS 40
3.1 Plasma Isolation and tissue collection 40
3.2 Bicinchoninic Acid Assay (BCA) 41
3.3 Biological sample preparation 41
3.4 Slot blot assay 41
3.5 Detection of oxidatively modified proteins 42

3.5.1 Protein carbonyl determination 42
3.5.2 Protein-bound HNE and 3-nitrotyrosine determination 43
3.6 Behavioral testing: Novel object recognition and open field testing 44
3.6.1 Novel object recognition 44
3.6.2 Motor activity in an open field 45
3.7 Hydrogen magnetic resonance imaging spectroscopy 45
3.8 Phospholipase C and Phospholipase D Activity Assays 46
3.9 Assessment of mitochondrial function 47
3.9.1 Isolation of Brain Mitochondria 47
3.9.2 Bioenergetic analysis in mitochondria 48
3.10 Superoxide experiments 49
3.10.1 Solvent selection and potassium superoxide solution preparation 49
3.10.2 Plasma oxidation with potassium superoxide 49
3.10.3 Macrophage stimulation with potassium superoxide 51
3.11 Proteomics (Butterfield et al. 2012)(Butterfield et al. 2012) 52
3.11.1 Isoelectric focusing (IEF) 52
3.11.2 Two-dimensional polyacrylamide gel electrophoresis (2D-PAGE) 53
3.11.3 SYPRO Ruby® staining 53
3.11.4 Image analysis: differential expression 54
3.11.5 In-gel trypsin digestion 54
3.11.6 Mass spectrometry 55
3.11.7 Database search and peptide identification 56
3.11.8 One-dimensional polyacrylamide gel electrophoresis 57
3.11.9 Western Blotting 57

CHAPTER 4: DOXORUBICIN-INDUCED ELEVATED OXIDATIVE STRESS IN BRAIN AND COGNITIVE DECLINE: PROTECTION BY MESNA AND INSIGHTS INTO MECHANISMS OF CHEMOTHERAPY-INDUCED COGNITIVE IMPAIRMENT (“CHEMOBRAIN”). 59

4.1 Overview of Study 59
4.2 Introduction 60
4.3 Materials and methods 64
4.3.1 Chemicals 64
4.3.2 Statistical analysis 64
4.3.3 Animals 65
4.3.4 Behavioral testing: Novel object recognition and open field testing 65
4.3.4.1 Novel object recognition 65
4.3.4.2 Motor activity in an open field 67
4.3.5 Hydrogen magnetic resonance imaging spectroscopy 67
4.3.6 Sample preparation 68
4.3.7 Slot blot assay 68

4.3.9 Phospholipase C and Phospholipase D Activity Assays 69
4.4 Results 70
4.4.1 Dox administration results in increases in oxidative stress markers in brain and plasma 70
4.4.2 Dox administration results in cognitive impairment 73
4.4.3 Dox administration results in changes to the neurochemical profile in the hippocampus determined by MRS 77
4.4.4 Dox administration results in decreased PC-PLC and PLD activity 79
4.5 Discussion 81

CHAPTER 5: PREVENTION OF MITOCHONDRIAL DAMAGE IN BRAIN AND OXIDATIVE STRESS IN PLASMA OF TNF-α KNOCKOUT MICE TREATED WITH THE ANTI-CANCER DRUG DOXORUBICIN: IMPLICATIONS FOR CHEMOTHERAPY-INDUCED COGNITIVE IMPAIRMENT (“CHEMOBRAIN”)..... 92

5.1 Overview of Study 92
5.2 Introduction 93
5.3 Methods and Materials 96
5.3.1 Chemicals 96
5.3.2 Statistical analysis 96
5.3.3 Animals 97
5.3.4 Sample preparation 97
5.3.5 Slot blot assay 98
5.3.6 Isolation of brain mitochondria 99
5.3.7 Bioenergetic analysis in mitochondria 100
5.3.8 Hydrogen magnetic resonance imaging spectroscopy 101
5.3.9 Phospholipase C and phospholipase D activity assays 102
5.4 Results 102
5.4.1 Dox administration results in increases in oxidative stress markers in brain and plasma of wild-type mice and plasma but not brain of TNFKO mice 102
5.4.2 Dox administration results in altered oxygen consumption rate in brain mitochondria that is absent in TNF-α null mice 106
5.4.3 Changes to the neurochemical profile following Dox administration the hippocampus determined by MRS 107
5.4.4 Dox administration to TNFKO mice results in preservation of PLD activity 110
5.5 Discussion 112

CHAPTER 6: SUPEROXIDE INDUCES PROTEIN OXIDATION IN PLASMA AND TNF-α ELEVATION IN MACROPHAGE CULTURE: INSIGHTS INTO MECHANISMS OF NEUROTOXICITY CAUSED BY DOXORUBICIN 117

6.1 Overview of study 117

6.2 Introduction 118
6.3 Methods and Materials 120
6.3.1 Chemicals 120
6.3.2 Statistical analysis 120
6.3.3 Animals 121
6.3.4 Sample preparation 121
6.3.5 Slot blot assay 122
6.3.6 Solvent selection and potassium superoxide solution preparation 122
6.3.7 Plasma oxidation with potassium superoxide 123
6.3.8 Macrophage stimulation with potassium superoxide 124
6.4 Results 126
6.4.1 Protocol development 126
6.4.2 Plasma oxidation from potassium superoxide 126
6.4.3 Superoxide induces TNF-α elevation in macrophage culture similar to that seen following doxorubicin administration 128
6.5 Discussion 130

CHAPTER 7: CONCLUSIONS AND FUTURE STUDIES 133

7.1 Conclusions 133
7.2 Future studies 140

APPENDIX A: DIETARY VITAMIN D DEFICIENCY IN RATS FROM MIDDLE- TO OLD-AGE LEADS TO ELEVATED TYROSINE NITRATION AND PROTEOMICS CHANGES IN LEVELS OF KEY PROTEINS IN BRAIN: IMPLICATIONS FOR LOW VITAMIN D-DEPENDENT AGE-RELATED COGNITIVE DECLINE 143

A.1 Overview of study 143
A.2 Introduction 146
A.3 Methods and Materials 148
A.3.1 Chemicals 148
A.3.2 Animals 149
A.3.3 Sample preparation 150
A.3.4 Slot blot assay 151
A.3.5 Proteomics (Butterfield et al. 2012) 152
A.3.5.1 Isoelectric focusing (IEF) 152
A.3.5.2 Two-dimensional polyacrylamide gel electrophoresis (2D-PAGE) 153
A.3.5.3 SYPRO Ruby® staining 153
A.3.5.4 Image analysis: differential expression 154
A.3.5.5 In-gel trypsin digestion 154
A.3.5.6 Mass spectrometry 155
A.3.5.7 One-dimensional polyacrylamide gel electrophoresis 156

A.3.5.8 Western Blotting 156
A.3.5.9 Validation 157
A.3.6 Statistical analysis 158
A.4 Results 161
A.4.1 Vitamin D deficiency leads to increased nitrosative protein damage in brain. 161
A.4.2 VitD deficiency elevation of peroxidases, glycolytic enzymes, and PPIA. 161
A.4.3 VitD deficiency leads to NF-κB activation and increased iNOS levels in brain. 166
A.5.3 Consequences of low dietary VitD 177
A.6 Conclusions 180
APPENDICES B AND C: DATA TO SUPPLEMENT TABLES AND FIGURES 206
REFERENCES 214
VITA 237
SCIENTIFIC PUBLICATIONS 238

LIST OF TABLES

TABLE 3.1. SUPEROXIDE PROTOCOL VOLUMES. 50
TABLE 6.1. SUPEROXIDE SAMPLE TREATMENT. 123
TABLE A.1. VITD DIETARY MANIPULATION 150
TABLE A.2. BRAIN PROTEIN IDENTIFICATIONS IN VITD DEFICIENCY 159
TABLE A.3. VITD 2D-GEL COMPARISON PDQUEST DATA..... 163

LIST OF FIGURES

Figure 2.1. Our early model of the stages following Dox administration that lead to chemotherapy-induced cognitive impairment (CICI). 9

Figure 2.2. Redox cycling of doxorubicin. 10

Figure 2.3. Unmodified vs. oxidatively modified ApoA-I. 20

Figure 2.4. MESNA scavenges free radicals and reactive aldehydes 30

Figure 2.5. ROS formation involving mitochondria-derived superoxide. 34

Figure 2.6. HNE formation from arachidonic acid. 37

Figure 2.7. A linear depiction of HNE adducts with amino acids. 37

Figure 2.8. Mechanism of tyrosine nitration. 38

Figure 3.1. Experimental design: macrophage simulation with potassium superoxide. 51

Figure 4.1. PC and protein-bound HNE levels in brain and plasma following Dox and MESNA treatments. 71

Figure 4.2. Behavior testing following Dox and MESNA administration. 76

Figure 4.3. H1-MRS of mouse hippocampus after Dox and MESNA treatment. 78

Figure 4.4. PC-PLC and PLD activity in brain following Dox and MESNA treatment, ... 80

Figure 4.5. A pathway to apoptosis. 91

Figure 5.1. PC and protein-bound HNE levels in brain and plasma following Dox treatment in wild-type and TNFKO mice. 105

Figure 5.2. Mitochondrial function in brain following Dox treatment in wild-type and TNFKO mice. 108

Figure 5.3. H1-MRS of mouse hippocampus following Dox treatment in wild-type and TNFKO mice. 109

Figure 5.4. PC-PLC, PLD activity in brain after Dox treatment in wild-type and TNFKO mice. 111

Figure 6.1. Experimental design: J774.A1 macrophage culture treatment with potassium superoxide. 125

Figure. 6.2. PC and protein-bound HNE levels in plasma after treatment with potassium superoxide. 128

Figure 6.3. TNF-α levels in macrophage culture after treatment with potassium superoxide. 129

Figure A.1. Graphical Abstract, Vitamin D deficiency study. 145

Figure A.2. Representative 2D gels used for proteomics identification of differentially expressed proteins. 160

Figure A.3. Slot-blot analysis of 3-NT levels in rat brain homogenates. 162

Figure A.4. Validation of expression proteomics results for PrxIII by 2D Western blot analysis. 164

Figure A.5. Validation of expression proteomics results by 1D Western blot analysis of PPIA levels. 165

Figure A.6. Potential mechanism for the biochemical consequences of VitD deficiency. 167

Figure A.7. Effect of VitD deficiency on NF-κB subcellular localization in rat brain. 170

Figure A.8. Effect of VitD deficiency on iNOS levels in rat brain. 172

Figure A.9. Proposed mechanism for the protein nitration regulatory effects of VitD in brain based on recent literature and results from the current study. 173

Figure B.1. Experimental Design: Dox/MESNA Human Clinical Pilot Study. 183

Figure B.2. Model estimates for percent change of protein carbonyl (PC) depending on an individual's baseline PC level. 184

Copyright © Jeriel T. R. Keeney 2013

CHAPTER 1

INTRODUCTION

The studies presented in this manuscript were conducted to examine the mechanisms likely underlying chemotherapy-induced cognitive impairment (CICI) and to outline potential preventative interventions thereby improving potential outcomes and quality of life for the increasing number of cancer survivors. We investigate the potential involvement of reactive oxygen species (ROS)-producing chemotherapy drugs in the cause and progression of CICI. Briefly, oxidative stress is widely viewed as an imbalance in the physiological levels of oxidants over antioxidants. This imbalance can be due to increased oxidant production or exposure, decrease anti-oxidant capacity, or both. Damage to biomolecules and changes in levels and function can occur as a result.

Doxorubicin (Dox), a representative chemotherapeutic agent used in these studies, is used to treat various solid tumors, often as part of a multi-drug chemotherapy regimen. Dox is known to produce reactive oxygen species (ROS) due to redox cycling of the quinone moiety within its structure. Oxidative damage of plasma proteins are observed following Dox treatment. Prior studies by the Butterfield laboratory have shown that oxidative protein damage, mitochondrial dysfunction, and apoptosis are also observed in brain following Dox treatment, even though this agent does not cross the blood-brain barrier (BBB) (Joshi et al.

2005; Tangpong et al. 2006; Joshi et al. 2007; Tangpong et al. 2007; Tangpong et al. 2008; Joshi et al. 2010). This plasma protein oxidative leads to plasma elevation of the inflammatory cytokine, tumor necrosis factor alpha (TNF-α). This cytokine crosses the BBB leading to mitochondrial damage and dysfunction, which, we hypothesize, can lead to a series of biochemical alterations ultimately resulting in cognitive dysfunction and memory impairment, a condition patients describe as “chemobrain” or “chemofog.”

In addition, samples from patients treated with Dox but not simultaneously treated with sodium-2-mercaptoethane sulfonate (MESNA) showed statistically significant increases markers of protein oxidation and lipid peroxidation. However, plasma samples from patients coincidentally treated with MESNA as part of their chemotherapy regimen did not exhibit the same levels of damage, suggesting that MESNA prevented Dox-induced oxidative stress. Our group demonstrated in mouse models that MESNA suppresses the Dox-induced increase in plasma oxidative stress evidenced by protein carbonyl and protein-bound HNE levels, suppressed oxidation of apolipoprotein A-I (ApoA-I), and suppressed the associated Dox-induced increase in peripheral TNF-α levels. Since MESNA is negatively charged, this agent does not penetrate cells and, consequently, is known not to interfere with chemotherapy.

The results of the current studies suggest that MESNA could reduce the systemic and neurotixic side effects of Dox. A NCI-funded human clinical trial involving

Dox and MESNA is ongoing to test this hypothesis. Our results presented here provide strong evidence in support of a plausible mechanism for Dox-initiated, TNF-α -mediated cognitive dysfunction that leads to CICI, and our results are consistent with a plausible means to prevent these harmful effects without interference with chemotherapy, thereby increasing the quality of life of cancer survivors. Given that about 50 percent of FDA-approved chemotherapeutic agents are associated with ROS, the conclusions of this present study conceivably might have widespread applicability. Studies to test this notion are ongoing in our laboratories.

This dissertation research was conducted test the following hypotheses:

1.) Co-administration of MESNA would prevent Dox-induced oxidation in brain.
2.) Co-administration of MESNA would prevent Dox-related cognitive decline.
3.) Dox-administration would alter the neurochemical profile indexed by proton MRS.
4.) Dox-induced mitochondrial dysfunction would be prevented in brain of TNF-α knockout mice.
5.) Dox-induced oxidative protein damage would be prevented in brain of TNF-α knockout mice.
6.) Superoxide produces oxidative damage to plasma proteins and TNF- α elevation in macrophages similar to that seen following Dox administration.

Copyright © Jeriel T. R. Keeney 2013

CHAPTER 2

BACKGROUND

2.1 Cancer: Incidence, mortality, and treatments

People everywhere get cancer. Few people could say that their lives have not been touched either directly or indirectly by cancer. In the United States, the highest cancer incidence rates per 100,000 population exist in the Northeast. Age-adjusted death rates across all cancer types is highest in states along the Ohio and Mississippi river valleys. (NCI http://statecancerprofiles.cancer.gov) The only state that ranks in the highest category in both of these statistics is Kentucky making it a prime area for the research presented in this dissertation. Kentucky ranks first in the U.S. in overall cancer mortality and second in overall cancer incidence. With regard to specific cancer types, Kentucky ranks first in the nation in incidence of lung, colorectal, and mouth and throat cancers, second in renal cancer, and third in brain cancer. Rates in the Appalachian region of Kentucky are even higher, especially for lung and cervical cancers. (ACS Cancer Facts & Figures 2012, SEER registries, and Kentucky Cancer Registry). Common anti-cancer treatments include surgery, radiation, and chemotherapy. The work presented here focus on the latter, more specifically on those chemotherapeutic agents that induce production of reactive oxygen species as a consequence of their use. The US FDA has approved over 130 anticancer drugs.

(http://www.fda.gov/cder/cancer/approved.htm). Approximately half of these have been reported to induce oxidative stress (Chen et al. 2007).

2.2 Chemotherapy-induced cognitive impairment (CICI, “Chemobrain”)

2.2.1 CICI, definition and prevalence

A large percentage of cancer patients report memory and cognitive impairment following chemotherapy, called “chemobrain” by patients, adversely affecting quality of life (Ahles et al. 2005). Chemotherapy-induced cognitive impairment (CICI) is now widely recognized as a complication of chemotherapy (Tannock et al. 2004; Ahles et al. 2007; Foley et al. 2008; Aluise et al. 2010; Cheng et al. 2013; Seigers et al. 2013). The complexity of cancer, lack of a scientific explanation, and lack of definitive diagnostic criteria, coupled to the fact that many anti-cancer drugs do not cross the BBB, likely contribute to the delay in dealing with CICI. Cognitive symptoms following cancer chemotherapy vary greatly, but memory and executive functions appear to be preferentially affected (Saykin et al. 2003).

2.2.2 Gray and white matter changes in CICI

Direct neurotoxic effects may include cerebral gray matter atrophy and white matter demyelination (Saykin et al. 2003). Several studies have reported white

matter changes in human breast cancer patients following adjuvant chemotherapy (Inagaki et al. 2007; Deprez et al. 2011; de Ruiter et al. 2012; Deprez et al. 2012). Indeed, the integrity of lipid-rich myelin covered white matter have been shown to be altered as well as damage to gray matter with associated functional deficits following systemic cancer chemotherapy, in some cases years after chemotherapy (de Ruiter et al. 2012; Briones et al. 2013; McDonald et al. 2013; Simo et al. 2013). Studies have shown that chemotherapy-induced neuroinflammation are correlated with changes in myelination and cognitive impairment (Briones et al. 2013). Neuroimaging techniques are already being used to detect axonal and white matter changes in subjects at risk of Mild Cognitive Impairment (MCI) and Alzheimer's Disease (AD) (Gold et al. 2010; Gold et al. 2012) and following traumatic brain injury (Kinnunen et al. 2011). Similar techniques may provide useful insights into diagnosis and progression of CICI.

2.2.3 Potential reasons for varied patient outcomes

Saykin and Ahles (2007) suggest that cancer and cognitive problems share genetic risk factors providing a possible explanation for why only some patients experience cognitive deficits following chemotherapy. Immune response dysregulation, DNA-repair deficits, inefficient efflux pumps, reduced antioxidant capacity, decreased neurotransmitter activity, and impaired capacity for neuronal

repair may all contribute to the neurotoxic consequences of chemotherapy (Ahles et al. 2007).

2.2.4 Clinical presentation of and current treatments for CICI

Clinically, consequences of chemotherapy can include both peripheral neuropathy and CNS neurotoxicity including cognitive deficits, encephalopathy, dementia, and beyond (Verstappen et al. 2003). Currently, management of these detrimental consequences is limited to dose reduction, though some ability to compensate for memory deficits has been reported using cognitive-behavioral treatment (Ferguson et al. 2007). The work presented in this manuscript outlines the central role played by TNF-α in CICI and the protective effects of MESNA versus the toxic consequences of the acti-cancer drug, doxorubicin.

2.2.5 Our model of CICI

Based on our previous studies, we proposed the following model. Plasma protein oxidation, including apolipoprotein A-I (ApoA-I), induced by the redox cycling of Dox leads to elevation of tumor necrosis factor-alpha (TNF-α) in the periphery. TNF-α crosses the BBB by receptor-mediated endocytosis to induce microglial activation, further TNF-α release, increased production of NO, mitochondrial dysfunction, neuronal death, and consequent cognitive impairment (Tangpong et al. 2006; Tangpong et al. 2007; Tangpong et al. 2008; Aluise et al. 2009; Aluise

et al. 2010; Joshi et al. 2010; Aluise et al. 2011). Studies presented in this dissertation led us to propose an expanded model of CICI presented in later chapters.

2.3 Doxorubicin (Dox)

Doxorubicin (Dox) is a prototypical chemotherapeutic agent known to produce reactive species (Handa et al. 1975; Gutteridge 1984; Cummings et al. 1991). Dox is an anthracycline antineoplastic agent commonly used in multidrug chemotherapy regimens primarily to treat solid tumors and leukemias. The cancer killing effects of Dox have been shown to involve three proposed mechanisms: DNA intercalation, inhibition of topoisomerase II, and production of ROS (Bachur et al. 1977; Chuang et al. 1979; Reich et al. 1979; Tanaka et al. 1980; Cummings et al. 1991; Fornari et al. 1994; Deres et al. 2005). The quinone moiety present in the Dox structure is capable of undergoing a one-electron reduction to the semi-quinone (Chen et al. 2007; Aluise et al. 2011). Through the redox cycling of this structure back to the quinone, *in vivo*, the reactive O_2^{-}• is produced from molecular oxygen (Figure 2.2).

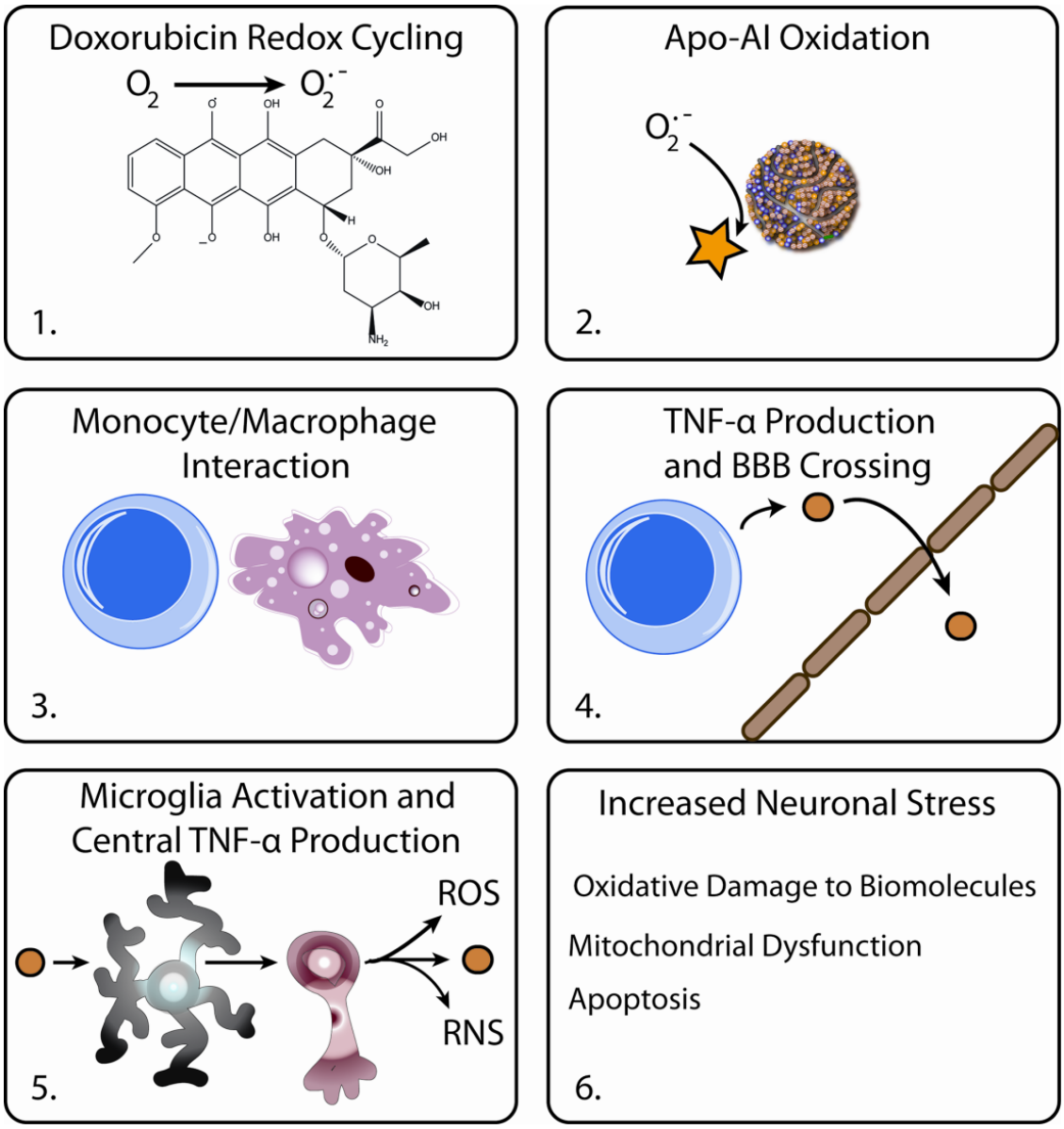

Figure 2.1. Our early model of the stages following Dox administration that lead to chemotherapy-induced cognitive impairment (CICI). In this proposed model, peripheral doxorubicin redox cycling between the quinone and semiquinone states within the circulatory system produces the reactive oxygen species superoxide ($O_2^{\cdot -}$) in abundance (Box 1) that oxidatively modifies ApoA-I on HDL particles (Box 2). This modified ApoA-I is no longer able to inhibit the

monocyte/macrophage interaction (Box 3) and because of this, TNF-α is produced. TNF-α is subsequently able to cross the BBB (Box 4) and activate microglia initiating the production of a host of pro-inflammatory mediators ultimately leading to central TNF-α production as well as increased ROS/RNS (Box 5), which damage neurons and ultimately lead to neuronal death (Box 6).

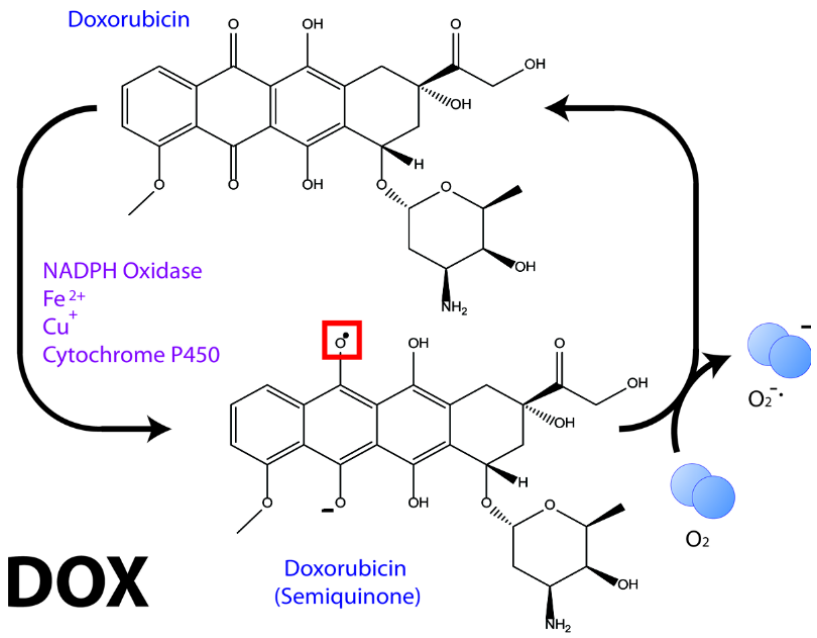

Figure 2.2. Redox cycling of doxorubicin. Redox cycling of doxorubicin back and forth between the semi-quinone and quinone produces superoxide from molecular oxygen.

Previous studies by our laboratory demonstrated that though neither Dox nor its primary metabolite crosses the blood-brain barrier (BBB), peripheral Dox treatment does cause brain injury as evidenced by increased oxidative stress,

the inflammatory cytokine, tumor necrosis factor-alpha (TNF-α), and mitochondrial dysfunction (Tangpong et al. 2006; Joshi et al. 2007; Tangpong et al. 2007; Tangpong et al. 2008).

Our laboratory and others previously demonstrated Dox-induced oxidative stress in blood and damage to plasma proteins leading to detrimental central nervous system consequences (Thayer 1988; Fadillioglu et al. 2003; Tangpong et al. 2006; Othman et al. 2008; Aluise et al. 2009; Aluise et al. 2011). Central to this paradigm is apolipoprotein A-I (ApoA-I) (Aluise et al. 2010; Aluise et al. 2011; Perluigi et al. 2011; Keeney et al. 2013). ApoA-I promotes cholesterol efflux as part of the high density lipoprotein (HDL) complex. Additionally, ApoA-I has been shown to suppress TNF-α in plasma (Hyka et al. 2001; Perry et al. 2002; Weber et al. 2011). Previous studies in our laboratory have shown that, when oxidized, ApoA-I loses this ability to suppress TNF-α release and may exacerbate the problem (Aluise et al. 2011).

2.4 Apolipoprotein A-I (ApoA-I)

ApoA-I is a multifunctional apolipoprotein that plays a variety of roles in human physiology among which are cholesterol transport and regulation of inflammation. Through the ATP-binding cassette protein (ABCA1), ApoA-I serves as the primary lipid acceptor protein for lipids such as cholesterol and phosphatidylcholine as they are effluxed from the lipid bilayer (Quazi et al. 2011)

as part of the high-density lipoprotein (HDL) complex taking excess cholesterol from tissues (Hyka et al. 2001). HDL is associated with a reduced risk of atherosclerosis through intervening in either lipoprotein and cholesterol metabolism or modulation of inflammatory processes (Rader et al. 2008).

In addition to its role in reverse cholesterol transport ApoA-I has been reported to have antioxidant and anti-inflammatory properties and other studies have reported decreased serum ApoA-I with inflammation (Tape et al. 1990) and increased ApoA-I levels in CSF after brain injury (Saito et al. 1997). As described further below, redox proteomics has identified ApoA-I as oxidatively modified in plasma of persons subjected to ROS/RNS as a result of chemotherapy.

2.4.1 Cholesterol and Its Transport

Cholesterol is predominantly an amphipathic molecule which is dominated by its hydrophobic sterol ring that allows for the insertion of cholesterol into the bilayer, yet is able to maintain its proper orientation due to the hydrophilic 3β-hydroxyl group present in the molecule. Cholesterol has been found to play a major stabilizing role, reducing membrane lipid bilayer fluidity and increasing turgidity. Cholesterol is also well known to play a role in bile acid production and steroid hormone synthesis while much more recently cholesterol has been implicated in the formation of micro-signaling domains called lipid- or membrane-rafts (Liscum et al. 1995; Dominiczak 2001; Waarts et al. 2002; Shadan et al. 2004; Oh et al.

2007; Chaudhuri et al. 2011). Because cholesterol is centrally stored in the liver, there must be a mechanism in place for the transport of cholesterol to and from the cells that require it. Due to the fact that the majority of the surface area of cholesterol is hydrophobic in nature, transport of cholesterol through the aqueous blood supply is facilitated by a group of proteins called lipoproteins.

Lipoprotein sub-classes are classified based on their hydrated density into five main groups (chylomicrons, very-low density lipoproteins (VLDL), intermediate density lipoproteins, low-density lipoproteins (LDL) and high-density lipoproteins (HDL)) that may also differ in the relative size as well as the overall lipid and apolipoprotein content (Dominiczak et al. 2011). Predominantly important to this discussion is the ability of apolipoproteins to direct the action of lipoproteins through direct interaction with other cell types by way of membrane lipoprotein receptors.

There are three main ways in which cholesterol and triglycerides are mobilized throughout the body: the fuel transport pathway (FTP), the over-flow pathway (OFP), and reverse cholesterol transport (RCT). In order to move triglycerides from the liver for use in peripheral tissues, the FTP employs both chylomicrons as well as VLDL using an array of apolipoproteins such as ApoA-I, A-II, A-IV and A-V, apoB48 and B100, apoC-I, C-II, and C-III, and apoE (Hill et al. 1997; Dominiczak 2001; Dominiczak et al. 2011). Once in the periphery, lipoprotein lipase acts on chylomicrons to release fatty acids to cells while returning

apolipoproteins to nearby HDL particles. VLDL particles remain partially intact after interaction with lipoprotein lipase, and the resulting VLDL remnants are returned by LDL receptors that bind apolipoprotein E (apoE). As a result of excessive remnant generation by the FTP, an increase in LDL, which has been referred to as an extracellular cholesterol depot, can accumulate in the blood supply, a process that has been linked to atherosclerosis. To combat this increase in LDL, the OFP is in place to metabolize LDL using apoB100, the predominant apolipoprotein in LDL, that interacts with the apoB/E LDL receptor and causes the internalization of the LDL particles (Dominiczak et al. 2011).

The RCT system comprises the metabolism of HDL and the subsequent transport of cholesterol from the periphery back to the liver, and because of this role, HDL levels have been found to have an inverse relationship with cardiovascular disease (Cucuianu et al. 2007; Yang et al. 2010; Zhao et al. 2012). The primary apolipoprotein component of HDL is ApoA-I, responsible for the free cholesterol loading of HDL from cells by binding to ABCA1 as well as the secretion of apoE, which stimulates Lecithin-cholesterol acyltransferase (LCAT) activity(Dominiczak 2001; Bencharif et al. 2010) (Figure 2.3). Once loaded, the cholesterol is esterified by LCAT, producing cholesteryl esters and transforming HDL to HDL3. HDL3 can then function to interchange the cholesteryl esters and apolipoproteins A, C and E for triglycerides from lipoproteins, in which triglycerides are abundant, forming HDL2 which can subsequently deposit the cholesteryl esters into the scavenger receptor BI (SRB-1) at the liver (Hill et al.

1997; Dominiczak et al. 2011). Interestingly, in bovine aortic endothelial cells oxidative modification of HDL, likely on ApoA-I, by myeloperoxidase was sufficient to decrease HDL interaction with SR-B1 as well as induce a pro-inflammatory state via tumor necrosis factor-α (TNF-α)-induced expression of the vascular cell adhesion molecule 1protein as well as nuclear factor kappa-B (NFκB) activation (Undurti et al. 2009).

2.4.2 HNE modification of ApoA-I

ApoA-I is particularly susceptible to modification by lipid peroxidation products such as the reactive aldehydes, 4-hydroxy-2-trans-nonenal (HNE) and acrolein. Electrophilic sites on these reactive aldehydes may be attacked by nucleophilic centers like those in the amino acid side chains of histidine (H), lysine (K), or cysteine (C) to form covalent adducts that has been shown to alter both the structure and function of proteins (Subramaniam et al. 1997; Liebler 2008; Kim et al. 2009; Butterfield et al. 2010). Liebler and colleagues (Szapacs et al. 2008) found ApoA-I to be highly modified by free radical oxidation using a novel biotin-modified linoleoylglycerylphosphatidylcholine probe (PLPBSO). Free radical oxidation of human plasma containing the probe produced covalent Michael-adducts to plasma proteins. These proteins were identified and phospholipid binding sites mapped using liquid chromatography-tandem mass spectrometry (LC-MS/MS) on streptavidin-purified proteins (Szapacs et al. 2008; Kim et al. 2009).

To determine potential binding sites, human plasma was oxidized using 2, 2-azobis(2-(2-imidazolin-2-yl)propane)-dihydrochloride (AIPH), a compound known to produce reactive aldehydes upon oxidation of the PLPBSO probe. In independent experiments, HNE was added in varying concentrations directly to isolated HDL. The formation of HNE adducts on ApoA-I was found at an increasing number of sites and with increasing frequency as concentrations of either AIPH in plasma or HNE in isolated HDL were increased (Szapacs et al. 2008). These sites include H162, H193 at HNE concentrations of 1uM; H155 at 10uM; H135, H199, K208, K94, K96; and K107, K238, K12, K23 at 1000uM. At low concentrations of AIPH or HNE respectively, HNE modifications on ApoA-I were found that included H162, located in a key functional region of ApoA-I(Szapacs et al. 2008). Oxidative modification of H162 on ApoA-I may disrupt the maturation of the HDL complex by structural changes in the ApoA-I domain responsible for activation of LCAT which, as discussed, converts free cholesterol to the more hydrophobic cholesteryl esters for packaging in the formation of HDL particles (Figure 2.3).

2.4.3 ApoA-I and ABCA1 interaction and subsequent signaling

The binding of ApoA-I to ABCA1 has been shown to have a major role in RCT and the exporting of free cholesterol from cells for return to the liver, a process believed to be of crucial importance for anti-atherosclerosis (Vergeer et al. 2010; Zhao et al. 2012). More recently this interaction has been found to affect many

areas of cellular processes, including not only direct cellular cholesterol and phospholipid efflux, but also various cell signaling pathways that may turn out to have more far reaching effects than were first thought.

Aside from the activation of Rho GTPases such as Cdc42, Rho, and Rac, small G-proteins that are responsible for the reorganization of cytoskeletal architecture, as well as the direct binding of calmodulin, the binding of ApoA-I and ABCA1 has been shown to cause the activation of Janus kinase 2 (JAK2).This activation has been implicated in the majority of the lipid transport conducted by ABCA1, a process that is significantly impaired when in the presence of JAK2-specific inhibitors (Matsunaga et al. 1991; Tsukamoto et al. 2001; Tang et al. 2004; Tang et al. 2006; Vaughan et al. 2009; Iwamoto et al. 2010). Interestingly, STAT3 also has been shown to be active post ApoA-I/ABCA1 interaction to decrease the secretion of inflammatory cytokines in macrophages, a process linked to anti-inflammation (Murray 2006; Tang et al. 2009; Yin et al. 2011).

In addition to JAK2/STAT3 activation, the ApoA-I/ABCA1 interaction has been shown to activate both protein kinase A (PKA) and protein kinase C (PKC). PKA is activated by increased cyclic-adenosine monophosphate by the activation of adenylyl cyclase through $G\alpha_s$ coupling with ABCA1. The result of PKA activation is the phosphorylation of ABCA1 and a subsequent increase in ApoA-I lipidation, a process blocked by specific PKA inhibition (Yang et al. 2007; Hu et al. 2009; Jeon et al. 2010; Zhao et al. 2012). PKC on the other hand is activated as a

result of an initial depletion of free cholesterol, phostphatidylcholine and sphingomyelin from the cell membrane by ApoA-I/ABCA1 interaction. This later interaction stimulates phosphatidylcholine-specific phospholipase C activity resulting in an increase of both phosphatidylcholine as well as diacylglycerol, a major activator of PKC. The activation of PKC not only leads to the phosphorylation of ABCA1, a process believed to increase the lifetime of ABCA1 via protection from degradation, but also increases cholesterol. The interaction of PKC-ζ with specificity protein-1 controls the expression level of ABCA1 (Yamauchi et al. 2003; Yamauchi et al. 2004; Chen et al. 2011; Zhao et al. 2012).

From the above, it is apparent that ApoA-I/ABCA1 interaction is a critical event that, if impaired through damage such as oxidative stress, could have much larger ramifications than simply cholesterol and fatty acid efflux impairment, i.e., may affect a large array of cellular processes directly or tangentially related to the activation or inactivation of this important intracellular signaling process.

In the context of atherosclerosis, increased oxidative modification of ApoA-I mediated by myeloperoxidase led to decreased ABCA1-dependent cholesterol efflux from macrophages (Zheng et al. 2004) as well as impaired activation of LCAT (Wu et al. 2007). A possible, albeit weak, link has been established between a polymorphism of the ApoA-I gene negatively affecting HDL function and cognitive decline (Helbecque et al. 2008).Overall, current evidence suggests

ApoA-I to be a promising diagnostic marker as well as a potential target for therapeutic strategies.

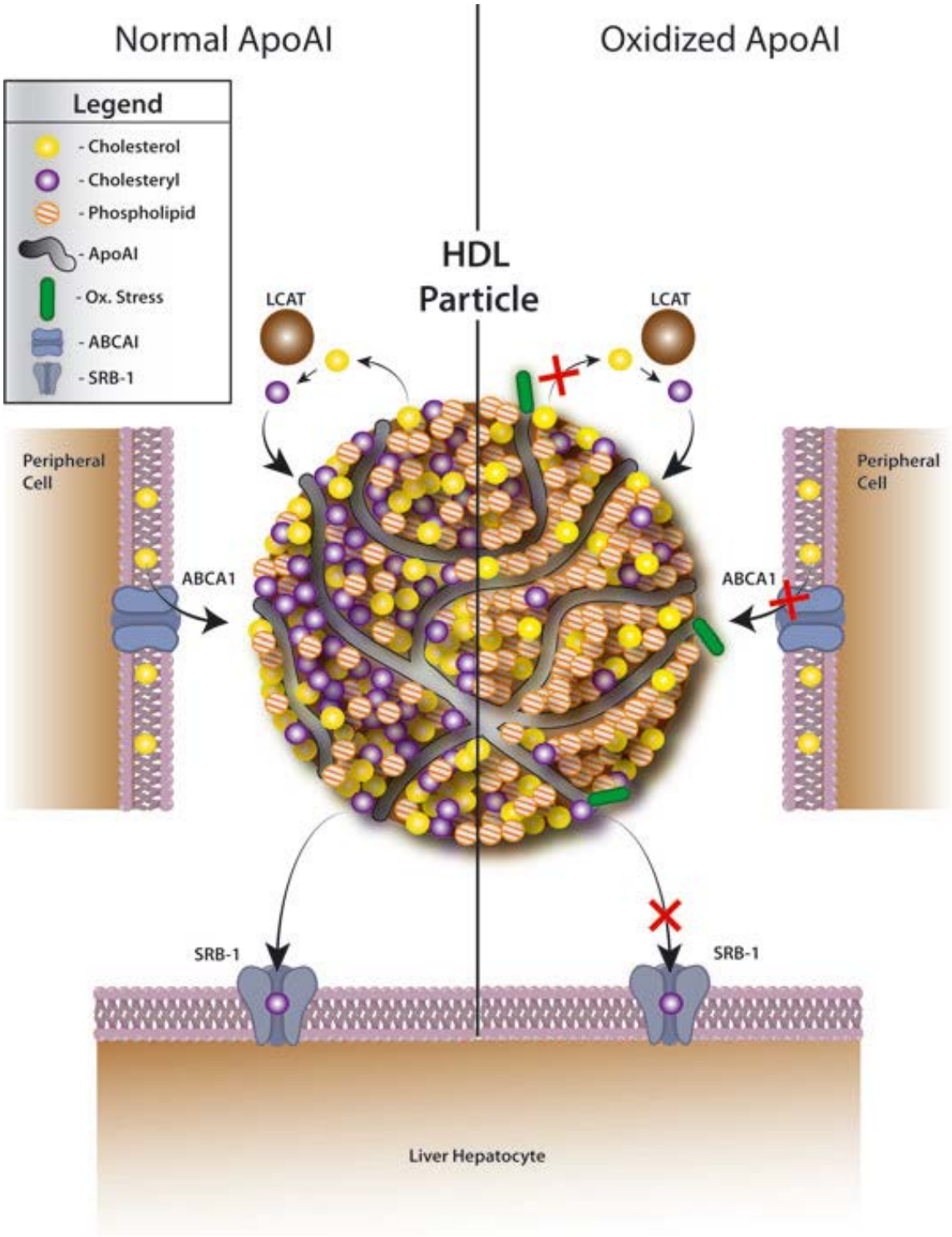

Figure 2.3. Unmodified vs. oxidatively modified ApoA-I. The left-hand side of the figure depicts an HDL particle with bound ApoA-I that has not undergone oxidative damage, and as shown, is able to function normally interacting with LCAT, peripheral ABCA1 and scavenger receptor BI (SRB-1). The right-hand side of the figure displays an HDL particle that has undergone extensive oxidative modification on ApoA-I, a process that has been shown to negatively affect the ability of the HDL particle to interact peripherally with ABCA-1, LCAT, and SRB-1. This loss of function of ApoA-I has many consequences such as impaired ABCA1 signaling and cholesterol deposition to HDL, impaired cholesterol to cholesteryl conversion by LCAT, and the inability to dock with SRB-1. See text. Used by permission of John Wiley and Sons.

2.4.4 ApoA-I and chemotherapy-induced cognitive impairment

Redox proteomics provided new insights into mechanisms involved in chemotherapy induced cognitive dysfunction (Aluise et al. 2011), found in up to 75% of breast cancer survivors (Raffa et al. 2006). Given that nearly 50 percent of FDA-approved chemotherapeutic agents are associated with ROS, a significant proportion of the millions of cancer survivors in the United States likely show symptoms of cognitive dysfunction.

Oxidative modification of ApoA-I has been implicated in a cascade of events involving elevation of inflammatory species leading to chemotherapy-induced cognitive dysfunction (Aluise et al. 2011). Chemotherapy patients often complain of noticeable memory impairment as well as cognitive decline following chemotherapy, an ailment described by the patients with the term “Chemobrain”, with symptoms that persist sometimes for years post-treatment. The anthracycline, doxorubicin (Dox), used to treat a variety of solid tumors and leukemias often as part of multidrug chemotherapy regimens, leads to the production of ROS and RNS(Bachur et al. 1977; Deres et al. 2005; Aluise et al. 2011) that can damage biomolecules including proteins, lipids, and DNA (Fornari et al. 1994; Jungsuwadee et al. 2006; Chen et al. 2007). A quinone in the Dox structure undergoes redox cycling to the semiquinone, accepting a single electron from an oxidant potentially involving NADPH oxidases, Fe^{2+}, Cu^{+}, or cytochrome P450. In the presence of molecular oxygen, the quinone is reformed by transferring the extra electron to oxygen producing the superoxide radical anion. Superoxide can damage biomolecules directly or indirectly through formation of other ROS/RNS (Aluise et al. 2010).

Oxidative stress analysis of plasma samples from human patients treated with Dox showed global elevation of plasma protein carbonylation compared to plasma samples from the same persons prior to Dox administration. A subset of these patients also showed elevated plasma protein-bound HNE, a lipid

peroxidation byproduct of arachidonic acid (Jungsuwadee et al. 2006; Aluise et al. 2010; Aluise et al. 2011).

Our group hypothesized that the oxidative damage to plasma resident ApoA-I, as a result of ROS/RNS induced by Dox and other chemotherapeutic agents, leads to peripheral elevation of the inflammatory cytokine, TNF-α, which, as mentioned above, crosses the BBB (Gutierrez et al. 1993; Osburg et al. 2002) via TNFR1 and TNFR2 endocytosis and activates distant receptors located in the CNS. In brain, TNF-α was shown to lead to biomolecule and mitochondrial damage, and neuronal death, and cognitive decline in these cancer patients is proposed to result from such changes (Tangpong et al. 2006; Tangpong et al. 2007; Aluise et al. 2011). An activated T-cell-monocyte contact interaction results in monocyte production of TNF-α. ApoA-I inhibits TNF-α release either by inhibition of the monocyte-macrophage contact interaction or by interaction with ABCA1 (Hyka et al. 2001; Tang et al. 2009). Our group showed, based on redox proteomic evidence, elevated oxidative alterations of ApoA-I induced by protein carbonylation and protein-bound HNE in the plasma of chemotherapy patients, results that were confirmed in Dox treated mouse models compared to saline treated controls (Aluise et al. 2011). Once oxidized, ApoA-I loses the ability to inhibit the monocyte-macrophage interaction thereby allowing increased TNF-α release (Aluise et al. 2011). Despite the inability of Dox or its metabolites to cross the BBB, through ApoA-I oxidation, Dox increases levels of TNF-α in the periphery which can migrate in the bloodstream to the brain and other tissues

and stimulate local inflammation and oxidative stress leading to apoptosis and, potentially, the deleterious cognitive effects experienced by chemotherapy patients (Tangpong et al. 2006; Aluise et al. 2011). Once in the CNS, TNF-α activates astrocytes, specifically microglia, elevation of iNOS is induced causing damage to mitochondrial MnSOD, leading to a cascade involving cytochrome C, caspase 3, and cell execution (Tangpong et al. 2007). Anti-TNF-α antibody prevents these effects (Tangpong et al. 2006). Sustained activation of microglia can lead to long-term elevation of TNF-α in the CNS (Dammann et al. 2001; Wang et al. 2012).

2.5 Tumor necrosis factor-alpha (TNF-α)

2.5.1 Overview of TNF-α and CICI

The inflammatory cytokine, tumor necrosis factor-alpha (TNF-α), plays a variety of roles including inflammatory responses and innate immunity (Dinarello 2007). The inflammatory and immune responses of TNF-α can be beneficial when acute, controlled, and localized, but quite detrimental if elevated or sustained demonstrating the pleiotropic nature of this and other cytokines. Macrophages are a principle cell source of TNF-α. Interaction of ApoA-I with the ATP-binding membrane cassette transporter A1 (ABCA1) involved in cholesterol transport (Quazi et al. 2011; Weber et al. 2011) results in inhibition of TNF-α release through production of a tristetraprolin (TTP) (Yin et al. 2011). TTP degrades the

mRNA message for TNF-α (Yin et al. 2011). Once oxidized, ApoA-I loses the ability to inhibit TNF-α release (Aluise et al. 2011). TNF-α, produced in the periphery, traverses the BBB via receptor-mediated endocytosis. Resulting microglial activation in the CNS results in further release of TNF-α, oxidative stress, and CNS toxicity (Tangpong et al. 2006; Tangpong et al. 2007; Tangpong et al. 2008; Joshi et al. 2010; Aluise et al. 2011).

2.5.2 TNF-α signaling, inflammation, and apoptosis

TNF-α is a multifunctional cytokine with involvement in pathways including pro-apoptotic, anti-apoptotic, inflammatory response, and immune function regulation and has been implicated in a large variety of diseases such as rheumatoid arthritis, Crohn's disease, and Alzheimer disease. Within the CNS, TNF-α has both neuroprotective and neurotoxic roles facilitating both necrosis and caspase-mediated apoptosis (Selmaj et al. 1990; Schneider-Brachert et al. 2004; Badiola et al. 2009). TNF-α is normally found in low levels in healthy brain, but can be found at high levels in cerebral and transient ischemic attacks, and in aged human brains (Gupta et al. 2005; Rubio-Perez et al. 2012).

Extracellular TNF-α binds and activates two main receptors, TNFR1 (p55) and TNFR2 (p75) that are responsible for mediating the intracellular cytokine activity. Because the two receptors lack metabolic activity, they must recruit and bind intracellular proteins in order to transduce the signal initiated by TNF-α. TNFR1

and TNFR2 are single transmembrane glycoproteins with similar extracellular structures, yet differ in their intracellular domains (MacEwan 2002).

TNFR1, also known as the death-receptor, has an intracellular death domain (DD) consisting of 80 amino acids and is located near the carboxy-terminus (MacEwan 2002). Silencer of death domain (SODD) is responsible for binding and silencing the DD of inactive TNFR1 and dissociates upon receptor activation facilitated by TNF binding to its extracellular domain. Dissociation of SODD from the DD of TNFR1 allows the binding of the adaptor protein, TNF-receptor-associated death-domain (TRADD), and its subsequent recruitment of additional proteins to the receptor, as demonstrated by the interaction between TNF receptor-associated factor (TRAF2) and receptor-interacting kinase (RIP). TRADD-dependent recruitment of proteins to TNFR1 allows the initiation of the following three main pathways: NFκB activation, mitogen-activated protein kinase (MAPK) pathway activation, and caspase-mediated apoptosis.

NFκB is a heterodimeric transcription factor responsible for a large variety of cellular responses under stress and anti-apoptotic actions. Inactive NFκB is sequestered in the cytoplasm by inhibitor of κB (IκB), which dissociates upon its phosphorylation at two serine residues by inhibitor of κB kinase β (IKKβ). Recruitment and activation of IKKβ to TNFR1 is dependent on the presence of TRAF2 and RIP, respectively (Song et al. 1997; Wajant et al. 2003). Once NFκB is released from the inhibitory subunit, IκB, it may then translocate to the nucleus

and induce the gene expression of its downstream anti-apoptotic proteins. Within the CNS this anti-apoptotic NFκB pathway, activated through TNF-α, generally has neuroprotective roles (Liu et al. 1996).

Of the three main MAPK pathways, the stress related and pro-apoptotic c-jun NH_2-terminal kinase (JNK) cascade is most strongly stimulated by the TNFR1/TRADD/TRAF2 complex (Chen et al. 2002). The recruited TRAF2 protein is believed to be responsible for activation of a mitogen-activated protein kinase kinase kinase (MAPKKK), for example, apoptosis-stimulated kinase 1 (ASK1) (Nishitoh et al. 1998). Stimulation of a variety of MAPKKKs can lead to the activation of a cascade of kinases that ultimately result in JNK activation. Once activated, JNK translocates to the nucleus where it then may phosphorylate and subsequently activate the pro-apoptotic transcription factor c-Jun.

Stimulation of caspase-mediated apoptosis by the TNF-α-activated TNFR1 receptor involves the recruitment and binding of fas-associated death domain (FADD) to TRADD. The TNFR1/TRADD/FADD complex then recruits and activates the cysteine protease caspase-8, which leads to the activation of caspase-3, the executioner of apoptosis. The mentioned pro-apoptotic caspase cascade and anti-apoptotic NFκB pathway both play negative regulatory roles of one another; caspase-8 and caspase-3 inhibits RIP and IKKβ respectively, and the NFκB-transcribed cellular inhibitor of apoptosis protein 1 and 2 inhibits both caspase-8 as well as caspase-3.

TNFR2, the less understood of the two TNF-α receptors, lacks a death domain and currently appears to have a stronger anti-apoptotic role than TNFR1. TRAF2 was initially recognized as a signal transduction protein of TNFR2, in which it may bind directly to the receptors intracellular domain of this receptor. In contrast to TNFR1 where TRAF2 indirectly interacts with the TNFR2 receptor by binding to the adaptor protein TRADD. Through direct interaction with TRAF2, TNFR1 is able to stimulate the anti-apoptotic transcriptional factor, NFκB.

An excitotoxic effect of excessive synaptic glutamate is promoted by the collaboration of TNF-α receptors located on the surfaces of microglia and astrocytes. Activation of microglial TNF-α receptors lead to the up regulation of the glutamate generating enzyme glutaminase and subsequent extracellular release of excess glutamate through hemichannels (Takeuchi et al. 2006). Extracellular TNF-α also has been found to stimulate the generation of microglial TNF-α (Tangpong et al. 2008), increasing its extracellular levels. In astrocytes TNFR1-associated caspase 3 and NFkB pathways work to decrease the reuptake of synaptic glutamate by respectively inactivating and reducing the expression of the influx transporter, excitatory amino acid transporter 2 (EAAT2), from the membrane of astrocytes (Sitcheran et al. 2005; Zou et al. 2005; Boston-Howes et al. 2006). EAAT2 is an important part of the glutamine shuttle, responsible for the reuptake of glutamate from the synaptic cleft and into astrocytes, where it can be converted to its inactive form of glutamine. With the TNF-α-associated down regulation of EAAT2 activity, and increased generation

and release of glutamate from microglia, this puts neurons in danger of excitotoxicity caused by high extracellular levels of glutamate.

Within neurons, TNF-α-mediated activation of TNFR1 contributes more directly to neuronal cell death through activation of the caspase-mediated apoptosis cascade described earlier (Kogo et al. 2006). Neuronal TNFR1 also has influence over Ca^{2+} -mediated cell death by increasing the membranous expression of iontropic glutamate receptor AMPA, through the activation of IP_3 (Stellwagen et al. 2005). The increased expression of ligand gated ion channel AMPA is yet another factor into the excitotoxic effect of high synaptic glutamate levels. Further jeopardizing neuronal survival is the TNF-α-mediated decrease of surface receptor $GABA_A$, responsible for inhibitory effects that work to counteract the excitatory effect of glutamate (Stellwagen et al. 2005).

Through activated TNF-α receptors on microglial, astrocyte, and neuronal cell surfaces, TNF-α is able to directly and indirectly contribute to neuronal cell death. These neurotoxic effects of TNF-α help highlight the cytokine's role in a variety of neurodegenerative diseases. Such processes are likely involved in chemotherapy-induced cognitive decline (Aluise et al. 2011).

2.6 MESNA

2-mercaptoethane sulfonate sodium (MESNA) is a drug developed for use to protect the urinary bladder from hemorrhagic cystitis caused by chemotherapy.

MESNA is FDA-approved for use with Dox as part of multidrug chemotherapy regimens that include ifosfamide or cyclophosphamide. MESNA does not enter cells, does not interfere with cancer chemotherapy (Bernacki et al. 1987). A biproduct of ifosfamide metabolism is acrolein [2-propen-1-al], an alpha, beta unsaturated aldehyde that can build up in the bladder leading to the complications. The structure of MESNA contains a free sulfhydryl group imparting much of its antioxidant properties by affording it the ability to scavenge free radicals and reactive aldehydes such as HNE and acrolein. Our laboratory has demonstrated that ApoA-I oxidation in plasma and subsequent increased TNF-α release is suppressed with co-administration of MESNA (Aluise et al. 2011).

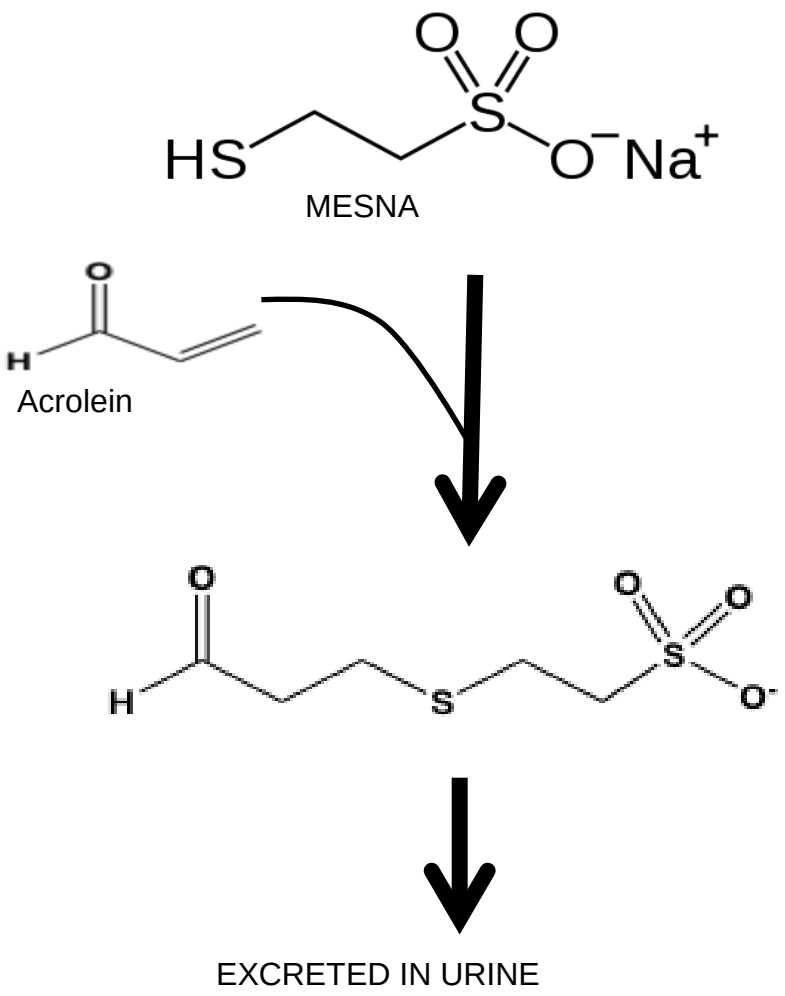

Figure 2.4. MESNA scavenges free radicals and reactive aldehydes such as HNE and acrolein and is excreted in urine.

2.7 Oxidative Stress

Oxidative stress refers a condition where an imbalance exists between those species that cause oxidative damage to biomolecules, reactive oxygen and reactive nitrogen species (ROS, RNS), and the antioxidant defenses intended to

protect against them (Sies 1997; Dasuri et al. 2012; Schulz et al. 2012). The brain is particularly vulnerable to oxidative damage due to relatively low antioxidant defenses, high oxygen consumption, areas rich in iron, and high concentrations of polyunsaturated fatty acids containing labile allylic hydrogens that are prime targets of free radical attack.

2.7.1 Reactive oxygen and reactive nitrogen species

ROS and RNS include, among many others, superoxide radical anion ($O_2^{-\cdot}$), hydrogen peroxide (H_2O_2), hydroxyl radical ($^{\cdot}OH$), nitric oxide ($NO^{\cdot}$), and peroxynitrite ($ONOO^-$), many of which are free radicals. ROS/RNS play necessary and beneficial roles in many biological processes (Dasuri et al. 2012). In addition to free radicals produced from environmental exposure, excess production of free radicals or other reactive species and a failure of antioxidant defense systems to adequately handle the ROS/RNS load results in damage to biomolecules including proteins, lipids, and genetic material (Valko et al. 2007; Uttara et al. 2009; Butterfield et al. 2012; Halliwell 2012).

2.7.2 Mitochondria as a source of ROS

Human mitochondria process oxygen at great potential self-risk due to production and leakage of the damaging $O_2^{-\cdot}$ (Figure 2.5) from age-related decreases in the efficiency of electron transport chain reactions, primarily from Complex I (Adam-

Vizi 2005; Calabrese et al. 2005; Dasuri et al. 2012; Scialo et al. 2012; De Giusti et al. 2013). The reactive $O_2^{-\cdot}$ has been shown to oxidize biomolecules directly through lipid peroxidation and protein oxidation (Halliwell et al. 1984; Fridovich 1986; Deby et al. 1990) and indirectly inducing oxidative/nitrosative stress in the brain through production of other reactive species and by mechanisms including the inflammatory cytokine tumor necrosis factor alpha (TNF-α) (Halliwell et al. 1984; Dean et al. 1997; Klamt et al. 2002; Tangpong et al. 2008; Aluise et al. 2011).

The mitochondrial resident superoxide scavenger, manganese superoxide dismutase (MnSOD) in the mitochondria react with $O_2^{-\cdot}$ producing H_2O_2 . H_2O_2 is only a weak oxidant otherwise but becomes much more damaging in the presence of free copper or iron ions through Fenton Chemistry as H_2O_2 is converted to the extremely reactive $^{\cdot}OH$ radical and OH^- (Halliwell et al. 1984; Halliwell 2012). The $^{\cdot}OH$ radical is responsible for much of the downstream indirect damage from superoxide. Hard nucleophiles such as the hydroxyl radical attack biomolecules at carbonyls resulting in structural and functional changes.

2.7.3 Free radicals and lipid peroxidation

Free radicals in close proximity to allylic hydrogens on biomolecules abstract such hydrogens leaving a carbon-centered radical. When this occurs to PUFA in the lipid bilayer, reaction of this radical with molecular oxygen forms a peroxyl

radical leading to a chain reaction involving further abstraction of other allylic hydrogens from nearby biomolecules, again forming a C-centered radical. Once initiated, lipid peroxidation can lead to increased production of reactive alkenals in the bilayer, loss of lipid asymmetry, and apoptosis (Castegna et al. 2004; Bader Lange et al. 2010; Butterfield et al. 2010; Perluigi et al. 2012; Sultana et al. 2013).

1. $LH + X^{\bullet} \rightarrow L^{\bullet} + XH$
2. $L^{\bullet} + O_2 \rightarrow LOO^{\bullet}$
3. $LOO^{\bullet} + LH \rightarrow LOOH + L^{\bullet}$
4. $LOO^{\bullet} + LOO^{\bullet} \rightarrow \text{nonradical} + O_2$

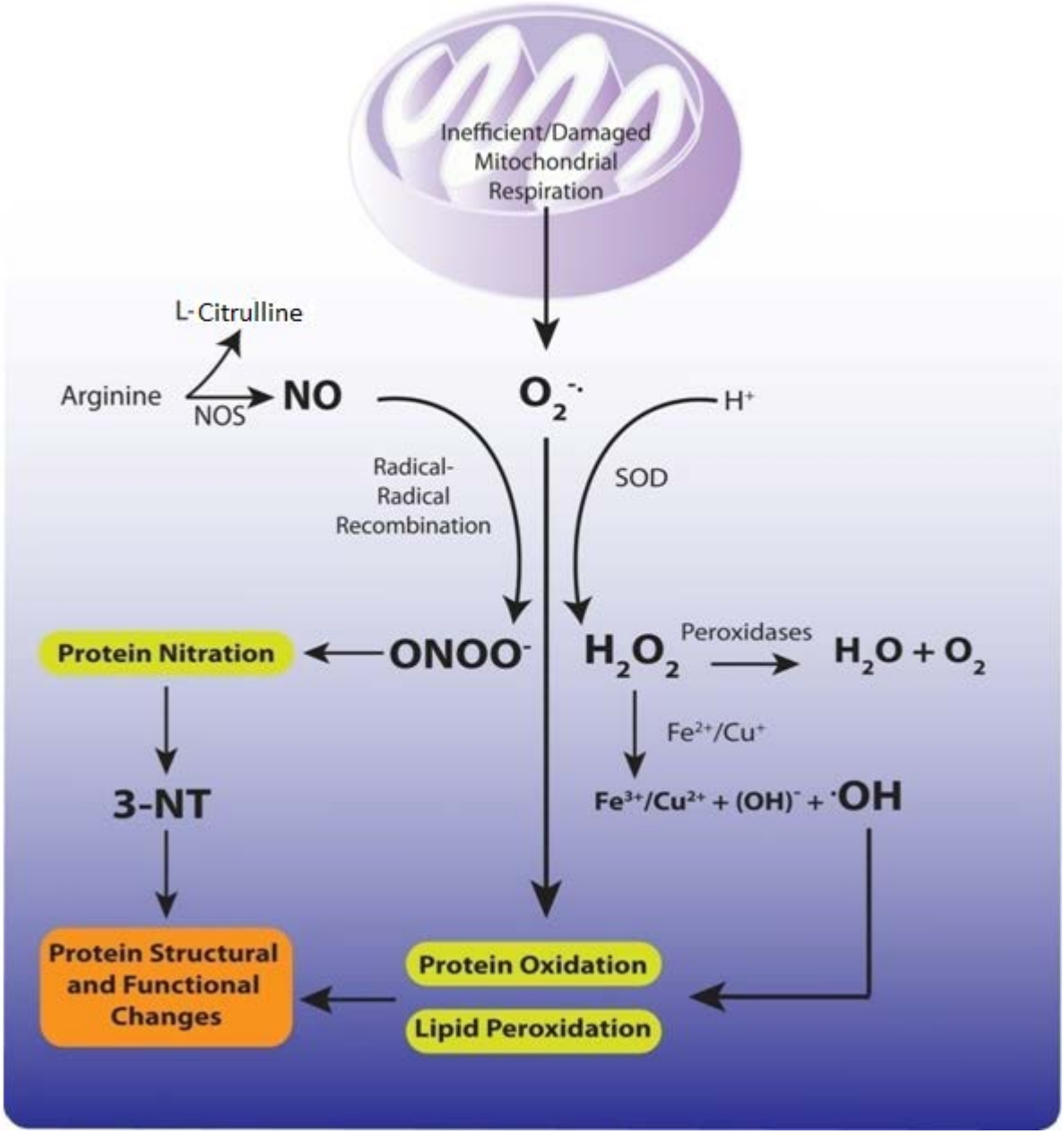

Figure 2.5. ROS formation involving mitochondria-derived superoxide. ROS formation involving mitochondria-derived superoxide free radicals and subsequent processing by MnSOD and Fenton chemistry and RNS formation following NO production via i-NOS and reaction of NO with superoxide free radicals. Used by permission from Elsevier Scientific Publishers, Inc.

A major reactive alkenal produced is 4-hydroxy-2-trans-nonenal (HNE). HNE is primarily produced in the brain via lipid peroxidation of arachidonic acid (Figure 2.6), an abundant omega-6 PUFA found in the lipid bilayer in brain (Butterfield et al. 2010). Arachidonic acid is released through cleavage of a phospholipid by phospholipase A2 (PLA2) and serves as a second messenger involved in cellular signaling and the regulation of signaling enzymes (Prentki et al. 1987; Jones et al. 1993; Frisardi et al. 2011). HNE binds proteins by Michael Addition to certain amino acids resulting in protein dysfunction (Figure 2.7) (Butterfield et al. 2002). Amyloid beta (Aβ)-peptide itself has been shown to be a source of ROS and an initiator of free radical damage to biomolecules in brain including lipid peroxidation (Harris et al. 1995; Hensley et al. 1995; Butterfield 1997; Butterfield et al. 1997; Varadarajan et al. 2000; Yatin et al. 2000; Lauderback et al. 2001; Butterfield et al. 2002; Boyd-Kimball et al. 2005).

2.7.4 NO and tyrosine nitration

A free radical in its natural form, $NO^{\cdot}$ is synthesized from L-arginine by endothelial, neuronal, or inducible nitric oxide synthases (NOS). $NO^{\cdot}$ has beneficial effects such as a biological mediator in several processes including neurotransmission, vascular smooth muscle contraction as well as having antitumor, and antimicrobial activities (Xu et al. 1994; Shinde et al. 2000; Cole et al. 2006) but becomes toxic at high concentrations (McCarty 2006).

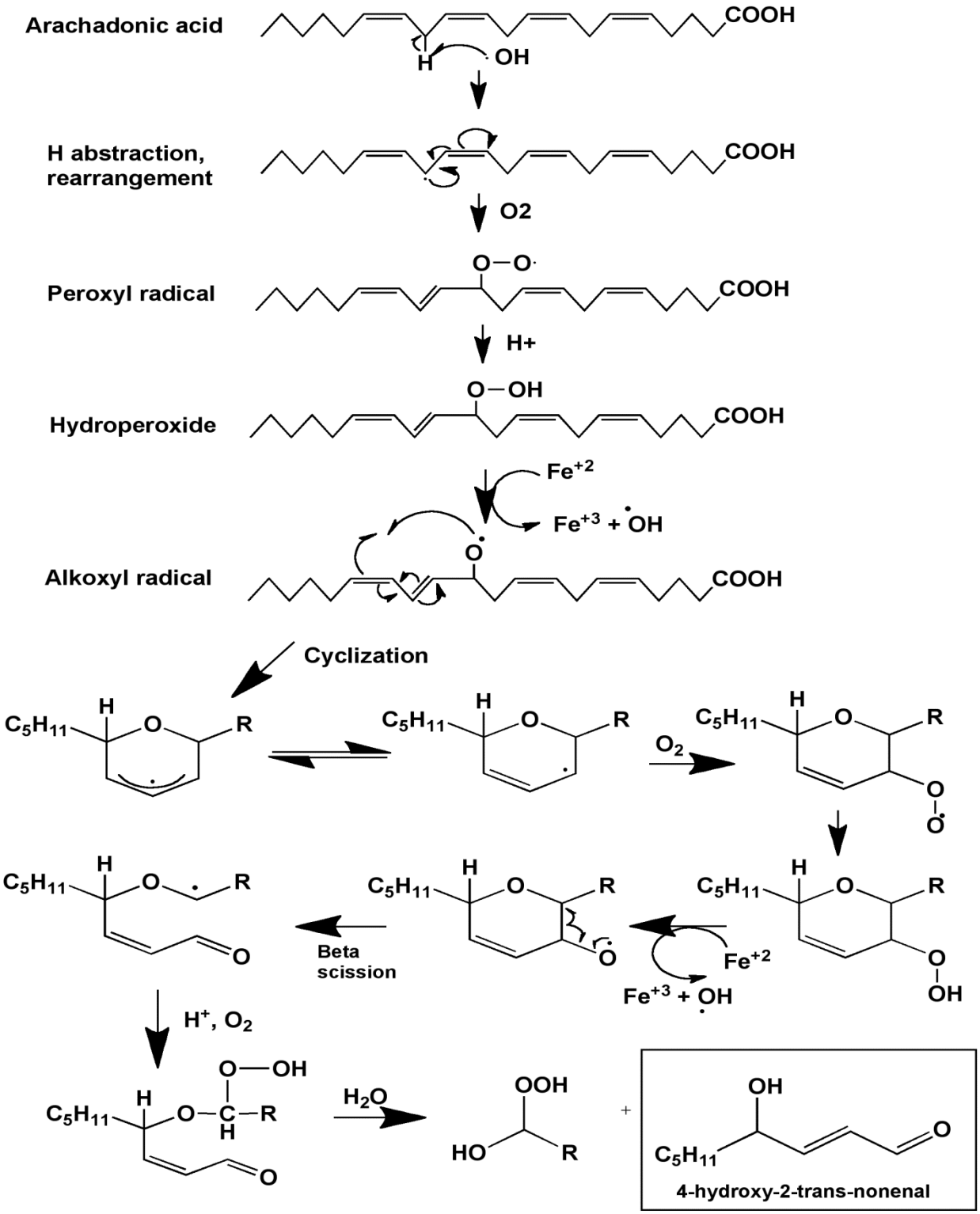
Arachadonic acid
COOH
H
OH
H abstraction, rearrangement
COOH
O2
Peroxyl radical
O—O·
COOH
H+
Hydroperoxide
O—OH
COOH
Fe+2
Fe+3 + ·OH
Alkoxyl radical
O·
COOH
Cyclization
C5H11
H
O
R
O2
O
O·
Fe+2
Fe+3 + ·OH
OH
Beta scission
H+, O2
O—OH
H2O
OOH
HO
R
+
OH
4-hydroxy-2-trans-nonenal

Figure 2.6. HNE formation from arachidonic acid.

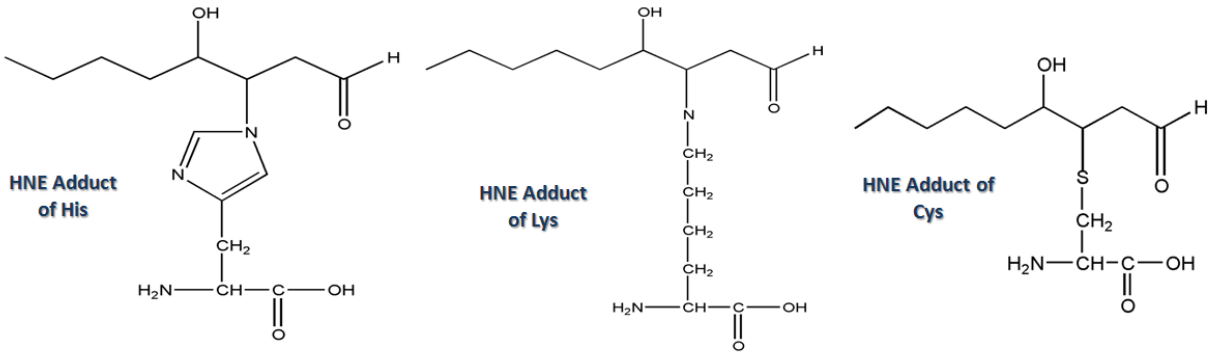

Figure 2.7. A linear depiction of HNE adducts with amino acids, histidine (His), lysine (Lys), and cysteine (Cys). Cyclization does occur in some of these products.

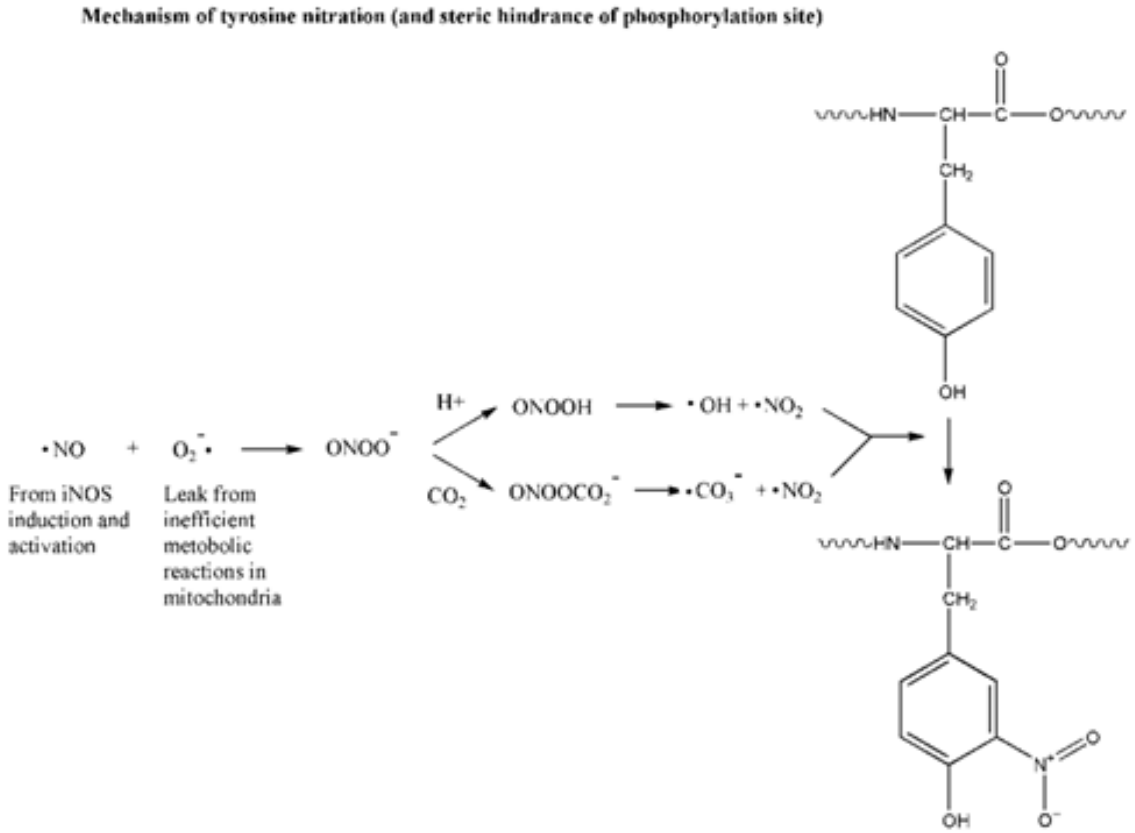

Figure 2.8. Mechanism of tyrosine nitration.

$NO^{\cdot}$ and $O_2^{-\cdot}$ exert more damaging effects together. Nitration of tyrosine occurs from the reaction $NO^{\cdot}$ with $O_2^{-\cdot}$ by radical-radical recombination producing the reactive intermediate peroxynitrite ($ONOO^-$) leading to tyrosine nitration by $^{\cdot}NO_2$ radical at the 3-position sterically blocking tyrosine kinase-mediated phosphorylation site at the 4-position (Figure 2.8). This effect would alter regulation of protein activity leading to changes in protein function (MacMillan-Crow et al. 1998; Amirmansour et al. 1999; Tangpong et al. 2007; Ischiropoulos 2009; Surmeli et al. 2010; Feeney et al. 2012). In addition to $^{\cdot}NO_2$, $^{\cdot}OH$ is another potential breakdown product of $ONOO^-$ (Amirmansour et al. 1999).

MnSOD itself has been shown to be susceptible to tyrosine nitration in the active site of the enzyme (MacMillan-Crow et al. 1998; Tangpong et al. 2007; Tangpong et al. 2008; Surmeli et al. 2010), potentially altering the affinity of MnSOD for the $O_2^{-\cdot}$ substrate by changing the redox potential of the active site (Feeney et al. 2012). Tyrosine nitration leads to damaged MnSOD and subsequent mitochondrial dysfunction (Tangpong et al. 2008; Surmeli et al. 2010). Increases in 3-nitrotyrosine (3NT) and protein-bound HNE have been found even in brain of subjects with early neurodegenerative disorders such as AD (Reed et al. 2009).

2.7.5 Protein carbonyl formation

Protein modification can occur through the formation of protein carbonyl groups, which can be introduced into proteins by direct oxidation of certain amino acid side chains, peptide backbone scission, by Michael addition reactions with alkenal products of lipid peroxidation, or glycooxidation (Berlett et al. 1997; Butterfield et al. 1997; Butterfield et al. 2002). The brain is rich in polyunsaturated fatty acids (PUFA) and has areas rich in iron coupled with high oxygen usage and a relatively low antioxidant capacity, which make the brain particularly susceptible to oxidative damage.

2.7.6 Oxidation of DNA and RNA

Similar to proteins and lipids, nucleic acids are also susceptible to oxidative modification by ROS, RNS (Cooke et al. 2003; Moreira et al. 2008), and by products of lipid peroxidation (Moreira et al. 2008) leading to alterations in replication or translation that lead to mutations or decreased protein synthesis. RNA may be more susceptible to ROS attack due to its closer proximity to mitochondria, RNA are single stranded entities not protected from ROS by hydrogen bonding, (Nunomura et al. 2009) and RNA are not protected by histones like DNA are. RNA oxidation has been detected in neurodegenerative diseases (Lovell et al. 2008).

Copyright © Jeriel T. R. Keeney 2013

CHAPTER 3

MATERIALS AND METHODS

3.1 Plasma Isolation and tissue collection

Plasma is the liquid portion of blood that suspends cells such as red blood cells, white blood cells, and platelets. Plasma is pale-yellow in color and rather viscous. Plasma can be isolated from whole blood by centrifugation at low speeds in the presence of an anticoagulant such as ethylenediaminetetraacetic acid (EDTA). For this research, mouse plasma was obtained by cardiac puncture and blood transferred into tubes containing EDTA. Tubes were inverted ten times to ensure proper mixing with anticoagulant. Blood was centrifuged at 3000 rpm at $4^{o}C$ for 10 minutes to separate blood components. 60 uL plasma was aliquots were placed into pre-labeled microfuge tubes, and immediately frozen in liquid nitrogen until analysis.

Following blood collection, brain from sacrificed animals were extracted, placed in pre-labeled microfuge tubes, and immediately frozen in liquid nitrogen until analysis.

3.2 Bicinchoninic Acid Assay (BCA)

Estimation of protein concentrations used for this dissertation were determined using the bicinchoninic acid (BCA) protein assay (Pierce, Rockford, IL, USA). This assay uses the Biuret reaction, protein-mediated reduction of Cu^{2+} to Cu^{+} by the peptide bond between amino acids. When reduced, Cu^{+} forms a complex with BCA that absorbs at 562 nm. Bovine serum albumin (BSA) was used a protein standard, and a Beer's law standard plot was used to calculate the protein concentration of plasma and brain samples.

3.3 Biological sample preparation

Protein estimation was performed using the bicinchoninic acid (BCA, Pierce) assay. Homogenized brain and plasma samples were diluted according to initial protein estimation results using 20 ug sample in isolation buffer [0.32 M sucrose, 2 mM EDTA, 2mM EGTA, and 20mM HEPES pH 7.4 with protease inhibitors, 0.2 mM PMSF, 20ug/mL trypsin inhibitor, 4 µg/ml leupeptin, 4 µg/ml pepstatin A, and 5 µg/ml aprotinin].

3.4 Slot blot assay

The slot-blot method is used to determine levels of protein carbonyl (PC), 3-nitrotyrosine (3NT) and protein-bound 4-hydroxy-2-transnonenal (HNE) in brain

as previously described [37, 38]. For protein carbonyl determination, samples were derivatized with 2,4-dinitrophenylhydrazine (DNPH) prior to analysis. For HNE and 3NT, samples were solubilized in Laemmli buffer. To standardize the protocol, a consistent amount of protein (250 ng) from each sample is loaded onto a nitrocellulose membrane in respective wells in a slot-blot apparatus (Bio-Rad) under vacuum. Development results in a colored product. Colorimetric intensity reflects of the levels of a specific modification in the sample. This technique requires only a small amount of sample (approximately 1 µg of protein), and a large number of samples can be run simultaneously.

3.5 Detection of oxidatively modified proteins

3.5.1 Protein carbonyl determination

For protein carbonyl determination, samples were derivatized with 2,4-dinitrophenylhydrazine (DNPH) prior to analysis. DNPH reacts with ketones and aldehydes with high specificity to form a Schiff base. Protein bound 2,4-dinitrophenylhydrazones can be detected using an antibody directed at the hydrazone adduct, which can be detected immunochemically or fluorescently. Membranes from slot blot or western blot are blocked in 3% bovine serum albumin (BSA) in PBS with 0.2% (v/v) Tween-20 for 1.5 h and then incubated in primary antibody (anti-dinitrophenylhydrazone primary produced in rabbit, Sigma-Aldrich) for 2 h, washed three times in PBS with 0.2% (v/v) Tween-20 and then

incubated for 1 h with secondary antibody (goat anti-rabbit secondary linked to alkaline phosphatase). Membranes were developed with 5-bromo-4-chloro-3-indolyl-phosphate (BCIP) dipotassium and nitro blue tetrazolium (NBT) chloride in alkaline phosphatase activity (ALP) buffer, dried, and scanned for analysis. Image analysis was performed using Scion Image (Scion Corporation, Frederick, MD).

3.5.2 Protein-bound HNE and 3-nitrotyrosine determination

Membranes from slot blot or western blot are blocked in 3% bovine serum albumin (BSA) in PBS with 0.2% (v/v) Tween-20 for 1.5 h and then incubated in primary antibody (anti-nitrotyrosine or anti-protein-bound HNE produced in rabbit, Sigma-Aldrich) for 2 h, washed three times in PBS with 0.2% (v/v) Tween-20 and then incubated for 1 h with secondary antibody (goat anti-rabbit secondary linked to alkaline phosphatase). Membranes were developed with 5-bromo-4-chloro-3-indolyl-phosphate (BCIP) dipotassium and nitro blue tetrazolium (NBT) chloride in alkaline phosphatase activity (ALP) buffer, dried, and scanned for analysis. Image analysis was performed using Scion Image (Scion Corporation, Frederick, MD). When measuring tyrosine nitration, a negative control for nitration should be performed by reducing nitrotyrosine to aminotyrosine according to the method of Miyagi and Crabb*et al*. (Miyagi et al. 2002) as follows. One replicate membrane is treated with 10 mM sodium

dithionite in 50 mM pyridine-acetate buffer (pH=5.0) for 1h at room temperature, rinsed thoroughly with nanopure water, and developed as above.

3.6 Behavioral testing: Novel object recognition and open field testing

3.6.1 Novel object recognition

Cognitive performance was evaluated using a NOR paradigm (Ennaceur et al. 1988; Schoch et al. 2012). One day prior to treatment, each mouse was acclimated for 1 h to an empty, Plexiglas cage which was dedicated to this mouse for all trials. Immediately thereafter, the mouse was introduced to two identical objects (object A) placed at opposite corners of the cage, and the time spent exploring each object was recorded. Several hours after the initial object exposure, mice were returned to the cage containing the two “familiar” objects (object A) to reinforce object recognition. Throughout the protocol, trial duration was 5 min unless total exploration time was less than 10 s. In this case, the trial was extended to ensure a minimum of 10 s of exploration. A mouse was considered to be exploring when it pointed its nose toward the object at a distance of 2 cm or less. The following morning, baseline memory function was evaluated by replacing one of the familiar objects with a novel object (object B). In the afternoon, mice received injections of MESNA or vehicle and then Dox or vehicle. The morning after injections, the mice were exposed to the original two (familiar) objects (object A) and, after a 4 h interval, one of the familiar objects

was replaced with a novel object (object C). At 3 days after treatment, memory was tested again (novel object D paired with familiar object A). Data are reported as a recognition index (RI), which represents the time spent exploring the novel object as a percentage of total exploration time. All trials were performed by an investigator blinded to treatment conditions.

3.6.2 Motor activity in an open field

Motor activity was tested using an Open Field test (Leibrock et al. 2013). Mice were placed in a 48 x 33cm empty Plexiglas box and videotaped from above for a 5 minute trial (EZVideoDV version 5.51). Trials were performed by an investigator blinded to treatment conditions. Behavioral testing was performed by the K. E. Saatman laboratory, Spinal Cord and Brain Injury Research Center, University of Kentucky.

3.7 Hydrogen magnetic resonance imaging spectroscopy

H^1-MRS (hydrogen magnetic resonance imaging spectroscopy) was used to quantify neurochemical changes in the mouse hippocampus. MRS data was acquired on a 7T BrukerClinscan horizontal bore system (7.0T, 30cm, 300Hz) equipped with a triple-axis gradient system (630 mT/m and 6300 T/m/s). A closed cycle, 14K quadrature cryocoil allowed for a 2.8 signal to noise increase relative to standard coils. The mice were anesthetized with 1.3 % percent isoflurane

using MRI compatible CWE Inc. equipment. Mice were held in place on a Bruker scanning bed with a tooth bar, ear bars and tape. Body temperature and respiration rate were monitored using equipment from SA Instruments Inc. The animals were maintained at 37°C with a water heating system built into the scanning bed. T2 weighted turbo spin echo sequences (TE 40ms, TR 2890ms, Turbo 7, FOV 20mm, 0.156 x 0.156 x 5.0 mm^3) were acquired and used for the placement of the spectroscopy voxel. The scanning procedure took 40 min. A 2x5.5x3mm^3 PRESS spectroscopic voxels (TE 135ms, TR 1500ms, 400avg, CHESS water suppression) was placed to cover both hippocampi. Spectrum analysis was performed using jMRUI (Naressi et al. 2001) to quantify the area under 10 peaks in the spectrum. The creatine peak was used to normalize the choline peak. H^1-MRS scans were performed by Dr. David Powell, Magnetic Resonance Imaging and Spectroscopy Center, University of Kentucky Medical Center.

3.8 Phospholipase C and Phospholipase D Activity Assays

Phosphatidylcholine-specific phospholipase C (PC-PLC) and phospholipase D (PLD) activity assays were performed using manufacturers' instructions provided with the EnzChek® Direct Phospolipase C Assay Kit and Amplex® Red Phospholipase D Assay Kit by Invitrogen/Life Technologies (Carlsbad, CA). Fluorescence intensity for each assay was measured using a SPECTRAFluor Plus instrument and quantified using associated Magellan™ software by TECAN

over a period of 24 h with the kinetic peaks of the positive controls used for comparison.

3.9 Assessment of mitochondrial function

3.9.1 Isolation of Brain Mitochondria

Mice were perfused via cardiac puncture with cold mitochondrial isolation buffer, the brain promptly removed, the cerebellum dissected away, and the mitochondria immediately isolated from the brain by a modification of the method described by Mattiazzi et al. (Mattiazzi et al. 2002). Brain mitochondria were isolated in cold mitochondrial isolation buffer, containing 0.07 M sucrose, 0.22 M mannitol, 20 mM HEPES, 1 mM EGTA, and 1% bovine serum albumin, pH 7.2. Tissues were homogenized with a Dounce homogenizer and centrifuged at 1500 × g at 4°C for 5 min before transferring the supernatants. The pellets were resuspended and centrifuged at 1500 × g at 4°C for 5 min. The supernatants were combined and recentrifuged at 1500 × g at 4°C for 5 min. The supernatants were separated and centrifuged at 13,500 × g at 4°C for 10 min. Non-synaptosomal mitochondrial fraction separation was performed using a 3%/6% (w/v) Ficoll gradient at 4°C prepared before use in 100 mL mitochondrial isolation buffer. Mitochondrial pellets were purified with a 4% Ficoll solution and the mitochondrial pellet was resuspended in 50 µL cold mitochondrial isolation buffer. This method allows rapid isolation of viable mitochondria from brain. Purity testing of resulting mitochondria samples was not performed due to time and

sample volume constraints to ensure mitochondrial viability. There is a tension between time of processing and purity of sample obtained. Thus, the results obtained required a short time to obtain viable mitochondria, but in so doing, the results may be affected by potential interfering contaminants. Protein concentration of isolated mitochondria was determined by the Bradford assay (Bradford 1976).

3.9.2 Bioenergetic analysis in mitochondria

The XF96 Analyzer, Seahorse Bioscience (North Billerica, MA, USA) was used to measure bioenergetic function in mitochondria freshly isolated by differential centrifugation from brain of adult male C57BL6 mice. The XF96 creates a transient 3µl chamber in specialized microplates that allows for the measurement of oxygen consumption rate (OCR) in real time. Respiration by the mitochondria (5 µg/well) was sequentially measured with substrate present (basal respiration) following conversion of ADP to ATP, induced with the addition of oligomycin. Next, maximal uncoupler-stimulated respiration was detected by the administration of the uncoupling agent FCCP. At the end of the experiment, the complex III inhibitor, antimycin A, was applied to completely inhibit mitochondrial respiration. Oxygen Consumption rate were measured four times and plotted as a function of cells, showing the relative contribution of oxygen consumption, ATP-linked oxygen consumption, the maximal OCR after the addition of FCCP, and the reserve capacity of the cells. Seahorse assays were performed by the D.K.

St. Clair laboratory, Graduate Center for Toxicology, Department of Radiation Medicine, Markey Cancer Center, University of Kentucky.

3.10 Superoxide experiments

3.10.1 Solvent selection and potassium superoxide solution preparation

KO_2 is a yellow solid that reacts readily with water and would decompose if exposed to water vapor or carbon dioxide in air. To avoid this situation, a saturated solution of KO_2 was prepared fresh, according to the method previously described (Valentine et al. 1975; McPherson et al. 2002; Miller 2003), in a solvent of anhydrous dimethyl sulfoxide (DMSO) containing 200mM crown ether (18crown6) to aid in solubility. To the prepared solvent, excess KO_2 was added and the KO_2 concentration estimated by UV-vis absorbance and using molecular absorptivity of (Kim et al. 1979; Miller 2003). A saturated solution of KO_2 was approximately 250 µM under the stated conditions. Serial dilutions of this saturated solution were performed using the DMSO+18crown6 solvent to obtain the desired O_2^{-}• concentrations.

3.10.2 Plasma oxidation with potassium superoxide

KO_2 was added to plasma from WT mice and incubated at 37°C for 0, 15, 30, and 90 min according to Table 3.1. Concentrations of 0, 0.1, 1.0, or 10 µM KO_2 were added to plasma to broadly encompass Dox concentrations used in

previous studies. The solvent, DMSO and 18crown6, was added to all control incubations.

Table 3.1. Superoxide protocol volumes. Plasma samples from 2-3 months old WT, male, SKH1 hairless, albino mice (purchased from the Jackson Laboratory) were treated with 0, 0.1, 1.0, or 10 µM KO_2 and incubated for 0, 15, 30, and 90 min.

Tube #	Incubation Time (min)	KO_2 conc to add (uM)	Plasma Volume (uL)	Solvent Vol (uL) (used for KO_2)
1	90	10	48	2
2	90	1.0	48	2
3	90	0.1	48	2
4	30	10	48	2
5	30	1.0	48	2
6	30	0.1	48	2
7	15	10	48	2
8	15	1.0	48	2
9	15	0.1	48	2
10	0	0 (control)	48	2

3.10.3 Macrophage stimulation with potassium superoxide

Cell culture experiments were carried out using mouse BALB/c monocyte macrophage cell line (J774A.1) collected form blood. The mouse macrophage cell line J774A.1 (American Type Culture Collection) was cultured in Dulbecco's modified Eagle's medium supplemented with 10% (v/v) fetal bovine serum, streptomycin (100µg/ml), and penicillin (100U/ml). All cultures were incubated at 37 °C in a humidified atmosphere with 5% CO_2. J774A.1 macrophage cells were plated at a density of 5×10^5 cells/well in 48-well plates. Potassium superoxide (KO_2) was prepared as previously described. Lipopolysaccharide (LPS; 1 µg/ml), KO_2 (0.1µM; 1µM; 10µM) was added and the cells were incubated for 24 h. The supernatant was collected and levels of TNF-α (pg/ml) were determined with a specific ELISA kit for mouse TNF-α (R&D Systems). Macrophage culture experiments were performed by the D.K. St. Clair laboratory, Graduate Center for Toxicology, Department of Radiation Medicine, Markey Cancer Center, University of Kentucky.

<u>Experimental design</u>

J774A.1
J774A.1+ Lipopolysaccharide (LPS) (1 µg/ml) – 24hours incubation
J774A.1+ DMSO+ Crown ether
J774A.1+KO_2 (0 µM) – 24hours incubation
J774A.1+KO_2 (0.1 µM) – 24hours incubation
J774A.1+KO_2 (10 µM) – 24hours incubation

Figure 3.1. Experimental design: macrophage simulation with potassium superoxide. J774.A1 macrophages were seeded onto a 48-well plate at 5×10^5

cells/well and allowed to grow overnight under standard culture conditions. Preincubation of solvent, lipopolysaccharide (LPS; 1 µg/ml), KO_2 (0.1µM; 1µM; 10µM) for 1 h was performed prior to addition to J774.A1 macrophages. Supernatants were collected and analyzed for TNF-α concentration.

3.11 Proteomics (Butterfield et al. 2012)

3.11.1 Isoelectric focusing (IEF)

Aliquots (containing 150ug of protein) of the homogenized cortical samples prepared above were precipitated using cold 100% trichloroacetic acid (TCA) to obtain a concentration of 15% (v/v) TCA in solution and incubated on ice for 15 minutes. Samples were centrifuged at 14,000 rpm for 10 min at 4 °C. The resulting pellets were resuspended and rinsed four times in a cold ethanol: ethyl acetate (1:1 v/v) mixture. After allowing the final pellets to dry completely at room temperature, the pellets were rehydrated for 2 h in rehydration buffer [8 M urea, 2 M thiourea, 50 mM DTT, 2.0% (w/v) CHAPS, 0.2% Biolytes, Bromophenol Blue] then sonicated for 10 s at 20% power. Each entire sample was added to an 11 cm pH 3-10 ReadyStrip™ IPG strip in a lane of the IEF tray. After 45 min of run time, 2 mL of mineral oil were added to each lane to prevent evaporation. Strips were actively rehydrated at 20 °C for 18 h at 50 V, focused at a constant temperature of 20 °C beginning at 300 V for 2 h, 500 V for 2 h, 1000 V for 2 h, 8000 V for 8 h, and finishing at 8000 V for 10 h rapidly. IPG strips were stored at −80 °C until needed for the second dimension of analysis.

3.11.2 Two-dimensional polyacrylamide gel electrophoresis (2D-PAGE)

IEF strips were allowed to come to room temperature (~30 min) and equilibrated for 10 min in the dark in 4 mL equilibration buffer A [50 mMTris–HCl, pH 6.8, 6 M urea, 1% (w/v) SDS, 30% v/v glycerol, 0.5% DTT] and then re-equilibrated for 10 min in the dark in equilibration buffer B [50 mMTris–HCl, pH 6.8, 6 M urea, 1% (w/v) SDS, 30% v/v glycerol, 4.5% IA]. All strips were rinsed in TGS running buffer to remove residual equilibration buffers before being placed onto Criterion precast linear gradient (8–16%) Tris–HCl polyacrylamide gels. Precision Plus Protein™ All Blue Standards and samples were run at a constant voltage of 200 V for 65 min.

3.11.3 SYPRO Ruby® staining

Following 2D-PAGE, gels were incubated in 50 mL fixing solution [7% (v/v) acetic acid, 10% (v/v) methanol] for 20 min at room temperature. SYPRO Ruby® Protein Gel Stain (50-55 mL) was added to gels and allowed to stain overnight at room temperature on a gently rocking platform. The stain was then removed and gels were rinsed with deionized (DI) water and stored in 50 mL DI water in the refrigerator until scanning. Gels were scanned into Adobe Photoshop 6.0 with a Molecular Dynamics STORM phosphoimager ($\lambda_{ex}/\lambda_{em}$: 470/618 nm) and stored in DI water at 4 °C.

3.11.4 Image analysis: differential expression

Spot intensities from SYPRO Ruby®-stained 2D-gel images of cortex samples were quantified according to total spot density using PDQuest software (Bio-RAD, Hercules, CA, USA). Intensities were normalized to total gel densities. Only low or high VitD samples with normalized spot densities that were significantly increased or decreased by at least 1.25 fold from control were considered for mass spectrometry (MS) analysis.

3.11.5 In-gel trypsin digestion

Protein spots identified as significantly altered in VitD deficient rat brain relative to normal VitD controls were excised from 2D-gels with new, sterilized micropipette tips and transferred to Eppendorfmicrocentrifuge tubes. Gel plugs were then washed with 0.1 M ammonium bicarbonate (NH_4HCO_3) at room temperature for 15 min, followed by incubation with 100% acetonitrile at room temperature for 15 min. Solvent was removed, and gel plugs were dried in their respective tubes in a biosafety cabinet at room temperature. Gel plugs were incubated for 45 min in 20 µl of 20 mM DTT in 0.1 M NH_4HCO_3 at 56 °C. The DTT solution was then removed and replaced with 20 µl of 55 mM IA in 0.1 M NH_4HCO_3 and incubated with gentle agitation at room temperature in the dark for 30 min. Excess IA solution was removed, and the gel plugs were incubated for

15 min with 200 µl of 50 mM NH_4HCO_3 at room temperature. 200 µL of 100% acetonitrile was added to this solution in each tube and incubated for 15 min at room temperature. All solvent was removed, and gel plugs were allowed to dry for 30 min at room temperature in a biosafety cabinet. Gel plugs were rehydrated with 20 ng/µL of modified trypsin (Promega, Madison, WI, USA) in 50 mM NH_4HCO_3 in a shaking incubator overnight at 37 °C. Enough trypsin solution was added in order to completely submerge the gel plugs (approximately 10uL).

3.11.6 Mass spectrometry

Salts and other contaminants were removed from tryptic digest solutions using C18 ZipTips (Sigma-Aldrich, St. Louis, MO, USA), reconstituted to a volume of approximately15 µl in a 50:50 DIwater:acetonitrile solution containing 0.1% formic acid. Tryptic peptides were analyzed with an automated Nanomate electrospray ionization (ESI) [Advion Biosciences, Ithaca, NY, USA] Orbitrap XL MS (ThermoScientific, Waltham, MA, USA) platform. The Orbitrap MS was operated in a data-dependent mode whereby the eight most intense parent ions measured in the Fourier Transform (FT) at 60,000 resolution were selected for ion trap fragmentation with the following conditions: injection time 50 ms, 35% collision energy, MS/MS spectra were measured in the FT at 7500 resolution, and dynamic exclusion was set for 120 s. Each sample was acquired for a total of approximately 2.5 min. MS/MS spectra were searched against the International Protein Index (IPI) database using SEQUEST and the following

parameters: two trypsin miscleavages, fixed carbamidomethyl modification, variable Methionine oxidation, parent tolerance 10 ppm, and fragment tolerance of 25 mmu or 0.01 Da. Results were filtered with the following criteria: Xcorr>1.5, 2.0, 2.5, 3.0 for +1, +2, +3, and +4 charge states, respectively, Delta CN>0.1, and *P*-value (protein and peptide) <0.01. IPI accession numbers were cross-correlated with SwissProt accession numbers for final protein identification (Robinson et al. 2011).

3.11.7 Database search and peptide identification

Results from the mass spectrum are compared to theoretical protein spectra in a database. The research in this dissertation was performed using the SEQUEST database. From the mass spectrum, exact peptide masses of the digested protein are compared with theoretical peptide masses in the database, producing a list of potential peptide matches. The database contains theoretical MS/MS spectra of the peptides with masses similar to the unidentified peptide. By subjecting the unidentified peptide to MS/MS, a fragmentation spectrum is generated. Using cross correlation analysis, the overlap in fragmentation patterns between the unidentified peptide and the database spectra of possible matches is compared. Proteins receive scores based on the quality of overlap. From these data, protein identification is made based on uniqueness of identity and probability of match with theoretical spectra.

3.11.8 One-dimensional polyacrylamide gel electrophoresis

Sample homogenates were incubated in sample buffer (0.5 M Tris (pH 6.8), 40% glycerol, 8% sodium dodecyl sulfate (SDS), 20% β-mercaptoethanol, and 0.01% bromophenol) for 5 min in a water bath at 95°C and loaded onto precast Criterion TGX (4-15%) or Criterion XT (12% Bis-Tris) Precast Gels as appropriate for the molecular weight of the protein of interest. Precision Plus Protein™ All Blue Standards and samples were run at 80 V for 15 min, increasing the voltage to 120 V and run for 90 min in TGS or MES running buffer as appropriate for the gel.

3.11.9 Western Blotting

In-gel proteins were transferred to a nitrocellulose membrane (0.45 μm) using a Trans-Blot® Turbo™ Blotting system at 25 V for 30 min (BioRAD, Hercules, CA, USA). After transfer, membranes were incubated in blocking solution [3% BSA in phosphate buffer (PBS) solution with 0.2% (v/v) Tween 20] at room temperature for 1.5 h.Membranes were then incubated with rabbit anti-inducible nitric oxide synthase (iNOS) antibody (Calbiochem/Millipore, Billerica, MA) or rabbit anti-NF-κB (p65) antibody (Enzo, Farmingdale, NY) for 2 h on a gentle rocking platform, followed by three rinses for 5 min each with PBS solution with 0.2% (v/v) Tween 20. Blots were then incubated for 1 h with ECL anti-rabbit IgG, horseradish peroxidase-linked whole antibody. The resulting blots were rinsed three times for

5, 10, and 10 min each in PBS solution with 0.2% (v/v) Tween 20 and signals were detected using Clarity™ Western ECL Substrate (BioRAD) and the ChemiDoc™MP Imaging System (BioRAD).Blots were stripped using Re-blot Plus Strong Solution (Millipore, Billerica, MA, USA) according to package instructions and re-probed with mouse anti-actin antibody (Sigma-Aldrich, St. Louis, MO) or mouse anti-histone H2B antibody (Chemicon, Temecula, CA) for normalization. Analysis was performed using the ImageLab software (BioRAD).

Copyright © Jeriel T. R. Keeney 2013

Chapter 4

Doxorubicin-induced elevated oxidative stress in brain and cognitive decline: protection by MESNA and insights into mechanisms of chemotherapy-induced cognitive impairment ("chemobrain").

4.1 Overview of Study

Chemotherapy-induced cognitive impairment (CICI) is now widely recognized as a real and too common complication of cancer chemotherapy experienced by an ever growing number of cancer survivors. Previously, we reported that Doxorubicin (Dox), a prototypical reactive oxygen species (ROS)-producing anti-cancer drug, results in oxidation of plasma proteins, including apolipoprotein A-I (ApoA-I) leading to tumor necrosis factor-alpha (TNF-α)-mediated oxidative stress in plasma and brain. We also reported that co-administration of the antioxidant drug, 2-mercaptoethane sulfonate sodium (MESNA), prevents Dox-induced protein oxidation and subsequent TNF-α elevation in plasma. In this study, we measured oxidative stress in both brain and plasma of Dox-treated mice both with and without MESNA. MESNA ameliorated Dox-induced oxidative protein damage in plasma, confirming our prior studies, and in a new finding led to decreased oxidative stress in brain. This study also provides further functional

and biochemical evidence of the mechanisms of CICI. Using novel object recognition (NOR), we demonstrated the Dox administration resulted in memory deficits, effects that were rescued by MESNA. Using hydrogen magnetic resonance imaging spectroscopy (H^1-MRS) techniques, we demonstrated that Dox administration led to a dramatic decrease in choline(phosphocholine)/creatine ratios in the hippocampus in mice. To better elucidate a potential mechanism for this MRS observation, we tested the activities of the phospholipase enzymes known to act on phosphatidylcholine (PtdCho), a key component of phospholipid membranes and a source of choline for the neurotransmitter, acetylcholine (ACh). The activities of both phosphatidylcholine-specific phospholipase C (PC-PLC) and phospholipase D were severely diminished following Dox administration. The activity of PC-PLC was preserved when MESNA was co-administered with Dox; however, PLD activity was not protected. This study is the first to demonstrate the protective effects of MESNA on Dox-related protein oxidation, cognitive decline, phosphocholine levels, and PC-PLC activity in the brain.

4.2 Introduction

Chemotherapy-induced cognitive impairment (CICI), termed “chemobrain” by patients, is increasingly recognized as a real complication of cancer chemotherapy (Tannock et al. 2004; Ahles et al. 2007; Foley et al. 2008; Konat et al. 2008; Aluise et al. 2010; Cheng et al. 2013; Seigers et al. 2013). CICI consists

of impairments in various aspects of memory and executive function (McDonald et al. 2013; Simo et al. 2013). Despite the increased attention this issue has garnered from the clinical and research communities, the mechanisms of the resulting cognitive impairment are still poorly understood but is thought to include peripheral toxic effects caused by the chemotherapy drugs leading to downstream structural and functional changes in the brain including neuroinflammatory consequences and even changes in neurotransmitter levels and function (Saykin et al. 2003; Joshi et al. 2010; Aluise et al. 2011; Raffa 2011). Reasons for the failure to address the problem may include the complexity of cancer and its treatments, especially by agents that do not cross the blood-brain barrier (BBB). Moreover, a hitherto lack of a scientific explanation for cognitive consequences of chemotherapy has hampered progress. A better understanding of the underlying mechanisms by which CICI occurs is necessary to allow cancer survivors to have a better quality of life by protecting non-targeted tissues against undesired toxicities of the anticancer drugs.

In the present studies, we used doxorubicin (Dox) as a representative chemotherapeutic agent known to produce reactive species (Handa et al. 1975; Gutteridge 1984; Cummings et al. 1991). Dox is an anthracycline antineoplastic agent commonly used in multidrug chemotherapy regimens primarily to treat solid tumors and leukemias. The cancer killing effects of Dox have been shown to involve three proposed mechanisms: DNA intercalation, inhibition of topoisomerase II, and production of ROS (Bachur et al. 1977; Chuang et al.

1979; Reich et al. 1979; Tanaka et al. 1980; Cummings et al. 1991; Fornari et al. 1994; Deres et al. 2005). The quinone moiety present in the Dox structure is capable of undergoing a one-electron reduction to the semi-quinone (Chen et al. 2007; Aluise et al. 2011). Through the redox cycling of this structure back to the quinone, *in vivo*, the reactive O_2^{-}• is produced from molecular oxygen. In addition, previous studies by our laboratories demonstrated that even though neither Dox nor its primary metabolite crosses the blood-brain barrier (BBB), peripheral Dox treatment does cause brain injury as evidenced by increased oxidative stress, the inflammatory cytokine, tumor necrosis factor-alpha (TNF-α), and mitochondrial dysfunction (Tangpong et al. 2006; Joshi et al. 2007; Tangpong et al. 2007; Tangpong et al. 2008).

Our laboratory and others previously demonstrated Dox-induced oxidative stress in blood and damage to plasma proteins leading to detrimental central nervous system consequences (Thayer 1988; Fadillioglu et al. 2003; Tangpong et al. 2006; Othman et al. 2008; Aluise et al. 2009; Aluise et al. 2011). Central to this paradigm is apolipoprotein A-I (ApoA-I) (Aluise et al. 2010; Aluise et al. 2011; Perluigi et al. 2011; Keeney et al. 2013). ApoA-I promotes cholesterol efflux as part of the high density lipoprotein (HDL) complex. Additionally, ApoA-I has been shown to suppress TNF-α in plasma (Hyka et al. 2001; Perry et al. 2002; Weber et al. 2011). Previous studies in our laboratory have shown that, when oxidized, ApoA-1 loses this ability to suppress TNF-α release and may exacerbate the problem (Aluise et al. 2011).

However, our group has also demonstrated that ApoA-I oxidation and subsequent increased TNF-α release is suppressed with co-administration of the drug MESNA (2-mercaptoethane sulfonate sodium) (Aluise et al. 2011). The structure of MESNA contains a free sulfhydryl group imparting much of its antioxidant properties by affording it the ability to scavenge free radicals and reactive aldehydes such as HNE and acrolein. MESNA is FDA approved for prevention of hemorrhagic cystitis and routinely used with Dox as part of multidrug chemotherapy regimens that include ifosfamide or cyclophosphamide. MESNA does not enter cells, does not interfere with cancer chemotherapy (Bernacki et al. 1987), and blocks protein oxidation, including ApoA-I, in the plasma (Aluise et al. 2011). Modulating the location and production of chemotherapy-induced production of ROS may be paramount in decreasing the unwanted toxicities associated with chemotherapy while enhancing the cancer-killing effects (Fang et al. 2009).

The current study was undertaken to test the hypothesis that MESNA would block Dox-induced, TNF-α-mediated markers of brain damage, indexed by changes in oxidative stress and magnetic resonance spectroscopy (MRS) spectra in brain, with consequent improved cognition.

4.3 Materials and methods

4.3.1 Chemicals

Precision Plus Protein™ All Blue Standards, BCA reagents, and nitrocellulose membranes were purchased from Bio-RAD (Hercules, CA, USA). EnzChek® Direct Phospolipase C Assay Kit and Amplex® Red Phospholipase D Assay Kit were purchased from Invitrogen/Life Technologies (Carlsbad, CA). Chemicals, proteases, protease inhibitors, and antibodies used in this study were purchased from Sigma-Aldrich (St. Louis, MO, USA) unless otherwise noted.

4.3.2 Statistical analysis

All data are presented as mean±SEM, and statistical analyses were performed using ANOVA with Bonferroni's Multiple Comparison Test followed by a two-tailed Student's *t*-test to make individual comparisons where relevant, with $p<0.05$ considered significant. The D'Agostino & Pearson omnibus normality test was used where appropriate.

4.3.3 Animals

Mice used in this study were the F1 progeny of C57BL/6 x C3H hybrids (B6C3) purchased from the Jackson Laboratory. B6C3 hybrids are more robust and tolerated the Dox dose better than inbred C57BL/6. Male B6C3 mice (2-3 months old), each weighing approximately 30 grams were kept under standard conditions housed in the University of Kentucky Animal Facility, and all experimental procedures were approved by the Institutional Animal Care and Use Committee of the University of Kentucky. Doxorubicin HCl was purchased from Bedford Laboratories™, and MESNA was purchased from Baxter Healthcare Corporation. Mice were injected using a single intraperitoneal (i.p.) dose of 25 mg/kg Dox or the same volume of saline as a control (Yen et al. 1996; Desai et al. 2013). MESNA was administered at 160 mg/kg i.p. 15 min before Dox as well as 3 h and 6 h after Dox. Animals tested using MRS were scanned 72 h post-treatment. Following MRS or novel object recognition (NOR) studies, these animals were euthanized and blood and tissues collected for molecular or biochemical analysis.

4.3.4 Behavioral testing: Novel object recognition and open field testing

4.3.4.1 Novel object recognition

Cognitive performance was evaluated using a NOR paradigm (Ennaceur et al. 1988; Schoch et al. 2012). One day prior to treatment, each mouse was acclimated for 1 h to an empty, Plexiglas cage which was dedicated to this mouse for all trials. Immediately thereafter, the mouse was introduced to two identical objects (object A) placed at opposite corners of the cage, and the time spent exploring each object was recorded. Several hours after the initial object exposure, mice were returned to the cage containing the two “familiar” objects (object A) to reinforce object recognition. Throughout the protocol, trial duration was 5 min unless total exploration time was less than 10 s. In this case, the trial was extended to ensure a minimum of 10 s of exploration. A mouse was considered to be exploring when it pointed its nose toward the object at a distance of 2 cm or less. The following morning, baseline memory function was evaluated by replacing one of the familiar objects with a novel object (object B). In the afternoon, mice received injections of MESNA or vehicle and then Dox or vehicle. The morning after injections, the mice were exposed to the original two (familiar) objects (object A) and, after a 4 h interval, one of the familiar objects was replaced with a novel object (object C). At 3 days after treatment, memory was tested again (novel object D paired with familiar object A). Data are reported as a recognition index (RI), which represents the time spent exploring the novel object as a percentage of total exploration time. All trials were performed by an investigator blinded to treatment conditions.

4.3.4.2 Motor activity in an open field

At 1 and 3 days after treatment, motor activity was tested using an Open Field test (Leibrock et al. 2013). Mice were placed in a 48 x 33cm empty Plexiglas box and videotaped from above for a 5 minute trial (EZVideoDV version 5.51). Trials were performed by an investigator blinded to treatment conditions. Behavioral testing was performed by the K. E. Saatman laboratory, Spinal Cord and Brain Injury Research Center, University of Kentucky.

4.3.5 Hydrogen magnetic resonance imaging spectroscopy

H^1-MRS (hydrogen magnetic resonance imaging spectroscopy) was used to quantify neurochemical changes in the mouse hippocampus. MRS data was acquired on a 7T BrukerClinscan horizontal bore system (7.0T, 30cm, 300Hz) equipped with a triple-axis gradient system (630 mT/m and 6300 T/m/s). A closed cycle, 14K quadrature cryocoil allowed for a 2.8 signal to noise increase relative to standard coils.

The mice were anesthetized with 1.3 % percent isoflurane using MRI compatible CWE Inc. equipment. Mice were held in place on a Bruker scanning bed with a tooth bar, ear bars and tape. Body temperature and respiration rate were monitored using equipment from SA Instruments Inc. The animals were maintained at 37°C with a water heating system built into the scanning bed. T2

weighted turbo spin echo sequences (TE 40ms, TR 2890ms, Turbo 7, FOV 20mm, 0.156 x 0.156 x 5.0 mm^3) were acquired and used for the placement of the spectroscopy voxel. The scanning procedure took 40 min. A 2x5.5x3mm^3 PRESS spectroscopic voxels (TE 135ms, TR 1500ms, 400avg, CHESS water suppression) was placed to cover both hippocampi. Spectrum analysis was performed using jMRUI (Naressi et al. 2001) to quantify the area under 10 peaks in the spectrum. The creatine peak was used to normalize the choline peak. H^1-MRS scans were performed by Dr. David Powell, Magnetic Resonance Imaging and Spectroscopy Center, University of Kentucky Medical Center.

4.3.6 Sample preparation

Protein estimation was performed using the bicinchoninic acid (BCA, Pierce) assay. Homogenized brain and plasma samples were diluted according to initial protein estimation results using 20 ug sample in isolation buffer [0.32 M sucrose, 2 mM EDTA, 2mM EGTA, and 20mM HEPES pH 7.4 with protease inhibitors, 0.2 mM PMSF, 20ug/mL trypsin inhibitor, 4 µg/ml leupeptin, 4 µg/ml pepstatin A, and 5 µg/ml aprotinin].

4.3.7 Slot blot assay

The slot-blot method was used to determine levels of protein carbonyl and HNE in brain as previously described [37, 38]. For protein carbonyl determination,

samples were derivatized with 2,4-dinitrophenylhydrazine (DNPH). For HNE, samples were solubilized in Laemmli buffer. Protein (250 ng) from each sample was loaded onto a nitrocellulose membrane in respective wells in a slot-blot apparatus (Bio-Rad) under vacuum. Membranes were blocked in 3% bovine serum albumin (BSA) in PBS with 0.2% (v/v) Tween-20 for 1.5 h and then incubated in primary antibody (anti-dinitrophenylhydrazone primary or anti-protein-bound HNE, respectively, each produced in rabbit, Sigma-Aldrich) for 2 h, washed three times in PBS with 0.2% (v/v) Tween-20 and then incubated for 1 h with secondary antibody (goat anti-rabbit secondary linked to alkaline phosphatase). Membranes were developed with 5-bromo-4-chloro-3-indolyl-phosphate (BCIP) dipotassium and nitro blue tetrazolium (NBT) chloride in alkaline phosphatase activity (ALP) buffer, dried, and scanned for analysis. Image analysis was performed using Scion Image (Scion Corporation, Frederick, MD).

4.3.9 Phospholipase C and Phospholipase D Activity Assays

Phosphatidylcholine-specific phospholipase C (PC-PLC) and phospholipase D (PLD) activity assays were performed using manufacturers' instructions provided with the EnzChek® Direct Phospolipase C Assay Kit and Amplex® Red Phospholipase D Assay Kit by Invitrogen/Life Technologies (Carlsbad, CA). Fluorescence intensity for each assay was measured using a SPECTRAFluor Plus instrument and quantified using associated Magellan™ software by TECAN

over a period of 24 h with the kinetic peaks of the positive controls used for comparison.

4.4 Results

4.4.1 Dox administration results in increases in oxidative stress markers in brain and plasma

We previously showed that, despite its inability to cross the BBB, peripheral Dox administration leads to increased levels of TNF-α and oxidative stress in brain (Joshi et al. 2005; Tangpong et al. 2006; Joshi et al. 2007; Joshi et al. 2010; Aluise et al. 2011). Here, we tested for indicators of oxidative stress in brain and plasma of animals used in this study. Test subjects were administered either saline, MESNA, Dox, or Dox plus MESNA. Brain and blood samples were collected at approximately 72 h post-Dox treatment, immediately following cognitive or MRS studies.

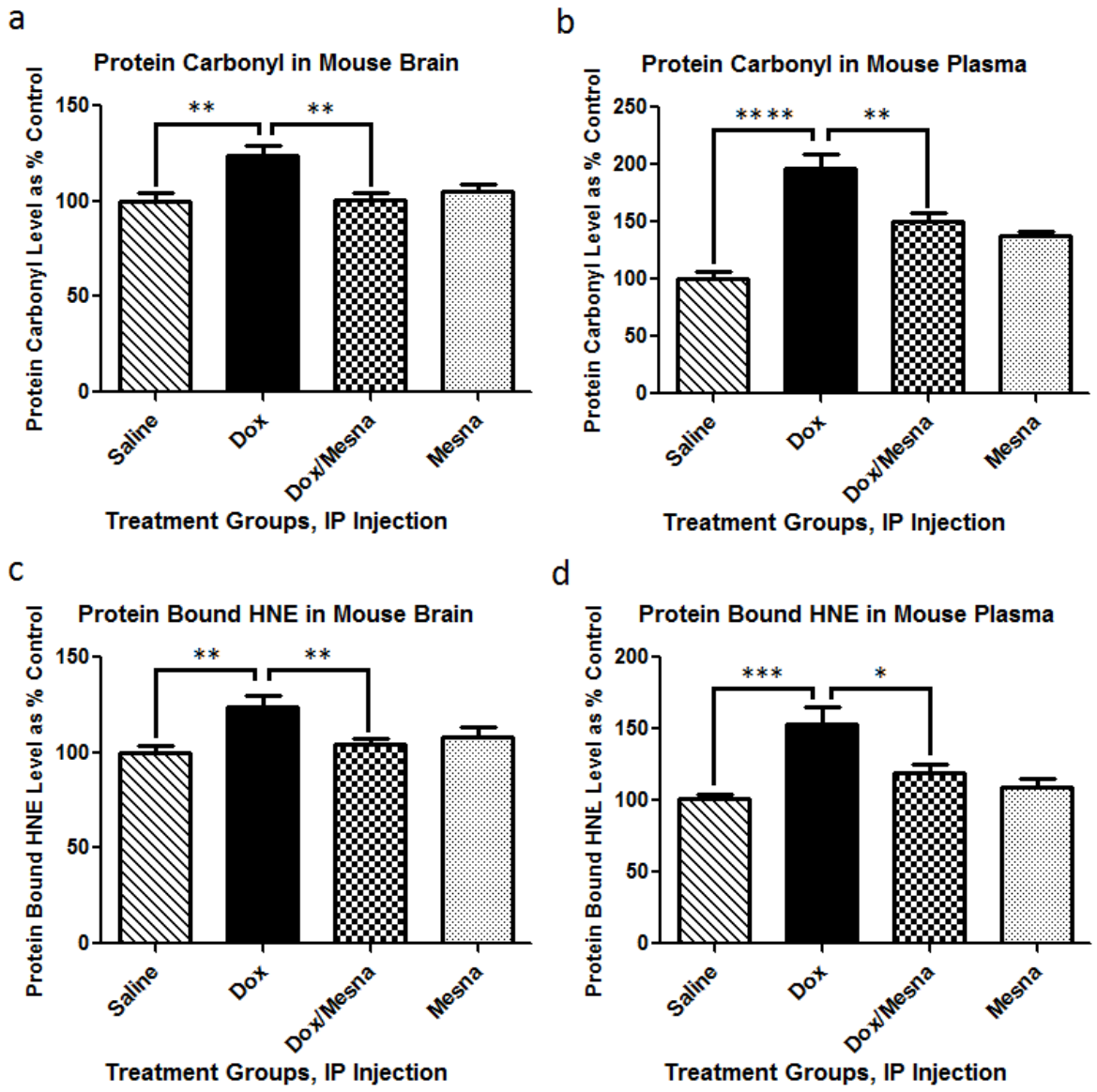

Figure 4.1. PC and protein-bound HNE levels in brain and plasma following Dox and MESNA treatments. Levels of protein carbonyl (PC) and protein-bound HNE are indicators of protein oxidation and lipid peroxidation respectively. Graphs a-d depict protein carbonyl and protein-bound HNE in brain and plasma of 2-3 month old, male B6C3 mice treated with saline, MESNA, Dox, or Dox with MESNA. Protein carbonyl levels were significantly increased in brain (a) and

plasma (b) of mice treated with Dox relative to saline. (In brain, the MESNA alone group did show slight but significant elevation in PC compared to saline.) MESNA, co-administered with Dox, ameliorated Dox-induced increases in PC in both brain and plasma. Protein-bound HNE levels were significantly elevated in brain and plasma of mice treated with Dox relative to saline. MESNA, co-administered with Dox, significantly suppressed Dox-induced elevation in protein-bound HNE in both brain and plasma. (n = 10 - 13 per treatment group; *$p<0.05$, **$p<0.005$, ***$p<0.001$, ****$p<0.001$).

Protein carbonyl levels and protein-bound HNE were used as a gauge of damage to proteins and lipids, respectively. Significantly higher levels of protein carbonyls and protein-bound HNE in brain of Dox-treated animals compared to saline-treated controls were observed ($p<0.005$, Figure 4.1a and $p<0.005$, Figure 4.1c, respectively). MESNA protected the brain from these oxidative damages ($p<0.005$, $p<0.005$). Plasma results revealed similarly increased protein carbonyl and protein-bound HNE levels in Dox vs. saline treated animals ($p<0.0001$, Figure 4.1b and $p<0.001$, Figure 4.1d, respectively). Both effects were ameliorated when MESNA was administered with Dox ($p<0.005$, $p<0.05$). These results are consistent with our previous findings in plasma (Aluise et al. 2011) and brain (Joshi et al. 2007; Joshi et al. 2010). These findings also provide further support that Dox induces oxidative stress in the plasma and brain, consistent with subsequent cognitive deficits and the notion that concomitant

MESNA administration may be able to reduce or prevent these consequences in brain.

4.4.2 Dox administration results in cognitive impairment

Behavior studies were performed by the K.E. Saatman laboratory. In order to determine the cognitive consequences of Dox-induced oxidative stress in brain and the potential for MESNA to protect brain function, NOR was performed on animals in each of the previously mentioned treatment groups (Figure 4.2a). NOR provides a measure of cognitive function in rodent models by assessing the preference for investigating a novel object in a familiar environment. Preference for the novel object indicates memory of a familiar object through the animal's natural propensity to explore an unfamiliar object.

Novelty recognition is thought to require complex cognitive function (Bevins et al. 2006; Antunes et al. 2012). NOR employs the executive function of the frontal cortex, which is thought to be a key brain region affected in CICI ("chemobrain"). Open field testing was employed as a measure of locomotor activity (Figure 4.2b).

Prior to treatment, animals spent an average of approximately 70% of total exploration time investigating a novel object with no difference among the treatment groups. The day after treatment, each subject was re-acclimated to the

environment containing the two original familiar objects followed by exposure to one familiar and one novel object. The RI used in these studies is a ratio of time spent exploring the novel object to total time spent exploring either object. (i.e., a RI of 70 means that 70% of the total object exploration time was spent exploring the novel object, while a RI of 50 means there was no preference of the novel object over the familiar one.) One day after treatment, there was no statistically significant difference among groups. However, Dox treated groups appeared to have slightly lower RI at 24 h.

At 72 h post-treatment, the saline and MESNA treatment groups maintained an average RI of approximately 70, similar to previous performance. Meanwhile, RI was significantly decreased in the Dox treatment group, which exhibited a mean RI of below 50 (approximately 40) suggesting a preference for the familiar over the novel object. This loss of the natural preference for novelty supplanted by a preference for the familiar has been seen in rodent models with perirhinal cortex lesions (Mumby et al. 2002). Processes involved in recognition memory may be deleteriously affected. A preference for the familiar may be due to incomplete encoding of the familiar stimulus or a discrepancy between the memory of the familiar object and the actual perception of the same object (Ennaceur 2010). Another plausible explanation is that the natural bias for novelty may have been eliminated or at least altered (Mumby 2001; Ennaceur 2010). Additionally, anxiety resulting from Dox treatment could be a possible reason for the RI being lower than 50 in these animals. The RI of Dox treated group at 72 h post-Dox

was significantly lower than the 72 h saline treated group ($p<0.001$) and significantly lower than the same group's performance at the 24 h post-Dox mark ($p<0.05$). At 72 h post-treatment, the group that received MESNA with Dox had a mean RI of approximately 60, significantly higher than the Dox-treated group ($p<0.01$), indicating a protection of memory function though not a full return to the RI of the 72 h saline-treated group.

Dox treatment was associated with a delayed decline in locomotor activity (Figure 4.2b). Both the Dox and Dox with MESNA groups exhibited a small, but non-significant, decrease in movement time at 24 h after treatment. However, at 72 h, Dox-induced decline in motor activity was clearly evident in both groups receiving Dox (Figure 4.2b; Dox $p<0.05$ and Dox+MESNA $p<0.005$ compared to their respective controls at 72 h; 72 h Dox $p<0.0001$ and 72 h Dox+MESNA $p<0.0001$ compared to 24 h). MESNA treatment did not alleviate this decrease in spontaneous locomotion. The similar decrease in total locomotor activity of the Dox and Dox with MESNA groups (Figure 4.2b) removes a potential cofounding variable when comparing cognitive function results between these two groups.

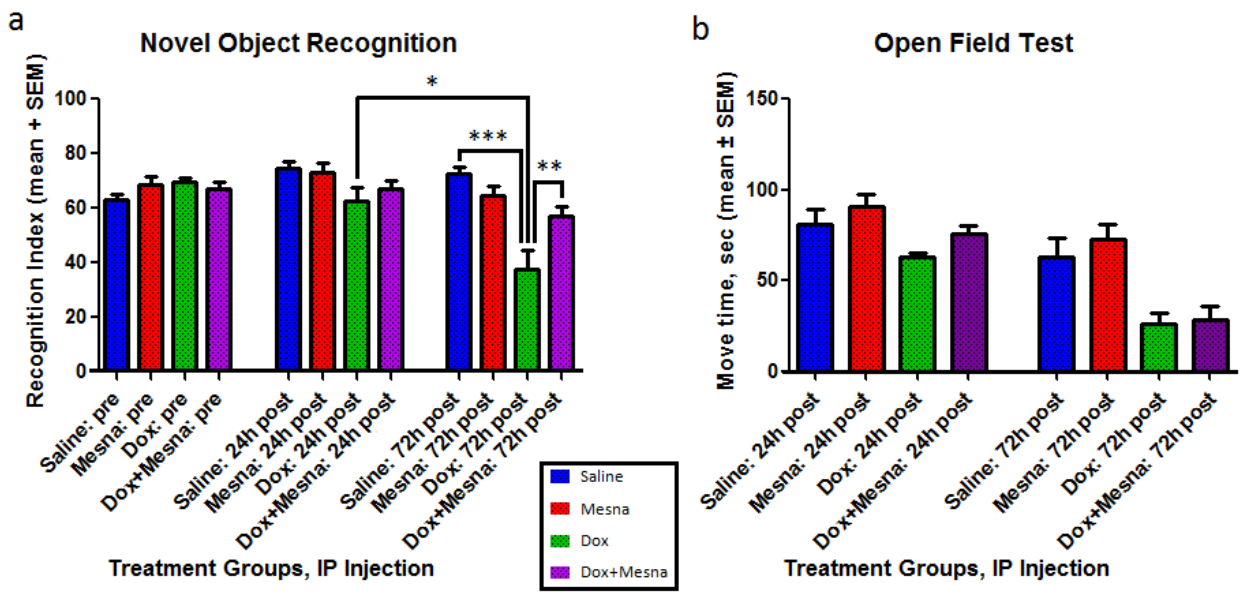

Figure 4.2. Behavior testing following Dox and MESNA administration. Behavior testing for male B6C3 mice treated with saline, MESNA, Dox, or Dox+MESNA. (n = 7 – 8 per group; Data is presented as mean±SEM.) (a) Novel Object Recognition (NOR) testing provides a measure of cognitive function through recognition memory. At 72 h post-treatment, the Dox group performed at a significantly lower RI ($p<0.001$, Dox vs. saline, and $p<0.05$, Dox-24 h vs. Dox-72 h). MESNA given with Dox rescued this measure of cognitive function ($p<0.01$, Dox+MESNA vs. Dox) though not fully to the level of the saline-treated group. (b) Open Field Testing was used to provide a comparison of average total locomotor activity among groups. Both the Dox and Dox+MESNA groups showed decreased average total movement 72 h post-treatment compared to their corresponding 24 h post-Dox levels and to the 72 h saline and MESNA groups. (*$p<0.05$, **$p<0.01$, ***$p<0.001$, ****$p<0.001$). Behavior studies were performed by the K.E. Saatman laboratory.

4.4.3 Dox administration results in changes to the neurochemical profile in the hippocampus determined by MRS

The involvement of the hippocampus in learning and memory (Sarkisyan et al. 2009; Clarke et al. 2010; Goulart et al. 2010; Antunes et al. 2012; Meck et al. 2013) led us to pursue MRS scans of the hippocampus in our murine chemotherapy treatment groups. H^1-MRS non-invasively measures neurochemical aspects of the living brain. The peaks observed in this spectrum (Figure 4.3a) include N-acetylaspartate (NAA), Choline (Cho)-containing compounds, creatine (Cr), myo-inositol, glutamate and glutamine, lipids, and lactate allowing quantification of these and other metabolites in the living brain (Jansen et al. 2006). Quantification is generally achieved using ratios to other species, commonly to Cr.

Unilateral and bilateral hippocampal H^1-MRS showed a slight, but significant, decrease in the NAA/Cr ratio in the Dox treated group compared to saline controls (*$p<0.05$, Figure 4.3b). A decrease in NAA/Cr is indicative of decreased neuronal integrity. Strikingly, MRS scans revealed, on average, a much larger six standard-deviation decrease in the choline/creatine (Cho/Cre) ratio in Dox-treated mice compared to saline-treated mice (***$p<0.0001$, Figure 4.3c). Though not significant, a slight increase in the Cho/Cr to peak was seen in the Dox+MESNA group compared to Dox alone (Figure 4.3d). This result suggests

that MESNA may be protecting cognition by a different mechanism other than restoration of the Cho/Cr ratio. Phosphocholine and glycerophosphorylcholine are the major contributors to the choline peak, while Cho itself is a smaller contributor.

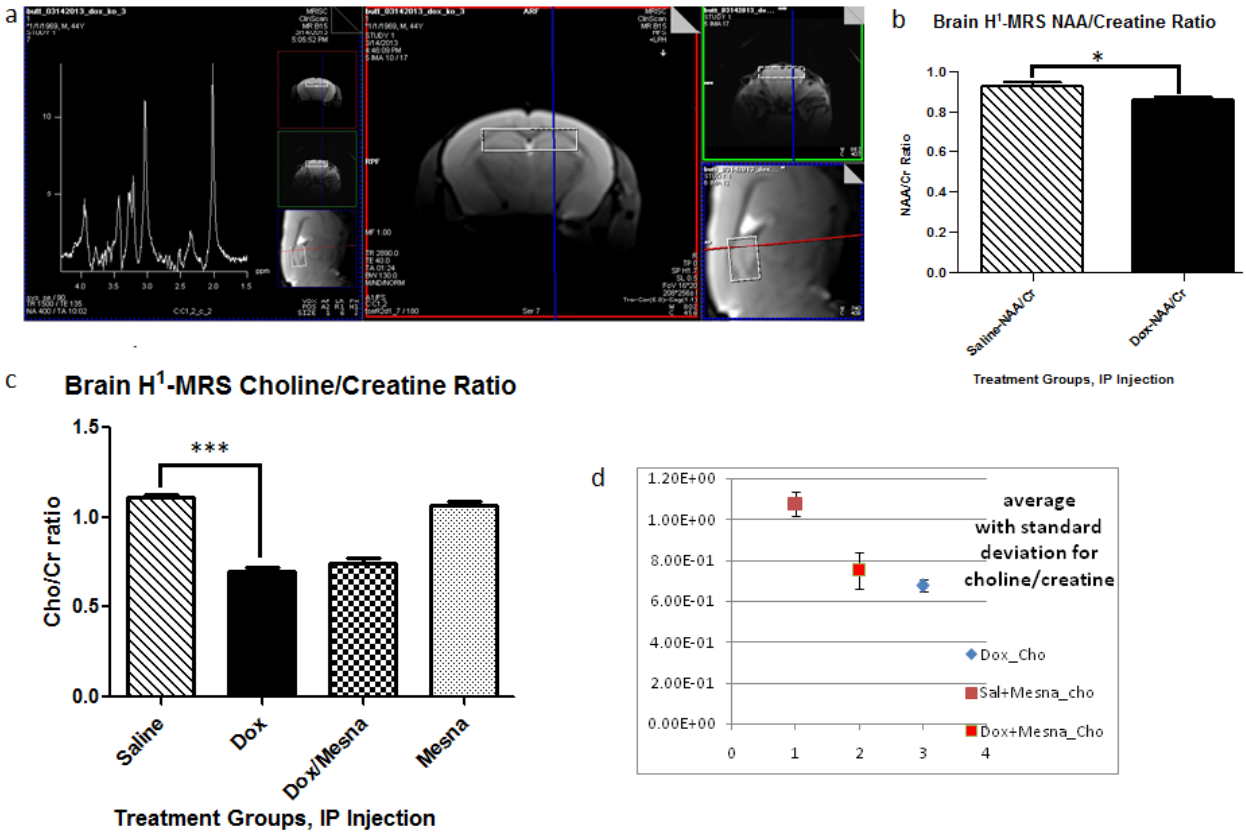

Figure 4.3. H1-MRS of mouse hippocampus after Dox and MESNA treatment. (a) H^1-MRS uses proton signatures from hydrogen in much the same way as NMR to create two-dimensional images of the tissue (right) and a spectrum of peaks reflecting a neurochemical profile that includes NAA, Cho, Cr, and others (left). (b) Bilateral H^1-MRS scans of mouse hippocampus revealed a

slight but statistically significant decrease in the NAA/Cr ratio (*$p<0.05$) and (c) a six standard deviation decrease in the Cho/Cr ratio in the Dox-treated group compared to saline control (***$p<0.0001$). (d) Co-administration of MESNA with Dox resulted in a trend toward rebound in Cho/Cr compared to Dox alone. Greater variability was seen in Cho/Cr in the Dox+MESNA group. H^1-MRS scans were performed by Dr. David Powell, Magnetic Resonance Imaging and Spectroscopy Center, University of Kentucky Medical Center.

4.4.4 Dox administration results in decreased PC-PLC and PLD activity

To gain insight into a possible mechanism for the MRS-indexed changes in the choline-containing compounds, the activities of phospholipase enzymes known to act on phosphatidylcholine (PtdCho), a major source of Cho and phosphocholine (PCho) in the brain were tested. Phosphatidylcholine-specific phospholipase C (PC-PLC) cleaves PtdCho at the glycerol-phosphate bond producing the second messenger, diacylglycerol (DAG), and phosphocholine. Phospholipase D (PLD), located in the plasma membrane, cleaves the headgroup from phospholipids thereby releasing soluble choline from PtdCho into the cytosol leaving phosphatidic acid. Activity of both PC-PLC and PLD in brain were severely impaired at 72 h following Dox administration ($p<0.01$ and $p<0.01$, respectively; Figure 4.4) providing a possible explanation for the dramatic decrease seen in the choline-containing peaks (as measured by MRS Cho/Cr ratio). MESNA, co-administered with Dox, completely rescued PC-PLC activity back to the activity

observed in the saline-treated group. However, adding MESNA to the treatment regimen with Dox did not prevent the Dox-related decrease in PLD activity.

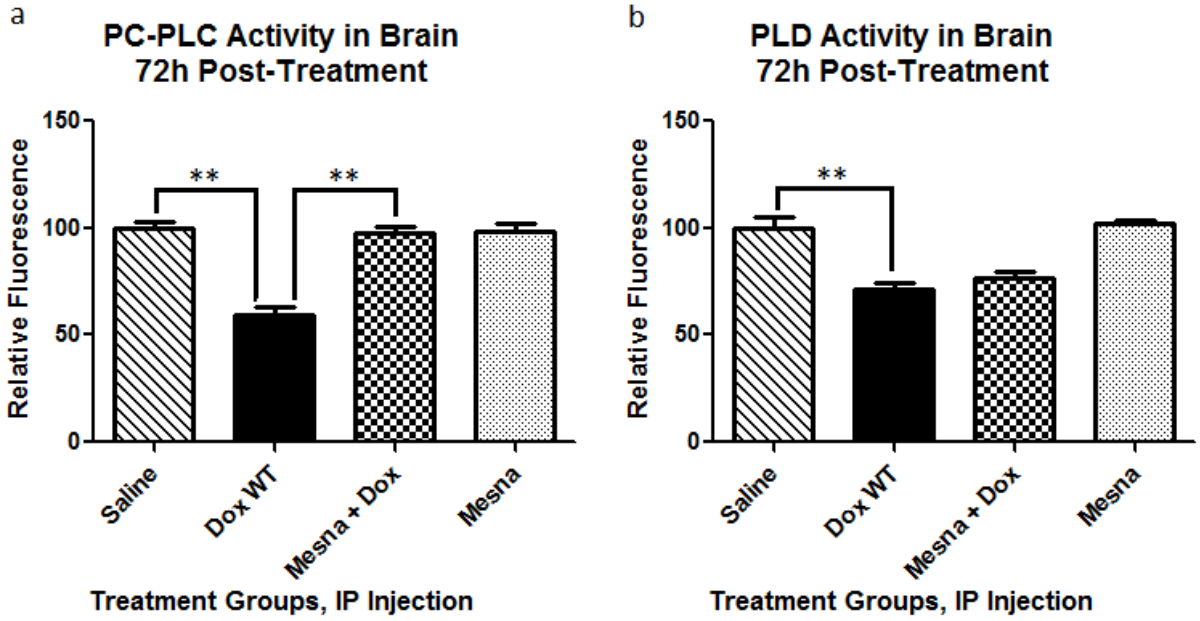

Figure 4.4. PC-PLC and PLD activity in brain following Dox and MESNA treatment, presented as percent saline control. (a) PC-PLC activity at 22.5h of incubation, the peak fluorescence of the corresponding positive control in these trials, at room temperature in the dark. Cleavage of the assay substrate by PC-PLC yields a dye-labeled DAG which fluoresces using an excitation and emission maxima of 509 and 516nm, respectively. Dox administration caused a significant decrease in PC-PLC activity compared to saline treated mice (**$p<0.01$). Co-administration of MESNA rescued PC-PLC activity (**$p<0.01$, Dox vs. Dox+MESNA). (b) PLD activity at 1h of incubation, the peak fluorescence of the corresponding positive control in these trials, at 37°C protected from light. PLD cleaves the headgroup from phospholipids thereby releasing the choline from

PtdCho. Assay reactions involving the choline produce a product that fluoresces using an excitation and emission maxima of 571 and 585nm, respectively. Dox treatment resulted in significantly decreased PLD activity compared to saline treated controls (**$p<0.01$). PLD activity in the Dox+MESNA group was not significantly different from the group receiving Dox alone.

4.5 Discussion

Based on our previous studies, we proposed this model. Plasma protein oxidation, including ApoA-I, induced by the redox cycling of Dox leads to elevation of TNF-α in the periphery. TNF-α crosses the BBB by receptor-mediated endocytosis to induce microglial activation, further TNF-α release, increased production of NO, mitochondrial dysfunction, neuronal death, and consequent cognitive impairment (Tangpong et al. 2006; Tangpong et al. 2007; Tangpong et al. 2008; Aluise et al. 2009; Aluise et al. 2010; Joshi et al. 2010; Aluise et al. 2011). Our laboratory has previously shown that oxidative damage occurs early in neurodegenerative processes (Reed et al. 2008; Owen et al. 2009; Sultana et al. 2009; Sultana et al. 2010; Aluise et al. 2011). Nearly half of the FDA-approved anti-cancer drugs have been shown to result in elevation of ROS and induce oxidative stress (Chen et al. 2007). A large percentage of cancer survivors suffer from CICI, now widely recognized as a chemotherapy complication (Tannock et al. 2004; Foley et al. 2008; Aluise et al. 2010; Cheng et al. 2013; Seigers et al. 2013). The goals of this study were to gain insight into

mechanisms of CICI and its potential prevention, with the long-term goal to progress toward prevention or at least successful management of CICI and an improved quality of life for an ever growing number of cancer survivors.

Direct toxic effects caused by the chemotherapy drugs leads to damage to biomolecules including lipids, proteins, lipoproteins, and genetic material (Sterrenberg et al. 1984; Bagchi et al. 1995; Chen et al. 2007; Nithipongvanitch et al. 2007; Joshi et al. 2010; Aluise et al. 2011). Oxidative stress caused by anticancer drugs leads to damage to biomolecules in non-targeted, non-cancerous tissues including the blood, heart, and brain (Chen et al. 2007).

Reactive oxygen and reactive nitrogen species (ROS, RNS) include such species as superoxide radical anion (O_2^{-}•), nitric oxide (NO), peroxynitrite ($ONOO^{-}$), and hydroxyl radical (HO•). Some of these have both functions essential to life and effects damaging to biomolecules necessary for life. O_2^{-}• is produced by inefficient reduction of molecular oxygen in the mitochondria (Raha et al. 2000; Chen et al. 2007; Barja 2013; Figueira et al. 2013). NO, a free radical, is produced from L-arginine by catalysis of various forms of the enzyme, nitric oxide synthase. Together, O_2^{-}• and NO combine to form another reactive species, $ONOO^{-}$ (Squadrito et al. 1998; Szabo et al. 2007). Hydrogen peroxide (H_2O_2), produced through the actions of superoxide dismutases (SOD) (Fridovich 1995; Liochev et al. 2007), is converted to water and molecular oxygen by peroxidases but can result in production of HO• in the presence of iron(II) or copper(I) ions via

Fenton Chemistry (Fenton 1894; Haber 1932; Stadtman et al. 1991; Wardman et al. 1996). These radical species can cause the formation carbon centered radicals, alkoxyl radicals, and peroxyl radicals further damaging biomolecules through a free radical chain reaction (Porter et al. 1995; Pratt et al. 2011). In particular, this type of oxidative stress can lead to lipid peroxidation in the lipid bilayer and the formation of reactive alkenals such as 4-hydroxy-2-transnonenal (HNE), a lipid peroxidation product of the brain abundant arachidonic acid, which can covalently bind proteins by Michael addition to alter protein structure and function (Halliwell et al. 1984; Butterfield et al. 1997; Butterfield et al. 2002; Sultana et al. 2013). The brain is particularly vulnerable to oxidative damage due to relatively low antioxidant defenses, high oxygen consumption, and high concentrations of polyunsaturated fatty acids.

Administration of the prototypical ROS generating anti-cancer drug, Dox, leads to oxidative damage to plasma proteins through both direct and indirect toxicity independent of its cancer killing ability. Dox directly continually causes oxidative stress in peripheral tissues by redox cycling of the quinone moiety in its structure. Dox-induced cardiac dysfunction in part is due to mitochondrial damage is well established and is used as a dose limiting criteria in treatment protocols (DeAtley et al. 1999; Chen et al. 2006; Jungsuwadee et al. 2006; Jungsuwadee et al. 2012). Indirectly, Dox elevates levels of TNF-α in the blood and, subsequently, the brain leading to neuronal death (Tangpong et al. 2006; Aluise et al. 2011). Macrophages are the principal cell source of TNF-α; however, cellular targets

and biological effects are varied including inflammation, neutrophil activation, catabolism in fat and muscle, triggering the synthesis of acute-phase proteins, and apoptosis in many cell types. Such responses can be beneficial if acute but quite harmful if chronic or sustained.

Under normal conditions, ApoA-I suppresses TNF-α release in plasma (Hyka et al. 2001; Yin et al. 2011). Once oxidized, ApoA-I loses this ability and may actually exacerbate TNF-α release (Aluise et al. 2011). The oxidative status of ApoA-I is crutial to its role in TNF-α suppression. Dox-induced ApoA-I oxidation and TNF-α increase is suppressed by co-administration of MESNA (Aluise et al. 2011). MESNA is rapidly oxidized, scavenging reactive species in circulation. MESNA's time in circulation is short-lived as it is rapidly renally eliminated, thereby, reducing the chance for potential unwanted side effects (Mashiach et al. 2001).

Oxidative stress data presented here supports the results of our previous studies. Dox administration leads to oxidative stress in both plasma and brain as evidenced by increases in both PC and protein-bound HNE. Both of these damages are prevented when MESNA is administered just prior to Dox. These results, shown for the first time in brain, confirm our prior results in plasma.

Cognitive testing of saline, Dox, MESNA, and Dox+MESNA treatment groups revealed learning and memory impairment in animals receiving Dox alone.

Cognitive performance, as measured by NOR, was largely rescued in the group that received MESNA with Dox. Open field testing was employed as a gauge of locomotor activity and ability. The treatment groups receiving Dox, both with and without MESNA displayed less total movement than those in the saline or MESNA treated groups. The Dox and Dox+MESNA treatment groups displayed similar total movement in the test environment decreasing potential confounds when comparing NOR performance between these two groups. Total object exploration time was similar among all treatment groups and decreased with repeated exposure to the environment. After only 24 h post-injection, animals in the Dox-treated group were already showing a trend of decreased preference for the novel object compared to the other treatment groups. By day three, the Dox-treated animals on average displayed a preference for the familiar object over the novel one. Incomplete encoding of the familiar stimulus or a discrepancy between the memory of the familiar object and the actual perception of the same object may be responsible for the apparent preference for the familiar object. This is compelling evidence for Dox-induced cognitive impairment. MESNA rescued much of this Dox-induced cognitive deficit (Figure 4.2a).

H^1-MRS of hippocampus of similarly treated animals revealed changes in the neurochemical profile in Dox-treated group versus saline control. A slight but significant decline in the NAA/Cr ratio was observed in the Dox group suggesting neuronal damage. More profoundly, MRS revealed, on average, a dramatic six standard deviation decline in the Cho/Cr ratio in the hippocampus of the Dox-

treated group compared to the saline-treated group. These results are consistent with results from another study in which Ciszkowska-Łysoń *et al*. observed a time-related decrease in the Cho/Cr ratio following chemotherapy which they attributed to potential myelin damage (Ciszkowska-Lyson et al. 2003). Three days after Dox treatment may be too soon to see measurable myelin damage in brain detectable on MRS.

Changes in choline-containing compounds on MRS are thought to be associated with membrane turnover (phospholipid synthesis and degradation) (Soares et al. 2009; Bertholdo et al. 2013). Cho levels have been shown to be proportional to cell density (Gupta et al. 2000) and to correlate with degree of malignancy in cancers (Soares et al. 2009; Bertholdo et al. 2013). A decrease in the Cho peaks in brain has also been seen in brain aging as well as a decrease in choline uptake in older adults (Cohen et al. 1995; Dezortova et al. 2008; Soares et al. 2009). A decrease in Cho/Cre ratio is seen as indicative of decreased cell density and necrosis (Gupta et al. 2000; Soares et al. 2009). Upon Dox administration, the decreased PCho and/or Cho is consistent with changes in the production or metabolism of PtdCho or the neurotransmitter, acetylcholine (ACh) (Mallampalli et al. 2000; Zhao et al. 2001). Due to the widespread functions of ACh in both the motor and somatic divisions of the autonomic nervous system, the effects of chemotherapy-induced changes to this neurotransmitter may be varied and dramatic and need to be further explored. Evidence exists that ACh-associated

memory, intelligence, and mood may, in part, be mediated by Cho levels and ACh metabolism in the brain (Poly et al. 2011).

The decrease in the Cho peak in brain revealed by MRS spectra of Dox-treated mice may be due to decreased membrane synthesis, decreased myelination, and potentially cell loss. Such changes in the MRS observed, conceivably, may be consistent with the white matter changes seen in human breast cancer patients (Inagaki et al. 2007; Deprez et al. 2011; de Ruiter et al. 2012; Deprez et al. 2012). Magnetic resonance imaging (MRI) and magnetic resonance spectroscopy (MRS) are proving to be useful tools both for visualization of white matter changes and changes in the neurochemical profile indicative of axonal degeneration and demyelination in the brains of living subjects following chemotherapy (de Ruiter et al. 2012). Indeed, the integrity of lipid-rich myelin covered white matter have been shown to be altered as well as damage to gray matter with associated functional deficits following systemic cancer chemotherapy, in some cases years after chemotherapy (de Ruiter et al. 2012; Briones et al. 2013; Simo et al. 2013). Studies have shown that chemotherapy-induced neuroinflammation, including increases in TNF-α, are correlated with changes in myelination and cognitive impairment (Briones et al. 2013). Coupled with neuropsychological tests, neuroimaging techniques can provide important information to help outline a mechanism for clinical and biochemical changes in the brain that results from chemotherapy and help researchers and clinicians

work together to decrease or prevent unnecessary cognitive decline in cancer patients (Correa et al. 2008; Raffa 2010; Raffa 2010).

Elevated TNF-α is reported to decrease synthesis of PtdCho (Mallampalli et al. 2000; Church et al. 2005). Our group previously hypothesized that TNF-α elevated in the periphery and in brain following cancer chemotherapy plays a central role in CICI (Joshi et al. 2005; Tangpong et al. 2006; Tangpong et al. 2008; Aluise et al. 2010; Aluise et al. 2011). PtdCho is also the principal phospholipid found in high-density lipoprotein (HDL), teaming with ApoA-I in cholesterol transport, one of the most common constituents found in biological membranes. PtdCho is usually located in the outer leaflet with the choline headgroup exposed to the aqueous cytosolic environment playing vital roles in membrane-mediated cell signaling. The turnover of PtdCho has been shown to be accelerated in models of mitochondrial dysfunction mimicking Alzheimer's Disease (AD) patterns of metabolic changes in the brain (Farber et al. 2000). Cleavage of PtdCho by PC-PLC yields PCho and the second messenger DAG whereas cleavage of PLD releases choline used in the synthesis of the neurotransmitter, ACh. PC-PLC plays vital roles in several cell signaling pathways involved in both apoptosis and cell survival and in a variety of disease processes. Hence, decreased DAG could severely impair normal cell signaling and be important for CICI. Dox-treatment severely impaired the activity of both PC-PLD and PLD in brain of the mouse model of chemotherapy used in this study. The decrease in activity of these two enzymes may, in part, explain the

changes in the Cho signal seen on hippocampal H^1-MRS. The slight though not statistically significant recovery of the Cho peaks when MESNA was co-administered with Dox may be due to protection of PC-PLC function by MESNA but no protection of PLD. Therefore, more studies are warranted to further elucidate this mechanism.

Based on previous work by our group and the results of the current study, we propose the following expanded model for CICI over that published by our group previously (Aluise et al. 2011). ROS-associated chemotherapeutic agents cause oxidative damage to plasma proteins, including ApoA-I, and lead to peripheral elevation of the inflammatory cytokine, TNF-α (Tangpong et al. 2006; Aluise et al. 2011). Unaltered ApoA-I interacts with the ATP-binding membrane cassette transporter A1 (ABCA1) involved in cholesterol transport (Weber et al. 2011; Yin et al. 2011). Given that protein structure changes when oxidized (Subramaniam et al. 1997), the initial interaction of ApoA-I with ABCA1 is altered when ApoA-I is oxidized. Hence, TNF-α would be elevated in plasma. Elevated TNF-α crosses the BBB leading to microglial activation, increased ROS and further TNF-α release in the brain, leading to mitochondrial dysfunction and subsequent cognitive decline (Aluise et al. 2010; Joshi et al. 2010). TNF-α inhibition of PtdCho synthesis may result in decreased PCho availability. Since ceramide couples with PCho to produce sphingomyelin (Siegel 2006), decreased PCho would lead to elevated ceramide. The latter is a known inducer of apoptosis (Geilen et al. 1997; Qin et al. 1998; De Nadai et al. 2000; Car et al. 2012; Wang

et al. 2012), and we previously showed elevated apoptosis in brain of Dox-treated mice (Tangpong et al. 2007) (Figure 4.5). Dox-induced decreased PC-PLC and PLD activities may result in dysregulation of cell survival and apoptosis pathways that involve PC-PLC and decreases in choline available for ACh synthesis via PLD.

CICI severely impacts the quality of life of cancer survivors. This paper shows for the first time strong evidence that brain oxidative stress following Dox administration leads to cognitive decline, and both are rescued by MESNA. These studies form the basis of additional investigations to gain insights into CICI.

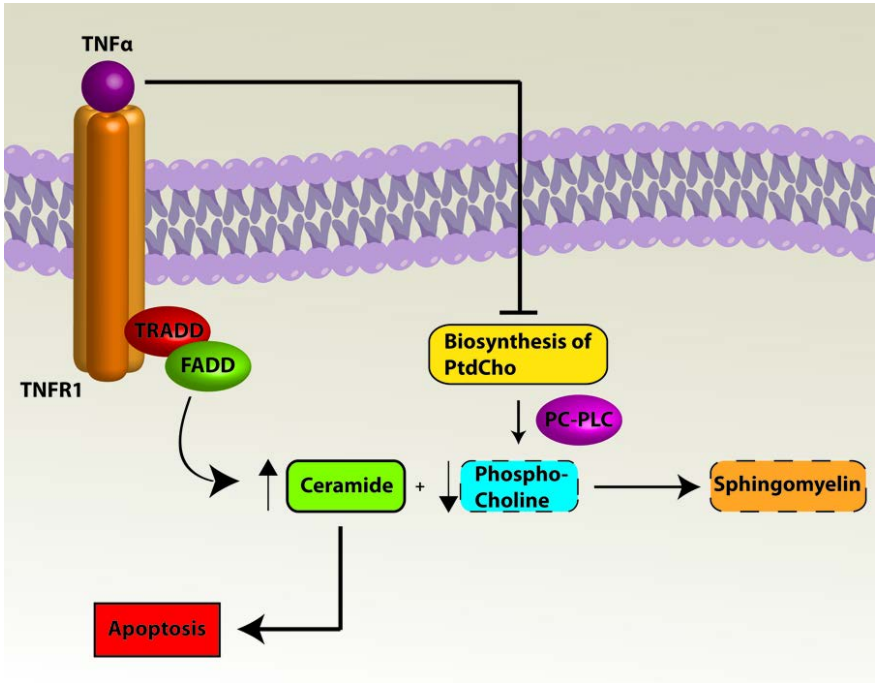

Figure 4.5. A pathway to apoptosis. Elevated TNF-α inhibits biosynthesis of PtdCho leading to decreased PC-PLC-mediated cleavage of PCho from PtdCho. Decreased PCho results in increased ceramide due to decreased conversion to sphingomyelin. Increased ceramide leads to apoptosis. (Figure designed by A. M. Swomley, Butterfield Laboratory, University of Kentucky).

Copyright © Jeriel T. R. Keeney 2013

CHAPTER 5

Prevention of mitochondrial damage in brain and oxidative stress in plasma of TNF-α knockout mice treated with the anti-cancer drug doxorubicin: Implications for chemotherapy-induced cognitive impairment ("Chemobrain")

5.1 Overview of Study

Approximately fifty percent of FDA-approved anti-cancer drugs generate reactive oxygen species (ROS). Doxorubicin (Dox) is a prototypical ROS generating chemotherapeutic agent used to treat solid tumors often as part of multi-drug chemotherapeutic regimens. Dox produces the reactive superoxide radical anion (O_2^{-}•) *in vivo* through redox cycling between the quinone and semi-quinone forms. We previously reported that peripheral Dox-administration leads to plasma protein damage and elevation of tumor necrosis factor-alpha (TNF-α) in plasma and brain of mice. TNF-α elevation in brain led to further central nervous system toxicity including mitochondrial dysfunction, neuronal death, and cognitive impairment. In the present study, we demonstrate that Dox-induced oxidative stress is ameliorated and mitochondrial oxygen consumption rate (OCR) is preserved in brain of TNF-α null (TNFKO) mice. Further, we show protection

against Dox-related decreases in the Cho/Cr ratio determined by magnetic resonance spectroscopy (MRS) and phospholipase D (PLD) activity of TNFKO mouse brain. This study demonstrates that, in the absence of TNF-α, MRS-indexed Cho/Cr ratio, PLD activity, and mitochondrial oxygen consumption are preserved in brain, and markers of oxidative stress are reduced. Together with results from our previous studies, these results provide strong evidence that TNF-α is responsible for chemotherapy-induced cognitive impairment (CICI), particularly by anti-cancer drugs like Dox that do not cross the BBB. These results have important implications for potential interventions to modulate the cognitive consequences of chemotherapy experienced by a large percentage of cancer survivors.

5.2 Introduction

Approximately half of FDA approved anti-cancer drugs are known to generate reactive oxygen species (ROS) resulting in oxidative stress (Chen et al. 2007). Doxorubicin (Dox), an antineoplastic anthracycline used primarily to treat solid tumors as part of multi-drug chemotherapy regimens, is one such ROS inducing chemotherapeutic agent (Handa et al. 1975; Bachur et al. 1977; Gutteridge 1984; Cummings et al. 1991; Deres et al. 2005; Aluise et al. 2011). The redox cycling of Dox between the quinone and semi-quinone forms results in production of superoxide radical anion (O_2^{-}•) (Handa et al. 1975; Bachur et al. 1977; Cummings et al. 1991). Dox-induced extracellular protein oxidation and resulting

toxicities are thought to be independent of the anti-tumor ability of Dox (Bernacki et al. 1987; Aluise et al. 2011). Oxidation of plasma proteins following Dox administration results in elevation of tumor necrosis factor-alpha (TNF-α) and oxidative and nitrosative stress in the brain, despite the inability of Dox to cross the blood-brain barrier (BBB) (Tangpong et al. 2006; Joshi et al. 2007; Tangpong et al. 2007; Tangpong et al. 2008; Aluise et al. 2010; Joshi et al. 2010).

Apolipoprotein A-I (ApoA-I) plays a variety of roles including cholesterol transport and regulation of inflammation (Rader et al. 2008; Keeney et al. 2013). ApoA-I acts as the primary lipid acceptor protein in the high-density lipoprotein (HDL) complex for lipids such as cholesterol and phosphatidylcholine (PtdCho) (Quazi et al. 2011). Interaction of ApoA-I with the ATP-binding membrane cassette transporter A1 (ABCA1) involved in cholesterol transport (Quazi et al. 2011; Weber et al. 2011) results in inhibition of TNF-α release through production of a tristetraprolin (TTP) (Yin et al. 2011). TTP degrades the mRNA message for TNF-α (Yin et al. 2011). Once oxidized, ApoA-I loses the ability to inhibit TNF-α release (Aluise et al. 2011). Subsequently, TNF-α crosses the BBB via receptor-mediated endocytosis to elicit microglial activation resulting in further TNF-α release, oxidative and nitrosative stress, mitochondrial dysfunction, and neuronal death (Tangpong et al. 2006; Tangpong et al. 2007; Tangpong et al. 2008; Joshi et al. 2010; Aluise et al. 2011). Our group has demonstrated these to be key events leading to chemotherapy-induced cognitive dysfunction (CICI) (Joshi et al. 2005; Joshi et al. 2010; Aluise et al. 2011; Keeney et al. 2014).

Mitochondrial dysfunction induced by Dox is well established, especially in the heart (DeAtley et al. 1999; Chen et al. 2006; Jungsuwadee et al. 2006). Cardiac toxicity is used as the dose-limiting factor in Dox treatment (Tangpong et al. 2007). Prior studies by our group demonstrated that Dox-induced mitochondrial dysfunction also occurs in brain via a mechanism involving nitration of the mitochondrial $O_2^{\cdot-}$• scavenger, manganese superoxide dismutase (MnSOD) (Tangpong et al. 2007). TNF-α and inducible nitric oxide synthase (iNOS) are both downstream products of the nuclear factor κ-light-chain enhancer of activated B-cells (NF-κB) pathway (Griscavage et al. 1996; Keeney et al. 2013). Mitochondrial ROS are thought to be involved in the activation of this pathway (Chandel et al. 2000).

Brain function is energetically expensive. The brain accounts for approximately 2% of body weight but accounts for about 20% of the body's total energy usage, most of this for signaling and maintaining membrane potentials. Due to low stores of energy and energy substrates, the brain relies primarily on continuous energy production via mitochondrial respiration for normal function (Siegel 2006). Therefore, Dox-induced mitochondrial dysfunction would lead to cognitive decline. Previously, we reported that Dox administration led to cognitive dysfunction in mice within a few days following treatment (Keeney et al. 2014). In the current study, given the centrality of TNF-α in our model for CICI, we tested the hypothesis that in TNFKO mice, brain oxidative stress, the magnetic

resonance spectroscopy (MRS)-indexed neurochemical profile, and mitochondrial function following Dox administration would be compromised in contrast to that of WT mice.

5.3 Methods and Materials

5.3.1 Chemicals

Precision Plus Protein™ All Blue Standards, BCA reagents, and nitrocellulose membranes were purchased from Bio-RAD (Hercules, CA, USA). Chemicals, proteases, protease inhibitors, and antibodies used in this study were purchased from Sigma-Aldrich (St. Louis, MO, USA) unless otherwise noted. EnzChek® Direct Phospolipase C Assay Kit and Amplex® Red Phospholipase D Assay Kit were purchased from Invitrogen/Life Technologies (Carlsbad, CA).

5.3.2 Statistical analysis

All data are presented as mean±SEM unless otherwise noted. Statistical analyses using GraphPad Prism 5 software were performed using ANOVA followed by a two-tailed Student's *t*-test to make individual comparisons between groups where relevant, with $p<0.05$ considered significant. The D'Agostino & Pearson omnibus normality test were used where appropriate.

5.3.3 Animals

All procedures were approved by the Institutional Animal Care and Use Committee of the University of Kentucky in accordance with the U.S. National Institutes of Health Guide for the Care and Use of Laboratory Animals. The animals were housed in an air-conditioned environment (22.1°C, 50.5% relative humidity, 12 h light-dark cycle), with free access to food and water.

Male, wild-type (WT) B6C3F1/J (B6C3) mice and B6.129S6-*Tnf*^{tm1Gkl}/J (TNF-α knockout, TNFKO) purchased from the Jackson Laboratory, 2-3 months old and each weighing approximately 30 grams, were kept under standard conditions housed in the University of Kentucky Animal Facility. Doxorubicin HCl was purchased from Bedford Laboratories™. Mice were injected using a single intraperitoneal (i.p.) dose of 25mg/kg Dox or the same volume of saline as a control. MRS was performed 72 h post treatment. Following MRS studies, animals were euthanized and blood and tissues collected for molecular or biochemical analysis.

5.3.4 Sample preparation

Protein estimation was performed using the bicinchoninic acid (BCA, Pierce) assay (Bradford 1976). Homogenized brain and plasma samples were diluted according to initial protein estimation results using 20 ug sample in isolation

buffer [0.32 M sucrose, 2 mM EDTA, 2mM EGTA, and 20mM HEPES pH 7.4 with protease inhibitors, 0.2 mM PMSF, 20ug/mL trypsin inhibitor, 4 µg/ml leupeptin, 4 µg/ml pepstatin A, and 5 µg/ml aprotinin].

5.3.5 Slot blot assay

The slot blot method was used to determine levels of protein carbonyl (PC) and protein-bound 4-hydroxy-2-transnonenal (HNE) in brain as previously described (Bernacki et al. 1987; Fang et al. 2009). For PC determination, samples were derivatized with 2,4-dinitrophenylhydrazine (DNPH). For HNE, samples were solubilized in Laemmli buffer. Protein (250 ng) from each sample was loaded onto a nitrocellulose membrane in respective wells in a slot-blot apparatus (Bio-Rad) under vacuum. Membranes were blocked in 3% bovine serum albumin (BSA) in PBS with 0.2% (v/v) Tween-20 for 1.5 h and then incubated in primary antibody (anti-dinitrophenylhydrazone primary or anti-protein-bound HNE, respectively, each produced in rabbit, Sigma-Aldrich) for 2 h, washed three times in PBS with 0.2% (v/v) Tween-20 and then incubated for 1 h with secondary antibody (goat anti-rabbit secondary linked to alkaline phosphatase). Membranes were developed with 5-bromo-4-chloro-3-indolyl-phosphate (BCIP) dipotassium and nitro blue tetrazolium (NBT) chloride in alkaline phosphatase activity (ALP) buffer, dried, and scanned for analysis. Image analysis was performed using Scion Image (Scion Corporation, Frederick, MD).

5.3.6 Isolation of brain mitochondria

Mice were perfused via cardiac puncture with cold mitochondrial isolation buffer, the brain promptly removed, the cerebellum dissected away, and the mitochondria immediately isolated from the brain by a modification of the method described by Mattiazzi et al. (Mattiazzi et al. 2002). Brain mitochondria were isolated in cold mitochondrial isolation buffer, containing 0.07 M sucrose, 0.22 M mannitol, 20 mM HEPES, 1 mM EGTA, and 1% bovine serum albumin, pH 7.2. Tissues were homogenized with a Dounce homogenizer and centrifuged at 1500 × g at 4°C for 5 min before transferring the supernatants. The pellets were resuspended and centrifuged at 1500 × g at 4°C for 5 min. The supernatants were combined and recentrifuged at 1500 × g at 4°C for 5 min. The supernatants were separated and centrifuged at 13,500 × g at 4°C for 10 min. Non-synaptosomal mitochondrial fraction separation was performed using a 3%/6% (w/v) Ficoll gradient at 4°C prepared before use in 100 mL mitochondrial isolation buffer. Mitochondrial pellets were purified with a 4% Ficoll solution and the mitochondrial pellet was resuspended in 50 µL cold mitochondrial isolation buffer. This method allows rapid isolation of viable mitochondria from brain. Purity testing of resulting mitochondria samples was not performed due to time and sample volume constraints to ensure mitochondrial viability. There is a tension between time of processing and purity of sample obtained. Thus, the results obtained required a short time to obtain viable mitochondria, but in so doing, the results may be affected by potential interfering contaminants. Protein

concentration of isolated mitochondria was determined by the Bradford assay (Bradford 1976).

5.3.7 Bioenergetic analysis in mitochondria

The XF96 Analyzer, Seahorse Bioscience (North Billerica, MA, USA) was used to measure bioenergetic function in mitochondria freshly isolated by differential centrifugation from brain of adult male C57BL6 mice. The XF96 creates a transient 3µl chamber in specialized microplates that allows for the measurement of oxygen consumption rate (OCR) in real time. Respiration by the mitochondria (5 µg/well) was sequentially measured with substrate present (basal respiration) following conversion of ADP to ATP, induced with the addition of oligomycin. Next, maximal uncoupler-stimulated respiration was detected by the administration of the uncoupling agent FCCP. At the end of the experiment, the complex III inhibitor, antimycin A, was applied to completely inhibit mitochondrial respiration. Oxygen Consumption rate were measured four times and plotted as a function of cells, showing the relative contribution of oxygen consumption, ATP-linked oxygen consumption, the maximal OCR after the addition of FCCP, and the reserve capacity of the cells. Seahorse assays were performed by the D.K. St. Clair laboratory, Graduate Center for Toxicology, Department of Radiation Medicine, Markey Cancer Center, University of Kentucky.

5.3.8 Hydrogen magnetic resonance imaging spectroscopy

H^1-MRS (hydrogen magnetic resonance imaging spectroscopy) was used to quantify neurochemical changes in the mouse hippocampus. MRI data was acquired on a 7T BrukerClinscan horizontal bore system (7.0T, 30cm, 300Hz) equipped with a triple-axis gradient system (630 mT/m and 6300 T/m/s). A closed cycle, 14K quadrature cryocoil allowed for a 2.8 signal to noise increase relative to standard coils.

The mice were anesthetized with 1.3 % percent isoflorane using MRI compatible CWE Inc. equipment. Mice were held in place on a Bruker scanning bed with a tooth bar, ear bars and tape. Body temperature and respiration rate were monitored using equipment from SA Instruments Inc. The animals were maintained at 37°C with a water heating system built into the scanning bed. T2 weighted turbo spin echo sequences (TE 40ms, TR 2890ms, Turbo 7, FOV 20mm, 0.156 x 0.156 x 5.0 mm^3) were acquired and used for the placement of the spectroscopy voxel. The scanning procedure took 40 min. A 2x5.5x3mm^3 PRESS spectroscopic voxels (TE 135ms, TR 1500ms, 400avg, CHESS water suppression) was placed to cover both hippocampi. Spectrum analysis was performed using jMRUI (naressi, *et al*. 2001) to quantify the area under 10 peaks in the spectrum. The creatine peak was used to normalize the choline peak. H^1-MRS scans were performed by Dr. David Powell, Magnetic Resonance Imaging and Spectroscopy Center, University of Kentucky Medical Center.

5.3.9 Phospholipase C and phospholipase D activity assays

Phosphatidylcholine-specific phospholipase C (PC-PLC) and phospholipase D (PLD) activity assays were performed using manufacturers' instructions provided with the EnzChek® Direct Phospolipase C Assay Kit and Amplex® Red Phospholipase D Assay Kit by Invitrogen/Life Technologies (Carlsbad, CA). Fluorescence intensity for each assay was measured using a SPECTRAFluor Plus instrument and quantified using associated Magellan™ software by TECAN over a period of 24h with the kinetic peaks of the positive controls used for comparison.

5.4 Results

5.4.1 Dox administration results in increases in oxidative stress markers in brain and plasma of wild-type mice and plasma but not brain of TNFKO mice

Our laboratory previously demonstrated that peripheral administration of Dox to WT mice caused increased global oxidative stress in plasma and brain (Joshi et al. 2007; Aluise et al. 2011; Keeney et al. 2014) as well as oxidative damage to key plasma and brain proteins (Joshi et al. 2010). The consequent Dox-induced elevation of plasma TNF-α resulted in elevation of TNF-α and oxidative stress in brain (Joshi et al. 2005; Tangpong et al. 2006; Joshi et al. 2007; Joshi et al.

2010; Aluise et al. 2011), which led us to examine the effects of Dox administration on oxidative stress in plasma and brain in a TNFKO mouse model. Test subjects were administered either saline or Dox. Samples were collected at approximately 72 h post-Dox treatment, immediately following MRS studies. PC levels were used as a gauge of protein oxidation (Butterfield et al. 1997), while lipid peroxidation product, protein-bound HNE, was used as a measure of lipid damage (Subramaniam et al. 1997). Confirming our prior studies, Dox administration resulted in elevation of oxidative stress markers, PC and protein-bound HNE, in both plasma and brain of WT mice (Figure 5.1a-d). Dox-treated TNFKO mice still exhibited elevated PC levels ($p<0.005$, Figure 5.1a) and protein-bound HNE ($p<0.05$, Figure 5.1b) in plasma, likely due to Dox redox cycling. However, in brain of TNFKO mice, PC and protein-bound HNE levels were not found to be significantly different from levels observed in saline-treated mice. This result is strong evidence to support our hypothesis that TNF-α plays a central role in Dox-induced oxidative stress in brain. Additionally, 3-NT was found to be significantly elevated in both plasma and brain of Dox-treated WT mice. In Dox-treated TNFKO mice, 3-NT was significantly elevated in plasma but not in brain compared to relevant control. Baseline 3-NT was significantly higher than the baseline observed in WT counterparts perhaps due to activation of the NF-κB pathway (Schreck et al. 1992; Griscavage et al. 1996; Chandel et al. 2000; Baker et al. 2011; Keeney et al. 2013). In the mouse's attempt to produce more TNF-α, a product of the NF-κB pathway, no TNF-α will be produced as it was genetically ablated. As this attempt to produce TNF-α continues, iNOS, another product of

NF-κB activation will consequently be produced resulting in increased production of NO and resulting protein nitration.

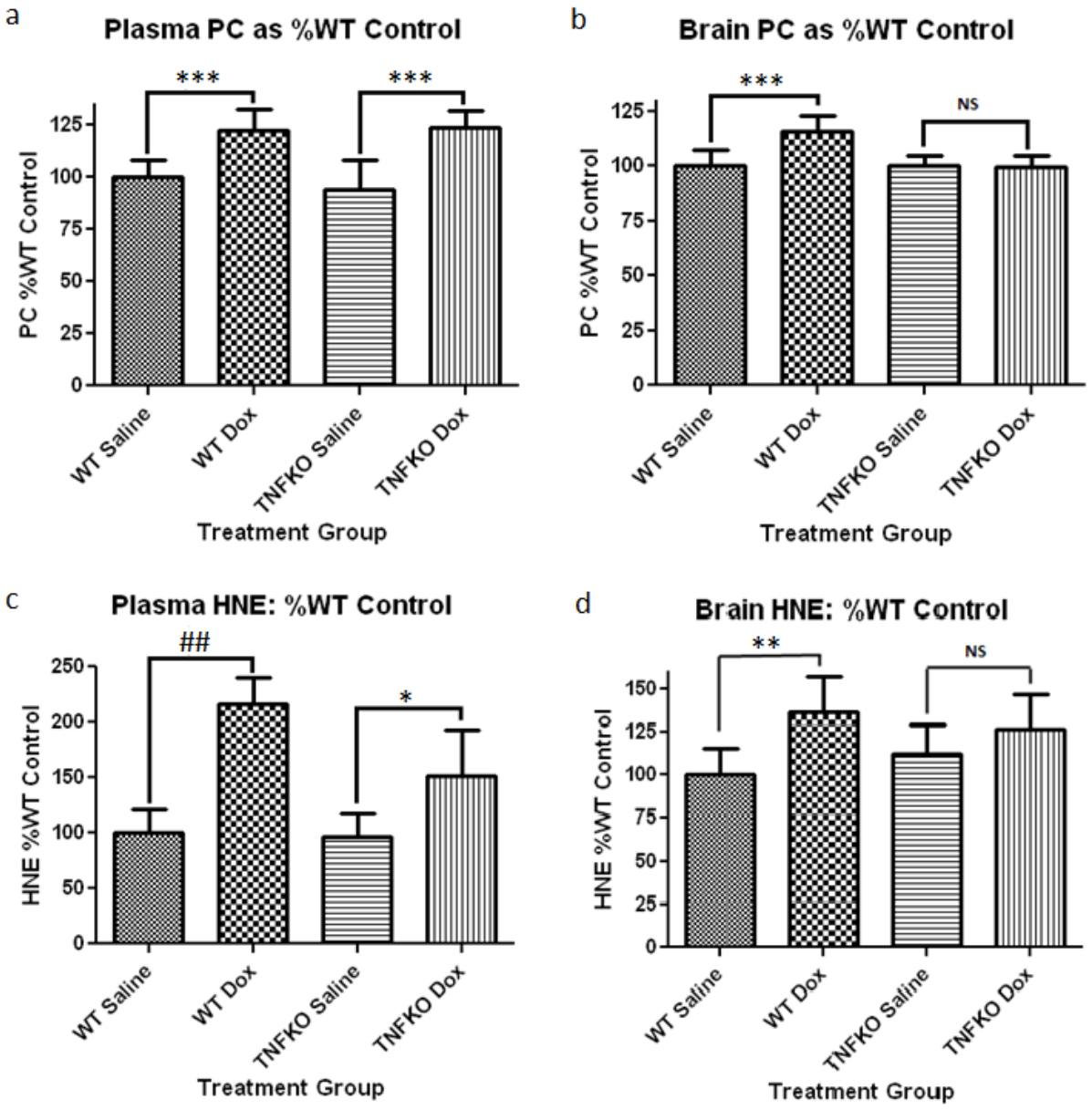

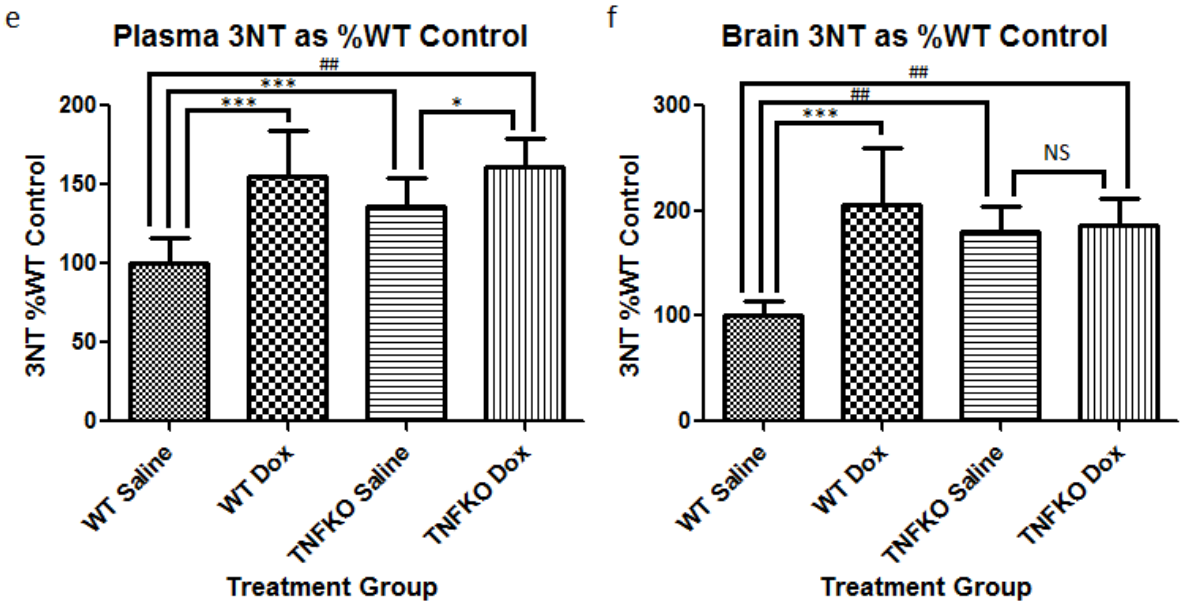

Figure 5.1. PC and protein-bound HNE levels in brain and plasma following Dox treatment in wild-type and TNFKO mice. Protein carbonyl (PC) and protein-bound HNE (HNE) are measures of protein oxidation and lipid peroxidation. Samples were collected approximately 72 h following treatment. (a) PC levels in plasma were significantly elevated following Dox administration in brain of both wild-type (WT) and tumor necrosis factor-alpha knockout (TNFKO) mice compared to saline-treated mice. (b) In brain, PC levels were significantly elevated following Dox treatment; however, PC levels in brain of TNFKO mice was similar to that observed in saline-treated control mice. (c, d) Dox administration resulted in significant elevation of protein-bound HNE in both plasma and brain of WT mice. In TNFKO mice, protein-bound HNE levels were significantly elevated in plasma; however, protein-bound HNE levels in brain were not significantly different than levels observed in saline-treated mice. (e) Dox administration resulted in significant elevation of 3-NT in plasma of both WT and TNFKO mice. (f) In brain, 3-NT was significantly elevated in WT but not

TNFKO mice compared to its relevant control. TNFKO baseline 3-NT was higher than WT in both brain and plasma. (n=6 per treatment group; *p<0.05, **p<0.01, ***p<0.005, ##p<0.0001, NS=not significant).

5.4.2 Dox administration results in altered oxygen consumption rate in brain mitochondria that is absent in TNF-α null mice

Our prior studies demonstrated TNF-α-mediated mitochondrial dysfunction in brain as a consequence of peripheral Dox administration (Tangpong et al. 2006; Tangpong et al. 2007; Tangpong et al. 2008). Previously, we observed a decline in brain mitochondrial respiration via complex I and increases in TNF-α following peripheral Dox administration (Tangpong et al. 2006). In the present study, we used Seahorse technology to measure mitochondrial oxygen consumption rate (OCR) in mitochondria isolated from brain of saline-treated WT (blue circles), Dox-treated WT (red squares), saline-treated TNFKO (purple x's), and Dox-treated TNFKO (green triangles) mice (Figure 5.2a) . Basal, ATP-linked, maximal capacity, and reserve capacity OCR were ascertained in fresh brain mitochondria of each treatment group (Figure 5.2b).

Consistent with our earlier study, here we observed a significant decline in mitochondrial respiration in brain of Dox-treated mice as indexed by OCR. Compared to saline-treated WT mice, Dox-treated WT mice exhibited decreased mitochondrial OCR at every phase measured (Figure 5.2b; basal, p<0.01; ATP-

linked, $p<0.01$; maximal capacity, $p<0.0001$; reserve capacity, $p<0.005$). Compellingly, mitochondrial OCR observed in brain of Dox-treated TNFKO mice was similar to that observed in brain of saline-treated WT and saline-treated TNFKO mice at every phase of mitochondrial OCR measured (Figure 5.2b). This result supports the notion that TNF-α is a key player in mitochondrial dysfunction in brain following chemotherapy involving ROS generating chemotherapeutic agents like Dox, which cannot cross the BBB.

5.4.3 Changes to the neurochemical profile following Dox administration the hippocampus determined by MRS

Bilateral H^1-MRS scans of hippocampus revealed a dramatic decrease in the Cho/Cr ratio in Dox-treated wild-type mice compared to saline-treated control mice (##$p<0.0001$, Figure 5.3) confirming our earlier studies (Keeney et al. 2014). Similar MRS analysis of hippocampus of Dox-treated TNFKO mice showed significant protection in the Cho/Cr ratio over that observed in Dox-treated wild-type mice (#$p<0.0005$, Figure 5.3). The Cho/Cr ratio in Dox-treated TNFKO mouse brain was still lower than that observed in saline-treated mice, but profoundly higher than that (the Cho/Cr in brain) of Dox-treated wild-type mice. This result also provides compelling evidence of TNF-α involvement in the Dox-induced decrease in the Cho/Cr ratio in brain.

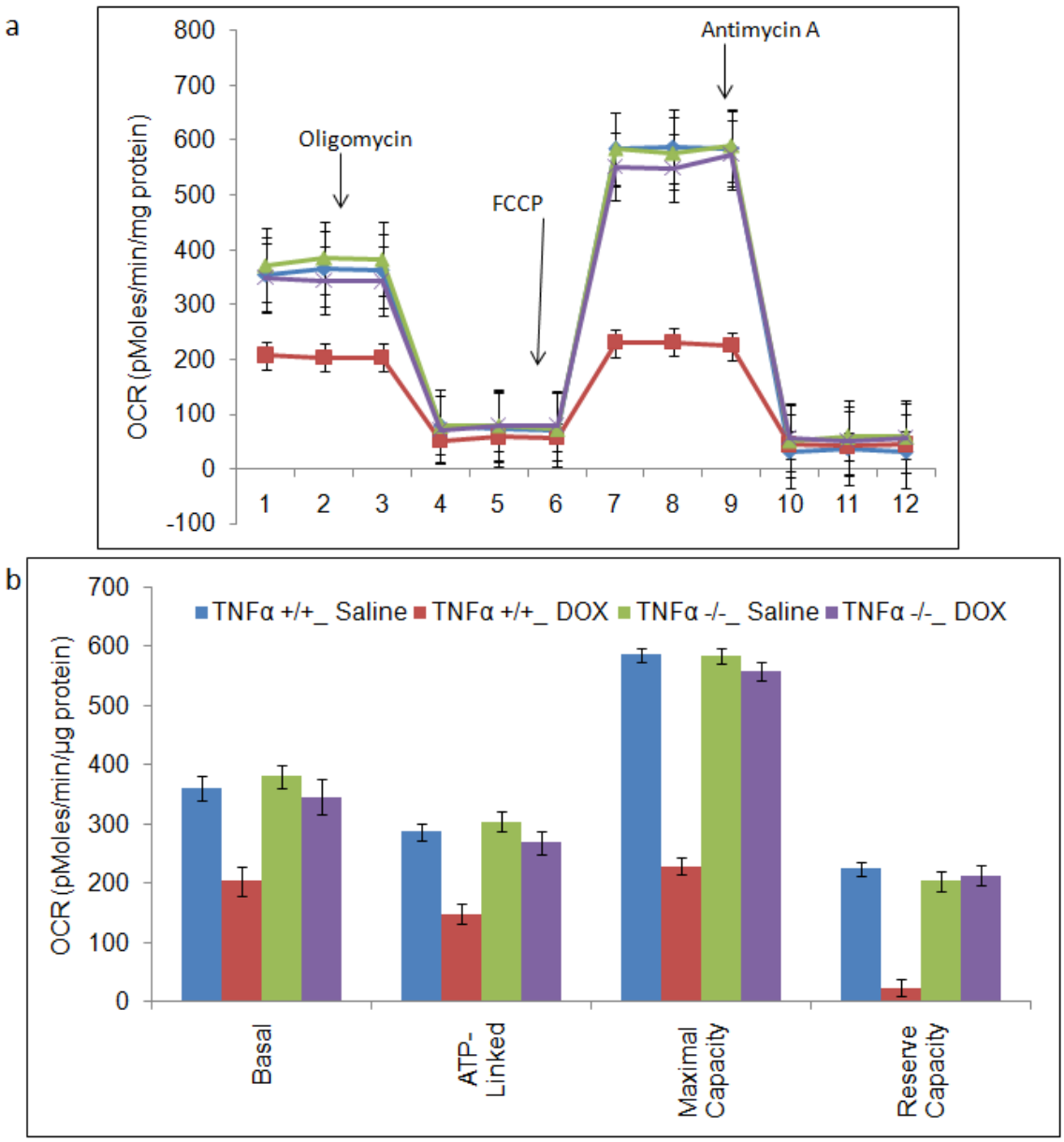

Figure 5.2. Mitochondrial function in brain following Dox treatment in wild-type and TNFKO mice. Measurement of mitochondrial function in brain mitochondria using the Seahorse XF96 analyzer. 5µg of mitochondrial protein were plated into Seahorse Bioscience tissue culture plates and centrifuged before the measurement of total oxygen consumption rate (OCR). (a) OCR were measured four times and plotted as a function of cells under the basal condition

followed by the sequential addition of Oligomycin (1µg/ml), FCCP (3µM) and Antimycin (2µM). (b) Quantification showing the relative contribution of oxygen consumption, ATP-linked oxygen consumption, the maximal OCR after the addition of FCCP, and the reserve capacity of the mitochondria. All data are the Mean±SEM, of triplicate samples and are representative of 3 independent experiments. Seahorse assays were performed by the D.K. St. Clair laboratory, Graduate Center for Toxicology, Department of Radiation Medicine, Markey Cancer Center, University of Kentucky.

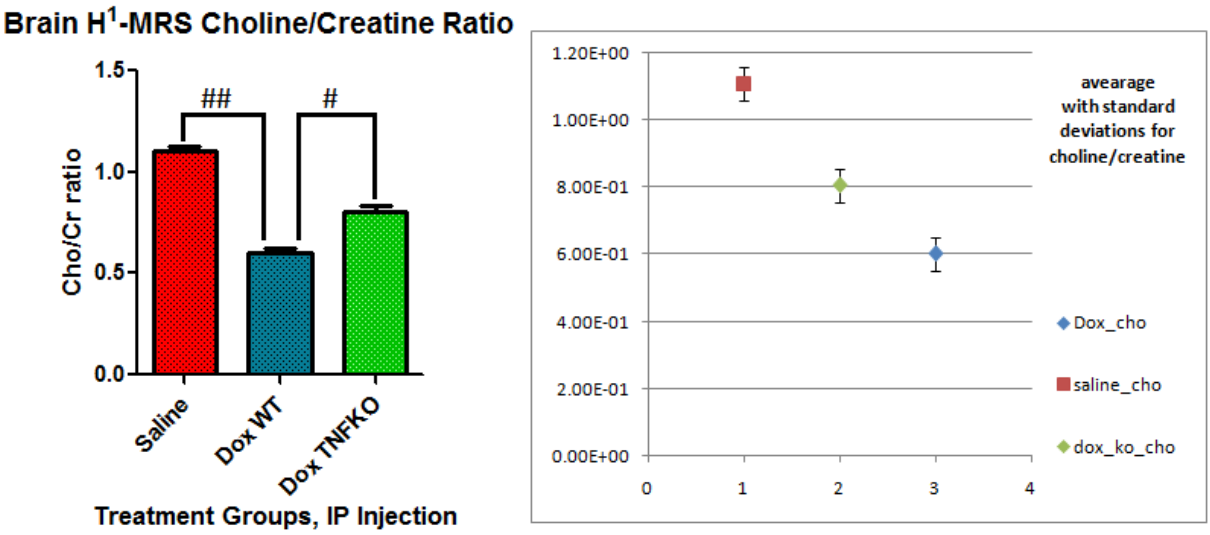

Figure 5.3. H1-MRS of mouse hippocampus following Dox treatment in wild-type and TNFKO mice. Bilateral H^1-MRS scans of hippocampus revealed a large decrease in the Cho/Cr ratio in the Dox-treated group compared to saline control mice (##p<0.0001). Dox treatment of TNFKO mice resulted in rebound of the Cho/Cr ratio over Dox-treated wild-type mice (#p<0.0005). H^1-MRS scans

were performed by Dr. David Powell, Magnetic Resonance Imaging and Spectroscopy Center, University of Kentucky Medical Center.

5.4.4 Dox administration to TNFKO mice results in preservation of PLD activity

Our laboratory reported previously that Dox administration resulted in significant decreases in the activities of both PC-PLC and PLD in mouse hippocampus as determined by MRS (Keeney et al. 2014). The protection of the Cho/Cr ratio observed by MRS in the hippocampus of TNFKO mice (Figure 5.3) led to examination of the effect of TNF-α on activities on phospholipases responsible for the cleavage of choline and phosphocholine from PtdCho. Confirming our prior studies, Dox administration to wild-type mice resulted in significant decline in PC-PLC (Figure 5.4a) and PLD (Figure 5.4b) activity compared to saline-treated mice (***$p<0.005$ and **$p<0.01$, respectively).

The observed Dox-induced decrease in PLD activity was ameliorated when Dox was administered to TNF null mice (*$p<0.05$, Dox-treated TNFKO compared to Dox-treated WT) demonstrating involvement of TNF-α in Dox-induced decline of PLD activity in brain. PC-PLC activity was not protected in the absence of TNF-α. In the face of Dox-adminstration, PLD activity was restored in brain of TNFKO mice to a level not significantly different from saline-treated WT mice. This results suggests that TNF-α plays a role in Dox-induced inhibition of PLD.

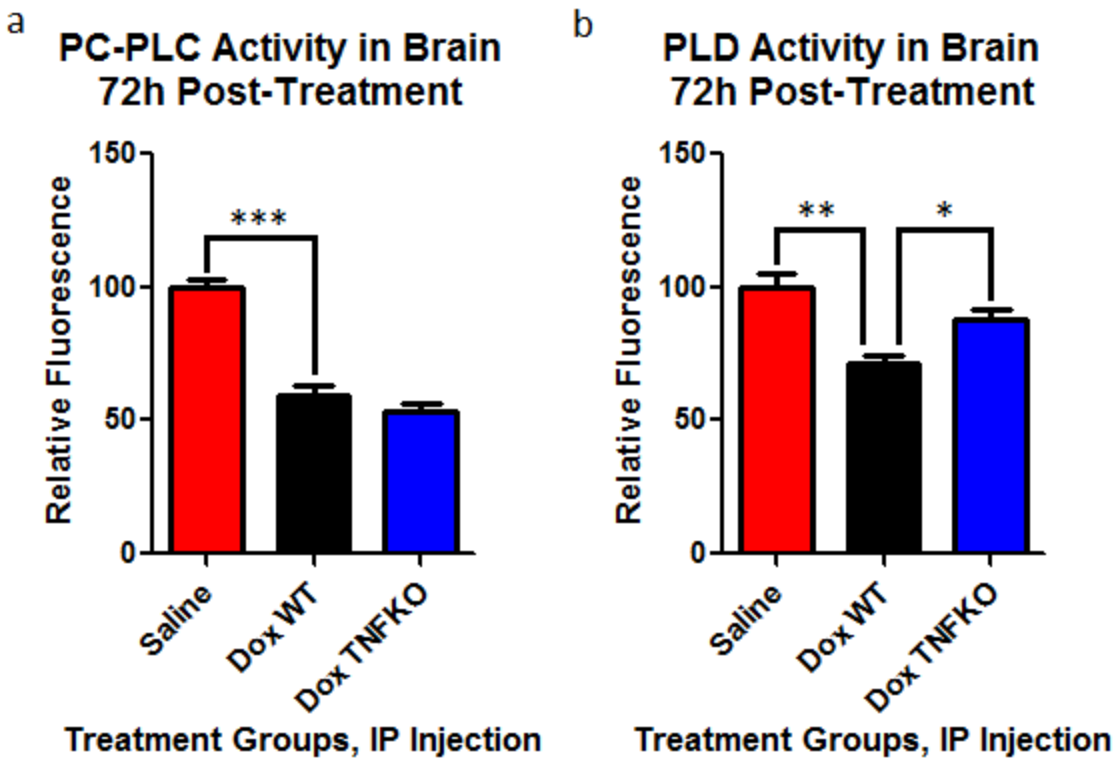

Figure 5.4. PC-PLC, PLD activity in brain after Dox treatment in wild-type and TNFKO mice. Phosphatidylcholine-specific phospholipase C (PC-PLC) and Phospholipase D (PLD) activity in brain post-treatment presented as percent saline control. (a) PC-PLC activity at 22.5h of incubation, the peak fluorescence of the corresponding positive control in these trials, at room temperature in the dark. Cleavage of the assay substrate by PC-PLC yields a dye-labeled diacylglycerol (DAG) which fluoresces using an excitation and emission maxima of 509 and 516nm, respectively. Dox administration caused a significant decrease in PC-PLC activity compared to saline treated mice (***$p<0.005$). Dox treatment of TNFKO mice resulted in similar decrease in PC-PLC activity compared to saline treated mice ($p<0.001$). (b) PLD activity at 1h of incubation, the peak fluorescence of the corresponding positive control in these trials, at

37°C protected from light. PLD cleaves the headgroup from phospholipids thereby releasing the choline from PtdCho. Assay reactions involving the choline produce a product that fluoresces using an excitation and emission maxima of 571 and 585nm, respectively. Dox treatment resulted in significantly decreased PLD activity compared to saline treated controls (**$p<0.01$). PLD activity was preserved in TNFKO mice, significantly higher than PLD activity in brain of Dox-treated wild-type mice (*$p<0.05$), but not significantly different from saline-treated controls.

5.5 Discussion

Prior studies by our group have shown that Dox administration leads to peripheral elevation of oxidative stress markers and TNF-α followed by elevation of TNF-α and oxidative stress in brain despite the inability of Dox or its primary metabolite to cross the BBB (Tangpong et al. 2006; Tangpong et al. 2007; Tangpong et al. 2008; Aluise et al. 2011). Resultant CNS toxicity included damage to key anti-oxidant enzymes, mitochontrial dysfunction, neuronal death, and cognitive dysfunction (Tangpong et al. 2006; Joshi et al. 2007; Tangpong et al. 2007; Joshi et al. 2010; Keeney et al. 2014). A large percentage of cancer survivors who underwent chemotherapy experience cognitive deficits following chemotherapy including memory impairment, difficulty reasoning, and problems multi-tasking (Raffa et al. 2010). Our laboratory recently demonstrated learning

and memory impairment in mice following Dox administration (Keeney et al. 2014).

In the current study, we investigated the central role played by the inflammatory cytokine, TNF-α in a potential mechanism for CICI that occurs following treatment with ROS-producing anti-cancer drugs using Dox as a prototype. We observed that oxidative stress present in plasma and brain of Dox-treated WT mice was also present in plasma of Dox-treated TNFKO mice but likely due to O_2^{-}• produced by redox cycling of Dox (Figure 5.1c, 5.1d). However, in brain of TNFKO mice, oxidative stress was absent. This result demonstrates that TNF-α is a key player in oxidative stress in brain following chemotherapy involving ROS-generating chemotherapy agents, even if they are unable to cross the BBB.

One of the most detrimental consequences in brain of chemotherapy is damage to mitochondrial function (Tangpong et al. 2006; Tangpong et al. 2007; Tangpong et al. 2008; Joshi et al. 2010). Evidence exists of mitochondrial dysfunction as a potential causal factor in a variety of neurodegenerative disorders including Alzheimer's disease, Parkinson's disease, amyotrophic lateral sclerosis, and Huntington's disease (Butterfield et al. 2012; Chaturvedi et al. 2013). The brain has a high and constant energy requirement coupled with low energy stores. Mitochondria are responsible for meeting much of this energy demand (Siegel 2006). Previously, our laboratory observed impairment of mitochondrial function in brain shown by a decrease in Complex I activity of the electron transport chain

following systemic Dox administration (Tangpong et al. 2006; Tangpong et al. 2007). Here, using Seahorse technology, we tested the hypothesis that Dox administration would not alter mitochondrial respiration indexed by OCR in mitochondria isolated from TNFKO mice brain (Figure 5.2). Peripheral Dox-treatment resulted in decreased mitochondrial basal and ATP-linked OCR as well as reduced OCR maximal and reserve capacities in mitochondria isolated from brain of WT mice (red, Figure 5.2b). Strikingly, mitochondrial OCR in brain of TNFKO mice was preserved to the level of that observed in saline-treated mice (purple, Figure 5.2) indicating a central role of TNF-α in the decreased mitochondrial function in brain present following chemotherapy.

H^1-MRS allows non-invasive measurement of neurochemical changes in living brain (Jansen et al. 2006). Previously, we observed changes in the neurochemical profile indexed by MRS in brain following Dox administration (Keeney et al. 2014). Dox-treatment resulted in dramaticly decreased Cho/Cr ratio in hippocampus. The hippocampus is involved in various aspects of learning and memory (Sarkisyan et al. 2009; Clarke et al. 2010; Goulart et al. 2010; Meck et al. 2013). In H^1-MRS, phosphocholine (PCho) and glycerophosphorylcholine (GPC) are major contributors to a cluster of peaks representing choline-containing compounds. Elevated TNF-α has been shown to inhibit synthesis of PtdCho, a major source of PCho and GPC in the brain (Mallampalli et al. 2000; Church et al. 2005). In the current study, bilateral hippocampal H^1-MRS showed profound decreases in the Cho/Cr ratio at 72 h following Dox treatment of WT

mice (Figure 5.3), confirming our earlier study (Keeney et al. 2014). Similar MRS measurements in brain of TNFKO mice showed a significant rebound of the Cho/Cr ratio from levels observed in Dox-treated WT mice (Figure 5.3). Changes in choline-containing compounds on MRS are thought to be associated with membrane turnover (phospholipid synthesis and degradation) (Soares et al. 2009; Bertholdo et al. 2013) and have been attributed to myelin damage following chemotherapy (Ciszkowska-Lyson et al. 2003). The absence of TNF-α afforded protection of the Cho/Cr ration in brain suggesting involvement of TNF-α in neuronal membrane damage and consistent with the oxidative stress indices.

In order to gain further insight into the involvement of TNF-α in the observed effect of Dox on the Cho/Cr ratio indexed by MRS in brain and a potential mechanism of eventual CICI, our laboratory investigated the activities of phospholipases responsible for the cleavage of choline and phosphocholine from PtdCho in the brain in our TNFKO model of cancer chemotherapy. Consistent with our prior studies (Keeney et al. 2014), activities of both PC-PLC and PLD were found to significantly diminished in brain of Dox-treated WT mice at 72 h post-treatment (Figure 5.4). PC-PLC activity remained decreased in brain of Dox-treated TNFKO mice. However, PLD activity was largely preserved in brain of TNFKO mice following Dox treatment providing evidence of TNF-α involvement in Dox-induced inhibition of PLD activity.

In addition to TNF-α-related inhibition of PtdCho biosynthesis (Mallampalli et al. 2000), TNF-α has been linked to decline in phosphatidic acid levels, an intermediate of the PLD pathway (Oprins et al. 2002). PLD activity as well as the mRNA message for PLD have been shown to be increased during cellular differention and decreased during apoptosis (Nakashima et al. 1999; Jang et al. 2008). Enzymatic activity of PLD is seen as essential to cell survival, and structural damage to PLD and decreased PLD activity are thought to promote apoptotic events (Nozawa 2002; Jang et al. 2008).

Taken together, the current study has demonstrated the central role played by TNF-α from the plasma in elevated oxidative stress, mitochondrial dysfunction, and neurochemical markers of membrane damage in brain. Potential therapeutic modulation of elevated TNF-α in plasma conceivably could modulate the cognitive consequences of chemotherapy (CICI). Studies to test this notion are undergoing in our laboratory.

Copyright © Jeriel T. R. Keeney 2013

Chapter 6

Superoxide induces protein oxidation in plasma and TNF-α elevation in macrophage culture: Insights into mechanisms of neurotoxicity caused by Doxorubicin

6.1 Overview of study

Chemotherapy-induced cognitive dysfunction (CICI) is a quality of life-altering consequence of chemotherapy experienced by a large percentage of cancer survivors. Approximately half of FDA-approved anti-cancer drugs are known to produce reactive oxygen species (ROS). Doxorubicin (Dox), primarily used to treat solid tumors often as part of multi-drug chemotherapy regimens, is a prototypical example of an ROS-generating chemotherapeutic agent. Redox cycyling of Dox, in the presence of molecular oxygen, generates the superoxide radical anion (O_2^{-}•). Our group previously demonstrated that Dox, which does not cross the blood brain barrier (BBB), induced oxidative damage to plasma proteins leads to TNF-α elevation in the periphery and, subsequently, in brain following cancer chemotherapy. We hypothesize that such processes play a central role in CICI. The current study tested the notion that O_2^{-}• is responsible for Dox-induced plasma protein oxidation and TNF-α release. Addition of O_2^{-}• as the potassium salt (KO_2) stabilized by the molecular cage of a crown ether (18crown6), to plasma resulted in significantly increased oxidative damage to

proteins, indexed by protein carbonyl (PC) and protein-bound HNE levels. We then adapted this protocol for use in cell culture. Incubation of J774A.1 macrophage culture with 1 and 10 μM KO_2 resulted in dramatically increased levels of TNF-α produced. These results are consistent with our previous results demonstrating increased protein oxidation and lipid peroxidation markers in plasma and subsequent TNF-α elevation following Dox administration *in vivo* and in macrophage culture. These findings, together with our prior results, provide strong evidence that O_2^{-}• is responsible for Dox-induced plasma protein oxidation and TNF-α release.

6.2 Introduction

More than half of the FDA approved anti-cancer drugs are known to cause reactive oxygen species (ROS) production (Chen et al. 2007). Doxorubicin (Dox), a prototypical ROS producing chemotherapeutic agent, generates the reactive superoxide radical anion (O_2^{-}•) via redox cycling (Handa et al. 1975; Bachur et al. 1977; Cummings et al. 1991). Dox is a quinone containing antineoplastic anthracycline used commonly in multi-drug chemotherapy regimens primarily to treat solid tumors (Aluise et al. 2011). Our group has demonstrated that, despite the inability of Dox or its major metabolite to cross the blood-brain barrier (BBB), Dox-induced oxidative damage to plasma proteins *in vivo* induces the elevation of the inflammatory cytokine, tumor necrosis factor-alpha (TNF-α), in the periphery (Joshi et al. 2005; Chen et al. 2007; Aluise et al. 2011).

TNF-α crosses the BBB via receptor mediated endocytosis resulting in central nervous system toxicities including further TNF-α elevation in brain, oxidative and nitrosative damage to key biomolecules, mitochondrial dysfunction, and neuronal death (Joshi et al. 2005; Tangpong et al. 2006; Joshi et al. 2007; Tangpong et al. 2007; Tangpong et al. 2008; Joshi et al. 2010). O_2^{-}• is considered a key reactive radical generated within the cell leading to protein oxidation, lipid peroxidation, and hydrogen peroxide (H_2O_2) and hydroxyl radical (•OH) production that can further damage biomolecules (Gutteridge 1984; McPherson et al. 2002; Halliwell et al. 2007). Additional biochemical complications could occur through pH elevation from the production of hydroxide anion, the other product of H_2O_2 produced via Fenton Chemistry (Fenton 1894; Stadtman et al. 1991). The goal of this study was to determine if O_2^{-}• produces oxidative protein damages in plasma and TNF-α elevation in macrophages similar to that observed following Dox administration in order to further elucidate the mechanism by which Dox may cause chemotherapy-induced cognitive impairment (CICI). Previously, our laboratory demonstrated that Dox-induced oxidation of apolipoprotein A-I (ApoA-I) in J774.A1 macrophage culture led to increased TNF-α production (Aluise et al. 2011).

To accomplish this goal, O_2^{-}• was added to plasma samples from wild-type (WT) mice in the form of potassium superoxide salt (KO_2) in an appropriate solvent including a stabilizer (Valentine et al. 1975; McPherson et al. 2002; Miller 2003), and oxidative stress parameters, protein carbonyl (PC) and protein-bound 4-

hydroxy-2-trans-nonenal (HNE), were measured. PC levels serve as a measure of protein oxidation, while protein-bound HNE, a lipid peroxidation product, indexes damage to lipids (Butterfield et al. 1997; Subramaniam et al. 1997).

The O_2^{-}• protocol we developed for our plasma experiments was then adapted for use in macrophage cell culture to determine if O_2^{-}• induces Dox-like TNF-α consequences. Macrophages are a principal source of TNF-α production *in vivo* (Old 1976; Aluise et al. 2010), and microglial activation in brain following Dox-induced TNF-α elevation leads to the previously mentioned central nervous system toxicities (Aluise et al. 2010; Raffa 2011).

6.3 Methods and Materials

6.3.1 Chemicals

Chemicals, proteases, protease inhibitors, and antibodies used in this study were purchased from Sigma-Aldrich (St. Louis, MO, USA) unless otherwise noted. Precision Plus Protein™ All Blue Standards, BCA reagents, and nitrocellulose membranes were purchased from Bio-RAD (Hercules, CA, USA).

6.3.2 Statistical analysis

All data are presented as mean±SEM. Statistical analyses were performed using ANOVA (and Bonferroni's multiple comparison post-test) followed by a two-tailed Student's *t*-test to make individual comparisons between groups where

appropriate, with $p<0.05$ considered significant. Normality of data sets was tested using the D'Agostino & Pearson omnibus normality test where appropriate.

6.3.3 Animals

Wild-type, male, SKH1 hairless, albino mice (2-3 months old) were purchased from the Jackson Laboratory. Mice were kept under standard conditions housed in the University of Kentucky Animal Facility, and all experimental procedures were approved by the Institutional Animal Care and Use Committee of the University of Kentucky. These animals were euthanized and blood and tissues collected for molecular or biochemical analysis. Whole blood collected by cardiac puncture, was immediately collected in EDTA tubes and plasma immediately separated by centrifugation.

6.3.4 Sample preparation

Protein estimation was performed using the bicinchoninic acid (BCA, Pierce) assay.

Homogenized plasma samples were diluted according to initial protein estimation results using 20 ug sample in isolation buffer [0.32 M sucrose, 2 mM EDTA, 2mM EGTA, and 20mM HEPES pH 7.4 with protease inhibitors, 0.2 mM PMSF, 20ug/mL trypsin inhibitor, 4 µg/ml leupeptin, 4 µg/ml pepstatin A, and 5 µg/ml aprotinin].

6.3.5 Slot blot assay

The slot-blot method was used to determine levels of protein carbonyl and protein-bound HNE in plasma as previously described [37, 38]. For protein carbonyl determination, samples were derivatized with 2,4-dinitrophenylhydrazine (DNPH). For protein-bound HNE, samples were solubilized in Laemmli buffer. Protein (250 ng) from each sample was loaded onto a nitrocellulose membrane in respective wells in a slot-blot apparatus (Bio-Rad) under vacuum. Nitrocellulose membranes were blocked in 3% bovine serum albumin (BSA) in PBS with 0.2% (v/v) Tween-20 for 1.5 h and then incubated in primary antibody (anti-dinitrophenylhydrazone primary or anti-protein-bound HNE, respectively, each produced in rabbit, Sigma-Aldrich) for 2 h, washed three times in PBS with 0.2% (v/v) Tween-20 and then incubated for 1 h with secondary antibody (goat anti-rabbit secondary linked to alkaline phosphatase). Nitrocellulose membranes were developed with 5-bromo-4-chloro-3-indolyl-phosphate (BCIP) dipotassium and nitro blue tetrazolium (NBT) chloride in alkaline phosphatase activity (ALP) buffer, dried, and scanned for analysis. Image analysis was performed using Scion Image (Scion Corporation, Frederick, MD).

6.3.6 Solvent selection and potassium superoxide solution preparation

KO_2 is a yellow solid that reacts readily with water and would decompose if exposed to water vapor or carbon dioxide in air. To avoid this, a saturated solution of KO_2 was prepared fresh, according to the method previously

described (Valentine et al. 1975; McPherson et al. 2002; Miller 2003), in a solvent of anhydrous dimethyl sulfoxide (DMSO) containing 200mM crown ether (18crown6) to aid in solubility. To the prepared solvent, excess KO_2 was added and the KO_2 concentration estimated by UV-vis absorbance and using Beer's law (Kim et al. 1979; Miller 2003). A saturated solution of KO_2 was approximately 250 µM under the stated conditions. Serial dilutions of this saturated solution were performed using the DMSO+18crown6 solvent to obtain the desired $O_2^{-}\bullet$ concentrations.

6.3.7 Plasma oxidation with potassium superoxide

KO_2 was added to plasma from WT mice and incubated at 37°C for 0, 15, 30, and 90 min according to Table 6.1. Concentrations of 0, 0.1, 1.0, or 10 µM KO_2 were added to plasma to broadly encompass Dox concentrations used in previous studies. The solvent, DMSO and 18crown6, was added to all control incubations.

Table 6.1. Superoxide sample treatment. Plasma samples from 2-3 months old WT, male, SKH1 hairless, albino mice (purchased from the Jackson Laboratory) were treated with 0, 0.1, 1.0, or 10 µM KO_2 and incubated for 0, 15, 30, and 90 min.

Tube#	Incubation Time(min)	KO_2 conc to add (uM)	Plasma Volume(uL)	Solvent Vol (uL) (used for KO_2)
1	90	10	48	2
2	90	1.0	48	2
3	90	0.1	48	2
4	30	10	48	2
5	30	1.0	48	2
6	30	0.1	48	2
7	15	10	48	2
8	15	1.0	48	2
9	15	0.1	48	2
10	0	0 (control)	48	2

6.3.8 Macrophage stimulation with potassium superoxide

Cell culture experiments were carried out using mouse BALB/c monocyte macrophage cell line (J774A.1) collected form blood. The mouse macrophage cell line J774A.1 (American Type Culture Collection) was cultured in Dulbecco's

modified Eagle's medium supplemented with 10% (v/v) fetal bovine serum, streptomycin (100µg/ml), and penicillin (100U/ml). All cultures were incubated at 37 °C in a humidified atmosphere with 5% CO_2. J774A.1 macrophage cells were plated at a density of 5×10^5 cells/well in 48-well plates. Potassium superoxide (KO_2) was prepared as previously described. Lipopolysaccharide (LPS; 1 µg/ml), KO_2 (0.1µM; 1µM; 10µM) was added and the cells were incubated for 24 h. The supernatant was collected and levels of TNF-α (pg/ml) were determined with a specific ELISA kit for mouse TNF-α (R&D Systems). Macrophage culture experiments were performed by the D.K. St. Clair laboratory, Graduate Center for Toxicology, Department of Radiation Medicine, Markey Cancer Center, University of Kentucky.

<u>Experimental design</u>

J774A.1
J774A.1+ Lipopolysaccharide (LPS) (1 µg/ml) – 24hours incubation
J774A.1+ DMSO+ Crown ether
J774A.1+KO_2 (0 µM) – 24hours incubation
J774A.1+KO_2 (0.1 µM) – 24hours incubation
J774A.1+KO_2 (10 µM) – 24hours incubation

Figure 6.1. Experimental design: J774.A1 macrophage culture treatment with potassium superoxide. J774.A1 macrophages were seeded onto a 48-well plate at 5×10^5 cells/well and allowed to grow overnight under standard culture conditions. Preincubation of solvent, lipopolysaccharide (LPS; 1 µg/ml), KO_2 (0.1µM; 1µM; 10µM) for 1 h was performed before their addition to J774.A1 macrophages. Supernatants were collected and analyzed for TNF-α concentration.

6.4 Results

6.4.1 Protocol development

A variety of solvents and combinations were explored to make a stable solution of KO_2. KO_2 releases O_2^{-}• upon addition to an aqueous environment (McPherson et al. 2002). O_2^{-}• then reacted rapidly with water present in any solvent combination forming H_2O_2. The reaction of KO_2 with water was more rapid and vigorous than expected. In fact, KO_2 reacted with water vapor in the air during any attempt at weighing KO_2, contrary to some methods (Olojo et al. 2005). Transition metals are known to influence the reactivity of dioxygen radicals including those present in O_2^{-}• and H_2O_2 (Aust et al. 1985) . Chelex removal of metal ions did not prevent this problem (Halliwell et al. 1986), and prior addition of catalase to the solvent only accelerated the reaction of KO_2 with water presumably by reacting away the formed H_2O_2 and shifting the reaction equilibrium toward product (Stadtman et al. 1991; Lardinois 1995; Aksenov et al. 1998). This prompted the pursuit of a suitable anhydrous solvent for KO_2. KO_2 is slightly soluble in anhydrous DMSO (Weber et al. 1977). A crown ether, 18crown6, was used to enhance solubility and stability (Valentine et al. 1975).

6.4.2 Plasma oxidation from potassium superoxide

Plasma samples were treated with 0, 0.1, 1.0, or 10 µM KO_2 for 0, 15, 30, and 90 min and analyzed via slot blot to determine relative levels of PC and protein-

bound HNE as measures of protein oxidation and lipid peroxidation, respectively (Butterfield et al. 1997; Subramaniam et al. 1997). PC damage to protein in plasma following incubation with KO_2 was rapid. After 15 min incubation at 37°C, significant increases in PC were observed at 0.1, 1, and 10 µM KO_2 (Figure 6.2a, ***p<0.005, ***p<0.005, and **p<0.01, respectively). At 10 µM KO_2, PC levels for each successive time point were significantly elevated over the previous one indicated by Bonferroni's Multiple Comparison Test. Significant increases in PC in plasma were also observed at each concentration, 0.1, 1, and 10 µM, of KO_2 measured after 15 min incubation at 37°C (Figure 6.2b, ***p<0.005, ***p<0.005, and **p<0.01, respectively). Similar experiments were performed to assess KO_2-induced protein-bound HNE in plasma. The higher concentrations of KO_2 and longer incubation were required to reach significant increases in protein-bound HNE following KO_2 addition (Figure 6.2c). Decisions for moving forward were based on these preliminary KO_2 dose-response results with varied incubation times.

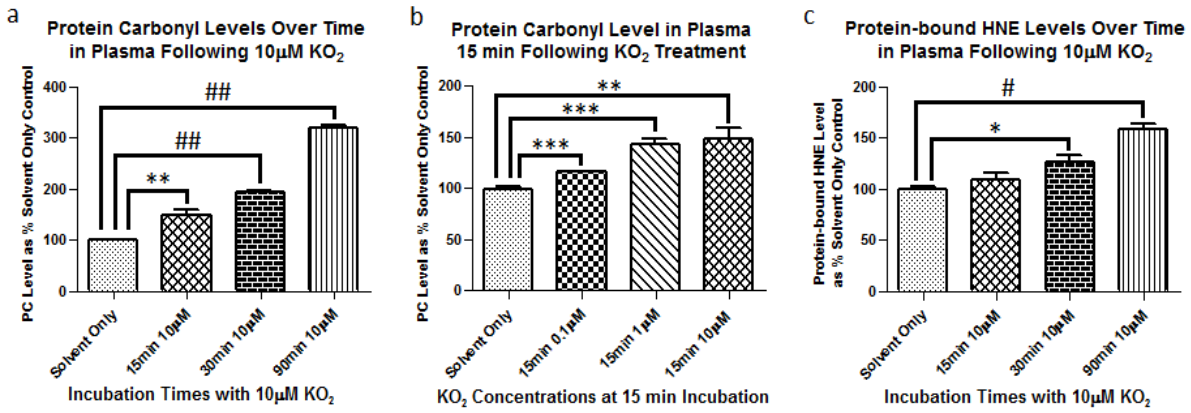

Figure. 6.2. PC and protein-bound HNE levels in plasma after treatment with potassium superoxide. Protein carbonyl (PC) and protein-bound HNE (HNE) are measures of protein oxidation and lipid peroxidation. (a) PC levels were assessed at 15, 30, and 90 min incubations with 10 µM KO_2 at 37°C. All incubation times tested at 10 µM KO_2 and 37°C , 15, 30, and 90 min, resulted in significantly increased PC compared to solvent alone (**p<0.01, ##p<0.0001, ##p<0.0001, respectively). PC for each successive time point at 10 µM KO_2 was significantly elevated over the previous one indicated by Bonferroni's Multiple Comparison Test. (b), Significant increases in PC were observed at 0.1, 1, and 10 µM KO_2 After 15 min incubation at 37°C (***p<0.005, ***p<0.005, and **p<0.01, respectively). (c) Protein-bound HNE was significantly elevated after 30 and 90 min incubations with 10 µM KO_2 at 37°C (*p<0.05, #p<0.001, respectively) but not at 15 min incubation or lower KO_2 concentrations.

6.4.3 Superoxide induces TNF-α elevation in macrophage culture similar to that seen following doxorubicin administration

Previously, we have reported TNF-α elevation in plasma following Dox treatment with O_2^{-}• produced through redox cycling of Dox as the likely cause (Tangpong et al. 2006; Aluise et al. 2011). Here, we test our hypothesis that O_2^{-}•, administered as KO_2, will lead to TNF-α elevation in macrophage culture similar to that observed following Dox administration (Aluise et al. 2011). Significantly increased TNF-α elevation in J774.A1 macrophage culture after incubation with KO_2 for 24 h was observed. TNF-α was increased in these cell lines following incubation

with 1 and 10 µM KO_2 (Figure 6.3; p<*** 0.0001). Incubation of these macrophages with the 10 µM KO_2 concentration resulted in TNF-α greater than treatment of the cells with lipopolysaccharide (LPS; 1 µg/ml), a known initiator of TNF-α transcription via nuclear factor κ-light-chain enhancer of activated B cells (NF-κB) (Schreck et al. 1992; Griscavage et al. 1996; Chandel et al. 2000; Baker et al. 2011; Keeney et al. 2013).

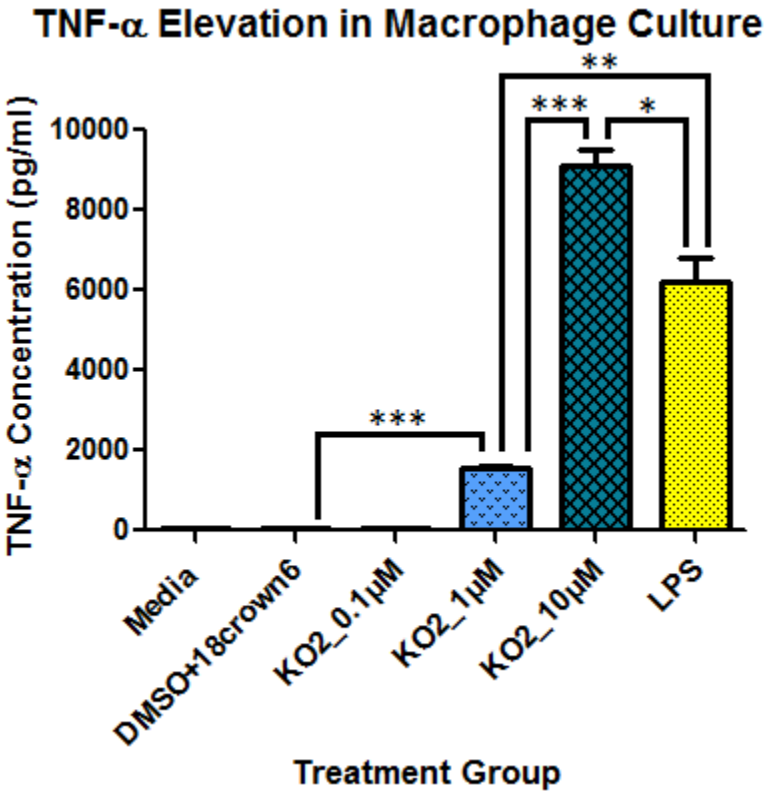

Figure 6.3. TNF-α levels in macrophage culture after treatment with potassium superoxide. Superoxide (O_2^{-}•) induces TNF-α production in J774.A1 macrophages. J774.A1 macrophages were seeded onto a 48-well plate at 5×10^5 cells/well and allowed to grow overnight. Preincubation of solvent, lipopolysaccharide (LPS; 1 µg/ml), KO_2 (0.1µM; 1µM; 10µM) for 1 h was

performed before their addition to J774.A1 macrophages. Supernatants were collected and analyzed for TNF-α concentration. Values are means±SEM (n=3). (*$p<0.05$, **$p<0.005$, ***$p<0.0001$ compared to solvent alone). One-way ANOVA ($p<0.0001$) with Bonferroni's Multiple Comparison Test also demonstrated these significant differences between groups. Macrophage culture experiments were performed by the D.K. St. Clair laboratory, Graduate Center for Toxicology, Department of Radiation Medicine, Markey Cancer Center, University of Kentucky.

6.5 Discussion

Prior studies by our laboratory have implicated O_2^{-}•, produced *in vivo* via the redox cycling of the chemotherapeutic agent Dox, in increased oxidative damage to plasma proteins, elevation of TNF-α in the periphery, followed by transfer of TNF-α to brain and further TNF-α elevation in the parenchyma, subsequent CNS toxicity including mitochondrial dysfunction, neuronal death, and chemotherapy-induced cognitive impairment (CICI) (Joshi et al. 2005; Tangpong et al. 2006; Chen et al. 2007; Joshi et al. 2007; Tangpong et al. 2007; Tangpong et al. 2008; Aluise et al. 2010; Joshi et al. 2010; Aluise et al. 2011; Keeney et al. 2014). The quinone moiety within the molecular structure of Dox cycles between the quinone and semi-quinone, producing superoxide free radical from molecular oxygen as it cycles back to the quinone (Handa et al. 1975; Bachur et al. 1977; Cummings et al. 1991; Aluise et al. 2010; Aluise et al. 2011). The current study was undertaken to test the plausibility of our hypothesis that O_2^{-}• from Dox is, in fact,

responsible for oxidative protein damage, TNF-α elevation, and cognitive consequences observed following chemotherapy with ROS-producing anti-cancer drugs, like Dox, that do not cross the BBB but result in these unwanted clinical signs and symptoms.

In the current study, superoxide caused oxidative damage to plasma proteins *in vitro* rapidly and at small concentrations of KO_2, similar to damage caused by doxorubicin. All incubation times tested, 15, 30, and 90 min, resulted in significantly increased plasma protein oxidative damage as indicated by PC elevation with PC at each successive time point significantly increased over the previous one (Figure 6.2a) (Butterfield et al. 1997). Significant PC elevation was observed in plasma even at the lowest concentrations of KO_2 tested ($p<0.005$, Figure 6.2b). Evidence of lipid damage was also found to be elevated in KO_2-treated plasma in the form of protein-bound HNE, a product of lipid peroxidation (Subramaniam et al. 1997). Higher concentrations of KO_2 and longer incubation times tested were required to reach significant increases in protein-bound HNE following KO_2 addition (Figure 6.2c) which might reflect the negative charge of O_2^{-}• being slow to enter a hydrophobic environment.

These results demonstrate that O_2^{-}•, when added to plasma in the form of KO_2 salt and incubated at physiologic 37°C, results protein oxidation in plasma and TNF-α elevation in macrophage culture similar to that observed following Dox administration in vivo. Together, these results are compelling evidence for O_2^{-}•

production as a result of Dox administration as the causative agent in the neurotoxicity associated with Dox and provides useful insights into the mechanism of CICI caused by cancer chemotherapy with ROS-producing chemotherapeutic agents like Dox.

Acknowledgements

The authors gratefully acknowledge insights from Dr. A.F. Miller, University of Kentucky, Department of Chemistry for her knowledge and insights into working with potassium superoxide. This work was supported in part by a grant from NIH [CA-148341].

Copyright © Jeriel T. R. Keeney 2013

CHAPTER 7

CONCLUSIONS AND FUTURE STUDIES

7.1 Conclusions

The works presented in this dissertation provide insights into the mechanisms of chemotherapy-induced cognitive impairment (CICI or “Chemobrain”) and take steps toward outlining a preventive strategy. These studies demonstrate the roles that oxidation of plasma proteins, like apolipoprotein A-I (ApoA-I), and elevation of the inflammatory cytokine, tumor necrosis factor-alpha (TNF-α), play in the neurotoxicity and cognitive impairment that occurs as a consequence of chemotherapy.

Chemotherapy-induced cognitive impairment (CICI) is now widely recognized as a real and too common complication of cancer chemotherapy experienced by an ever growing number of cancer survivors. Approximately fifty percent of existing FDA-approved anti-cancer drugs generate reactive oxygen species (ROS). Doxorubicin (Dox) is a prototypical ROS-generating chemotherapeutic agent used to treat solid tumors often as part of multi-drug chemotherapeutic regimens. Dox produces the reactive superoxide radical anion (O_2^{-}•) *in vivo* through redox cycling between the quinone and semi-quinone forms within the Dox molecular structure. Dox treatment results in oxidation of plasma proteins, including ApoA-I,

leading to TNF-α-mediated oxidative stress in plasma and brain. TNF-α elevation in brain leads to further central nervous system toxicity including mitochondrial dysfunction, neuronal death, and cognitive impairment. Co-administration of the antioxidant drug, 2-mercaptoethane sulfonate sodium (MESNA), prevents Dox-induced protein oxidation and subsequent TNF-α elevation in plasma without interfering with the cancer-killing ability of Dox.

In studies presented in this dissertation, we measured oxidative stress in both brain and plasma of Dox-treated mice both with and without MESNA. MESNA ameliorated Dox-induced oxidative protein damage in plasma, confirming our prior studies, and in a new finding led to decreased oxidative stress in brain. This study also provides further functional and biochemical evidence of the mechanisms of CICI. Using novel object recognition (NOR), we demonstrated the Dox administration resulted in memory deficits, effects that were rescued by MESNA. Using hydrogen magnetic resonance imaging spectroscopy (H^1-MRS) techniques, we demonstrated that Dox administration led to a dramatic decrease in choline (phosphocholine)/creatine (Cho/Cr) ratios in the hippocampus in mice. To better elucidate a potential mechanism for this MRS observation, we tested the activities of the phospholipase enzymes known to act on phosphatidylcholine (PtdCho), a key component of phospholipid membranes and a source of choline for the neurotransmitter, acetylcholine (ACh). The activities of both phosphatidylcholine-specific phospholipase C (PC-PLC) and phospholipase D were severely diminished following Dox administration. The activity of PC-PLC

was preserved when MESNA was co-administered with Dox; however, PLD activity was not protected. This study is the first to demonstrate the protective effects of MESNA on Dox-related protein oxidation, cognitive decline, phosphocholine levels, and PC-PLC activity in the brain.

Further, we demonstrate that Dox-induced oxidative stress is ameliorated and mitochondrial oxygen consumption rate (OCR) is preserved in brain of TNF-α null (TNFKO) mice. Further, we show protection against Dox-related decreases in the Cho/Cr ratio determined by magnetic resonance spectroscopy (MRS) and phospholipase D (PLD) activity of TNFKO mouse brain. This study demonstrates that, in the absence of TNF-α, MRS-indexed Cho/Cr ratio, PLD activity, and mitochondrial oxygen consumption are preserved in brain, and markers of oxidative stress are reduced. Together with results from our previous studies, these results provide strong evidence that TNF-α is responsible for chemotherapy-induced cognitive impairment (CICI), particularly by anti-cancer drugs like Dox that do not cross the BBB.

Additional studies presented here tested the notion that O_2^{-}• is responsible for Dox-induced plasma protein oxidation and TNF-α release. Addition of O_2^{-}• as the potassium salt (KO_2) to plasma resulted in significantly increased oxidative damage to proteins, indexed by protein carbonyl (PC) and protein-bound HNE levels. We then adapted this protocol for use in cell culture. 24 h incubation of J774A.1 macrophage culture with 1 and 10 μM KO_2 resulted in dramatically

increased levels of TNF-α produced. These results are consistent with our previous results demonstrating increased protein oxidation and lipid peroxidation markers in plasma and subsequent TNF-α elevation following Dox administration *in vivo* and in macrophage culture. These findings, together with our prior results, provide strong evidence that O_2^{-}• is responsible for Dox-induced plasma protein oxidation and TNF-α release. These results have important implications for potential interventions to modulate the cognitive consequences of chemotherapy experienced by a large percentage of cancer survivors.

The work presented in this dissertation examined the mechanisms of cognitive impairment that occur following chemotherapy in a mouse model of CICI and probed some potential points of intervention. More specifically, this work elucidated further the functional and biochemical mechanisms by which chemotherapy-induced cognitive impairment occurs as a result of doxorubicin (Dox) administration, the central role of tumor necrosis factor-alpha (TNF-α) in these mechanisms, and the protective effects of the antioxidant drug, MESNA, against Dox-induced neurotoxic effects. A large percentage of current anti-cancer drugs, including Dox, result in increased levels of reactive oxygen species (ROS). Despite the inability of Dox to cross the blood-brain barrier, mounting evidence demonstrates CNS toxicity as a result of Dox treatment.

Results of oxidative stress analyses confirmed the presence of increased oxidative damage to proteins in both plasma and brain following Dox treatment.

These data show that co-administration of MESNA not only ameliorated Dox-induced oxidative protein damage in plasma but also led to decreased oxidative stress in brain. Using novel object recognition (NOR), we demonstrated the Dox administration resulted in memory deficits, effects that were fully rescued by MESNA. Further explorations of the mechanisms of cognitive deficit led us to measure Dox-related changes in the neurochemical profile using hydrogen magnetic resonance imaging spectroscopy (H^1-MRS) techniques. Unilateral and bilateral hippocampal MRS scans in mice revealed a dramatic decrease in the choline(phosphocholine)/creatine ratios (Cho/Cr) following Dox treatment. MESNA only provided a slight, but not significant, return in these values. So, why do we see a decrease in choline-containing compounds in the brain of subjects with CICI? The answer may lie in the choline metabolic pathways being altered subsequent to chemotherapy. To better elucidate a potential mechanism for this MRS observation, we tested the activities of the phospholipase enzymes known to act on phosphatidylcholine (PtdCho), a key component of phospholipid membranes and a source of choline for the neurotransmitter, acetylcholine (ACh). The activities of both phosphatidylcholine-specific phospholipase C (PC-PLC) and phospholipase D were severely diminished following Dox administration. MESNA fully protected PC-PLC activity against Dox-related decrease, but PLD activity was not protected. These studies are the first to demonstrate the protective effects of MESNA on Dox-related protein oxidation, cognitive decline, phosphocholine levels, and PC-PLC activity in the brain.

Elevation of TNF-α occurs both in the periphery and in the brain following peripheral Dox administration (Tangpong et al. 2006). In this dissertation research, oxidative stress measures revealed, in TNF-α knockout (TNFKO) mice, Dox-related oxidative stress still exists in plasma as a direct consequence of redox cycling but is absent in brain. This is strong evidence that TNF-α is a major moderator of oxidative damage in brain following treatment with brain impenetrable-Dox. Using Seahorse technology, we demonstrated that mitochondrial oxygen consumption rate (OCR) in brain is severely diminished as a result of Dox administration. Strikingly, OCR patterns in mitochondria from brain of Dox-treated TNFKO mice is preserved to the level of that observed in saline treated mice. H^1-MRS results show a partial but significant protection the Cho/Cr ratio in living brain of Dox-treated TNFKO mice compared to saline-treated mice. Additionally, TNF-α is known to inhibit phosphatidylcholine (PtdCho) biosynthesis (Mallampalli et al. 2000). TNF-α inhibition of PtdCho synthesis may result in decreased PCho availability. Since ceramide couples with PCho to produce sphingomyelin (Siegel 2006), decreased PCho would lead to elevated ceramide. The latter is a known inducer of apoptosis (Geilen et al. 1997; Qin et al. 1998; Car et al. 2012; Wang et al. 2012), and we previously showed elevated apoptosis in brain of Dox-treated mice (Tangpong et al. 2007). Extracellular TNF-α binds and activates two main receptors, TNFR1 and TNFR2, that are responsible for mediating the intracellular cytokine activity. TNFR1, also known as the death-receptor, has an intracellular death domain (DD) known as TRADD (Hsu et al. 1995). Ceramide potentiates rapidly TNF-α-induced TRADD

recruitment and initiator caspase, caspase 8, activity. TNFR1 activation stimulates ceramide production and its pro-apoptotic pathways (Rath et al. 1999; De Nadai et al. 2000). Dox-induced decreased PC-PLC and PLD activities may result in dysregulation of cell survival and apoptosis pathways that involve PC-PLC and decreases in choline available for ACh synthesis via PLD.

PLD activity was fully preserved in the face of Dox treatment in brain of TNFKO mice. Conceivably, preservation of PtdCho production and PLD activity in the absence of TNF-α would maintain the Cho levels available for synthesis of ACh. The loss of function of ACh as an inhibitory neurotransmitter that lowers heart rate may, in part, explain some of the cardiac effects of Dox. These studies demonstrate that, in the absence of TNF-α, MRS-indexed Cho/Cr ratio, PLD activity, and mitochondrial oxygen consumption are preserved in brain, and markers of oxidative stress are reduced. Together, these results provide compelling evidence for the central role TNF-α in chemotherapy-induced mitochondrial and neuronal damage and the mechanisms of CICI.

There are currently millions of cancer survivors. Thankfully, that number continues to grow. A large percentage of them experience cognitive symptoms following chemotherapy. Approximately half of the FDA-approved anti-cancer drugs are known to generate ROS. As with Dox, the extracellular ROS production appears to be independent of the cancer-killing ability of the drug. Preventing plasma protein oxidation and resultant TNF-α-related cardiac and

neurotoxic consequences may allow cancer patients to become cancer free without compromising quality of life.

7.2 Future studies

Based on the results in this dissertation, the following experiments may warrant future investigation:

1. Due to the central involvement of ApoA-I and TNF-α in the mechanism of CICI, further examination of the mechanisms of their involvement are warranted. Unaltered ApoA-I interacts with the ATP-binding membrane cassette transporter A1 (ABCA1) involved in cholesterol transport, through the JAK2/STAT3 pathways, leads to production of tristetraprolin (TTP). TTP destabilizes the mRNA message for TNF-α. Examination of the impact of co-administration of MESNA and in TNFKO models on ABCA1 and TTP involvement in CICI following Dox administration would further elucidate the mechanism of CICI.
2. HNE preferentially binds certain amino acids (Cys, Lys, and His), thereby altering protein structure and function. ApoA-I contains several such sites where HNE has been shown to bind *in vitro*. Examination of HNE binding sites on ApoA-I following Dox administration *in vivo* would provide specific insights into the inability of oxidized ApoA-I to inhibit TNF-α related consequences.
3. More insights into definitive diagnosis, progression, and prevention of CICI may be elucidated using MRS and neuroimaging techniques. Gray and

white matter status should be examined following Dox treatment in TNFKO model and with co-administration of MESNA. These techniques non-invasively provide information of the CNS status in living systems. Ultimately, the author of this dissertation would like to see all chemotherapy patients examined for gray and white matter changes and MRS-indexed neurochemical profile status at every phase of treatment. Of course, such an appeal would be ridiculously expensive.

4. H^1-MRS does not currently allow resolution of the choline cluster of peaks to allow identification of individual choline-containing compounds that are changing following Dox administration to be identified. More precise methods do exist. P^{31}-MRS may allow these peaks to be resolved and individual neurochemical species to be identified.
5. Based on MESNA protection of PC-PLC activity and protection of PLD activity in TNFKO in mouse brain, further examination of the impact of chemotherapy on choline metabolism including ACh production and ceramide and sphingomyelin levels is warranted. Perhaps, a combination of MESNA and anti-TNF antibody, administered during chemotherapy may completely preserve choline metabolism.
6. VitD deficits are common, especially with advanced age. As people age, they tend to become more sedentary spending less time outside and nutritional status declines further exacerbating VitD deficiency. More studies are necessary to determine the effects VitD deficiency has on

cognition and the biochemical consequences of such deficiency. Further protein activity and gene studies may provide more insight.

Copyright © Jeriel T. R. Keeney 2013

APPENDIX A

Dietary Vitamin D Deficiency in Rats from Middle- to Old-age Leads to Elevated Tyrosine Nitration and Proteomics Changes in Levels of Key Proteins in Brain: Implications for Low Vitamin D-dependent Age-Related Cognitive Decline

A.1 Overview of study

In addition to the well-known effects of vitamin D (VitD) in maintaining bone health, there is increasing appreciation that this vitamin may serve important roles in other organs and tissues, including the brain. Given that VitD deficiency is especially widespread among the elderly, it is important to understand how the range of serum VitD levels that mimic those found in humans (from low to high) affects the brain during aging from middle-age to old-age. To address this issue, twenty-seven male F344 rats were split into three groups and fed isocaloric diets containing low (100 IU/kg food), control (1000 IU/kg food), or high (10000 IU/kg food) VitD beginning at middle-age (12 months) and continued for a period of 4-5months.We compared the effects of these dietary VitD manipulations on oxidative and nitrosative stress measures in posterior brain cortices. The low VitD group showed global elevation of 3-nitrotyrosine (3-NT) compared to control

and high VitD treated groups. Further investigation showed that this elevation may involve dysregulation of the nuclear factor kappa-light-chain-enhancer of activated B cells (NF-κB) pathway and NF-κB mediated transcription of inducible nitric oxide synthase (iNOS) as indicated by translocation of NF-κB to the nucleus and elevation of iNOS levels. Proteomic techniques were used to provide insights into potential mechanisms underlying these effects. Several brain proteins were found at significantly elevated levels in low VitD group compared to the control and high VitD groups. Three of these proteins, 6-phosphofructokinase, triosephosphate isomerase, and pyruvate kinase, are involved directly in glycolysis. Two others, peroxiredoxin-3 and DJ-1/PARK7, have peroxidase activity and are found in mitochondria. Peptidyl-prolylcis-trans isomerase A (PPIA or cyclophilin A) has been shown to have multiple roles including protein folding, regulation of protein kinases and phosphatases, immunoregulation, cell signaling, and redox status. Together, these results suggest that dietary VitD deficiency contributes to significant nitrosative stress in brain and may promote cognitive decline in middle-aged and elderly adults.

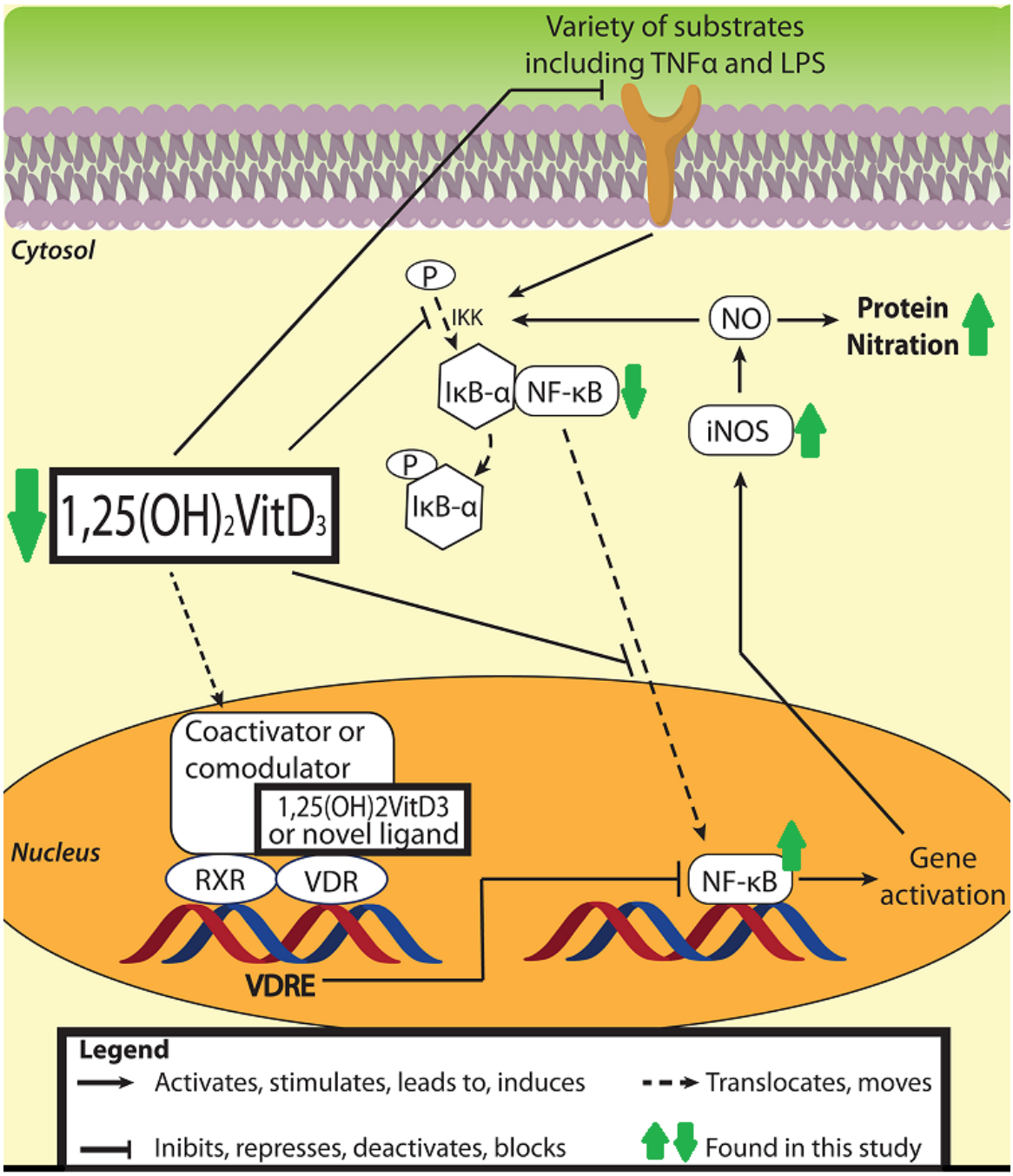

Graphical Abstract: The figure depicts a potential mechanism for the protein nitration regulatory effects of VitD in brain and the consequences of VitD deficiency. Results obtained in this study supporting this mechanism are marked with wide green arrows, up arrows designating a found increase and down arrows designating a found decrease.

Figure A.1. Graphical Abstract, Vitamin D deficiency study. Used by permission from Elsevier Scientific Publishers, Inc.

A.2 Introduction

The steroid hormone Vitamin D (VitD) can be produced by the body or obtained through the diet. VitD is synthesized in the skin from the cholesterol precursor, 7-dehydrocholesterol and is converted to cholecalciferol (VitD3) upon exposure to sunlight (Holick 2004). VitD3 can also be obtained through several dietary sources and is transported in the blood via vitamin D-binding protein. In the liver, VitD3 is converted to calcidiol, 25-hydroxy vitamin D (25-OH VitD) followed by further conversion to calcitriol, 1α, 25-dihydroxy vitamin D (1α, 25-$(OH)_2$VitD) primarily in the kidneys where it helps to regulate calcium homeostasis(Nezbedova et al. 2004; Brewer et al. 2006). VitD also plays roles in autoimmunity (Cantorna et al. 2004), mental health (Brewer et al. 2001; Brewer et al. 2006; Fernandes de Abreu et al. 2009; Farid et al. 2012; Mizwicki et al. 2013), and inhibition of tumor growth through reductions in proliferation and angiogenesis(Deeb et al. 2007; Holick 2008; Holick et al. 2008; Holick 2012).

VitD deficiency has long been associated with osteoporosis, brittle bones, and muscle weakness, but recently low levels of VitD have been linked to increased overall mortality (Semba et al. 2009; Zittermann et al. 2009). VitD status is typically assessed using serum concentration of 25-OH VitD because it is longer lived than the biologically active 1α, 25-$(OH)_2$VitD (Weaver et al. 2004; Ginter et al. 2009; Zittermann et al. 2009). VitD deficiency is highly prevalent in Europe and North America (Holick 2004; Vieth et al. 2007) with the elderly particularly at risk (Holick 2006; Holick et al. 2008; Zittermann et al. 2009; Holick 2010;

Llewellyn et al. 2011). Current estimates suggest that as many as 40-100% of the elderly populations in these areas are VitD deficient (Holick 2007). Poor diet and lower exposure to UV-B from the sun limits VitD synthesis in the skin and an age-related decrease in the VitD synthesis machinery may contribute to the observed lower VitD levels (Ginter et al. 2009).

The elderly represent those at greatest risk of age-related cognitive decline and neurodegenerative disorders (Poon et al. 2006). Recent retrospective studies on elderly human subjects provide correlative evidence that those with VitD deficiency have a much higher incidence of cognitive impairment than those with normal VitD levels (Przybelski et al. 2007; Llewellyn et al. 2009). Thus, it appears that VitD deficiency may accelerate cognitive decline in aging (Llewellyn et al. 2010). A recent meta-analysis also shows that patients with Alzheimer disease (AD)typically have lower serum concentrations of VitD (Annweiler et al. 2013). AD is associated with defects in amyloid-β (Aβ) processing and an upregulation of inflammatory cytokines and nuclear factor kappa-light-chain-enhancer of activated B cells (NF-κB) (Mizwicki et al. 2013). Interestingly, 1α,25$(OH)_2$VitD helped to reverse soluble Aβ and inflammatory issues (Mizwicki et al. 2013).In addition to these actions, VitD is neuroprotective against Ca^{2+}-mediated excitotoxicity, reduces biomarkers of brain aging associated with Ca^{2+}dyshomeostasis(Brewer et al. 2001; Brewer et al. 2006), and helps to regulate glutathione levels, a primary antioxidant in the brain, by modulating γ-glutamyltranspeptidase activity(Garcion et al. 1999). VitD also prevents onset of

autoimmune demyelination in animal models of multiple sclerosis (Lemire et al. 1991; Garcion et al. 2002).

Here, we manipulated serum VitD status by dietary supplementation with low, moderate/control or high levels of VitD in order to identify changes in the VitD-dependent proteome in the brains of rats from middle- to old-age. Prior studies have shown that cognitively impaired subjects have significant levels of mitochondrial dysfunction and oxidative protein damage. In particular, nitration of protein resident tyrosine residues is a common marker observed in brain of cognitively impaired subjects (Beckman 1996; Souza et al. 2001; Castegna et al. 2003; Butterfield et al. 2007; Feeney et al. 2012). Therefore, we tested the hypothesis that manipulating serum VitD levels would alter protein nitration and key protein markers of mitochondrial function. Our results identify several possible targets of VitD action that may mechanistically link circulating VitD levels with risk forage-related cognitive decline.

A.3 Methods and Materials

A.3.1 Chemicals

Criterion precast polyacrylamide gels, tris-glycine-SDS (TGS) and MES electrophoresis running buffers, ReadyStrip™ IPG strips, mineral oil, Precision Plus Protein™ All Blue Standards, SYPRO Ruby® Protein Stain, nitrocellulose

membranes, dithiothreitol (DTT), iodoacetamide (IA), Biolytes, and urea were purchased from Bio-RAD (Hercules, CA, USA). Chemicals, proteases, protease inhibitors, and antibodies used in this study were purchased from Sigma-Aldrich (St. Louis, MO, USA) unless otherwise noted.

A.3.2 Animals

All animal studies were approved by the University of Kentucky Institutional Animal Care and Use Committee and followed NIH Guidelines for the Care and Use of Laboratory Animals. Middle-aged (12 month old) male F344 rats, a standard model for studies of brain aging, were obtained from the National Institutes on Aging rodent colony. Four-to five-month dietary manipulation of VitD was carried outusing cholecalciferol (VitD3) added to an isocaloric diet in the following amounts (based on pilot studies intended to mimic the range of human levels): control VitD = 1000 IU/kg food, low VitD = 100 IU/kg food, and high VitD = 10,000 IU/kg food with nine animals in each group (Table A.1). Animals were weighed and food intake measured 2-3 times per week. Serum 25-OH VitD levels were monitored as a measure of circulating VitD. Dietary manipulation of VitD resulted in different serum levels of VitD. Upon conclusion of the long-term treatment, animals were euthanatized and samples isolated from the right posterior corticalarea. Samples were then stored at −80°C until needed for oxidative stress and expression proteomics determinations (Robinson et al. 2011; Butterfield et al. 2012).

Table A.1. VitD dietary manipulation [*p < 0.0001 (one-way ANOVA)].

	Control	**Low**	**High**
Weight at 12 months	480g	485g	475g
Weight at 18 months	538g	565g	548g
Daily Food Intake	16.5 g/day	16.4 g/day	15.9 g/day
Daily intake of Cholecalciferol	16.5 IU/day	1.64 IU/day	159 IU/day
***Serum levels of 25(OH)VitD**	12.7 ng/mL	5.8 ng/mL	31.7 ng/mL

A.3.3 Sample preparation

Protein estimation was performed using the bicinchoninic acid (BCA, Pierce) assay. Homogenized cortex samples were diluted according to initial protein estimation results 20 µg sample in 140 µL of media-I buffer [0.32 M sucrose, 0.6 mM $MgCl_2$, and 0.125 M Tris pH 8.0 with protease inhibitors, 4 µg/ml leupeptin, 4 µg/ml pepstatin A, and 5 µg/ml aprotinin].

A.3.4 Slot blot assay

The slot-blot method was used to determine levels of protein 3-nitrotyrosine (3-NT) in brain as previously described (Sultana et al. 2008; Aluise et al. 2011). For 3-NT determination, samples were solubilized in Laemmli buffer. Protein (250 ng) from each sample was loaded onto a nitrocellulose membrane in respective wells in a slot-blot apparatus (Bio-Rad) under vacuum. Membranes were blocked in 3% bovine serum albumin (BSA) in PBS with 0.2% (v/v) Tween-20 for 1.5 h and then incubated in primary antibody (anti-nitrotyrosine produced in rabbit, Sigma-Aldrich) for 2 h, washed three times in PBS with 0.2% (v/v) Tween-20 and then incubated for 1 h with secondary antibody (goat anti-rabbit secondary linked to alkaline phosphatase). Membranes were developed with 5-bromo-4-chloro-3-indolyl-phosphate (BCIP) dipotassium and nitro blue tetrazolium (NBT) chloride in alkaline phosphatase activity (ALP) buffer, dried, and scanned for analysis. Image analysis was performed using Scion Image (Scion Corporation, Frederick, MD). A negative control for nitration was performed by reducing nitrotyrosine to aminotyrosine according to the method of Miyagi and Crabb *et al*. (Miyagi et al. 2002) as follows. One replicate membrane was treated with 10 mM sodium dithionite in 50 mM pyridine-acetate buffer (pH=5.0) for 1h at room temperature, rinsed thoroughly with nanopure water, and developed as above. No staining of the membrane was observed (data not shown), indicating that the anti-3NT antibody was specific for this specific posttranslational modification.

A.3.5 Proteomics (Butterfield et al. 2012)

A.3.5.1 Isoelectric focusing (IEF)

Aliquots (containing 150ug of protein) of the homogenized cortical samples prepared above were precipitated using cold 100% trichloroacetic acid (TCA) to obtain a concentration of 15% (v/v) TCA in solution and incubated on ice for 15 minutes. Samples were centrifuged at 14,000 rpm for 10 min at 4 °C. The resulting pellets were resuspended and rinsed four times in a cold ethanol: ethyl acetate (1:1 v/v) mixture. After allowing the final pellets to dry completely at room temperature, the pellets were rehydrated for 2 h in rehydration buffer [8 M urea, 2 M thiourea, 50 mM DTT, 2.0% (w/v) CHAPS, 0.2% Biolytes, Bromophenol Blue] then sonicated for 10 s at 20% power. Each entire sample was added to an 11 cm pH 3-10 ReadyStrip™ IPG strip in a lane of the IEF tray. After 45 min of run time, 2 mL of mineral oil were added to each lane to prevent evaporation. Strips were actively rehydrated at 20 °C for 18 h at 50 V, focused at a constant temperature of 20 °C beginning at 300 V for 2 h, 500 V for 2 h, 1000 V for 2 h, 8000 V for 8 h, and finishing at 8000 V for 10 h rapidly. IPG strips were stored at −80 °C until needed for the second dimension of analysis.

A.3.5.2 Two-dimensional polyacrylamide gel electrophoresis (2D-PAGE)

IEF strips were allowed to come to room temperature (~30 min) and equilibrated for 10 min in the dark in 4 mL equilibration buffer A [50 mM Tris–HCl, pH 6.8, 6 M urea, 1% (w/v) SDS, 30% v/v glycerol, 0.5% DTT] and then re-equilibrated for 10 min in the dark in equilibration buffer B [50 mM Tris–HCl, pH 6.8, 6 M urea, 1% (w/v) SDS, 30% v/v glycerol, 4.5% IA]. All strips were rinsed in TGS running buffer to remove residual equilibration buffers before being placed onto Criterion precast linear gradient (8–16%) Tris–HCl polyacrylamide gels. Precision Plus Protein™ All Blue Standards and samples were run at a constant voltage of 200 V for 65 min.

A.3.5.3 SYPRO Ruby® staining

Following 2D-PAGE, gels were incubated in 50 mL fixing solution [7% (v/v) acetic acid, 10% (v/v) methanol] for 20 min at room temperature. SYPRO Ruby® Protein Gel Stain (50-55 mL) was added to gels and allowed to stain overnight at room temperature on a gently rocking platform. The stain was then removed and gels were rinsed with deionized (DI) water and stored in 50 mL DI water in the refrigerator until scanning. Gels were scanned into Adobe Photoshop 6.0 with a Molecular Dynamics STORM phosphoimager ($\lambda_{ex}/\lambda_{em}$: 470/618 nm) and stored in DI water at 4 °C.

A.3.5.4 Image analysis: differential expression

Spot intensities from SYPRO Ruby®-stained 2D-gel images of cortex samples were quantified according to total spot density using PDQuest software (Bio-RAD, Hercules, CA, USA). Intensities were normalized to total gel densities. Only low or high VitD samples with normalized spot densities that were significantly increased or decreased by at least 1.4-fold from control were considered for mass spectrometry (MS) analysis. This is a conservative cut-off criterion, but does greatly minimize false positives.

A.3.5.5 In-gel trypsin digestion

Protein spots identified as significantly altered in VitD deficient rat brain relative to normal VitD controls were excised from 2D-gels with new, sterilized micropipette tips and transferred to Eppendorf microcentrifuge tubes. Gel plugs were then washed with 0.1 M ammonium bicarbonate (NH_4HCO_3) at room temperature for 15 min, followed by incubation with 100% acetonitrile at room temperature for 15 min. Solvent was removed, and gel plugs were dried in their respective tubes in a biosafety cabinet at room temperature. Gel plugs were incubated for 45 min in 20 µl of 20 mM DTT in 0.1 M NH_4HCO_3 at 56 °C. The DTT solution was then removed and replaced with 20 µl of 55 mM IA in 0.1 M NH_4HCO_3 and incubated with gentle agitation at room temperature in the dark for 30 min. Excess IA solution was removed, and the gel plugs were incubated for

15 min with 200 µl of 50 mM NH_4HCO_3 at room temperature. 200 µL of 100% acetonitrile was added to this solution in each tube and incubated for 15 min at room temperature. All solvent was removed, and gel plugs were allowed to dry for 30 min at room temperature in a biosafety cabinet. Gel plugs were rehydrated with 20 ng/µL of modified trypsin (Promega, Madison, WI, USA) in 50 mM NH_4HCO_3 in a shaking incubator overnight at 37 °C. Enough trypsin solution was added in order to completely submerge the gel plugs (approximately 10uL).

A.3.5.6 Mass spectrometry

Salts and other contaminants were removed from tryptic digest solutions using C18 ZipTips (Sigma-Aldrich, St. Louis, MO, USA), reconstituted to a volume of approximately15 µl in a 50:50 DI water:acetonitrile solution containing 0.1% formic acid. Tryptic peptides were analyzed with an automated Nanomate electrospray ionization (ESI) [Advion Biosciences, Ithaca, NY, USA] Orbitrap XL MS (ThermoScientific, Waltham, MA, USA) platform. The Orbitrap MS was operated in a data-dependent mode whereby the eight most intense parent ions measured in the Fourier Transform (FT) at 60,000 resolution were selected for ion trap fragmentation with the following conditions: injection time 50 ms, 35% collision energy, MS/MS spectra were measured in the FT at 7500 resolution, and dynamic exclusion was set for 120 s. Each sample was acquired for a total of approximately 2.5 min. MS/MS spectra were searched against the International Protein Index (IPI) database using SEQUEST and the following

parameters: two trypsin miscleavages, fixed carbamidomethyl modification, variable Methionine oxidation, parent tolerance 10 ppm, and fragment tolerance of 25 mmu or 0.01 Da. Results were filtered with the following criteria: Xcorr>1.5, 2.0, 2.5, 3.0 for +1, +2, +3, and +4 charge states, respectively, Delta CN>0.1, and *P*-value (protein and peptide) <0.01. IPI accession numbers were cross-correlated with SwissProt accession numbers for final protein identification (Robinson et al. 2011).

A.3.5.7 One-dimensional polyacrylamide gel electrophoresis

Sample homogenates were incubated in sample buffer (0.5 M Tris (pH 6.8), 40% glycerol, 8% sodium dodecyl sulfate (SDS), 20% β-mercaptoethanol, and 0.01% bromophenol) for 5 min in a water bath at 95°C and loaded onto precast Criterion TGX (4-15%) or Criterion XT (12% Bis-Tris) Precast Gels as appropriate for the molecular weight of the protein of interest. Precision Plus Protein™ All Blue Standards and samples were run at 80 V for 15 min, increasing the voltage to 120 V and run for 90 min in TGS or MES running buffer as appropriate for the gel.

A.3.5.8 Western Blotting

In-gel proteins were transferred to a nitrocellulose membrane (0.45 µm) using a Trans-Blot® Turbo™ Blotting system at 25 V for 30 min (BioRAD, Hercules, CA,

USA). After transfer, membranes were incubated in blocking solution [3% BSA in phosphate buffer (PBS) solution with 0.2% (v/v) Tween 20] at room temperature for 1.5 h. Membranes were then incubated with rabbit anti-inducible nitric oxide synthase (iNOS) antibody (Calbiochem/Millipore, Billerica, MA) or rabbit anti-NF-κB antibody (Enzo, Farmingdale, NY) for 2 h on a gentle rocking platform, followed by three rinses for 5 min each with PBS solution with 0.2% (v/v) Tween 20. Blots were then incubated for 1 h with ECL anti-rabbit IgG, horseradish peroxidase-linked whole antibody. The resulting blots were rinsed three times for 5, 10, and 10 min each in PBS solution with 0.2% (v/v) Tween 20 and signals were detected using Clarity™ Western ECL Substrate (BioRAD) and the ChemiDoc™MP Imaging System (BioRAD).Blots were stripped using Re-blot Plus Strong Solution (Millipore, Billerica, MA, USA) according to package instructions and re-probed with mouse anti-actin antibody (Sigma-Aldrich, St. Louis, MO) or mouse anti-histone H2B antibody (Chemicon, Temecula, CA) for normalization. Analysis was performed using the ImageLab software (BioRAD).

A.3.5.9 Validation

Proteomics results were validated by IEF and 2D-PAGE as described above followed by Western blot (Robinson et al. 2011) for peroxiredoxin 3 (PrxIII) and 1D-gel electrophoresis followed by Western blot for peptidyl-prolylcis-trans isomerase A (PPIA or cyclophilin A). PrxIII blots were probed for PrxIII as described above using rabbit polyclonal to PrxIII primary antibody (Abcam,

Cambridge, MA, USA), mouse anti-actin primary antibody and anti-rabbit whole molecule IgG alkaline phosphatase oranti-mouse whole molecule IgG alkaline phosphatase secondary antibody respectively. The resulting blots were developed colorimetrically with a solution of BCIP combined with NBT in ALP buffer [0.1 M Tris, 0.1 M NaCl, 5 mM $MgCl_2 \cdot 6\ H_2O$ (pH 9.5)]. Developed blots were allowed to dry overnight at room temperature and scanned into Adobe Photoshop 6.0 using a Canon CanoScan 8800F scanner. The resulting images were analyzed using Image Quant software. PPIA blots were probed for PPIA by incubation with anti-cyclophilin A rabbit antiserum (Upstate/Millipore, Billerica, MA, USA,) primary antibody and ECL anti-rabbit IgG, horseradish peroxidase-linked whole antibody and developed chemiluminescently as described above. PPIA blots were stripped and re-probed for the actin. Analysis was performed using the ImageLab software (BioRAD).

A.3.6 Statistical analysis

All data are presented as mean±SD or mean±SEM, and statistical analyses were performed using a two-tailed Student's *t*-test or ANOVA where indicated, with $p<0.05$ considered significant for spot comparison. A Mann–Whitney U statistical analysis was performed to determine the significance of differential expression fold-change values, where a $p<0.05$ was considered significant. Significance was also confirmed using a Student's *t*-test. Only spots that were significant by both tests were further evaluated. Protein and peptide identifications obtained with the

SEQUEST search algorithm with a $p < 0.01$ were considered as statistically significant. To further validate PD-Quest analysis, identities of protein spots were verified matching calculated molecular weight (MW) and isoelectric point (pI) values from MS results and SwissProt database information to spot locations on the gels (Table A.2 and Figure A.2).

Table A.2. Brain protein identifications in VitD deficiency based on MS/MS results and in-gel spot locations.

SSP	Protein Identification	Score	Coverage	Unique Peptides	MW [kDa]	CalcpI
5201	Triosephosphate isomerase	67.52	48.59	10	26.8	7.24
8103	Pyruvate kinase isozymes M1/M2	241.21	50.85	21	57.8	7.06
6701	6-phosphofructokinase type C	69.17	19.54	11	85.7	7.28
3207	Peroxiredoxin 3	154.94	33.85	6	28.3	7.55
4201	DJ-1/PARK7	61.73	58.20	11	20.0	6.77
8104	Peptidyl-prolyl cis-trans isomerase A(cyclophilin A)	56.18	28.66	7	17.9	8.16

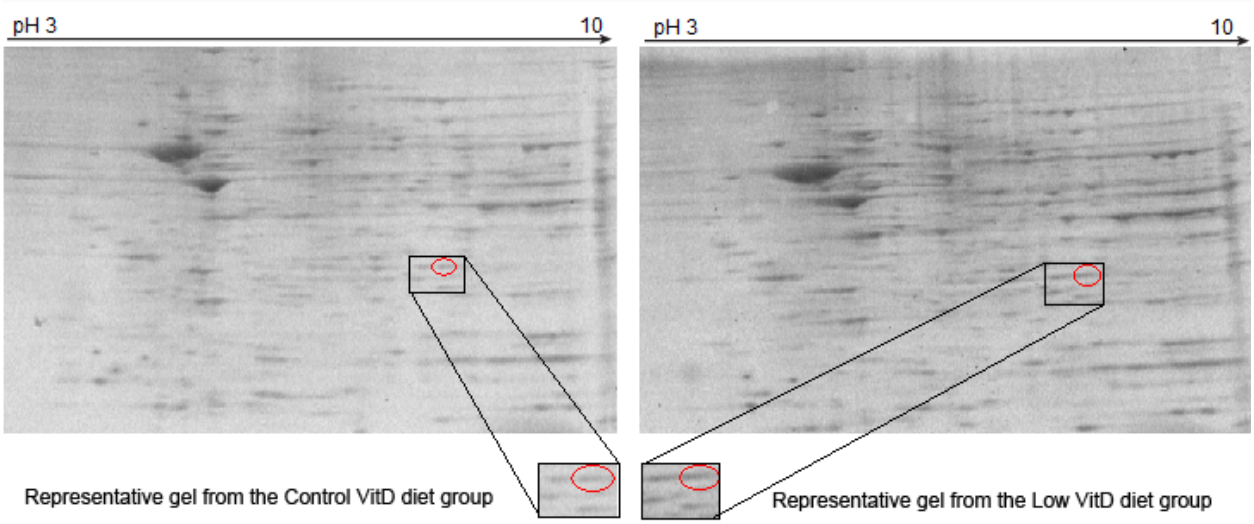

Figure A.2. Representative 2D gels used for proteomics identification of differentially expressed proteins. Brain samples of rats fed a control, low-VitD, or high-VitD diet from middle age to old age were separated by IEF using IPG strips pH 3–10 followed by SDS–PAGE using 8–16% Tris–HCl gels. Separated proteins were visualized with SYPRO Ruby protein gel stain. Acquired images were analyzed using PDQuest software and spots showing different intensities were chosen for further analysis. A comparison of the PrxIII spot as a representative of those found with significant expression differences in low vs control VitD groups as identified by PDQuest analysis is shown. Below are expansions of the spot images showing clearly that the PrxIII level is elevated in brain of rats on a chronic low-VitD diet. Used by permission from Elsevier Scientific Publishers, Inc.

A.4 Results

A.4.1 Vitamin D deficiency leads to increased nitrosative protein damage in brain.

Tyrosine nitration is a common indicator/biomarker of the aging brain and of age-related neurodegenerative disorders (Souza et al. 2001; Castegna et al. 2003), both of which typically are accompanied by different extents of cognitive deficit. Here, we tested for indicators of oxidative and nitrosative stress in brain tissue samples from rats in which we manipulated serum VitD levels from middle-age to old-age. Significantly increased global 3-NT (Figure A.3) in the brains of rats on a low VitD diet compared to rats on control or high VitD diets was observed.3-NT measures of brain samples from rats fed high VitD diets were similar to the control group. No significant differences were observed for the other oxidative stress parameters measured.

A.4.2 VitD deficiency elevation of peroxidases, glycolytic enzymes, and PPIA.

In order to determine changes, possible causes, consequences, or mechanisms for the elevated nitrosative stress, expression proteomics experiments (Butterfield et al. 2012) were performed on brain of rats fed a low VitD, control, or high VitD diet to determine which proteins were altered. PDQuest analysis was

performed on all groups as well. Only spots that were found to be statistically different in relative intensity by statistical tests were further evaluated. Compared to control, the high VitD group was similar to control in terms of protein levels for easily discernible protein spots. In contrast, a number of protein spots with significant differences in intensity were found between the control and low VitD groups. Table A.3 shows the PDQuest software generated I.D. numbers (SSP) of these protein spots. Spot intensities between control and low VitD groups were used to calculate fold changes reflecting significant increases in protein amounts. These proteins were identified by MS/MS and database interrogation as 6-phosphofructokinase (6-PFK) type C, PPIA, triosephosphate isomerase (TPI), PrxIII, DJ-1/PARK7, and pyruvate kinase (PK) isozymes M1/M2 (Table A.3).

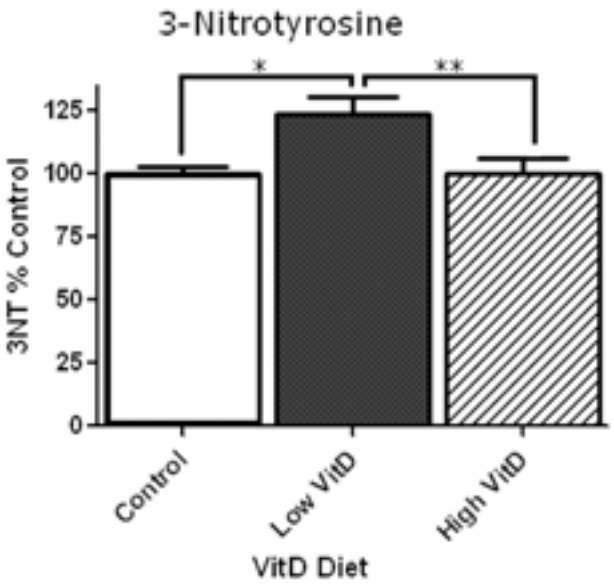

Figure A.3. Slot-blot analysis of 3-NT levels in rat brain homogenates. Slot-blot analyses were performed using brain samples of rats fed a control, low-VitD,

or high-VitD diet from middle age to old age (*n*=9). Data show a significant increase in 3-NT levels in rat brains between control and low-VitD diet (**p*<0.01). No difference was observed in high-VitD diet compared to control. High-VitD diet decreased 3-NT levels compared to low-VitD diet (***p*<0.05). Used by permission from Elsevier Scientific Publishers, Inc.

Table A.3. VitD 2D-Gel Comparison PDQuest Data: spot matching Low VitD (L) vs. Control (C), Levels. (SSP=PDQuest software-generated ID numbers).

SSP	Fold Change	Direction of change L vs C	p-value L vs C
6701	1.41	Increased	0.0114
8104	2.49	Increased	0.0130
5201	60.3	Increased	0.0291
3207	1.53	Increased	0.0347
8103	1.48	Increased	0.0373
4201	1.53	Increased	0.0473

To validate protein identity from proteomics, 2D and 1D Western blots were performed, selecting PrxIII and PPIA as representative proteins. 2D Western

blots showed a 1.5-fold increase in PrxIII levels confirming the 1.5-fold increase suggested by 2D-PAGE. Further, the position of the PrxIII spot appears at approximately 26 kDa and 7.2 pI on 2D Western blot (Figure A.4). 1D Western blot showed a 2.24-fold increase in PPIA levels, further validating the 2.49-fold increase seen in the proteomics results (Figure 4). These validation results provide confidence in the proteomics identification of other proteins reported in this study.

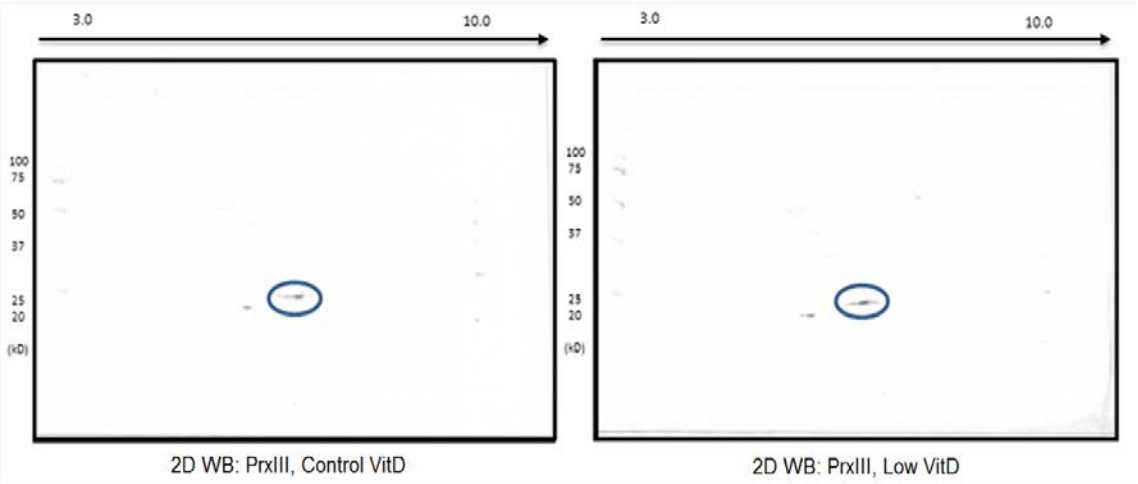

Figure A.4. Validation of expression proteomics results for PrxIII by 2D Western blot analysis. Depicted are representative blots showing a 1.5-fold increase in PrxIII in brain samples of rats fed the low-VitD diet from middle age to old age compared to those fed the control diet. Circled spots are PrxIII from control-VitD brain samples shown on the left and low-VitD brain samples on the right. Used by permission from Elsevier Scientific Publishers, Inc.

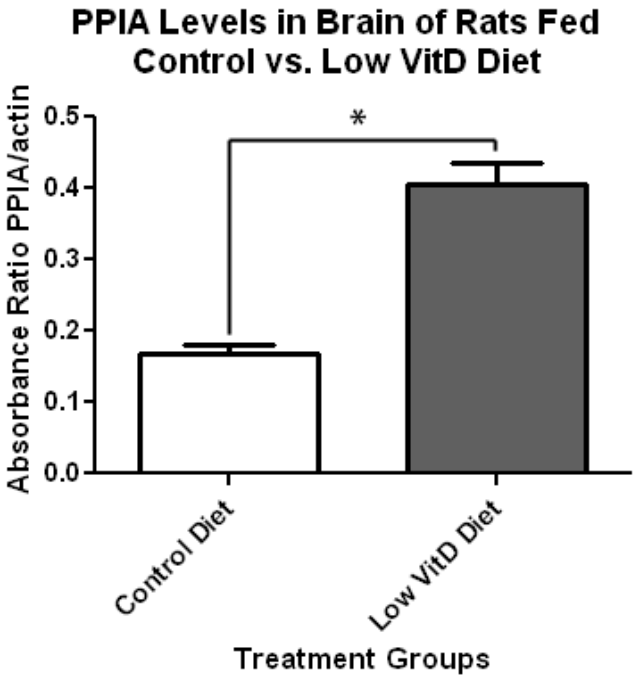

A

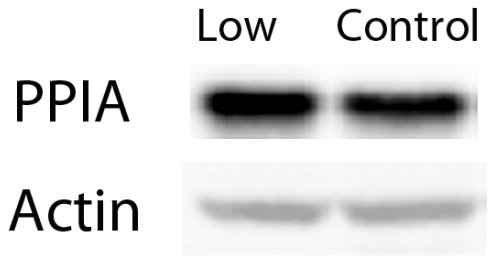

B

Figure A.5. Validation of expression proteomics results by 1D Western blot analysis of PPIA levels. 1D Western blot analysis was used to determine PPIA levels of brain samples of rats fed a control or low-VitD diet from middle age to old age (*n*=9). (A) Analysis using a specific antibody against PPIA showed a 2.24-fold increase in PPIA levels in brain of the low-VitD group compared to control (*$p<0.01$). This result confirms the increase in PPIA levels found by expression proteomics. (B) Representative lanes from 1D Western blot showing

probes for PPIA and the actin loading control. Used by permission from Elsevier Scientific Publishers, Inc.

A.4.3 VitD deficiency leads to NF-κB activation and increased iNOS levels in brain.

Preliminary results of this study coupled with previous studies in our laboratory and existing literature led us to propose a model to connect the observed increases in nitrosative protein damage and expression proteomics results showing elevated levels of the above mentioned peroxidases, glycolytic enzymes, and PPIA to VitD deficiency (Figure A.6). Based on this proposed model, we examined the hypothesis that VitD deficiency would lead to increased NF-κB activation and iNOS levels, resulting in the observed increase in protein tyrosine nitration seen in the low-VitD group compared to control.

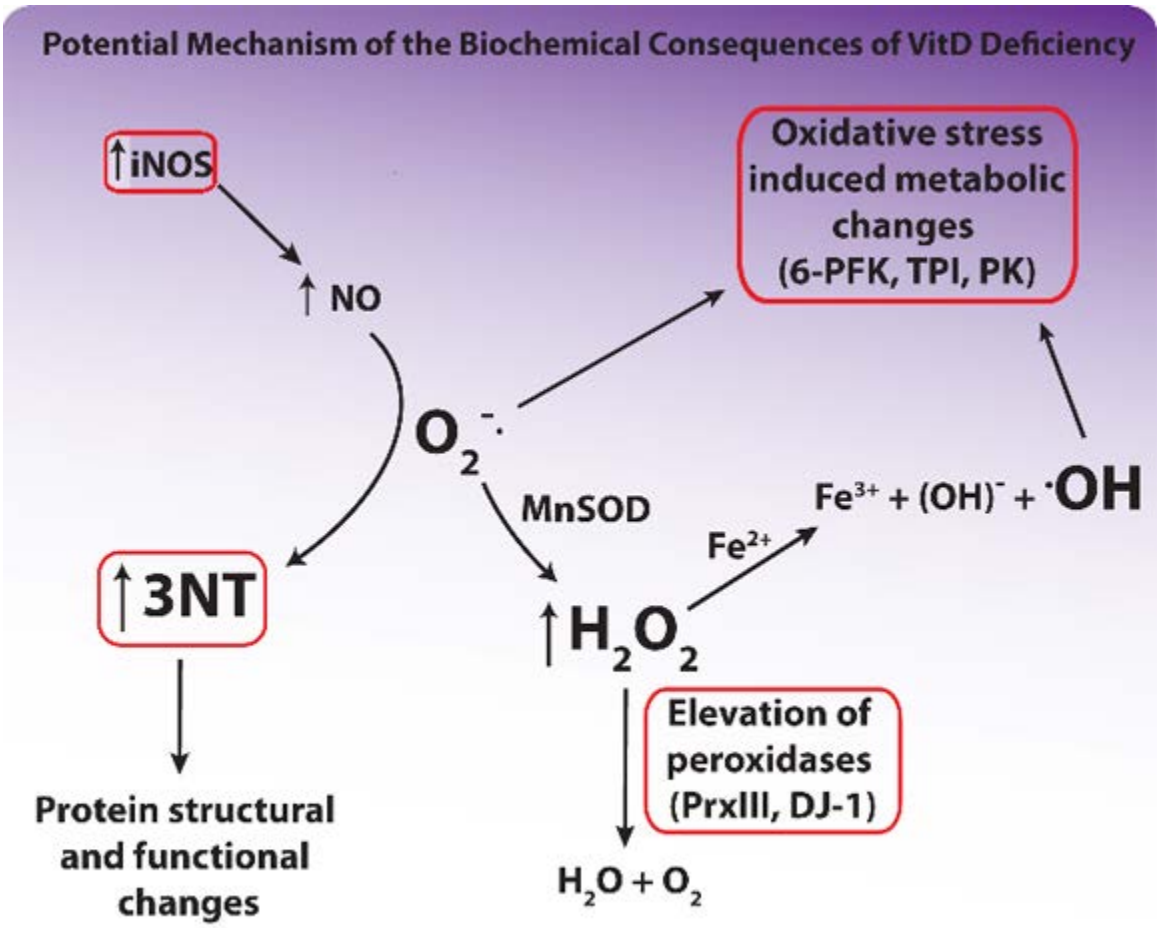

Figure A.6. Potential mechanism for the biochemical consequences of VitD deficiency. Circled areas indicate data collected in this study. Increased tyrosine nitration was found by slot-blot analysis, increased iNOS levels were found by 1D Western blot analysis, and elevation of glycolytic enzymes and peroxidases was found by expression proteomics using brain samples of rats fed a control or low-VitD diet from middle age to old age. Items in large type are the most potentially damaging agents in this diagram. Used by permission from Elsevier Scientific Publishers, Inc.

NF-κB is a redox-sensitive nuclear transcription factor that can be activated by oxidizing agents such as H_2O_2 (Schreck et al. 1992). Hypoxic activation of NF-κB and gene transcription has been found to require mitochondrial ROS (Chandel et al. 2000). Among downstream products of NF-κB pathway activation are tumor necrosis factor-α (TNFα) and iNOS (Griscavage et al. 1996; Chandel et al. 2000; Feo et al. 2009). Using 1D Western blotting, we investigated whether NF-κB activation of iNOS expression may be a plausible reason for the nitration of tyrosine residues through overproduction of $NO^{\cdot}$ (Kim et al. 1999; Akama et al. 2000; Fitzgerald et al. 2007; Tangpong et al. 2007; Tangpong et al. 2008) seen in these samples.

Under normal conditions, NF-κB exists in an inactive form bound to inhibitor of kB-α (IkB-α). Upon activation of a Toll-like receptor by a variety of substrates including lipopolysaccharide (LPS) and TNFα (Chagas et al. 2012), phosphorylation of IkB-α occurs through IkB kinase (IKK) allowing IkB-α proteasomal degradation and NF-κB activation. NF-κB is translocated to the nucleus leading to bursts of iNOS activation, subsequent $NO^{\cdot}$ elevation (Akama et al. 2000; Feo et al. 2009), and further transcriptional activation of the *TNFα gene*(Kim et al. 1999; Baker et al. 2011). Pro-inflammatory cytokines such as TNFα lead to further and rapid phosphorylation of IkBs (Pomerantz et al. 2002). Overproduction of $NO^{\cdot}$ as a consequence of iNOS activation results in protein nitration events and further stimulation of IKK (Mendes et al. 2002; Feo et al. 2009). 1α, 25-$(OH)_2$VitD has been shown to interfere with these processes

through decreasing TNFα levels and TNFα-induced inflammatory cytokines (Furman et al. 1996; Giulietti et al. 2007; Diaz et al. 2009), down-regulating Toll-like receptors (Sadeghi et al. 2006), up-regulating IkB-α, decreasing IkB-α phosphorylation, and decreasing translocation of NF-κB (Chagas et al. 2012), thereby reducing many downstream consequences. Further decrease of NF-κB action may occur through the suppression of NF-κB-directed expression by the VitD responsive element (Haussler et al. 2008). Thus, VitD can inhibit protein nitration in the brain via its suppressive effects on the NF-κB pathway. VitD deprivation may exacerbate NF-κB-directed nitrosative damage and subsequent neurodegenerative consequences. As an estimate of NF-κB activity, subcellular fractionation was done on control and low VitD brain samples. NF-κB levels were found to be significantly decreased in the cytosolic fraction and significantly increased in the nuclear fraction of the low VitD group compared to control (Figure A.7) indicating NF-κB translocation to the nucleus.

Our analysis further revealed a significant increase in iNOS levels in the low VitD samples compared to control (Figure A.8). These NF-κB and iNOS results provide evidence to support the proposed mechanism of protein nitration due to VitD deficiency. TNFα is one of several initiators of the NF-κB activation cascade. 1D Western blot analysis of these samples for TNFα showed a trend toward increase (data not shown) in the low VitD group compared to control consistent with NF-κB activation and iNOS elevation. Figure A.9 depicts a suggested mechanism for the protein nitration regulatory effects of VitD in brain.

A

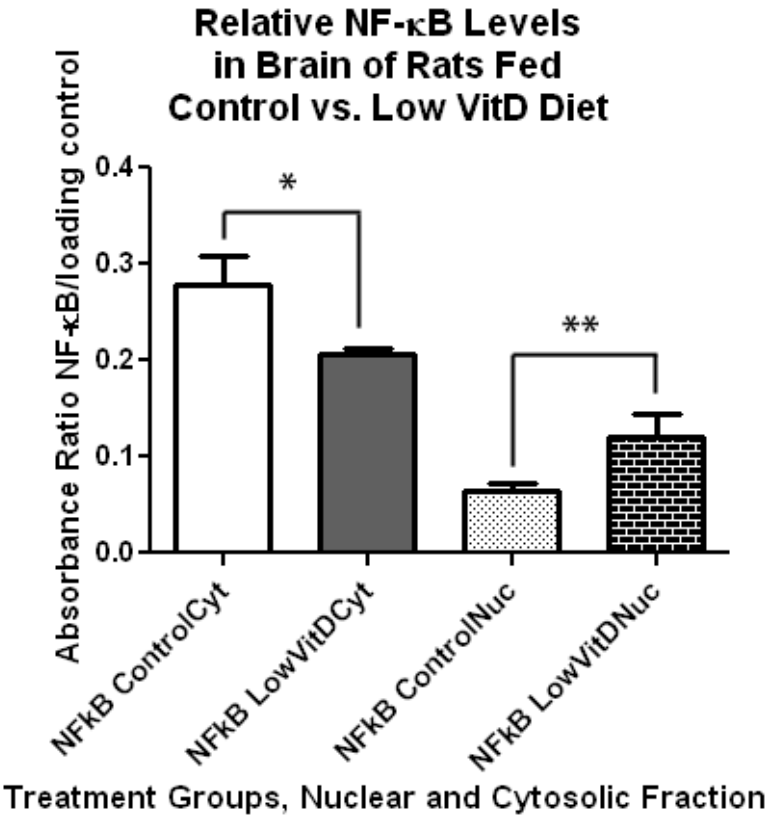

B

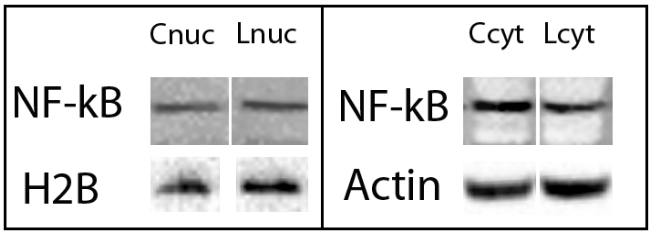

Figure A.7. Effect of VitD deficiency on NF-κB subcellular localization in rat brain. 1D Western blots were used to determine the NF-κB (p65) levels in the cytosolic and nuclear fractions of brain samples of rats fed a control or a low-VitD diet from middle age to old age (*n*=9). The NF-κB (p65) subunit is common in the NF-κB signaling pathway. NF-κB (p65) levels in the cytosolic fraction were

normalized to β-actin, and NF-κB (p65) levels in the nuclear fraction were normalized to histone H2B. (A) A decrease in NF-κB (p65) in the cytosolic fraction (*p<0.05) and increase in the nuclear fraction (**p<0.05) in brain samples from the low-VitD group compared to control is observed, indicative of NF-κB activation and translocation. (B) Representative bands from 1D Western blot are shown here side by side for comparison. Nuclear and cytosolic fractions were alternated across all gels. Blots were probed for NF-κB (p65), stripped, probed for β-actin, and then stripped and probed for histone H2B. Used by permission from Elsevier Scientific Publishers, Inc.

A

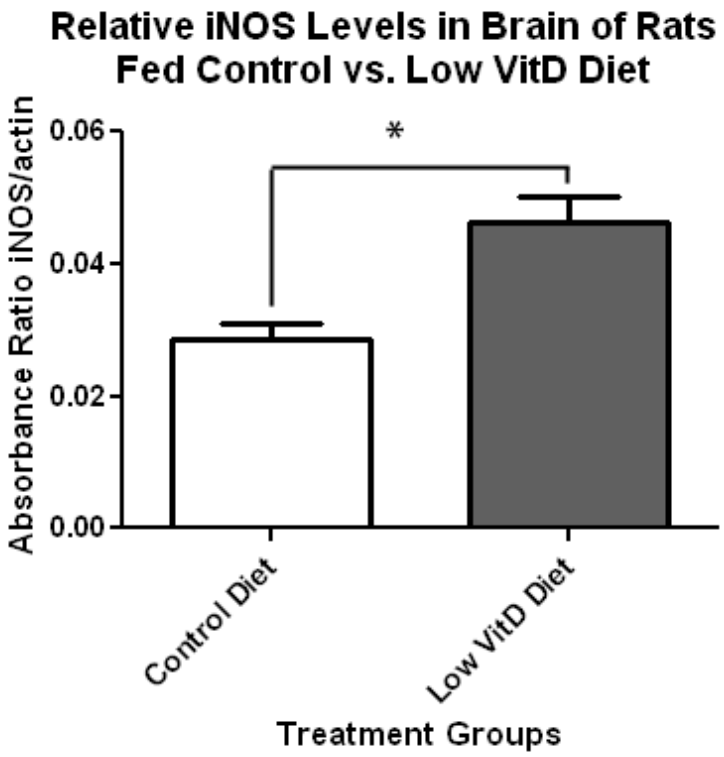

B

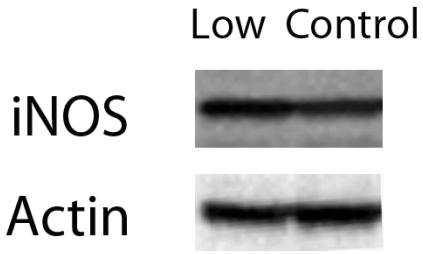

Figure A.8. Effect of VitD deficiency on iNOS levels in rat brain. 1D Western blot was performed to compare iNOS levels between brain samples of rats fed a control or a low-VitD diet from middle age to old age (*n*=9). iNOS signals were normalized to β-actin. (A) iNOS levels were significantly higher in brain samples from the low-VitD group compared to control (**p*<0.01). (B) Representative lanes from 1D Western blot. Used by permission from Elsevier Scientific Publishers, Inc.

A.5 Discussion

We have previously shown that tyrosine nitration occurs early in neurodegenerative processes, i.e., in mild cognitive impairment (MCI), arguably the earliest form of AD (Butterfield et al. 2007). Nitration of tyrosine occurs from the reaction $NO^{\cdot}$ with the $O_2^{-\cdot}$through the reactive intermediate $ONOO^-$in the presence of CO_2 (Beckman 1996; Labetoulle et al. 2001) leading to tyrosine nitration by $NO_2^{\cdot}$ radical. Nitrosative stress measures on these cortical samples showed approximately a 25% elevation of 3-NT globally in brain protein in the low VitD group versus the control and high VitD-treated groups.

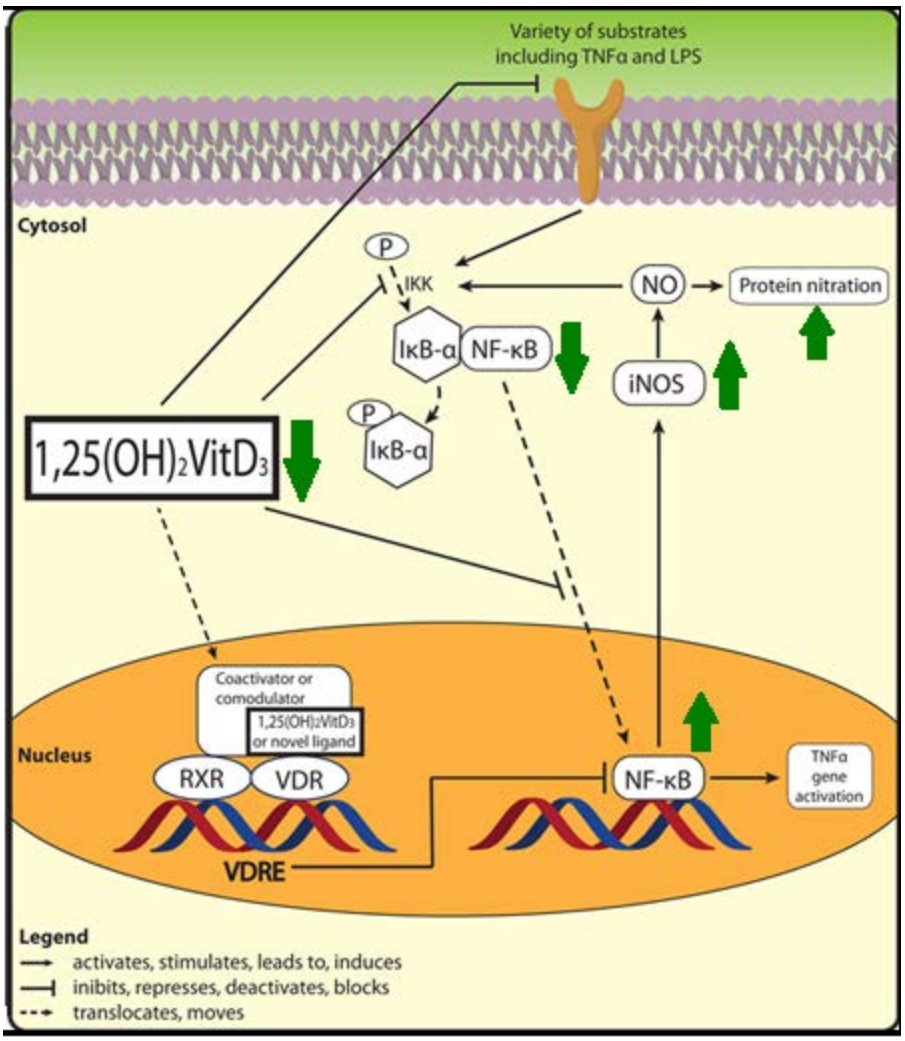

Figure A.9. Proposed mechanism for the protein nitration regulatory effects of VitD in brain based on recent literature and results from the current study. Results obtained from this study are marked with dark green arrows. The deficient serum levels of VitD in the low-VitD group in brain led to decreased NF-κB in the cytosolic fraction, increased NF-κB in the nuclear fraction, iNOS elevation, increased protein tyrosine nitration, and elevations in mitochondrial and regulatory proteins. Used by permission from Elsevier Scientific Publishers, Inc.

A.5.1 Glycolytic enzymes targeted by low VitD

The brain proteins identified by proteomics in the present study to be at increased levels (Table A.2) fall primarily in the following functional categories: glycolysis, mitochondrial peroxidase activity, and protein folding. Three of these proteins, 6-PFK, TPI, and PK, are enzymes involved in the production of ATP in the cell during glycolysis in response to the need for energy. PK catalyzes the conversion of phosphoenolpyruvate (PEP) to pyruvate transferring a phosphate group from PEP to ADP to produce ATP. Pyruvate, NADH, and H^+ from glycolysis continue onto the tricarboxylic acid (TCA) cycle for further ATP production. PK has been identified by redox proteomics as oxidatively modified in brain regions, such as cortex and hippocampus, during brain aging (Poon et al. 2006; Perluigi et al. 2010) and neurodegeneration resulting in reduced enzymatic activity (Reed et al. 2008). 6-PFK catalyzes a key regulatory step, the conversion of fructose-6-phosphate to fructose-1,6-bisphosphate at the expense of ATP, committing the path of glucose through glycolysis. This rate-limiting glycolytic enzyme was found by Tang and colleagues to be upregulated in several biological systems as part of the oxidative stress response including the response to H_2O_2 induced oxidative stress (Tang et al. 2012). TPI catalyzes the interconversion of the trioses, glyceraldehyde-3-phosphate (G3P) and dihydroxyacetone phosphate (DHAP). Significant increases of TPI have been found by our group using proteomic analysis in the Alzheimer's disease

hippocampus (Sultana et al. 2007). Further studies identified TPI as significantly nitrated in the inferior parietal lobe (IPL) in early AD brain (Reed et al. 2009) and in both AD hippocampus and IPL (Sultana et al. 2006). Dysfunction of this enzyme leads to the buildup of a toxic species, methylglyoxal, leading to neurodegenerative consequences (Sultana et al. 2009; Pun et al. 2012).Thus, metabolic effects in brain are evident from the effect of a low-VitD diet.

A.5.2 Other identified targets of VitD deficiency (DJ-1, PPIA, PRXIII)

Mutations of the *DJ-1* gene are believed to be one possibility that leads to Parkinson disease (PD) (van Duijn et al. 2001). DJ-1 is thought to be involved in cell cycle regulation, gene transcription, spermatogenesis, and the cellular stress response (Bonifati et al. 2004) among other functions. Evidence exists that DJ-1, in response to oxidative stress, may have roles as an anti-oxidant (Mitsumoto et al. 2001; Mitsumoto et al. 2001) and a redox sensitive chaperone (Zucchelli et al. 2009; Foti et al. 2010). Accordingly, elevation of DJ-1 in brain could be a consequent cell-stress response to elevated protein nitration.

PPIases regulate activity of target proteins to which they bind by catalyzing the cis-trans isomerization of proline of these target proteins(Andreotti 2003; Sarkar et al. 2007), typically a rate limiting step in protein folding. PPIA, or cyclophilin A, is also known to play a variety of roles from immunoregulation to cellular signaling and proliferation, but more recently has been identified as a potential

marker of inflammation in a variety of disease states (Zhang et al. 2001; Satoh et al. 2008; Satoh et al. 2010; Bannon et al. 2012; Ramachandran et al. 2012) and may play a regulatory role in the NF-κB pathway in some cell types (Sanchez-Tillo et al. 2006; Bahmed et al. 2012). In addition, PPIA treatment was shown to reduce reactive oxygen species (ROS) and alleviate some forms of Aβ-induced neurotoxicity in PC12 cell culture while maintaining activities of certain key anti-oxidant enzymes including SOD (Ge et al. 2009). PPIA binds Prxs and activates their peroxidase activity acting as an immediate electron donor (Lee et al. 2001). PPIA may also indirectly stimulate PrxIII, a downstream consequence of tumor necrosis factor-α (TNFα) (Regent et al. 2011).

PrxIII is a mitochondria resident, thioredoxin-dependent peroxide reductase that acts to scavenge as much as 90% of H_2O_2in mitochondria, with GPx 1 and 4 and PrxV thought to account for the rest (Netto et al. 1996; Kang et al. 1998; Rhee et al. 1999; Bentley et al. 2008; Jones 2008; Cox et al. 2010). Rhee and colleagues elegantly showed that peroxiredoxin over expression inhibited NF-κB (Rhee et al. 1999), and over expression of PrxIII has been shown to protect against H_2O_2-dependent apoptosis in cancer cells (Nonn et al. 2003). Further, PrxIII was shown to be essential in maintaining normal mitochondrial homeostasis (Wonsey et al. 2002). Dysfunctional PrxIII leads to increased ROS and subsequent DNA damage and apoptosis linked to loss of peroxidase activity in mitochondria (Mukhopadhyay et al. 2006). Prxs have been shown to detoxify peroxynitrite, thereby decreasing biomolecule damage caused by more reactive products of

$ONOO^-$ and protecting human cells in culture from iNOS-related cell death (Bryk et al. 2000).

Tyrosine nitration can and does have functional consequences on the affected proteins (Labetoulle et al. 2001; Ischiropoulos 2009; Feeney et al. 2012). Steric hindrance by the NO_2 groupin the 3-position of tyrosine may prevent phosphorylation at the 4-position thereby causing dysregulation of activation/deactivation processes in the affected proteins (MacMillan-Crow et al. 1998; Tangpong et al. 2008; Ischiropoulos 2009; Surmeli et al. 2010; Feeney et al. 2012; Frau et al. 2012). Such considerations have implications for cognitive dysfunction following low dietary VitD.

A.5.3 Consequences of low dietary VitD

Based on this experimental evidence, the biochemical consequences of low dietary VitD include increased 3-NT in the brain as well as increases in certain proteins with peroxidase activity. A likely link between these two pathways is $O_2^{-\cdot}$ (Figure A.6). The high O_2 usage in energy metabolism coupled with age-related decreases in the efficiency of these reactions results in the production and leakage of $O_2^{-\cdot}$ from the electron transport chain. MnSOD in the mitochondria react with $O_2^{-\cdot}$ producing H_2O_2. $NO^\cdot$ reacts with $O_2^{-\cdot}$ by radical-radical recombination producing the potentially more reactive species, $ONOO^-$, that leads to the nitration of tyrosine (Beckman 1996; Squadrito et al. 1998; Koppal et

al. 1999; Butterfield et al. 2011) residues, hindering protein activity regulation by sterically blocking the phosphorylation site. The findings of this study are consistent with current literature hypothesizing that oxidative damage during the aging process leads to mitochondrial dysfunction (Perluigi et al. 2010; Tang et al. 2012). Increased glycolytic enzymes could be a compensatory mechanism reflecting changes in energy production, changes in mitochondrial redox status, and oxidative stress (Tang et al. 2012) reminiscent of the Warburg effect in cancer (Warburg et al. 1924; Warburg 1930; Vander Heiden et al. 2009; Sotgia et al. 2012).

Collectively, these results reflect a change in mitochondrial redox potential, glucose metabolism, and structural changes in proteins. Data from the current study are consistent with recent findings that VitD: a) increases SOD activity, b) decreases levels of endogenous oxidants, c) attenuates H_2O_2 induced changes, d) decreases release of inflammatory cytokines, and e) may have natural anti-oxidant and anti-inflammatory properties (Halicka et al. 2012; Tukaj et al. 2012). In contrast, VitD deficiency contributes to inflammation through increased production of inflammatory cytokines, effects that are attenuated by 1,25$(OH)_2$VitD supplementation (Muller et al. 1992; Zhu et al. 2005; Zittermann et al. 2009; Farid et al. 2012).

More recently, VitD has been shown to play potential roles in CNS homeostasis (Lefebvre d'Hellencourt et al. 2003). The VitD receptor (VDR) is expressed in

microglia, and 1α-hydroxylase, the enzyme that converts 25-OH VitD to 1α, 25-$(OH)_2$VitD, is present in activated but not resting microglia (Neveu et al. 1994; Garcion et al. 1998; Garcion et al. 2002; McCarty 2006). In activated microglia, 1α,25$(OH)_2$VitD suppresses the production of $NO^{\cdot}$ and the inflammatory mediators, TNFα and interleukin-6 (IL-6), in a dose-dependent manner suggesting direct anti-inflammatory roles for VitD in the brain (Lefebvre d'Hellencourt et al. 2003). Local conversion of VitD to the active 1α,25$(OH)_2$VitD in the brain may be a direct neuroprotective response to CNS inflammation followed by inhibition of NF-κB related iNOS induction (Garcion et al. 1998).NF-κB leads to mitochondrial dysfunction inhibition of MnSOD through nitration via activation of iNOS, an effect that is absent in iNOS knockout animal models (Tangpong et al. 2007).

Our data are consistent with existing evidence that sufficient VitD is known to be anti-inflammatory and to suppress the NF-κB cellular stress response pathway (Yu et al. 1995; Cohen-Lahav et al. 2006; Haussler et al. 2008; Chagas et al. 2012; Minelli et al. 2012). Hydrogen peroxide (H_2O_2) has been shown to modulate NF-κB activity thereby helping to regulate NF-κB-dependent processes including inflammation (Schreck et al. 1992; Li et al. 2001; Wang et al. 2002; Oliveira-Marques et al. 2009). During inflammatory events in the CNS, iNOS generates excessive amounts of $NO^{\cdot}$. This increased activity of iNOS and resulting overproduction of $NO^{\cdot}$ may occur in brief bursts. In rat models with experimental allergic encephalomyelitis (EAE), Garcion and colleagues showed

that 1α,25$(OH)_2$VitD inhibited the iNOS increases (Garcion et al. 1997). VitD restriction led to slight worsening of clinical symptoms (Garcion et al. 2003). Nitration of protein resident tyrosine residues also occurs during brain aging leading to mitochondrial dysfunction and neurodegeneration (MacMillan-Crow et al. 1998; Anantharaman et al. 2006; Tangpong et al. 2008).

A.6 Conclusions

This study is the first to demonstrate that a chronic low-VitD diet and consequential low levels of VitD in the bloodstream result in significant increases in tyrosine nitration in brain proteins, alterations in glucose metabolism and mitochondrial changes in brain of elderly rats, an animal model of brain in older human subjects (Figure A.1). A shift from the TCA cycle to glycolysis may be indicative of metabolic dysfunction. Further, ATP generated from glycolysis is important for maintaining a proper resting membrane potential in neurons (e.g., via NA^+/K^+ATPase), which is, in turn, important for neurotransmission. The results of this study are consistent with the notion that nitration of brain proteins occurs via NF-κB activation of iNOS. These results provide biochemical evidence to support the conclusions, consistent with other studies, that suggest that higher serum VitD levels may have direct and indirect anti-oxidant properties and be beneficial to modulate damaging effects of brain aging. Based on evidence from the present study and the literature as noted above, it is our opinion that current

daily VitD intake in the general adult population is too low and should be increased.

The present study used brain tissue from animals as part of a larger study examining the effects of serum VitD status and brain aging. A component of these larger studies examined learning and memory and a preliminary report indicated that low VitD animals displayed poorer performance, but that performance improved with high VitD (Latimer CS, et al., personal communication, 2011). Hence, these data support the present findings and conclusions.

As people age, their lifestyles become more sedentary, physically and mentally. Perhaps due to limited access, physical or financial limitations, or lack of motivation, nutritional status often declines. Concurrently, time spent outside decreases. Less sun exposure further decreases circulating VitD levels. Our studies, together with those of others, indicate that higher VitD may be beneficial for older individuals and, thus, it would appear that further studies are warranted to determine whether VitD supplementation can offset some of the changes associated with unhealthy brain aging. Further studies to address this issue are ongoing in our laboratory.

Copyright © Jeriel T. R. Keeney 2013

Appendix B

Insights into the mechanism of chemotherapy-induced cognitive impairment caused by the anti-cancer drug doxorubicin: Perspectives from a human clinical pilot study. In progress.

B.1 Overview of study

Our preliminary results are consistent with a novel hypothesis involving Doxorubicin(Dox)-induced, ROS-mediated plasma protein oxidation leading to peripheral TNF-α elevation which crosses the blood-brain barrier leading to CNS oxidative stress, mitochondrial damage, and cognitive impairment. The data presented here is from a human pilot study based on this hypothesis. Patients who entered the trial were randomly assigned into one of two treatment groups. For the first two cycles of chemotherapy, patients agreed to receive only Dox with or without MESNA, each combination for one of the first two cycles. A naïve blood sample was obtained prior to any treatment. Treatment then followed the schedule presented in figure B.1. Preliminary oxidative stress data as assessed by protein carbonyl levels is presented in figure B.2. The project is ongoing.

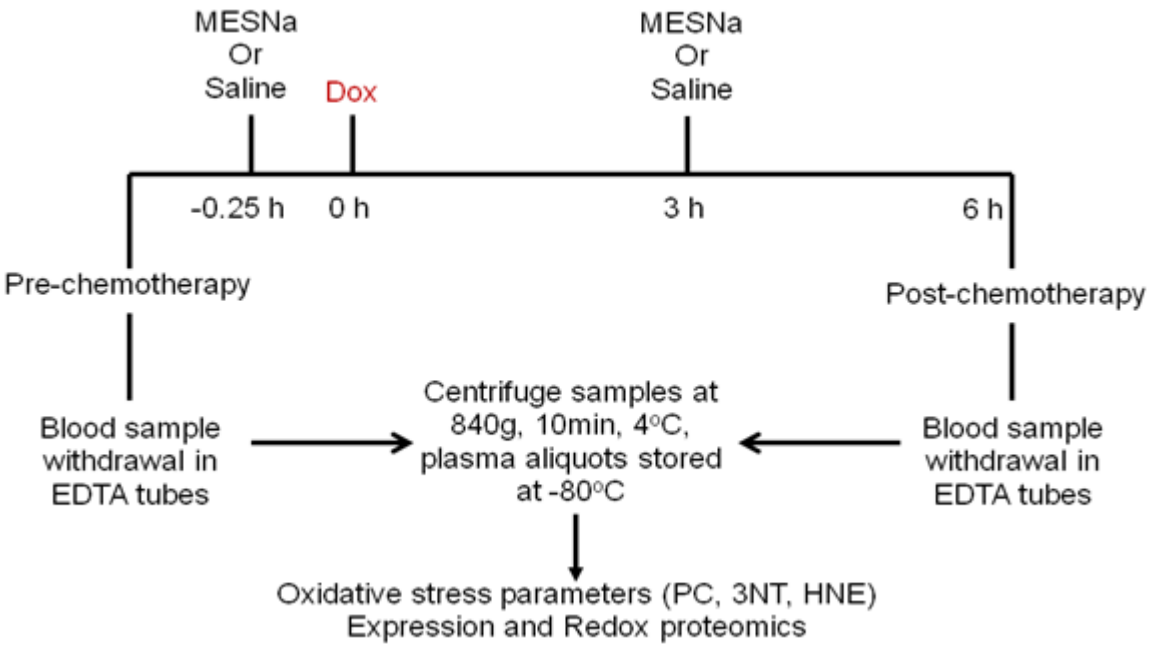

Figure B.1. Experimental Design: Dox/MESNA Human Clinical Pilot Study.

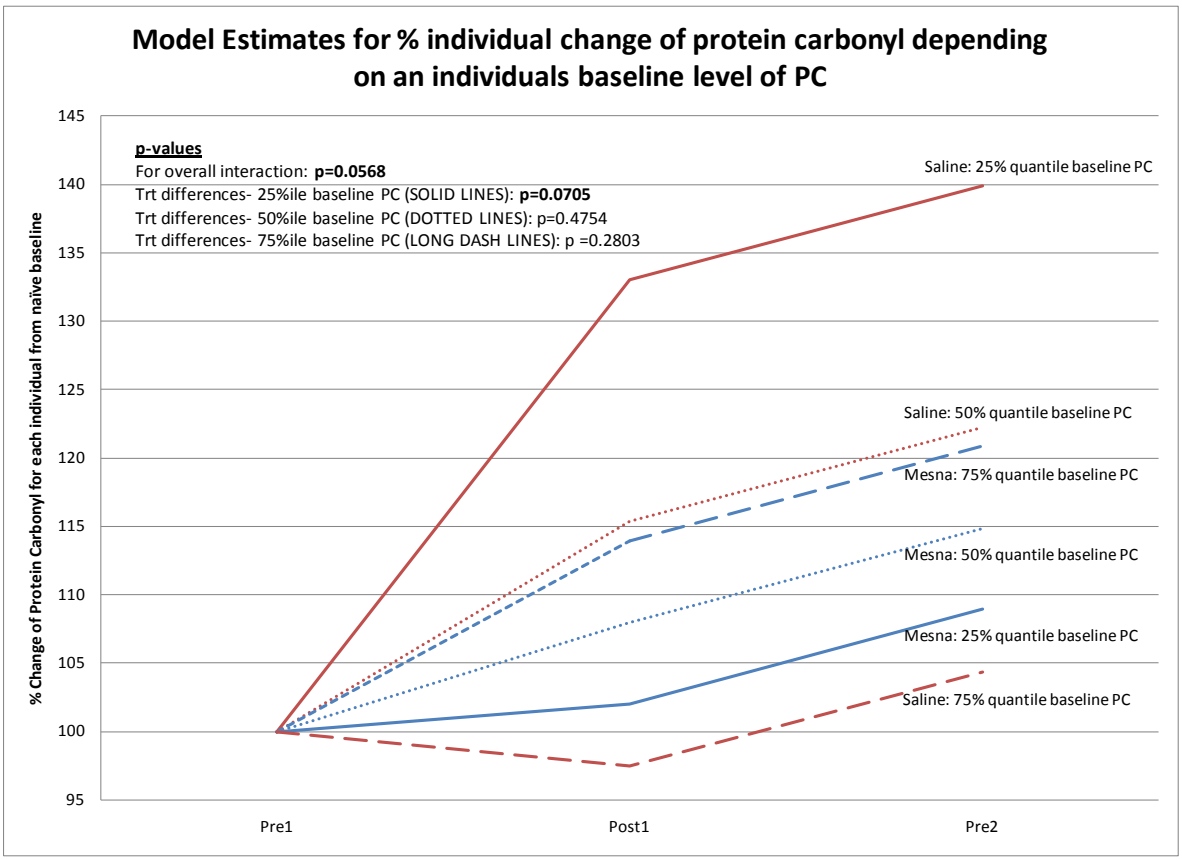

Figure B.2. Model estimates for percent change of protein carbonyl (PC) depending on an individual's baseline PC level.

Preliminary protein carbonyl (PC) data from our human pilot study show those patients who would potentially get the most PC prevention benefit from co-administration of MESNA with Dox.

B.2 Raw data from ongoing human trials

plasma	HNE-modified ApoA1, Human trial random 10				Ratio of change
Sample #	**HNE**	**ApoA1**	**HNE+ ApoA1**	**HNE/(HNE+ ApoA1)**	**post/pre**
AC4 1A	2347434	876672	3224106	0.728088344	0.914474405
AC4 1B	1485680	745680	2231360	0.665818156	
AC5 1A	3872838	696174	4569012	0.847631392	0.932328001
AC5 1B	3374240	895488	4269728	0.790270481	
CH2 1A	2756149	1115608	3871757	0.711860016	0.642612825
CH2 1B	1910020	2265340	4175360	0.457450376	
CH4 1A	3347280	1656256	5003536	0.668982895	1.162201598
CH4 1B	2091848	598656	2690504	0.77749299	
CH7 1A	2870784	1785434	4656218	0.616548452	0.6844679
CH7 1B	1825659	2500469	4326128	0.422007624	
CH8 1A	2263653	1533042	3796695	0.59621671	0.751527042
CH8 1B	972520	1197930	2170450	0.44807298	
CH10 1A	5246010	3124914	8370924	0.626694257	1.090927401
CH10 1B	4575129	2116807	6691936	0.683677937	
CH14 1A	1418877	44720	1463597	0.969445141	0.928934405
CH14 1B	1911124	211048	2122172	0.900550945	
CH18 1A	497670	9854	507524	0.980584169	0.891939481
CH18 1B	3670030	526104	4196134	0.874621735	
TA2 1A	2214449	1610648	3825097	0.578926234	0.48807523
TA2 1B	473246	1201608	1674854	0.282559554	

Collection Date	Sample Number	Collection Code	Approx vol collected (uL)	# of vials aliquoted	Sample Notes Collector
10/22/10	CH1	C1A	3300	7	R
10/22/10	CH1	C1B	3300	7	J
11/12/10	CH1	C2A	3300	7	R
11/12/10	CH1	C2B	3300	7	J
12/16/10	CH2	C1A	3300	7	J
12/16/10	CH2	C1B	4000	7	J
12/21/10	CH3	C1A	3200	10	T
12/21/10	CH3	C1B	3200	10	T
1/11/11	CH4	C1A	2000	5	J
1/11/11	CH4	C1B	2700	7	J
1/12/11	CH3	C2A	3600	7	J
1/12/11	CH3	C2B	4000	7	J
1/14/11	AC2	C1A	3100	7	J
1/14/11	AC2	C1B	2800	7	J
1/14/11	CH2	C2A	4000	7	J
1/14/11	CH2	C2B	4000	7	J
1/27/11	AC2	C2A	3300	7	J
1/27/11	AC2	C2B	3300	7	J
2/2/11	CH4	C2A	2800	7	J
2/2/11	CH5	C1A	4000	7	J
2/2/11	CH4	C2B	3200	7	J
2/2/11	CH5	C1B	3200	7	J
2/10/11	CH6	C1A	3600	7	J
2/10/11	CH6	C1B	3600	7	J
2/22/11	AC4	C1A	3200	6	T
2/22/11	AC4	C1B	3200	7	J
2/22/11	AC5	C1A	3600	7	J
2/22/11	AC5	C1B	3200	7	J
2/23/11	CH5	C2A	3600	7	J
2/23/11	CH5	C2B	3200	7	J
2/25/11	TA1	C1A	3600	7	J
2/25/11	TA1	C1B	3600	7	J
3/1/11	CH7	C1A	3600	7	J
3/1/11	CH7	C1B	3600	7	J
3/3/11	CH6	C2A	3300	7	J
3/3/11	CH8	C1A	3300	7	J
3/3/11	CH6	C2B	3300	7	J
3/3/11	CH8	C1B	3100	7	J
3/7/11	CH9	C1A	4000	7	J

3/7/11	CH9	C1B	4000	7	J
3/15/11	AC4	C2A	3200	7	J
3/15/11	CH7	C2A	3600	7	J
3/15/11	AC4	C2B	2800	7	J
3/15/11	CH7	C2B	4000	7	J
3/17/11	TA1	C2A	3200	7	J
3/17/11	TA1	C2B	3600	7	J
3/22/11	AC5	C2A	3600	7	J
3/22/11	AC5	C2B	3600	7	J
3/24/11	CH8	C2A	4000	7	J
3/24/11	CH8	C2B	3600	7	J
3/28/11	CH9	C2A	3600	7	J
3/28/11	CH9	C2B	3200	7	J
4/15/11	AC6	C1A	4000	7	J
4/15/11	AC6	C1B	4000	7	J
4/25/11	AC7	C1A	3200	7	J
4/25/11	AC7	C1B	2900	7	J
5/6/11	AC6	C2A	3300	7	J
5/6/11	AC6	C2B	3600	7	G
5/13/11	CH10	C1A	3500	7	G
5/13/11	CH10	C1B	3500	7	G
5/16/11	AC7	C2A	3500	7	J
5/16/11	AC7	C2B	3600	7	J
5/19/11	CH11	C1A	2900	7	J
5/19/11	CH11	C1B	3300	7	J
6/2/11	CH10	C2A	3200	7	J
6/2/11	CH10	C2B	3300	7	J
6/9/11	CH11	C2A	3200	7	J
6/9/11	CH11	C2B	3100	7	J
6/28/11	AC8	C1A	3600	7	J
6/28/11	AC8	C1B	3300	7	J
7/26/11	AC8	C2A	2800	7	J
7/26/11	AC8	C2B	2800	7	J
8/25/11	CH14	C1A	2900	7	J
8/25/11	CH13	C1A	3300	7	J
8/25/11	CH14	C1B	2900	7	J
8/25/11	CH13	C1B	3300	7	J
9/15/11	CH15	C1A	3300	7	J
9/15/11	CH13	C2A	3300	7	J
9/15/11	CH13	C2B	3300	7	J
9/15/11	CH15	C1B	3500	7	J

9/16/11	AC9	C1A	2900	6(+1)	T
9/16/11	AC9	C1B	2800	7	T
9/20/11	CH14	C2A	2800	7	J
9/20/11	CH14	C2B	2700	7	J
9/23/11	AC10	C1A	3700	7	J
9/23/11	AC10	C1B	3600	7	J
9/29/11	AC9	C2A	3100	7	J
9/29/11	AC9	C2B	3200	7	J
10/6/11	CH15	C2A	3100	7	J
10/6/11	CH15	C2B	3100	7	J
10/24/11	AC10	C2A	3700	7	J
10/24/11	AC10	C2B	3500	7	J
12/29/11	CH16	C1A	4000	8	T
12/29/11	CH16	C1B	4000	8	T
1/6/12	CH17	C1A	4000	7	J
1/6/12	CH17	C1B	4000	7	J
1/17/12	CH18	C1A	3400	7	J
1/17/12	CH18	C1B	3400	7	J
1/19/11	CH16	C2A	3600	7	J
1/19/11	CH16	C2B	3500	7	J
1/20/11	TA2	C1A	3300	7	J
1/20/11	TA2	C1B	3400	7	J
1/25/12	AC11	C1A	3400	7	J
1/25/12	AC11	C1B	3400	7	J
1/27/12	CH17	C2A	3500	7	T
1/27/12	CH17	C2B	3500	7	T
1/30/12	AC12	C1A	3400	7	J
1/30/12	AC12	C1B	3600	7	J
2/7/12	CH18	C2A	3300	7	J
2/7/12	CH18	C2B	3400	7	J
2/8/12	TA2	C2A	3500	7	J
2/8/12	TA2	C2B	3500	7	J
2/8/12	AC11	C2A	3500	7	J
2/8/12	AC11	C2B	3500	7	J
3/27/12	CH19	C1A	3400	7	J
3/27/12	CH19	C1B	3600	7	J
4/17/12	CH19	C2A	3400	7	J
4/17/12	CH19	C2B	3800	7	J
4/24/12	CH20	C1A	3700	7	J

4/24/12	CH20	C1B	3800	7	J
5/15/12	CH20	C2A	3800	7	J
5/15/12	CH20	C2B	3800	7	J
5/25/12	AC13	C1A	3500	7	J
5/25/12	AC13	C1B	3500	7	J
6/15/12	AC13	C2A	3500	7	T
6/15/12	AC13	C2B	3500	7	T

Eureka Grant Human Trial Graphs
PC slotblot set1 avg%control 5Jun2012

	Blot 1 % naïve control	**Blot 2 % naïve control**	**Avg %** control	**trend from naïve**	**trend from pre to post**
CH1 C1A	100	100	100		
CH1 C1B	30.48887	47.21279	38.85083	**DOWN**	**DOWN**
CH1 C2A	53.19467	59.98822	56.59145	**DOWN**	
CH1 C2B	4.831667	20.9032	12.86743	**DOWN**	**DOWN**
CH2 C1A	100	100	100		
CH2 C1B	104.5881	91.70973	98.14891	same	same
CH2 C2A	56.10178	36.1957	46.14874	**DOWN**	
CH2 C2B	33.33926	15.5469	24.44308	**DOWN**	**DOWN**
CH3 C1A	100	100	100		
CH3 C1B	344.2072	129.3153	236.7612	**UP**	**UP**
CH3 C2A	176.1221	141.4497	158.7859	**UP**	
CH3 C2B	330.952	213.7081	272.3301	**UP**	**UP**
CH4 C1A	100	100	100		
CH4 C1B	5.106001	16.05881	10.5824	**DOWN**	**DOWN**

CH4 C2A	91.37903	87.67585	89.52744	down	
CH4 C2B	81.37535	70.52749	75.95142	down	same

Eureka Grant Human Trial
PC slotblot set2 blot1 5Jun2012

	Rep1	Rep2	Rep3	RepAvg	RepStdDev	%CV	Blot 1 % naïve control
AC2 C1A	42.38	62.07	73.14	59.19667	15.580001	26.31905	100
AC2 C1B	45.34	53.14	55.85	51.44333	5.4565587	10.60693	86.90242
AC2 C2A	133.15	136.58	127.37	132.3667	4.6547001	3.51652	223.6049
AC2 C2B	94.96	96.46	89.75	93.72333	3.5217941	3.757649	158.3254
CH5 C1A	127.32	126.77	123.71	125.9333	1.9450021	1.54447	100
CH5 C1B	124.25	125.18	118.26	122.5633	3.7556935	3.064288	97.32398
CH5 C2A	101.08	116.42	117.06	111.52	9.0469663	8.112416	88.55479
CH5 C2B	88.64	103.92	104.22	98.92667	8.9097774	9.006447	78.55479
CH6 C1A	117.37	105.65	102.16	108.3933	7.9674609	7.350508	100
CH6 C1B	74.71	78.25	77.5	76.82	1.8653954	2.428268	70.87152
CH6 C2A	155.85	157.11	151.55	154.8367	2.9152244	1.882774	142.847
CH6 C2B	144.15	142.56	146.35	144.3533	1.903164	1.318407	133.1755
AC4 C1A	87.87	84.84	80.31	84.34	3.8047208	4.51117	100
AC4 C1B	86.68	83.15	76.14	81.99	5.3648952	6.543353	97.21366
AC4 C2A	87.5	87.78	77.73	84.33667	5.7232537	6.786199	99.99605
AC4 C2B	73.45	68.7	65.6	69.25	3.9537956	5.709452	82.10813

Eureka Grant Human Trial
PC slotblot set2 blot2 5Jun2012

	Rep1	Rep2	Rep3	RepAvg	RepStdDev	%CV	Blot 2 % naïve control
AC2 C1A	63.98	94.15	103.49	87.20667	20.649877	23.67924	100
AC2 C1B	50.51	70.38	77.31	66.06667	13.910918	21.05588	75.75873
AC2 C2A	109.05	136.98	139.39	128.4733	16.864206	13.12662	147.3205
AC2 C2B	77.46	95.52	100.5	91.16	12.123019	13.29862	104.5333
CH5 C1A	88.27	98.81	81.94	89.67333	8.5221026	9.503497	100
CH5 C1B	79.11	92.47	81.4	84.32667	7.1446787	8.472621	94.03762

CH5 C2A	74.9	85.66	77.9	79.48667	5.552705	6.985706	88.64025
CH5 C2B	63.52	70.19	70.45	68.05333	3.9281336	5.77214	75.89027
CH6 C1A	118.27	115.87	129.37	121.17	7.202083	5.943784	100
CH6 C1B	80.11	79.83	77.46	79.13333	1.4558961	1.839801	65.30769
CH6 C2A	170	176.06	164.57	170.21	5.7478779	3.376933	140.4721
CH6 C2B	171.82	167.45	158.8	166.0233	6.6262081	3.991131	137.0169
AC4 C1A	81.31	94.29	101.33	92.31	10.155806	11.00185	100
AC4 C1B	73.93	90.4	85.74	83.35667	8.4897252	10.18482	90.3008
AC4 C2A	98.16	114.2	113.4	108.5867	9.0386135	8.32387	117.6326
AC4 C2B	76.66	88.49	89.13	84.76	7.0221008	8.284687	91.82104

Eureka Grant Human Trial Graphs
PC slotblot set2 blot1 5Jun2012

	Blot 1 % naïve control	**Blot 2 % naïve control**	**Avg % naïve control**	**trend from naïve**	**trend from pre to post**
AC2 C1A	100	100	100		
AC2 C1B	86.90242	75.75873	81.330575	**down**	**down**
AC2 C2A	223.6049	147.3205	185.46274	**UP**	
AC2 C2B	158.3254	104.5333	131.42932	up	down
CH5 C1A	100	100	100		
CH5 C1B	97.32398	94.03762	95.680799	same	same
CH5 C2A	88.55479	88.64025	88.59752	down	
CH5 C2B	78.55479	75.89027	77.22253	**down**	**down**
CH6 C1A	100	100	100		
CH6 C1B	70.87152	65.30769	68.089606	**DOWN**	**DOWN**
CH6 C2A	142.847	140.4721	141.65955	up	
CH6 C2B	133.1755	137.0169	135.09617	up	same
AC4 C1A	100	100	100		
AC4 C1B	97.21366	90.3008	93.757229	same	same
AC4 C2A	99.99605	117.6326	108.81433	up	
AC4 C2B	82.10813	91.82104	86.964586	**down**	**down**

Set 3 PC

Set 3 PC

	rep1	**rep2**	**rep3**	**repAvg**	**RepStdDev**	**%CV**
AC5 C1A	217.69	215.7	219.61	217.6667	1.9551044	0.89821

AC5 C1B	245.61	248.61	236.37	243.53	6.3795925	2.619633
AC5 C2A	305.02	278.61	290.83	291.4867	13.21724	4.534424
AC5 C2B	262.19	216.78	210.81	229.9267	28.099862	12.22123
TA1 C1A	253.25	230.52	218.62	234.13	17.594979	7.515047
TA1 C1B	303.42	246.53	258.53	269.4933	29.987731	11.12745
TA1 C2A	286.4	252.64	264.05	267.6967	17.172887	6.415054
TA1 C2B	251.54	261.39	271.46	261.4633	9.9602025	3.809407
CH7 C1A	234.05	225.31	237.27	232.21	6.1886671	2.665117
CH7 C1B	316.97	260.14	233.5	270.2033	42.635235	15.77894
CH7 C2A	282.18	253.9	228.54	254.8733	26.833243	10.52807
CH7 C2B	281.89	243.5	220.92	248.77	30.824745	12.39086
CH8 C1A	239.87	236.52	239.22	238.5367	1.7764665	0.744735
CH8 C1B	246.98	249.84	267.78	254.8667	11.274331	4.423619
CH8 C2A	238.86	236.13	234.33	236.44	2.2808551	0.964665
CH8 C2B	250.55	254.05	241.55	248.7167	6.448514	2.592715
					avg%cv	6.201824

	rep1	**rep2**	**rep3**	**repAvg**	**RepStdDev**	**%CV**
AC5 C1A	188.49	230.94	206.42	208.6167	21.310083	10.21495
AC5 C1B	121.79	150.35	145.68	139.2733	15.320001	10.99995
AC5 C2A	312.3	319.79	349.39	327.16	19.612616	5.994809
AC5 C2B	258.75	246.61	248.7	251.3533	6.4903801	2.582174
TA1 C1A	255.35	248.21	236.71	246.7567	9.4046017	3.811286
TA1 C1B	160.43	173.62	163.03	165.6933	6.986704	4.216648
TA1 C2A	251.3	273.52	289.14	271.32	19.015688	7.008583
TA1 C2B	249.66	261.02	278.07	262.9167	14.299652	5.438853
CH7 C1A	295.45	256.45	275.54	275.8133	19.501437	7.07052
CH7 C1B	193.83	156.21	144.22	164.7533	25.884927	15.71132
CH7 C2A	266.86	282.42	255.06	268.1133	13.722993	5.118355
CH7 C2B	267.75	228.2	220.37	238.7733	25.398083	10.6369
CH8 C1A	238.48	222.74	220.89	227.37	9.665904	4.251178
CH8 C1B	373.33	333.28	324.04	343.55	26.200777	7.626481
CH8 C2A	304.81	261.67	239.47	268.65	33.224527	12.36722
CH8 C2B	353.29	335.03	331.34	339.8867	11.753341	3.458018
					avg%cv	7.281703

			Avg%Con
AC5 C1A	100	100	100
AC5 C1B	111.8821	66.76041	89.32124
AC5 C2A	133.9142	156.8235	145.3689
AC5 C2B	105.6325	120.4857	113.0591
TA1 C1A	100	100	100
TA1 C1B	115.1041	67.14847	91.12631

TA1 C2A	114.3368	109.9545	112.1456
TA1 C2B	111.6744	106.549	109.1117
CH7 C1A	100	100	100
CH7 C1B	116.3616	59.73364	88.04763
CH7 C2A	109.7598	97.20826	103.4841
CH7 C2B	107.1315	86.57063	96.85105
CH8 C1A	100	100	100
CH8 C1B	106.8459	151.0973	128.9716
CH8 C2A	99.12103	118.1554	108.6382
CH8 C2B	104.2677	149.4862	126.8769

PC Set4 CH9, AC6, AC7, CH10

Blot 1

Sample	**Rep1**	**Rep2**	**Rep3**	**RepAvg**	**RepStdDev**	**%CV**
CH9 C1A	218.87	258.06	284.92	253.95	33.216257	13.07984
CH9 C1B	264.74	284.32	315.32	288.126667	25.503963	8.85165
CH9 C2A	168.19	187.83	202.4	186.14	17.167501	9.222897
CH9 C2B	210.59	218.69	248.53	225.936667	19.981154	8.843697
AC6 C1A	166.88	175.28	202.67	181.61	18.715841	10.30551
AC6 C1B	274.96	307.59	318.78	300.443333	22.767394	7.577933
AC6 C2A	248.5	301.67	343.66	297.943333	47.689332	16.00618
AC6 C2B	231.76	261.15	289.25	260.72	28.747412	11.02616
AC7 C1A	201.62	186.26	179.91	189.263333	11.162259	5.89774
AC7 C1B	271	249.6	230.66	250.42	20.182497	8.059459
AC7 C2A	295.05	269.85	254.69	273.196667	20.387068	7.462415
AC7 C2B	239.18	239.78	222.65	233.87	9.7214351	4.156769
CH10 C1A	288.3	267.33	249.42	268.35	19.460059	7.251746
CH10 C1B	305.6	279.75	251.47	278.94	27.074089	9.706062
CH10 C2A	278.54	253.18	239.36	257.026667	19.871229	7.731193
CH10 C2B	248.21	241.87	272.15	254.076667	15.969751	6.285406
Blot 2	**Rep1**	**Rep2**	**Rep3**	**RepAvg**	**RepStdDev**	**%CV**
CH9 C1A	93.19	99.77	97.94	96.9666667	3.3962676	3.50251
CH9 C1B	118.9	144.25	155.12	139.423333	18.586141	13.33072
CH9 C2A	100.76	126.51	138.2	121.823333	19.154948	15.72355
CH9 C2B	80.8	79.13	83.09	81.0066667	1.9880728	2.454209
AC6 C1A	147.79	148.37	148.98	148.38	0.595063	0.40104
AC6 C1B	140.83	162.35	156.39	153.19	11.111148	7.253181
AC6 C2A	171.85	184.11	181.99	179.316667	6.552628	3.654221
AC6 C2B	194.8	184.97	178.22	185.996667	8.3375436	4.482631
AC7 C1A	111.79	113.3	113.39	112.826667	0.8989067	0.796715
AC7 C1B	155.13	140.34	139.95	145.14	8.6537911	5.962375
AC7 C2A	164.51	153.9	130.09	149.5	17.626801	11.7905

AC7 C2B	144.91	127.77	113.32	128.666667	15.814077	12.29073
CH10 C1A	246.33	234.63	208.47	229.81	19.384767	8.435128
CH10 C1B	239.98	234.57	205.88	226.81	18.326639	8.080172
CH10 C2A	106.5	109.96	106.12	107.526667	2.1158765	1.967769
CH10 C2B	250.27	247.2	250	249.156667	1.6998922	0.682258

comparison	Blot1 %Con	Blot2 %Con	Blot Avg	Blot StdDev	Blot%CV	Graph Lanes
CH9 C1A	100	100	100	0	0	1
CH9 C1B	113.45803	143.784806	128.6214	21.4442689	16.672394	2
CH9 C2A	73.2978933	125.634239	99.46607	37.0073847	37.20604	3
CH9 C2B	88.9689571	83.5407356	86.25485	3.83833223	4.4499902	4
AC6 C1A	100	100	100	0	0	5
AC6 C1B	165.433254	103.241677	134.3375	43.9760863	32.735534	6
AC6 C2A	164.056678	120.84962	142.4531	30.5520036	21.447054	7
AC6 C2B	143.560377	125.351575	134.456	12.8755673	9.5760469	8
AC7 C1A	100	100	100	0	0	9
AC7 C1B	132.313003	128.639801	130.4764	2.59734575	1.9906632	10
AC7 C2A	144.347382	132.504136	138.4258	8.37443943	6.0497696	11
AC7 C2B	123.568573	114.039234	118.8039	6.73825999	5.6717497	12
CH10 C1A	100	100	100	0	0	13
CH10 C1B	103.946339	98.6945738	101.3205	3.71355862	3.6651618	14
CH10 C2A	95.7803863	46.7893767	71.28488	34.6418751	48.596384	15
CH10 C2B	94.6810757	108.418549	101.5498	9.71386028	9.5656113	16

Set 5					%control	%control	%control	%control
Blot 1	**Rep1**	**Rep2**	**Rep3**	**Rep Avg**	**Rep1**	**Rep2**	**Rep3**	**Rep Avg**
CH11 C1A	174.9	155.34	164.12	164.1867	106.1372	94.26734	99.59544	100
CH11 C1B	186.39	172.15	161.38	173.3067	113.1099	104.4684	97.93268	105.1703
CH11 C2A	152.91	190.54	152.31	165.2533	92.7927	115.6283	92.42859	100.2832
CH11 C2B	126.57	127.26	134.52	129.45	76.8084	77.22712	81.63282	78.55611
AC8 C1A	221.12	250.99	246.96	239.69	92.25249	104.7144	103.0331	100
AC8 C1B	137.11	203.33	222.18	187.54	57.20305	84.83041	92.69473	78.24273
AC8 C2A	104.67	112.63	110.08	109.1267	43.66891	46.98986	45.92599	45.52825
AC8 C2B	174.77	183.74	180.32	179.61	72.91502	76.65735	75.23051	74.93429

CH13 C1A	219.86	223.24	184.89	209.33	105.0303	106.645	88.32465	100
CH13 C1B	277	305.54	257.87	280.1367	132.3269	145.9609	123.1883	133.8254
CH13 C2A	217.08	243.29	200.3	220.2233	103.7023	116.2232	95.68624	105.2039
CH13 C2B	279.2	289.15	292.41	286.92	133.3779	138.1312	139.6885	137.0659
CH14 C1A	534.29	527.76	494.42	518.8233	102.9811	101.7225	95.29641	100
CH14 C1B	472.96	475.02	458.03	468.67	91.16013	91.55718	88.28246	90.33325
CH14 C2A	435.37	442.27	422.49	433.3767	83.91488	85.24482	81.43234	83.53068
CH14 C2B	256.14	260.39	184.74	233.7567	49.36941	50.18857	35.6075	45.05516
Blot 2	**Rep1**	**Rep2**	**Rep3**	**Rep Avg**				
CH11 C1A	147.11	177.89	197.08	174.0267	84.53302	102.22	113.247	100
CH11 C1B	127.47	141.73	146.6	138.6	73.2474	81.44154	84.23996	79.64297
CH11 C2A	210.59	260.23	249.34	240.0533	121.0102	149.5346	143.2769	137.9405
CH11 C2B	565.63	672.26	704.3	647.3967	325.0249	386.2971	404.7081	372.01
AC8 C1A	208.67	258.12	280.07	248.9533	83.81892	103.6821	112.499	100
AC8 C1B	227.76	317.83	331.16	292.25	91.48703	127.6665	133.0209	117.3915
AC8 C2A	204.49	273.45	277.23	251.7233	82.13989	109.8399	111.3582	101.1127
AC8 C2B	142.4	184.83	176.27	167.8333	57.19948	74.24283	70.80443	67.41558
CH13 C1A	233.98	230.42	206.03	223.4767	104.7	103.107	92.19307	100
CH13 C1B	175.37	175.52	162.03	170.9733	78.47352	78.54064	72.50421	76.50612
CH13 C2A	299.53	285.59	239.42	274.8467	134.0319	127.7941	107.1342	122.9867
CH13 C2B	217.79	233.43	206.24	219.1533	97.45536	104.4539	92.28704	98.06542
CH14 C1A	401.63	359.32	318.85	359.9333	111.5846	99.8296	88.58585	100
CH14 C1B	288.92	228.6	247.88	255.1333	80.27042	63.51176	68.86831	70.8835
CH14 C2A	172.81	176.05	176.56	175.14	48.01167	48.91184	49.05353	48.65901
CH14	153.53	167.15	160.83	160.503	42.6551	46.4391	44.6832	

C2B				3	2	6	7	
Set 6					%control	%control	%control	%control
Blot 1	**Rep1**	**Rep2**	**Rep3**	**Rep Avg**	**Rep1**	**Rep2**	**Rep3**	**Rep Avg**
CH15 C1A	965.87	988.29	1027.3	993.82	97.18762	99.4435 6	103.3688	100
CH15 C1B	864.36	886.32	894.67	881.7833	86.9735	89.18315	90.02334	88.72666
CH15 C2A	627.54	663.48	567.61	619.5433	63.14423	66.76058	57.11396	62.33959
CH15 C2B	583.47	632.45	542.21	586.0433	58.70983	63.63828	54.55817	58.96876
AC9 C1A	360.39	415.34	325.26	366.9967	98.1998	113.1727	88.62751	100
AC9 C1B	594.49	593.44	563.25	583.7267	161.9878	161.7017	153.4755	159.055
AC9 C2A	258.14	241.15	216.01	238.4333	70.33851	65.70904	58.85885	64.9688
AC9 C2B	272.71	254.68	260.78	262.7233	74.30858	69.39573	71.05787	71.58739
AC10 C1A	297.92	304.68	250	284.2	104.8276	107.2062	87.96622	100
AC10 C1B	472.56	465.41	393.37	443.78	166.2773	163.7614	138.4131	156.1506
AC10 C2A	893.39	814.33	713.12	806.9467	314.3526	286.5341	250.9219	283.9362
AC10 C2B	506.37	429.38	341.09	425.6133	178.1738	151.0837	120.0176	149.7584
CH16 C1A	812.43	713.28	628.03	717.9133	113.1655	99.35461	87.47992	100
CH16 C1B	464.96	405.41	348.01	406.1267	64.76548	56.4706	48.47521	56.57043
CH16 C2A	564.06	542.57	443.9	516.8433	78.56937	75.57597	61.83198	71.99244
CH16 C2B	661.26	578.35	533.76	591.1233	92.10861	80.55986	74.34881	82.33909
Blot 2	**Rep1**	**Rep2**	**Rep3**	**Rep Avg**				
CH15 C1A	364.42	380.43	404.48	383.11	95.12151	99.30046	105.578	100
CH15 C1B	175.95	216.11	203.99	198.6833	45.92676	56.40939	53.2458	51.86065
CH15 C2A	204.2	237.97	230.14	224.1033	53.30062	62.11532	60.07152	58.49582
CH15 C2B	252.08	289.14	278.28	273.1667	65.79833	75.4718	72.6371	71.30241

AC9 C1A	164.04	150.69	138.03	150.92	108.6933	99.8476	91.45905	100
AC9 C1B	273.06	276.41	258.05	269.1733	180.9303	183.15	170.9846	178.355
AC9 C2A	269.83	268.21	259.86	265.9667	178.7901	177.7167	172.1839	176.2302
AC9 C2B	263.16	277.77	272.62	271.1833	174.3705	184.0512	180.6387	179.6868
AC10 C1A	212.86	188.76	189.2	196.94	108.0837	95.84645	96.06987	100
AC10 C1B	267.29	261.55	229.19	252.6767	135.7215	132.8069	116.3755	128.3013
AC10 C2A	230.78	212.28	204.59	215.8833	117.1829	107.7892	103.8844	109.6188
AC10 C2B	237.74	231.33	201.22	223.43	120.717	117.4622	102.1733	113.4508
CH16 C1A	290.02	288.16	284.58	287.5867	100.8461	100.1994	98.95452	100
CH16 C1B	306.4	275.65	262.17	281.4067	106.5418	95.84937	91.16208	97.85108
CH16 C2A	287.18	282.6	253.11	274.2967	99.85859	98.26603	88.01173	95.37878
CH16 C2B	237.93	221.27	235.23	231.4767	82.73332	76.94028	81.79447	80.48936

Set 7					%control	%control	%control	%control
Blot 1	**Rep1**	**Rep2**	**Rep3**	**Rep Avg**	**Rep1**	**Rep2**	**Rep3**	**Rep Avg**
CH17 C1A	228.35	309.37	338.81	292.1767	78.15477	105.8846	115.9607	100
CH17 C1B	369.84	493.85	505.2	456.2967	126.5809	169.0244	172.9091	156.1715
CH17 C2A	261.38	409.34	543.15	404.6233	89.45957	140.1002	185.8978	138.4858
CH17 C2B	217.85	251.61	315.62	261.6933	74.56105	86.11571	108.0237	89.56681
CH18 C1A	343.27	331.38	322.75	332.4667	103.2494	99.67315	97.0774	100
CH18 C1B	311.31	326.42	314.78	317.5033	93.63645	98.18127	94.68017	95.4993
CH18 C2A	371.56	450.89	462.73	428.3933	111.7586	135.6196	139.1809	128.853
CH18 C2B	250	263.81	253.95	255.92	75.19551	79.34931	76.3836	76.97614
TA2 C1A	286.17	276.8	299.37	287.4467	99.55586	96.29612	104.148	100
TA2	277.06	300.47	245.2	274.243	96.3865	104.530	85.3027	95.4066

C1B				3	8	7	8	8
TA2				328.096	120.171	119.211	103.041	114.141
C2A	345.43	342.67	296.19	7	9	7	7	8
TA2					94.5149	100.216	73.4188	89.3835
C2B	271.68	288.07	211.04	256.93	2	9	4	4
AC11				288.003	101.689		87.1552	
C1A	292.87	320.13	251.01	3	8	111.155	4	100
AC11				299.776	108.137	122.394	81.7316	104.087
C1B	311.44	352.5	235.39	7	6	4	9	9
AC11				328.473	115.932	132.248	93.9746	114.051
C2A	333.89	380.88	270.65	3	7	5	1	9
AC11				281.033	94.0162	107.929	90.7940	97.5798
C2B	270.77	310.84	261.49	3	7	3	9	9
Blot 2	**Rep1**	**Rep2**	**Rep3**	**Rep Avg**				
CH17					85.2830	100.593	114.123	
C1A	208.5	245.93	279.01	244.48	5	1	9	100
CH17				208.096	71.4455	86.7269	97.1817	85.1180
C1B	174.67	212.03	237.59	7	2	3	7	7
CH17					86.3015	113.980	120.566	106.949
C2A	210.99	278.66	294.76	261.47	4	7	1	4
CH17				180.933	75.0449	69.5844	77.3928	74.0074
C2B	183.47	170.12	189.21	3	9	2	3	2
CH18					95.4441	107.440	97.1149	
C1A	380.45	428.27	387.11	398.61	7	9	7	100
CH18					48.0243	60.4851	61.5062	56.6719
C1B	191.43	241.1	245.17	225.9	8	9	3	3
CH18				392.523	88.0785	105.499	101.841	98.4730
C2A	351.09	420.53	405.95	3	7	1	4	3
CH18				264.176	54.6850	71.4482		66.2744
C2B	217.98	284.8	289.75	7	3	8	72.6901	7
TA2				210.503	92.8963	108.102	99.0008	
C1A	195.55	227.56	208.4	3	9	8	1	100
TA2					141.755	152.919	142.719	145.798
C1B	298.4	321.9	300.43	306.91	5	2	8	2
TA2					112.691	127.185	115.513	118.463
C2A	237.22	267.73	243.16	249.37	8	6	6	7
TA2				126.263	53.5003	59.6712	66.7732	59.9816
C2B	112.62	125.61	140.56	3	4	6	9	3
AC11				227.943	102.516	106.386		
C1A	233.68	242.5	207.65	3	7	1	91.0972	100
AC11				234.013	105.394	110.110	92.4835	102.662
C1B	240.24	250.99	210.81	3	6	7	1	9
AC11					113.787	107.355	95.3833	105.508
C2A	259.37	244.71	217.42	240.5	1	6	6	7
AC11				228.316	110.220	99.8844		100.163
C2B	251.24	227.68	206.03	7	4	7	90.3865	8

Set 8					%control	%control	%control	%control
Blot 1	**Rep1**	**Rep2**	**Rep3**	**Rep Avg**	**Rep1**	**Rep2**	**Rep3**	**Rep Avg**
AC12 C1A	249.52	247.51	310.13	269.0533	92.73998	91.99291	115.2671	100
AC12 C1B	173.59	198.52	216.37	196.16	64.51881	73.78463	80.419	72.90748
AC12 C2A	182.47	190.8	196.23	189.8333	67.81927	70.91531	72.9335	70.55602
AC12 C2B	203.74	209.67	219.11	210.84	75.72476	77.92879	81.43739	78.36365
CH19 C1A	218.65	275.27	293.43	262.45	83.31111	104.8847	111.8042	100
CH19 C1B	245.94	279.53	302.41	275.96	93.70928	106.5079	115.2258	105.1476
CH19 C2A	264.86	276.66	297.75	279.7567	100.9183	105.4144	113.4502	106.5943
CH19 C2B	177.13	190.89	215.14	194.3867	67.49095	72.73385	81.97371	74.06617
CH20 C1A	293.78	294.27	320.29	302.78	97.02754	97.18938	105.7831	100
CH20 C1B	360.05	375.56	408.46	381.3567	118.9147	124.0373	134.9032	125.9517
CH20 C2A	292.05	279.57	319.35	296.99	96.45617	92.33437	105.4726	98.08772
CH20 C2B	221.85	223.4	264.04	236.43	73.27102	73.78294	87.20523	78.0864
AC13 C1A	265.95	255.55	276.37	265.9567	99.99749	96.08708	103.9154	100
AC13 C1B	223.37	213.15	238.12	224.88	83.98737	80.14464	89.53338	84.55513
AC13 C2A	208.64	219.51	241.24	223.13	78.44887	82.536	90.70651	83.89713
AC13 C2B	180.09	188.88	201.12	190.03	67.71404	71.01909	75.62134	71.45149
Blot 2	**Rep1**	**Rep2**	**Rep3**	**Rep Avg**				
AC12 C1A	106.02	127.3	132.18	121.8333	87.02052	104.487	108.4925	100
AC12 C1B	157.2	169.92	169.64	165.5867	129.0287	139.4692	139.2394	135.9124
AC12 C2A	152.07	203.04	194.45	183.1867	124.8181	166.6539	159.6033	150.3584
AC12 C2B	143.61	145.9	153.07	147.5267	117.8741	119.7538	125.6389	121.0889
CH19 C1A	305.91	301.1	263.15	290.0533	105.4668	103.8085	90.72469	100
CH19 C1B	307.92	379.68	364.32	350.64	106.1598	130.9001	125.6045	120.8881

CH19 C2A	313.48	377.77	382.72	357.99	108.0767	130.2416	131.9481	123.4221
CH19 C2B	267.7	311.41	305.91	295.0067	92.29337	107.363	105.4668	101.7077
CH20 C1A	434.8	402.79	394.5	410.6967	105.8689	98.07482	96.05629	100
CH20 C1B	436.35	420.98	419.16	425.4967	106.2463	102.5039	102.0607	103.6036
CH20 C2A	307.37	320.08	323.19	316.88	74.84112	77.93587	78.69311	77.1567
CH20 C2B	312.41	305.98	332.68	317.0233	76.06831	74.50267	81.00382	77.1916
AC13 C1A	219.6	236.41	279.38	245.13	89.58512	96.4427	113.9722	100
AC13 C1B	243.29	220.28	237.59	233.72	99.24938	89.86252	96.92408	95.34533
AC13 C2A	331.11	303.3	316.46	316.9567	135.0753	123.7303	129.0988	129.3015
AC13 C2B	253.46	258.06	250	253.84	103.3982	105.2748	101.9867	103.5532

Dox/MESNA human clinical trial HNE Set 6 blot 1

Sample	**Rep1**	**Rep2**	**Rep3**	RepAvg	RepStdDev	Rep%CV
	2,494,029	2,563,026	3,741,861	2,932,972	701367.38	23.9132
	2,947,251	2,659,164	2,813,835	2,806,750	144174.12	5.136693
	2,356,362	2,325,297	2,668,102	2,449,920	189588.21	7.738546
	2,724,891	2,879,671	2,933,953	2,846,172	108482.18	3.811512
	2,508,635	3,406,904	3,414,643	3,110,061	520864.28	16.74772
	2,315,269	2,474,518	3,453,011	2,747,599	616071.65	22.42218
	2,923,925	2,891,770	3,532,363	3,116,019	360922.46	11.58281
	2,664,505	2,724,019	2,708,977	2,699,167	30946.02	1.146503
	6,547,957	7,026,031	6,859,915	6,811,301	242716.25	3.563435
	4,457,119	4,420,822	5,395,064	4,757,668	552299.1	11.60861
	3,864,159	3,855,875	3,630,899	3,783,644	132346.17	3.497849

	4,130,991	4,164,454	4,109,627	4,135,024	27635.101	0.668318
	4,630,102	3,983,623	3,769,002	4,127,576	448235.52	10.85953
	3,805,190	5,005,498	4,170,558	4,327,082	615272.01	14.2191
	3,477,536	3,632,752	3,740,553	3,616,947	132218.89	3.655538
	3,288,966	3,313,600	4,242,062	3,614,876	543298.64	15.02952
						9.725066

Sample	**Rep1**	**Rep2**	**Rep3**	RepAvg	RepStdDev	Rep%CV
	3,280,464	4,887,560	5,462,099	4,543,374	1130809.7	24.8892
	2,971,885	3,412,790	3,788,077	3,390,917	408535.38	12.04793
	2,633,876	2,311,127	2,408,573	2,451,192	165541.58	6.753513
	2,960,113	2,714,536	3,729,762	3,134,804	529677.81	16.89668
	2,780,699	2,780,045	3,362,977	2,974,574	336367.31	11.30808
	2,486,726	2,883,377	3,433,500	2,934,534	475455.63	16.20208
	3,165,687	3,103,557	3,214,192	3,161,145	55457.153	1.754337
	5,568,156	3,805,844	4,332,096	4,568,699	904666.52	19.8014
	5,218,484	4,755,997	3,519,610	4,498,030	878324.15	19.52686
	4,088,481	3,859,690	4,490,691	4,146,287	319447.56	7.704424
	4,442,513	4,131,863	4,320,215	4,298,197	156491.05	3.640853
	3,512,852	3,237,409	3,519,828	3,423,363	161078.66	4.705275
	4,024,498	4,078,453	3,887,921	3,996,957	98206.298	2.457026
	6,179,755	6,027,700	4,767,878	5,658,444	774991.27	13.69619
	4,210,997	4,223,750	4,337,001	4,257,249	69360.695	1.629237
	4,716,757	5,026,208	3,591,223	4,444,729	755178.64	16.99043
						11.25022

HNE set1 blot1 analysis 6/12/2012 Dox Mesna Human Trial

Sample	Rep1	Rep2	Rep3	RepAvg	RepStdDev	%CV	%naïve control
CH1 C1A	74.4	85.66	90.48	83.51333	8.2521351	9.881219	100
CH1 C1B	74.61	90.2	85.59	83.46667	8.0089596	9.595399	99.9441207
CH1 C2A	75.87	82.82	81.71	80.13333	3.7336354	4.659279	95.95274208
CH1 C2B	71.02	70.61	66.95	69.52667	2.2408555	3.223016	83.2521753
CH2 C1A	71.34	70.71	61.01	67.68667	5.7907369	8.555211	100
CH2 C1B	66.55	70.66	61.16	66.12333	4.7643503	7.205248	97.69033783
CH2 C2A	75.67	81.63	73.3	76.86667	4.2919964	5.58369	113.5624938
CH2 C2B	86.11	87.06	73.79	82.32	7.4024523	8.992289	121.6192258
CH3 C1A	92.16	82.1	100	91.42	8.9729148	9.815046	100
CH3 C1B	113.31	93.43	107.93	104.89	10.282743	9.803359	114.7341938
CH3 C2A	82.9	81.75	79	81.21667	2.0039544	2.467418	88.83905783
CH3 C2B	71.59	73.62	81.7	75.63667	5.3481991	7.070908	82.73536061
CH4 C1A	62.83	65.45	66.52	64.93333	1.8984818	2.92374	100
CH4 C1B	68.68	63.14	60.42	64.08	4.2094655	6.569079	98.68583162
CH4 C2A	70.13	70.75	66.88	69.25333	2.0786133	3.001463	106.6529774
CH4 C2B	75.18	72.06	72.81	73.35	1.6285883	2.220298	112.9620123
						6.347916	

HNE set1 blot2 analysis 6/12/2012 Dox Mesna Human Trial

	Rep1	Rep2	Rep3	RepAvg	RepStdDev	%CV	%naïve control

CH1 C1A	86	89.93	80.42	85.45	4.7787969	5.592507	100
CH1 C1B	96.07	105.29	84.83	95.39667	10.246606	10.74105	111.6403355
CH1 C2A	91.68	91.93	88.83	90.81333	1.7221595	1.896373	106.276575
CH1 C2B	101.85	101.99	96.79	100.21	2.962634	2.956425	117.2732592
CH2 C1A	77.16	61.41	63.46	67.34333	8.5630505	12.71551	100
CH2 C1B	103.3	101.8	94.35	99.81667	4.7933113	4.802115	148.2205613
CH2 C2A	105.73		87.93	96.83	12.586501	12.99855	143.7855764
CH2 C2B	100	92.44	83.64	92.02667	8.1878284	8.897235	136.6529723
CH3 C1A	108.83	104.32	96.64	103.2633	6.1633135	5.96854	100
CH3 C1B	109.02	113.14	108.91	110.3567	2.4110648	2.184793	106.8691694
CH3 C2A	102.76	98.04	99.21	100.0033	2.4579734	2.457891	96.84302269
CH3 C2B	96.78	91.94	85.95	91.55667	5.4251667	5.925474	88.66328803
CH4 C1A	70.37	66.3	67.63	68.1	2.0753072	3.047441	100
CH4 C1B	65.9	61.94	72.32	66.72	5.2383585	7.851257	97.97356828
CH4 C2A	70.05	73.98	75.47	73.16667	2.8000417	3.826936	107.4400392
CH4 C2B	72.57	84.06	81.03	79.22	5.9550063	7.517049	116.328928
						6.211197	

HNE set2 blot1 analysis ######## Dox Mesna Human Trial

	Rep1	**Rep2**	**Rep3**	**RepAvg**	**RepStdDev**	**%CV**	**%naïve control**
AC2 C1A	100	91.51	88.46	93.32333	5.9798857	6.407707	100
AC2 C1B	78.55	78.49	71.43	76.15667	4.0935233	5.375135	81.60517198
AC2 C2A	78.32	87.91	83.63	83.28667	4.80421	5.768282	89.24527628
AC2 C2B	87	84.67	78	83.22333	4.671149	5.612788	89.17741187
CH5 C1A	121.84	118.95	121.93	120.9067	1.6951204	1.402007	100
CH5 C1B	111.45	125.85	122.45	119.9167	7.5268409	6.276726	99.18118659
CH5 C2A	94.48	98.17	102.65	98.43333	4.0913608	4.156479	81.4126599
CH5 C2B	115.66	109.39	95.16	106.7367	10.50441	9.841426	88.28021614
CH6 C1A	110.4	110.15	113.53	111.36	1.8834277	1.691296	100
CH6 C1B	92.25	91.01	86.63	89.96333	2.9525808	3.281982	80.78603927
CH6 C2A	108.09	100.85	97.33	102.09	5.486128	5.373815	91.67564655
CH6 C2B	102.26	90.23	91.1	94.53	6.7084946	7.096683	84.88685345
AC4 C1A	103.44	90.84	85.1	93.12667	9.3813929	10.0738	100
AC4 C1B	112.93	95.91	93.84	100.8933	10.475315	10.38256	108.3398955
AC4 C2A	113.14	96.36	83.57	97.69	14.829798	15.18047	104.900136
AC4 C2B	112.05	98.45	103.87	104.79	6.8465174	6.53356	112.5241606
						6.52842	
HNE Set 2 blot 2							
	Rep1	**Rep2**	**Rep3**	**RepAvg**	**RepStdDev**	**%CV**	**%naïve control**
AC2 C1A	77.55	95.34	87.19	86.69333	8.9053935	10.2723	100
AC2 C1B	62.5	75.58	67.47	68.51667	6.6025172	9.63637	79.03337435
AC2 C2A	59.15	64.07	59.4	60.87333	2.77121514	4.55243	70.21685635
AC2 C2B	53.16	50.32	44.64	49.37333	4.33817166	8.78647	56.95170717

CH5 C1A	93.98	89.86	96.1	93.31333	3.17296917	3.40034	100
CH5 C1B	89.18	87.45	99.89	92.17333	6.73857799	7.31077	98.77830964
CH5 C2A	81.13	91.23	90.17	87.51	5.55060357	6.34282	93.78081017
CH5 C2B	84.65	98.83	77.99	87.15667	10.6437274	12.2122	93.40215761
CH6 C1A	88.53	93.26	102.9	94.89667	7.3234714	7.71731	100
CH6 C1B	85.27	81.82	81.73	82.94	2.0183409	2.4335	87.40033018
CH6 C2A	100.03	94.27	111.5	101.9333	8.77127319	8.60491	107.4150831
CH6 C2B	84.94	84.79	106.28	92.00333	12.3641835	13.4388	96.95106958
AC4 C1A	80.35	79.24	93.9	84.49667	8.1624159	9.66004	100
AC4 C1B	95.12	98.66	98.48	97.42	1.99389067	2.0467	115.2944889
AC4 C2A	106.06	117.77	110.83	111.5533	5.88841518	5.27856	132.020987
AC4 C2B	110.92	113.59	100	108.17	7.20027083	6.65644	128.0168843
						7.39687	

HNE set 3 blot 1

Sample	Rep1	Rep2	Rep3	RepAvg	RepStdDev	%CV
AC5 C1A	138.36	126.21	102.92	122.4967	18.00944	14.70199
AC5 C1B	191.38	180.64	149.8	173.94	21.58452	12.40918
AC5 C2A	178.53	190.93	146.43	171.9633	22.96526	13.35474
AC5 C2B	238.21	257.12	189.7	228.3433	34.7761	15.22974
TA1 C1A	262.18	249.81	177.73	229.9067	45.60765	19.83746
TA1 C1B	291.19	263.76	180.29	245.08	57.76166	23.56849
TA1 C2A	143.02	153.81	109.21	135.3467	23.26908	17.19221
TA1 C2B	137.63	117.02	125.26	126.6367	10.37374	8.191733
CH7 C1A	286	323.62		304.81	26.60136	8.727193
CH7 C1B	209.18	253.08	234.13	232.13	22.01823	9.485302
CH7 C2A	215.2	248.12	218.37	227.23	18.16057	7.992153
CH7 C2B	269.54	321.67	337.73	309.6467	35.64954	11.51297
CH8 C1A	358.69	339.72	328.92	342.4433	15.07069	4.400929
CH8 C1B	299.07	304.91	296.19	300.0567	4.442942	1.480701
CH8 C2A	382.63	382.37	381.98	382.3267	0.327159	0.085571
CH8 C2B	323.97	358.83	241.62	308.14	60.18711	19.53239

783.31 Blot abnormality

3NT set 3 blot1

rep1	rep2	rep3	rep avg	rep stddev	%cv
276.44	271.67	274.61	274.24	2.406429	0.8774901
298.1	280.32	282.05	286.8233	9.804113	3.4181714
284.01	295.82	277.4	285.7433	9.331529	3.2657031
261.06	252	230.34	247.8	15.78479	6.3699718
277.23	280.47	247.86	268.52	17.96527	6.6904792
274	266.2	238.39	259.53	18.71857	7.2124863
257.57	239.36	220.09	239.0067	18.7425	7.8418307
250	263.06	239.04	250.7	12.02529	4.7966853
422.02	446.75	467.73	445.5	22.88062	5.1359423
366.75	409.41	420.57	398.91	28.40485	7.1206166
351.89	404.51	470.37	408.9233	59.36317	14.516943
310.9	379.04	393.37	361.1033	44.0638	12.202545
291.96	321.62	341.58	318.3867	24.96752	7.8418854
299.93	321.46	332.14	317.8433	16.40674	5.1618964
336.96	337.91	368.94	347.9367	18.19562	5.2295785
279.5	301.53	342.67	307.9	32.06314	10.413491
					6.7559823

3NT set 3 blot2

rep1	rep2	rep3	rep avg	rep stddev	%cv
147.95	152.75	151.28	150.66	2.459329	1.6323704
157.82	175.83	175.83	169.8267	10.39808	6.1227595
175.97	178.59	173.5	176.02	2.545368	1.4460677
173.01	185.97	177.96	178.98	6.539931	3.6540011
179.51	198.82	188.48	188.9367	9.663096	5.1144633
179.48	182.2	176.96	179.5467	2.620636	1.4595849
186.85	174.07	168.93	176.6167	9.227445	5.2245605
277.29	266.96	248.01	264.0867	14.84997	5.623143
230.22	233.65	250	237.9567	10.56989	4.4419402
235.55	269.33	298.49	267.79	31.49825	11.762294
246.56	275.17	297.71	273.1467	25.63496	9.3850522
236.42	246.65	259.76	247.61	11.69958	4.7250018
211.34	226.55	248.67	228.8533	18.77129	8.2023221
222.17	234.71	263.87	240.25	21.39489	8.90526
245.03	267.66	322.51	278.4	39.84091	14.310673
216.53	262.29	286.76	255.1933	35.64878	13.969321
					6.6236759

3NT set 4 blot1

rep1	rep2	rep3	rep avg	rep stddev	%cv
141.02	161.38	173.51	158.6367	16.41781	10.34932
153.54	149.59	159.4	154.1767	4.935892	3.201452
134.59	132.51	142.14	136.4133	5.06731	3.714674
156.63	139.76	151.01	149.1333	8.590147	5.760045
162.47	148.37	163.83	158.2233	8.560288	5.410256
189.93	174.66	194.35	186.3133	10.33123	5.545081
164.26	151.92	170.32	162.1667	9.376915	5.78227
173.94	185.53	200.56	186.6767	13.34699	7.149792
169.16	147.79	163.43	160.1267	11.06134	6.907869
188.41	180.37	174.85	181.21	6.818915	3.76299
180.86	170.72	172.23	174.6033	5.47078	3.133262
197.38	178.21	200.99	192.1933	12.2437	6.370513
214.78	250	218.69	227.8233	19.3048	8.473585
244.34	217.09	229.21	230.2133	13.65268	5.930447
230.15	220.56	246.62	232.4433	13.18049	5.670412
220.45	226.06	241.36	229.29	10.82274	4.72011
					5.74263

3NT set4 blot2

rep1	rep2	rep3	rep avg	rep stddev	%cv
253.45	228.02	239.94	240.47	12.72328	5.291006
228.25	208.16	241.64	226.0167	16.85136	7.455805
221.33	194.17	222.68	212.7267	16.08471	7.561212
259.53	233.79	229.51	240.9433	16.23816	6.739409
295	268.44	264.41	275.95	16.62038	6.022969
291.63	278.42	275.05	281.7	8.763156	3.110811
264.93	245.87	251.78	254.1933	9.756487	3.838215
261.86	275.02	264.18	267.02	7.024642	2.630755
242.31	231.42	250	241.2433	9.335815	3.869875
250.72	238.35	276.23	255.1	19.3161	7.571974
303.95	198.57	239.42	247.3133	53.13158	21.48351
237.32	221.93	253.91	237.72	15.99375	6.727979
254.69	274.16	280.48	269.7767	13.44214	4.982693
301.41	283.02	327.84	304.09	22.52987	7.408947
269.23	248.03	269.91	262.39	12.44077	4.741328
271.82	235.39	258.93	255.38	18.47263	7.23339
					6.666867

Copyright © Jeriel T. R. Keeney 2013

APPENDIX C

DATA TO SUPPLEMENT TABLES AND FIGURES

Table A.3

L1u	L9u	L4m	L4u	L5m	L5u	L8m	L8u	L9m	LowGrpAvg	rel avgs	ttest C vs L
908.7	1596.1	964.8	2.6	2365.8	0.7	2171.6	1433.8	877.6	1146.86	1474.06	0.0114
233.2	1392.7	518.8	2.6	1844.6	0.7	1083	716	158.4	661.11	849.53	0.013
5.9	192.5	10.1	2.6	256.9	0.7	289.1	132.9	5.4	99.57	217.85	0.0291
596	439.4	284.7	402.7	**565.9**	0.7	**560.8**	**554.2**	198.8	400.37	450.33	0.0347
654.2	**1192**	648.5	2.6	**861.2**	0.7	668.9	**1039**	812.1	653.23	839.40	0.0374
527.2	569.2	10.1	2.6	442.9	0.7	345.8	387.6	5.4	254.61	454.54	0.0428
1279	968.1	286.3	1397	811.5	0.7	943	931.5	499.3	790.72	889.48	0.0473

c2u	C5m	c5u	c7m	c7u	c8m	c8u	c10m	c10u	ConGrpAvg	rel avgs	SSP
1.9	2.8	1	1230	2.4	2.1	855.8	0.7	7	233.78	1043.05	6701
1.9	2.8	1	5.3	2.4	341	9.3	0.7	7	41.22	340.60	8104
1.9	2.8	1	5.3	2.4	2.1	9.3	0.7	7	3.61	3.61	5201
1.9	2.8	439	337.8	2.4	**272**	**291.9**	98.4	**321.6**	196.43	293.47	3207
1.9	2.8	1	**722**	2.4	**381**	**746.8**	0.7	**454.8**	257.00	576.05	8103
1.9	2.8	1	409.8	2.4	2.1	9.3	0.7	7	48.56	409.80	6203
1.9	393.1	826.4	699.2	2.4	367	430	0	770.7	387.86	581.07	4201

Figure 4.1a

Saline	Dox	Dox/Mesna	Mesna
114.211100	144.368400	114.845500	111.258800
115.865400	121.518800	79.936560	114.057500
76.136580	116.023500	85.624480	79.725110
93.786930	136.252300	124.420100	102.165800
105.439300	130.082700	117.864300	82.058710
78.108630	140.650000	92.583140	119.199000
104.720800	154.927900	104.017500	107.208900
95.797170	96.394610	86.593690	124.123900
111.349300	120.250300	97.355030	112.744600
104.584700	123.812200	98.228500	103.544900
	100.107800	103.246200	98.028090
	129.208000	102.713000	100.787600
	93.456600		110.975000

Figure 4.1b

Saline	Dox	Dox/Mesna	Mesna
100.91140	176.76120	137.7715	135.9275
96.48774	244.86560	187.7915	113.0395
105.06910	183.87210	192.7291	150.1657
65.85894	183.63090	179.1203	156.4663
131.67280	194.70600	137.5846	145.0312
109.58880	113.53540	121.9427	133.9293
104.78480	191.96110	149.6186	147.6161
114.10410	265.92170	133.9399	122.7599
71.52222	199.68350	139.3021	143.0786
	199.42160	144.5231	129.9210
	211.44900	129.4157	137.5026

Figure 4.1c

Saline	Dox	Dox/Mesna	Mesna
81.251690	146.112900	83.237210	90.048170
110.488300	99.782270	96.098500	104.642400
	124.289200	98.182530	105.289600
101.049300		96.464420	126.252600
84.680970	100.498700	102.083900	76.547280
92.671120	112.701400	112.828000	108.201200
83.158990	115.561900	94.730650	103.397200
91.005530	98.692420	100.249100	123.983400
93.320320	110.675800	110.800100	75.171490
79.791340	143.486800	81.741170	88.429730
108.502500	97.988870	94.371310	102.761700
99.233120	122.055300	96.417880	106.256500

Figure 4.1d

Saline	Dox	Dox/Mesna	Mesna
104.90500	127.349600	127.981800	129.492300
109.59960	183.059100	110.467300	114.426900
95.15001	236.767600	109.689600	101.863400
92.96438	142.945200	120.337100	126.933000
109.23120	137.152600	143.589200	103.220500
88.14976	139.096100	135.459700	137.841700
114.77500	101.369100	101.872300	103.074600
99.95960	145.713300	87.930920	91.082730
115.50100	188.464800	87.311880	81.082310
102.83960	113.783000	146.135300	132.877100
89.56430	209.172200	131.704400	82.162540
88.98714	110.719200	127.094800	109.720700

Figure 4.2a

Saline: 24h post	Mesna: 24h post	Dox: 24h post	Dox+Mesna: 24h post
71.3	94.0	58.3	63.6
80.4	71.4	48.1	75.4
82.9	69.1	80.2	70.6
79.6	74.2	53.1	72.4
75.3	66.5	53.3	64.3
66.8	81.5	79.5	46.3
66.5	62.1	66.3	67.3
	64.1		75.6

Saline: 72h post	Mesna: 72h post	Dox: 72h post	Dox+Mesna: 72h post
81.6	72.4	35.8	67.8
70.2	73.3	23.0	60.3
70.6	53.6	49.1	48.6
81.9	53.5	7.8	51.9
67.4	64.2	34.3	62.7
67.5	57.0	45.7	38.8
67.8	70.3	66.9	65.1
	73.5		62.7

Figure 4.2b

Saline: 24h post	Mesna: 24h post	Dox: 24h post	Dox+Mesna: 24h post
90.	56.	52.	61.
62.	82.	63.	92.
47.	115.	59.	74.
77.	90.	71.	67.
81.	98.	65.	92.
108.	91.	61.	74.
103.	80.	71.	83.
	114.		65.

Saline: 72h post	Mesna: 72h post	Dox: 72h post	Dox+Mesna: 72h post
64.	49.	24.	34.
75.	117.	35.	68.
24.	86.	28.	10.
34.	52.	5.	23.
54.	62.	8.	19.
97.	80.	42.	6.
92.	55.	44.	44.
	82.		26.

Figure 4.3b

Saline-NAA/Cr	Dox-NAA/Cr
0.916	0.908
1.01	0.836
0.897	0.761
0.828	0.877
0.888	0.844
0.983	0.870
1.01	0.879
0.853	0.926
0.858	0.860
0.974	0.837
0.966	0.857

Figure 4.3c

Saline	Dox	Dox/Mesna	Mesna
1.07	0.722	0.775	1.09
1.01	0.769	0.693	1.05
1.10	0.709	0.735	
1.22	0.870	0.840	
1.11	0.728	0.662	
1.17	0.764		
1.05	0.757		
1.14	0.723		
1.08	0.727		
1.13	0.650		
	0.624		
	0.532		
	0.581		
	0.624		

Figure 4.4a

Dox WT	Mesna + Dox	Mesna
50.973450	103.008900	101.946900
64.778760	96.637170	94.513280
61.592920	93.982300	

Figure 4.4b

Saline	Dox WT	Mesna + Dox	Mesna
89.484500	73.930950	80.608760	103.454400
103.401300	66.001410	77.968190	101.144700

107.114200	74.922520	70.264420

Figure 5.1a

WT Saline	WT Dox	TNFKO Saline	TNFKO Dox
86.63986	111.1058	109.53350	116.42410
95.34743	112.8020	110.51390	123.68740
97.86980	122.5462	93.32509	136.13900
107.12850	119.1486	72.68974	115.04000
105.95090	136.4738	91.81253	125.36520
107.06360	131.4830	84.97487	*84.38054**

Figure 5.1b

WT Saline	WT Dox	TNFKO Saline	TNFKO Dox
88.15740	118.98880	100.01450	100.42200
94.39760	102.92840	106.30080	105.59410
99.28319	111.69250	101.44710	99.18892
105.59560	123.30750	95.95238	103.48660
105.83720	115.52690	93.36102	98.48431
106.72900	120.73220	102.92420	90.31973

Figure 5.1c

WT Saline	WT Dox	TNFKO Saline	TNFKO Dox
71.095600	218.330700	92.911650	84.438200
87.822320	210.183900	87.490140	153.609500
114.774100	225.073300	101.581500	207.733600
87.949420	176.257200	137.170200	148.166000
127.240000	230.395600	76.334820	177.535500
111.118600	242.003600	84.357960	136.842200

Figure 5.1d

WT Saline	WT Dox	TNFKO Saline	TNFKO Dox
95.800510	139.883900	98.885800	108.506900
98.048670	142.535200	118.339000	121.187200
89.461560	168.325000	129.850200	153.977600
80.535320	103.493600	122.408500	129.876200
115.744600	128.140300	117.537500	143.801600
120.409300	134.465100	84.208740	100.349000

Figure 5.2 mitochOCR

	TNFα $^{+/+}$_ Saline	TNFα $^{+/+}$_ DOX	TNFα $^{-/-}$_ Saline	TNFα $^{-/-}$_ DOX
Basal	360.82	204.34	380.46	345.20
Oligomycin	74.20	55.38	76.10	76.37
FCCP	585.29	228.55	584.15	558.16
Antimycin A	33.79	42.98	55.95	55.17

Mean				
	TNFα $^{+/+}$_ Saline	TNFα $^{+/+}$_ DOX	TNFα $^{-/-}$_ Saline	TNFα $^{-/-}$_ DOX
Basal	360.82	204.34	380.46	345.20
ATP-Linked	286.62	148.96	304.35	268.83
Maximal Capacity	585.29	228.55	584.15	558.16
Reserve Capacity	224.47	24.21	203.69	212.97
SEM				
	TNFα $^{+/+}$_ Saline	TNFα $^{+/+}$_ DOX	TNFα $^{-/-}$_ Saline	TNFα $^{-/-}$_ DOX
Basal	20.00	25.00	20.00	30.00
ATP-Linked	15.00	18.00	17.00	19.00
Maximal Capacity	12.00	14.00	12.00	15.00
Reserve Capacity	12.00	14.00	16.00	17.00

Figure 5.3

Saline	Dox WT	Dox TNFKO
1.08	0.650	0.789
1.13	0.624	0.772
	0.532	0.783
	0.581	0.882
	0.624	

Figure 5.4a

Saline	Dox WT	Dox TNFKO
98.230090	50.973450	58.407080
96.637170	64.778760	54.690270
105.132700	61.592920	46.194690

Figure 5.4b

Saline	Dox WT	Dox TNFKO
89.484500	73.930950	83.728570
103.401300	66.001410	86.060370
107.114200	74.922520	94.679360

Figure 6.2a

Solvent Only	15min 10μM	30min 10μM	90min 10μM
103.855400	164.209800	190.819800	316.414800
99.705090	151.931100	188.336700	315.159300
96.439480	129.959800	200.688300	330.723500

Figure 6.2b

Solvent Only	15min 0.1μM	15min 1μM	15min 10μM
103.855400	114.004000	139.111400	164.209800
99.705090	117.545900	138.877900	151.931100
96.439480	116.706300	153.318800	129.959800

Figure 6.2c

Solvent Only	15min 10μM	30min 10μM	90min 10μM
101.301300	100.008200	129.288600	148.036400
95.601140	106.499500	113.216000	167.626000
103.097500	121.054800	136.601600	159.441000

Figure 6.3

Media	DMSO+Crown ether	KO_2_0.1μM	KO_2_1μM	KO_2_10μM	LPS
58.276	60.254000	54.213	1535.877	8535.877	5065.467
55.711	61.248000	57.263	1589.112	9891.112	6598.405
54.236	63.548000	55.897	1600.780	8934.589	7023.548

Figure A.4

1	18499		**2D validation**	**Original 2D gel PDQuest analysis**	
2	56270		**fold change**	**Ovr fold change**	**Rel fold change**
		2	*1.29115*	2.038697	*1.534242*
1	23389	1	1.264339	increase in low VitD compared to control	
2	72653				

Figure A.5

Control Diet	Low VitD Diet
0.1552208	0.450910
0.192403	0.346070
0.154096	0.417273

Figure A.7

NFkB ControlCyt	NFkB LowVitDCyt	NFkB ControlNuc	NFkB LowVitDNuc
0.349778	0.193625	0.124206	0.264936
0.385451	0.212839	0.048534	0.075577
0.250173	0.220648	0.044043	0.091913
0.151604	0.182924	0.037732	0.086837
0.190344	0.224332	0.102414	0.204766
0.327843	0.189652	0.050578	0.095727
0.391415	0.202379	0.038098	0.092418
0.272194	0.230036	0.036522	0.076946
0.191043	0.190335	0.042182	0.114980

Figure A.8

Control Diet	Low VitD Diet
0.025247	0.043433
0.021871	0.035006
0.038149	0.060472
0.025479	0.058023
0.020323	0.045006
0.039095	0.063172
0.026288	0.033450
0.022176	0.037236
0.037210	0.040988

Copyright © Jeriel T. R. Keeney 2013

References

Adam-Vizi, V. (2005). "Production of reactive oxygen species in brain mitochondria: contribution by electron transport chain and non-electron transport chain sources." Antioxid Redox Signal **7**(9-10): 1140-1149.

Ahles, T. A. and A. J. Saykin (2007). "Candidate mechanisms for chemotherapy-induced cognitive changes." Nat Rev Cancer **7**(3): 192-201.

Ahles, T. A., A. J. Saykin, C. T. Furstenberg, B. Cole, L. A. Mott, L. Titus-Ernstoff, K. Skalla, M. Bakitas and P. M. Silberfarb (2005). "Quality of life of long-term survivors of breast cancer and lymphoma treated with standard-dose chemotherapy or local therapy." J Clin Oncol **23**(19): 4399-4405.

Akama, K. T. and L. J. Van Eldik (2000). "Beta-amyloid stimulation of inducible nitric-oxide synthase in astrocytes is interleukin-1beta- and tumor necrosis factor-alpha (TNFalpha)-dependent, and involves a TNFalpha receptor-associated factor- and NFkappaB-inducing kinase-dependent signaling mechanism." The Journal of biological chemistry **275**(11): 7918-7924.

Aksenov, M. Y., H. M. Tucker, P. Nair, M. V. Aksenova, D. A. Butterfield, S. Estus and W. R. Markesbery (1998). "The expression of key oxidative stress-handling genes in different brain regions in Alzheimer's disease." J Mol Neurosci **11**(2): 151-164.

Aluise, C. D., S. Miriyala, T. Noel, R. Sultana, P. Jungsuwadee, T. J. Taylor, J. Cai, W. M. Pierce, M. Vore, J. A. Moscow, D. K. St Clair and D. A. Butterfield (2011). "2-Mercaptoethane sulfonate prevents doxorubicin-induced plasma protein oxidation and TNF-alpha release: implications for the reactive oxygen species-mediated mechanisms of chemobrain." Free Radic Biol Med **50**(11): 1630-1638.

Aluise, C. D., R. A. Robinson, J. Cai, W. M. Pierce, W. R. Markesbery and D. A. Butterfield (2011). "Redox proteomics analysis of brains from subjects with amnestic mild cognitive impairment compared to brains from subjects with preclinical Alzheimer's disease: insights into memory loss in MCI." J Alzheimers Dis **23**(2): 257-269.

Aluise, C. D., D. St Clair, M. Vore and D. A. Butterfield (2009). "In vivo amelioration of adriamycin induced oxidative stress in plasma by gamma-glutamylcysteine ethyl ester (GCEE)." Cancer Lett **282**(1): 25-29.

Aluise, C. D., R. Sultana, J. Tangpong, M. Vore, D. St Clair, J. A. Moscow and D. A. Butterfield (2010). "Chemo brain (chemo fog) as a potential side effect of doxorubicin administration: role of cytokine-induced, oxidative/nitrosative stress in cognitive dysfunction." Adv Exp Med Biol **678**: 147-156.

Amirmansour, C., P. Vallance and R. G. Bogle (1999). "Tyrosine nitration in blood vessels occurs with increasing nitric oxide concentration." Br J Pharmacol **127**(3): 788-794.

Anantharaman, M., J. Tangpong, J. N. Keller, M. P. Murphy, W. R. Markesbery, K. K. Kiningham and D. K. St Clair (2006). "Beta-amyloid mediated nitration of manganese superoxide dismutase: implication for oxidative stress in a APPNLH/NLH X PS-1P264L/P264L double knock-in mouse model of Alzheimer's disease." The American journal of pathology **168**(5): 1608-1618.

Andreotti, A. H. (2003). "Native state proline isomerization: an intrinsic molecular switch." Biochemistry **42**(32): 9515-9524.

Annweiler, C., D. J. Llewellyn and O. Beauchet (2013). "Low serum vitamin D concentrations in Alzheimer's disease: a systematic review and meta-analysis." Journal of Alzheimer's disease : JAD **33**(3): 659-674.

Antunes, M. and G. Biala (2012). "The novel object recognition memory: neurobiology, test procedure, and its modifications." Cogn Process **13**(2): 93-110.

Aust, S. D., L. A. Morehouse and C. E. Thomas (1985). "Role of metals in oxygen radical reactions." J Free Radic Biol Med **1**(1): 3-25.

Bachur, N. R., S. L. Gordon and M. V. Gee (1977). "Anthracycline antibiotic augmentation of microsomal electron transport and free radical formation." Mol Pharmacol **13**(5): 901-910.

Bader Lange, M. L., D. St Clair, W. R. Markesbery, C. M. Studzinski, M. P. Murphy and D. A. Butterfield (2010). "Age-related loss of phospholipid asymmetry in APP(NLh)/APP(NLh) x PS-1(P264L)/PS-1(P264L) human double mutant knock-in mice: relevance to Alzheimer disease." Neurobiol Dis **38**(1): 104-115.

Badiola, N., C. Malagelada, N. Llecha, J. Hidalgo, J. X. Comella, J. Sabria and J. Rodriguez-Alvarez (2009). "Activation of caspase-8 by tumour necrosis factor receptor 1 is necessary for caspase-3 activation and apoptosis in oxygen-glucose deprived cultured cortical cells." Neurobiol Dis **35**(3): 438-447.

Bagchi, D., M. Bagchi, E. A. Hassoun, J. Kelly and S. J. Stohs (1995). "Adriamycin-induced hepatic and myocardial lipid peroxidation and DNA damage, and enhanced excretion of urinary lipid metabolites in rats." Toxicology **95**(1-3): 1-9.

Bahmed, K., C. Henry, M. Holliday, J. Redzic, M. Ciobanu, F. Zhang, C. Weekes, R. Sclafani, J. Degregori and E. Eisenmesser (2012). "Extracellular cyclophilin-A stimulates ERK1/2 phosphorylation in a cell-dependent manner but broadly stimulates nuclear factor kappa B." Cancer Cell Int **12**(1): 19.

Baker, R. G., M. S. Hayden and S. Ghosh (2011). "NF-kappaB, inflammation, and metabolic disease." Cell Metab **13**(1): 11-22.

Bannon, J. H., D. S. O'Donovan, S. M. Kennelly and M. M. Mc Gee (2012). "The peptidyl prolyl isomerase cyclophilin A localizes at the centrosome and the midbody and is required for cytokinesis." Cell cycle **11**(7): 1340-1353.

Barja, G. (2013). "Updating the Mitochondrial Free Radical Theory of Aging: An Integrated View, Key Aspects, and Confounding Concepts." Antioxid Redox Signal **19**(12): 1420-1445.

Beckman, J. S. (1996). "Oxidative damage and tyrosine nitration from peroxynitrite." Chemical research in toxicology **9**(5): 836-844.

Bencharif, K., L. Hoareau, R. K. Murumalla, E. Tarnus, F. Tallet, R. G. Clerc, C. Gardes, M. Cesari and R. Roche (2010). "Effect of apoA-I on cholesterol release and apoE secretion in human mature adipocytes." Lipids Health Dis **9**: 75.

Bentley, A. R., P. Emrani and P. A. Cassano (2008). "Genetic variation and gene expression in antioxidant related enzymes and risk of COPD: a systematic review." Thorax **63**(11): 956-961.

Berlett, B. S. and E. R. Stadtman (1997). "Protein oxidation in aging, disease, and oxidative stress." J Biol Chem **272**(33): 20313-20316.

Bernacki, R. J., S. K. Bansal and H. L. Gurtoo (1987). "Combinations of mesna with cyclophosphamide or adriamycin in the treatment of mice with tumors." Cancer Res **47**(3): 799-802.

Bertholdo, D., A. Watcharakorn and M. Castillo (2013). "Brain proton magnetic resonance spectroscopy: introduction and overview." Neuroimaging Clin N Am **23**(3): 359-380.

Bevins, R. A. and J. Besheer (2006). "Object recognition in rats and mice: a one-trial non-matching-to-sample learning task to study 'recognition memory'." Nat Protoc **1**(3): 1306-1311.

Bonifati, V., B. A. Oostra and P. Heutink (2004). "Linking DJ-1 to neurodegeneration offers novel insights for understanding the pathogenesis of Parkinson's disease." J Mol Med (Berl) **82**(3): 163-174.

Boston-Howes, W., S. L. Gibb, E. O. Williams, P. Pasinelli, R. H. Brown, Jr. and D. Trotti (2006). "Caspase-3 cleaves and inactivates the glutamate transporter EAAT2." J Biol Chem **281**(20): 14076-14084.

Boyd-Kimball, D., R. Sultana, H. F. Poon, B. C. Lynn, F. Casamenti, G. Pepeu, J. B. Klein and D. A. Butterfield (2005). "Proteomic identification of proteins specifically oxidized by intracerebral injection of amyloid beta-peptide (1-42) into rat brain: implications for Alzheimer's disease." Neuroscience **132**(2): 313-324.

Bradford, M. M. (1976). "A rapid and sensitive method for the quantitation of microgram quantities of protein utilizing the principle of protein-dye binding." Anal Biochem **72**: 248-254.

Brewer, L. D., N. M. Porter, D. S. Kerr, P. W. Landfield and O. Thibault (2006). "Chronic 1alpha,25-(OH)2 vitamin D3 treatment reduces Ca2+ -mediated hippocampal biomarkers of aging." Cell Calcium **40**(3): 277-286.

Brewer, L. D., V. Thibault, K. C. Chen, M. C. Langub, P. W. Landfield and N. M. Porter (2001). "Vitamin D hormone confers neuroprotection in parallel with downregulation of L-type calcium channel expression in hippocampal neurons." The Journal of neuroscience : the official journal of the Society for Neuroscience **21**(1): 98-108.

Briones, T. L. and J. Woods (2013). "Dysregulation in myelination mediated by persistent neuroinflammation: Possible mechanisms in chemotherapy-related cognitive impairment." Brain Behav Immun.

Bryk, R., P. Griffin and C. Nathan (2000). "Peroxynitrite reductase activity of bacterial peroxiredoxins." Nature **407**(6801): 211-215.

Butterfield, D. A. (1997). "beta-Amyloid-associated free radical oxidative stress and neurotoxicity: implications for Alzheimer's disease." Chem Res Toxicol **10**(5): 495-506.

Butterfield, D. A., M. L. Bader Lange and R. Sultana (2010). "Involvements of the lipid peroxidation product, HNE, in the pathogenesis and progression of Alzheimer's disease." Biochim Biophys Acta **1801**(8): 924-929.

Butterfield, D. A., A. Castegna, C. M. Lauderback and J. Drake (2002). "Evidence that amyloid beta-peptide-induced lipid peroxidation and its sequelae in Alzheimer's disease brain contribute to neuronal death." Neurobiol Aging **23**(5): 655-664.

Butterfield, D. A. and I. Dalle-Donne (2012). "Redox proteomics." Antioxid Redox Signal **17**(11): 1487-1489.

Butterfield, D. A. and C. M. Lauderback (2002). "Lipid peroxidation and protein oxidation in Alzheimer's disease brain: potential causes and consequences involving amyloid beta-peptide-associated free radical oxidative stress." Free Radic Biol Med **32**(11): 1050-1060.

Butterfield, D. A., M. Perluigi, T. Reed, T. Muharib, C. P. Hughes, R. A. Robinson and R. Sultana (2012). "Redox proteomics in selected neurodegenerative disorders: from its infancy to future applications." Antioxid Redox Signal **17**(11): 1610-1655.

Butterfield, D. A., T. Reed and R. Sultana (2011). "Roles of 3-nitrotyrosine- and 4-hydroxynonenal-modified brain proteins in the progression and pathogenesis of Alzheimer's disease." Free radical research **45**(1): 59-72.

Butterfield, D. A., T. T. Reed, M. Perluigi, C. De Marco, R. Coccia, J. N. Keller, W. R. Markesbery and R. Sultana (2007). "Elevated levels of 3-nitrotyrosine in brain from subjects with amnestic mild cognitive impairment: implications for the role of nitration in the progression of Alzheimer's disease." Brain research **1148**: 243-248.

Butterfield, D. A. and E. R. Stadtman (1997). "Protein Oxidation Processes in Aging Brain." Adv. Cell Aging and Gerontol. **2**: 161-191.

Calabrese, V., R. Lodi, C. Tonon, V. D'Agata, M. Sapienza, G. Scapagnini, A. Mangiameli, G. Pennisi, A. M. Stella and D. A. Butterfield (2005). "Oxidative stress, mitochondrial dysfunction and cellular stress response in Friedreich's ataxia." J Neurol Sci **233**(1-2): 145-162.

Cantorna, M. T. and B. D. Mahon (2004). "Mounting evidence for vitamin D as an environmental factor affecting autoimmune disease prevalence." Exp Biol Med (Maywood) **229**(11): 1136-1142.

Car, H., M. Zendzian-Piotrowska, A. Fiedorowicz, S. Prokopiuk, A. Sadowska and K. Kurek (2012). "[The role of ceramides in selected brain pathologies: ischemia/hypoxia, Alzheimer disease]." Postepy Hig Med Dosw (Online) **66**: 295-303.

Castegna, A., C. M. Lauderback, H. Mohmmad-Abdul and D. A. Butterfield (2004). "Modulation of phospholipid asymmetry in synaptosomal membranes by the lipid peroxidation products, 4-hydroxynonenal and acrolein: implications for Alzheimer's disease." Brain Res **1004**(1-2): 193-197.

Castegna, A., V. Thongboonkerd, J. B. Klein, B. Lynn, W. R. Markesbery and D. A. Butterfield (2003). "Proteomic identification of nitrated proteins in Alzheimer's disease brain." Journal of neurochemistry **85**(6): 1394-1401.

Chagas, C. E., M. C. Borges, L. A. Martini and M. M. Rogero (2012). "Focus on vitamin D, inflammation and type 2 diabetes." Nutrients **4**(1): 52-67.

Chandel, N. S., W. C. Trzyna, D. S. McClintock and P. T. Schumacker (2000). "Role of oxidants in NF-kappa B activation and TNF-alpha gene transcription induced by hypoxia and endotoxin." J Immunol **165**(2): 1013-1021.

Chaturvedi, R. K. and M. Flint Beal (2013). "Mitochondrial diseases of the brain." Free Radic Biol Med **63**: 1-29.

Chaudhuri, A. and A. Chattopadhyay (2011). "Transbilayer organization of membrane cholesterol at low concentrations: Implications in health and disease." Biochim Biophys Acta **1808**(1): 19-25.

Chen, G. and D. V. Goeddel (2002). "TNF-R1 signaling: a beautiful pathway." Science **296**(5573): 1634-1635.

Chen, X., Y. Zhao, Z. Guo, L. Zhou, E. U. Okoro and H. Yang (2011). "Transcriptional regulation of ATP-binding cassette transporter A1 expression by a novel signaling pathway." J Biol Chem **286**(11): 8917-8923.

Chen, Y., C. Daosukho, W. O. Opii, D. M. Turner, W. M. Pierce, J. B. Klein, M. Vore, D. A. Butterfield and D. K. St Clair (2006). "Redox proteomic identification of oxidized cardiac proteins in adriamycin-treated mice." Free Radic Biol Med **41**(9): 1470-1477.

Chen, Y., P. Jungsuwadee, M. Vore, D. A. Butterfield and D. K. St Clair (2007). "Collateral damage in cancer chemotherapy: oxidative stress in nontargeted tissues." Mol Interv **7**(3): 147-156.

Cheng, H., Z. Yang, B. Dong, C. Chen, M. Zhang, Z. Huang, Z. Chen and K. Wang (2013). "Chemotherapy-induced prospective memory impairment in patients with breast cancer." Psychooncology.

Chuang, R. Y. and L. F. Chuang (1979). "Inhibition of chicken myeloblastosis RNA polymerase II activity by adriamycin." Biochemistry **18**(10): 2069-2073.

Church, L. D., G. Hessler, J. E. Goodall, D. A. Rider, C. J. Workman, D. A. Vignali, P. A. Bacon, E. Gulbins and S. P. Young (2005). "TNFR1-induced sphingomyelinase activation modulates TCR signaling by impairing store-operated Ca2+ influx." J Leukoc Biol **78**(1): 266-278.

Ciszkowska-Lyson, B., L. Krolicki, A. Teska, A. Janowicz-Zebrowska, M. Krzakowski and M. Tacikowska (2003). "[Brain metabolic disorders after chemotherapy in the study by magnetic resonance spectroscopy]." Neurol Neurochir Pol **37**(4): 783-798.

Clarke, J. R., M. Cammarota, A. Gruart, I. Izquierdo and J. M. Delgado-Garcia (2010). "Plastic modifications induced by object recognition memory processing." Proc Natl Acad Sci U S A **107**(6): 2652-2657.

Cohen-Lahav, M., S. Shany, D. Tobvin, C. Chaimovitz and A. Douvdevani (2006). "Vitamin D decreases NFkappaB activity by increasing IkappaBalpha levels." Nephrol Dial Transplant **21**(4): 889-897.

Cohen, B. M., P. F. Renshaw, A. L. Stoll, R. J. Wurtman, D. Yurgelun-Todd and S. M. Babb (1995). "Decreased brain choline uptake in older adults. An in vivo proton magnetic resonance spectroscopy study." JAMA **274**(11): 902-907.

Cole, M. P., L. Chaiswing, T. D. Oberley, S. E. Edelmann, M. T. Piascik, S. M. Lin, K. K. Kiningham and D. K. St Clair (2006). "The protective roles of nitric oxide and superoxide dismutase in adriamycin-induced cardiotoxicity." Cardiovasc Res **69**(1): 186-197.

Cooke, M. S., M. D. Evans, M. Dizdaroglu and J. Lunec (2003). "Oxidative DNA damage: mechanisms, mutation, and disease." FASEB J **17**(10): 1195-1214.

Correa, D. D. and T. A. Ahles (2008). "Neurocognitive changes in cancer survivors." Cancer J **14**(6): 396-400.

Cox, A. G., C. C. Winterbourn and M. B. Hampton (2010). "Mitochondrial peroxiredoxin involvement in antioxidant defence and redox signalling." The Biochemical journal **425**(2): 313-325.

Cucuianu, M., M. Coca and N. Hancu (2007). "Reverse cholesterol transport and atherosclerosis. A mini review." Rom J Intern Med **45**(1): 17-27.

Cummings, J., L. Anderson, N. Willmott and J. F. Smyth (1991). "The molecular pharmacology of doxorubicin in vivo." Eur J Cancer **27**(5): 532-535.

Dammann, O., S. Durum and A. Leviton (2001). "Do white cells matter in white matter damage?" Trends in neurosciences **24**(6): 320-324.

Dasuri, K., L. Zhang and J. N. Keller (2012). "Oxidative stress, neurodegeneration, and the balance of protein degradation and protein synthesis." Free Radic Biol Med.

De Giusti, V. C., C. I. Caldiz, I. E. Ennis, N. G. Perez, H. E. Cingolani and E. A. Aiello (2013). "Mitochondrial reactive oxygen species (ROS) as signaling molecules of intracellular pathways triggered by the cardiac renin-angiotensin II-aldosterone system (RAAS)." Front Physiol **4**: 126.

De Nadai, C., P. Sestili, O. Cantoni, J. P. Lievremont, C. Sciorati, R. Barsacchi, S. Moncada, J. Meldolesi and E. Clementi (2000). "Nitric oxide inhibits tumor necrosis factor-alpha-induced apoptosis by reducing the generation of ceramide." Proc Natl Acad Sci U S A **97**(10): 5480-5485.

de Ruiter, M. B., L. Reneman, W. Boogerd, D. J. Veltman, M. Caan, G. Douaud, C. Lavini, S. C. Linn, E. Boven, F. S. van Dam and S. B. Schagen (2012). "Late effects of high-dose adjuvant chemotherapy on white and gray matter in breast cancer survivors: converging results from multimodal magnetic resonance imaging." Hum Brain Mapp **33**(12): 2971-2983.

Dean, R. T., S. Fu, R. Stocker and M. J. Davies (1997). "Biochemistry and pathology of radical-mediated protein oxidation." The Biochemical journal **324 (Pt 1)**: 1-18.

DeAtley, S. M., M. Y. Aksenov, M. V. Aksenova, B. Jordan, J. M. Carney and D. A. Butterfield (1999). "Adriamycin-induced changes of creatine kinase activity in vivo and in cardiomyocyte culture." Toxicology **134**(1): 51-62.

Deby, C. and R. Goutier (1990). "New perspectives on the biochemistry of superoxide anion and the efficiency of superoxide dismutases." Biochem Pharmacol **39**(3): 399-405.

Deeb, K. K., D. L. Trump and C. S. Johnson (2007). "Vitamin D signalling pathways in cancer: potential for anticancer therapeutics." Nat Rev Cancer **7**(9): 684-700.

Deprez, S., F. Amant, A. Smeets, R. Peeters, A. Leemans, W. Van Hecke, J. S. Verhoeven, M. R. Christiaens, J. Vandenberghe, M. Vandenbulcke and S. Sunaert (2012). "Longitudinal assessment of chemotherapy-induced structural changes in cerebral white matter and its correlation with impaired cognitive functioning." J Clin Oncol **30**(3): 274-281.

Deprez, S., F. Amant, R. Yigit, K. Porke, J. Verhoeven, J. Van den Stock, A. Smeets, M. R. Christiaens, A. Leemans, W. Van Hecke, J. Vandenberghe, M. Vandenbulcke and S. Sunaert (2011). "Chemotherapy-induced structural changes in cerebral white matter and its correlation with impaired cognitive functioning in breast cancer patients." Hum Brain Mapp **32**(3): 480-493.

Deres, P., R. Halmosi, A. Toth, K. Kovacs, A. Palfi, T. Habon, L. Czopf, T. Kalai, K. Hideg, B. Sumegi and K. Toth (2005). "Prevention of doxorubicin-induced acute cardiotoxicity by an experimental antioxidant compound." J Cardiovasc Pharmacol **45**(1): 36-43.

Desai, V. G., E. H. Herman, C. L. Moland, W. S. Branham, S. M. Lewis, K. J. Davis, N. I. George, T. Lee, S. Kerr and J. C. Fuscoe (2013). "Development of doxorubicin-induced chronic cardiotoxicity in the B6C3F1 mouse model." Toxicol Appl Pharmacol **266**(1): 109-121.

Dezortova, M. and M. Hajek (2008). "(1)H MR spectroscopy in pediatrics." Eur J Radiol **67**(2): 240-249.

Diaz, L., N. Noyola-Martinez, D. Barrera, G. Hernandez, E. Avila, A. Halhali and F. Larrea (2009). "Calcitriol inhibits TNF-alpha-induced inflammatory cytokines in human trophoblasts." J Reprod Immunol **81**(1): 17-24.

Dinarello, C. A. (2007). "Historical insights into cytokines." Eur J Immunol **37 Suppl 1**: S34-45.

Dominiczak, M. H. (2001). "Risk factors for coronary disease: the time for a paradigm shift?" Clin Chem Lab Med **39**(10): 907-919.

Dominiczak, M. H. and M. J. Caslake (2011). "Apolipoproteins: metabolic role and clinical biochemistry applications." Ann Clin Biochem **48**(Pt 6): 498-515.

Ennaceur, A. (2010). "One-trial object recognition in rats and mice: methodological and theoretical issues." Behav Brain Res **215**(2): 244-254.

Ennaceur, A. and J. Delacour (1988). "A new one-trial test for neurobiological studies of memory in rats. 1: Behavioral data." Behav Brain Res **31**(1): 47-59.

Fadillioglu, E. and H. Erdogan (2003). "Effects of erdosteine treatment against doxorubicin-induced toxicity through erythrocyte and plasma oxidant/antioxidant status in rats." Pharmacol Res **47**(4): 317-322.

Fang, J., T. Seki and H. Maeda (2009). "Therapeutic strategies by modulating oxygen stress in cancer and inflammation." Adv Drug Deliv Rev **61**(4): 290-302.

Farber, S. A., B. E. Slack and J. K. Blusztajn (2000). "Acceleration of phosphatidylcholine synthesis and breakdown by inhibitors of mitochondrial function in neuronal cells: a model of the membrane defect of Alzheimer's disease." FASEB J **14**(14): 2198-2206.

Farid, K., L. Volpe-Gillot, S. Petras, C. Plou, N. Caillat-Vigneron and J. Blacher (2012). "Correlation between serum 25-hydroxyvitamin D concentrations and regional cerebral blood flow in degenerative dementia." Nuclear medicine communications **33**(10): 1048-1052.

Feeney, M. B. and C. Schoneich (2012). "Tyrosine modifications in aging." Antioxid Redox Signal **17**(11): 1571-1579.

Fenton, H. J. H. (1894). "Oxidation of tartaric acid in presence of iron." J. Chem. Soc. **65**: 899-910.

Feo, F., M. Frau, M. L. Tomasi, S. Brozzetti and R. M. Pascale (2009). "Genetic and epigenetic control of molecular alterations in hepatocellular carcinoma." Exp Biol Med (Maywood) **234**(7): 726-736.

Ferguson, R. J., T. A. Ahles, A. J. Saykin, B. C. McDonald, C. T. Furstenberg, B. F. Cole and L. A. Mott (2007). "Cognitive-behavioral management of chemotherapy-related cognitive change." Psychooncology **16**(8): 772-777.

Fernandes de Abreu, D. A., D. Eyles and F. Feron (2009). "Vitamin D, a neuro-immunomodulator: implications for neurodegenerative and autoimmune diseases." Psychoneuroendocrinology **34 Suppl 1**: S265-277.

Figueira, T. R., M. H. Barros, A. A. Camargo, R. F. Castilho, J. C. Ferreira, A. J. Kowaltowski, F. E. Sluse, N. C. Souza-Pinto and A. E. Vercesi (2013). "Mitochondria as a source of reactive oxygen and nitrogen species: from molecular mechanisms to human health." Antioxid Redox Signal **18**(16): 2029-2074.

Fitzgerald, D. C., K. G. Meade, A. N. McEvoy, L. Lillis, E. P. Murphy, D. E. MacHugh and A. W. Baird (2007). "Tumour necrosis factor-alpha (TNF-alpha) increases nuclear factor kappaB (NFkappaB) activity in and interleukin-8 (IL-8) release from bovine mammary epithelial cells." Veterinary immunology and immunopathology **116**(1-2): 59-68.

Foley, J. J., R. B. Raffa and E. A. Walker (2008). "Effects of chemotherapeutic agents 5-fluorouracil and methotrexate alone and combined in a mouse model of learning and memory." Psychopharmacology (Berl) **199**(4): 527-538.

Fornari, F. A., J. K. Randolph, J. C. Yalowich, M. K. Ritke and D. A. Gewirtz (1994). "Interference by doxorubicin with DNA unwinding in MCF-7 breast tumor cells." Mol Pharmacol **45**(4): 649-656.

Foti, R., S. Zucchelli, M. Biagioli, P. Roncaglia, S. Vilotti, R. Calligaris, H. Krmac, J. E. Girardini, G. Del Sal and S. Gustincich (2010). "Parkinson disease-associated DJ-1 is required for the expression of the glial cell line-derived neurotrophic factor receptor RET in human neuroblastoma cells." The Journal of biological chemistry **285**(24): 18565-18574.

Frau, M., M. M. Simile, M. L. Tomasi, M. I. Demartis, L. Daino, M. A. Seddaiu, S. Brozzetti, C. F. Feo, G. Massarelli, G. Solinas, F. Feo, J. S. Lee and R. M. Pascale (2012). "An expression signature of phenotypic resistance to hepatocellular carcinoma identified by cross-species gene expression analysis." Cell Oncol (Dordr) **35**(3): 163-173.

Fridovich, I. (1986). "Biological effects of the superoxide radical." Arch Biochem Biophys **247**(1): 1-11.

Fridovich, I. (1995). "Superoxide radical and superoxide dismutases." Annu Rev Biochem **64**: 97-112.

Frisardi, V., F. Panza, D. Seripa, T. Farooqui and A. A. Farooqui (2011). "Glycerophospholipids and glycerophospholipid-derived lipid mediators: a complex meshwork in Alzheimer's disease pathology." Prog Lipid Res **50**(4): 313-330.

Furman, I., C. Baudet and P. Brachet (1996). "Differential expression of M-CSF, LIF, and TNF-alpha genes in normal and malignant rat glial cells: regulation by lipopolysaccharide and vitamin D." Journal of neuroscience research **46**(3): 360-366.

Garcion, E., S. Nataf, A. Berod, F. Darcy and P. Brachet (1997). "1,25-Dihydroxyvitamin D3 inhibits the expression of inducible nitric oxide synthase in rat central nervous system during experimental allergic encephalomyelitis." Brain research. Molecular brain research **45**(2): 255-267.

Garcion, E., L. Sindji, G. Leblondel, P. Brachet and F. Darcy (1999). "1,25-dihydroxyvitamin D3 regulates the synthesis of gamma-glutamyl transpeptidase and glutathione levels in rat primary astrocytes." Journal of neurochemistry **73**(2): 859-866.

Garcion, E., L. Sindji, C. Montero-Menei, C. Andre, P. Brachet and F. Darcy (1998). "Expression of inducible nitric oxide synthase during rat brain inflammation: regulation by 1,25-dihydroxyvitamin D3." Glia **22**(3): 282-294.

Garcion, E., L. Sindji, S. Nataf, P. Brachet, F. Darcy and C. N. Montero-Menei (2003). "Treatment of experimental autoimmune encephalomyelitis in rat by 1,25-dihydroxyvitamin D3 leads to early effects within the central nervous system." Acta neuropathologica **105**(5): 438-448.

Garcion, E., N. Wion-Barbot, C. N. Montero-Menei, F. Berger and D. Wion (2002). "New clues about vitamin D functions in the nervous system." Trends in Endocrinology and Metabolism **13**(3): 100-105.

Ge, Y. S., W. Y. Teng and C. D. Zhang (2009). "Protective effect of cyclophilin A against Alzheimer's amyloid beta-peptide (25-35)-induced oxidative stress in PC12 cells." Chin Med J (Engl) **122**(6): 716-724.

Geilen, C. C., T. Wieder and C. E. Orfanos (1997). "Ceramide signalling: regulatory role in cell proliferation, differentiation and apoptosis in human epidermis." Arch Dermatol Res **289**(10): 559-566.

Ginter, E. and V. Simko (2009). "Vitamin D deficiency, atherosclerosis and cancer." Bratisl Lek Listy **110**(12): 751-756.

Giulietti, A., E. van Etten, L. Overbergh, K. Stoffels, R. Bouillon and C. Mathieu (2007). "Monocytes from type 2 diabetic patients have a pro-inflammatory profile. 1,25-Dihydroxyvitamin D(3) works as anti-inflammatory." Diabetes research and clinical practice **77**(1): 47-57.

Gold, B. T., Y. Jiang, D. K. Powell and C. D. Smith (2012). "Multimodal imaging evidence for axonal and myelin deterioration in amnestic mild cognitive impairment." J Alzheimers Dis **31 Suppl 3**: S19-31.

Gold, B. T., D. K. Powell, A. H. Andersen and C. D. Smith (2010). "Alterations in multiple measures of white matter integrity in normal women at high risk for Alzheimer's disease." Neuroimage **52**(4): 1487-1494.

Goulart, B. K., M. N. de Lima, C. B. de Farias, G. K. Reolon, V. R. Almeida, J. Quevedo, F. Kapczinski, N. Schroder and R. Roesler (2010). "Ketamine impairs recognition memory consolidation and prevents learning-induced increase in hippocampal brain-derived neurotrophic factor levels." Neuroscience **167**(4): 969-973.

Griscavage, J. M., S. Wilk and L. J. Ignarro (1996). "Inhibitors of the proteasome pathway interfere with induction of nitric oxide synthase in macrophages by blocking activation of transcription factor NF-kappa B." Proc Natl Acad Sci U S A **93**(8): 3308-3312.

Gupta, R. K., T. F. Cloughesy, U. Sinha, J. Garakian, J. Lazareff, G. Rubino, L. Rubino, D. P. Becker, H. V. Vinters and J. R. Alger (2000). "Relationships between choline magnetic resonance spectroscopy, apparent diffusion coefficient and quantitative histopathology in human glioma." J Neurooncol **50**(3): 215-226.

Gupta, S., R. Bi, C. Kim, S. Chiplunkar, L. Yel and S. Gollapudi (2005). "Role of NF-kappaB signaling pathway in increased tumor necrosis factor-alpha-induced apoptosis of lymphocytes in aged humans." Cell Death Differ **12**(2): 177-183.

Gutierrez, E. G., W. A. Banks and A. J. Kastin (1993). "Murine tumor necrosis factor alpha is transported from blood to brain in the mouse." Journal of neuroimmunology **47**(2): 169-176.

Gutteridge, J. M. (1984). "Lipid peroxidation and possible hydroxyl radical formation stimulated by the self-reduction of a doxorubicin-iron (III) complex." Biochem Pharmacol **33**(11): 1725-1728.

Gutteridge, J. M. (1984). "Lipid peroxidation initiated by superoxide-dependent hydroxyl radicals using complexed iron and hydrogen peroxide." FEBS Lett **172**(2): 245-249.
Haber, F., Weiss, J. (1932). "Über die Katalyse des Hydroperoxydes." Naturwissenschaften **20**: 948-950.
Halicka, H. D., H. Zhao, J. Li, F. Traganos, G. P. Studzinski and Z. Darzynkiewicz (2012). "Attenuation of constitutive DNA damage signaling by 1,25-dihydroxyvitamin D3." Aging **4**(4): 270-278.
Halliwell, B. (2012). "Free radicals and antioxidants: updating a personal view." Nutr Rev **70**(5): 257-265.
Halliwell, B. and J. M. Gutteridge (1984). "Free radicals, lipid peroxidation, and cell damage." Lancet **2**(8411): 1095.
Halliwell, B. and J. M. Gutteridge (1984). "Oxygen toxicity, oxygen radicals, transition metals and disease." Biochem J **219**(1): 1-14.
Halliwell, B. and J. M. Gutteridge (1986). "Iron and free radical reactions: two aspects of antioxidant protection." Trends Biochem Sci **11**(9): 372-375.
Halliwell, B. and J. M. C. Gutteridge (2007). Free radicals in biology and medicine. Oxford ; New York, Oxford University Press.
Handa, K. and S. Sato (1975). "Generation of free radicals of quinone group-containing anti-cancer chemicals in NADPH-microsome system as evidenced by initiation of sulfite oxidation." Gann **66**(1): 43-47.
Harris, M. E., K. Hensley, D. A. Butterfield, R. A. Leedle and J. M. Carney (1995). "Direct evidence of oxidative injury produced by the Alzheimer's beta-amyloid peptide (1-40) in cultured hippocampal neurons." Exp Neurol **131**(2): 193-202.
Haussler, M. R., C. A. Haussler, L. Bartik, G. K. Whitfield, J. C. Hsieh, S. Slater and P. W. Jurutka (2008). "Vitamin D receptor: molecular signaling and actions of nutritional ligands in disease prevention." Nutr Rev **66**(10 Suppl 2): S98-112.
Helbecque, N., V. Codron, D. Cottel and P. Amouyel (2008). "An apolipoprotein A-I gene promoter polymorphism associated with cognitive decline, but not with Alzheimer's disease." Dementia and geriatric cognitive disorders **25**(2): 97-102.
Hensley, K., D. A. Butterfield, M. Mattson, M. Aksenova, M. Harris, J. F. Wu, R. Floyd and J. Carney (1995). "A model for beta-amyloid aggregation and neurotoxicity based on the free radical generating capacity of the peptide: implications of "molecular shrapnel" for Alzheimer's disease." Proc West Pharmacol Soc **38**: 113-120.
Hill, S. A. and M. J. McQueen (1997). "Reverse cholesterol transport--a review of the process and its clinical implications." Clin Biochem **30**(7): 517-525.
Holick, M. F. (2004). "Sunlight and vitamin D for bone health and prevention of autoimmune diseases, cancers, and cardiovascular disease." The American journal of clinical nutrition **80**(6 Suppl): 1678S-1688S.
Holick, M. F. (2006). "Resurrection of vitamin D deficiency and rickets." The Journal of clinical investigation **116**(8): 2062-2072.
Holick, M. F. (2007). "Vitamin D deficiency." The New England journal of medicine **357**(3): 266-281.
Holick, M. F. (2008). "The vitamin D deficiency pandemic and consequences for nonskeletal health: mechanisms of action." Molecular aspects of medicine **29**(6): 361-368.
Holick, M. F. (2010). "The vitamin D deficiency pandemic: a forgotten hormone important for health." Public Health Reviews **32**: 267-283.
Holick, M. F. (2012). "Evidence-based D-bate on health benefits of vitamin D revisited." Dermatoendocrinol **4**(2): 183-190.

Holick, M. F. and T. C. Chen (2008). "Vitamin D deficiency: a worldwide problem with health consequences." The American journal of clinical nutrition **87**(4): 1080S-1086S.

Hsu, H., J. Xiong and D. V. Goeddel (1995). "The TNF receptor 1-associated protein TRADD signals cell death and NF-kappa B activation." Cell **81**(4): 495-504.

Hu, Y. W., X. Ma, X. X. Li, X. H. Liu, J. Xiao, Z. C. Mo, J. Xiang, D. F. Liao and C. K. Tang (2009). "Eicosapentaenoic acid reduces ABCA1 serine phosphorylation and impairs ABCA1-dependent cholesterol efflux through cyclic AMP/protein kinase A signaling pathway in THP-1 macrophage-derived foam cells." Atherosclerosis **204**(2): e35-43.

Hyka, N., J. M. Dayer, C. Modoux, T. Kohno, C. K. Edwards, 3rd, P. Roux-Lombard and D. Burger (2001). "Apolipoprotein A-I inhibits the production of interleukin-1beta and tumor necrosis factor-alpha by blocking contact-mediated activation of monocytes by T lymphocytes." Blood **97**(8): 2381-2389.

Inagaki, M., E. Yoshikawa, Y. Matsuoka, Y. Sugawara, T. Nakano, T. Akechi, N. Wada, S. Imoto, K. Murakami and Y. Uchitomi (2007). "Smaller regional volumes of brain gray and white matter demonstrated in breast cancer survivors exposed to adjuvant chemotherapy." Cancer **109**(1): 146-156.

Ischiropoulos, H. (2009). "Protein tyrosine nitration--an update." Arch Biochem Biophys **484**(2): 117-121.

Iwamoto, N., R. Lu, N. Tanaka, S. Abe-Dohmae and S. Yokoyama (2010). "Calmodulin interacts with ATP binding cassette transporter A1 to protect from calpain-mediated degradation and upregulates high-density lipoprotein generation." Arterioscler Thromb Vasc Biol **30**(7): 1446-1452.

Jang, Y. H., B. H. Ahn, S. Namkoong, Y. M. Kim, J. K. Jin, Y. S. Kim and S. Min do (2008). "Differential regulation of apoptosis by caspase-mediated cleavage of phospholipase D isozymes." Cell Signal **20**(12): 2198-2207.

Jang, Y. H., S. Namkoong, Y. M. Kim, S. J. Lee, B. J. Park and D. S. Min (2008). "Cleavage of phospholipase D1 by caspase promotes apoptosis via modulation of the p53-dependent cell death pathway." Cell Death Differ **15**(11): 1782-1793.

Jansen, J. F., W. H. Backes, K. Nicolay and M. E. Kooi (2006). "1H MR spectroscopy of the brain: absolute quantification of metabolites." Radiology **240**(2): 318-332.

Jeon, K. I., H. Jono, C. L. Miller, Y. Cai, S. Lim, X. Liu, P. Gao, J. Abe, J. D. Li and C. Yan (2010). "Ca2+/calmodulin-stimulated PDE1 regulates the beta-catenin/TCF signaling through PP2A B56 gamma subunit in proliferating vascular smooth muscle cells." FEBS J **277**(24): 5026-5039.

Jones, D. P. (2008). "Radical-free biology of oxidative stress." American journal of physiology. Cell physiology **295**(4): C849-868.

Jones, P. M. and S. J. Persaud (1993). "Arachidonic acid as a second messenger in glucose-induced insulin secretion from pancreatic beta-cells." J Endocrinol **137**(1): 7-14.

Joshi, G., C. D. Aluise, M. P. Cole, R. Sultana, W. M. Pierce, M. Vore, D. K. St Clair and D. A. Butterfield (2010). "Alterations in brain antioxidant enzymes and redox proteomic identification of oxidized brain proteins induced by the anti-cancer drug adriamycin: implications for oxidative stress-mediated chemobrain." Neuroscience **166**(3): 796-807.

Joshi, G., S. Hardas, R. Sultana, D. K. St Clair, M. Vore and D. A. Butterfield (2007). "Glutathione elevation by gamma-glutamyl cysteine ethyl ester as a potential therapeutic strategy for preventing oxidative stress in brain mediated by in vivo administration of adriamycin: Implication for chemobrain." J Neurosci Res **85**(3): 497-503.

Joshi, G., R. Sultana, J. Tangpong, M. P. Cole, D. K. St Clair, M. Vore, S. Estus and D. A. Butterfield (2005). "Free radical mediated oxidative stress and toxic side effects in brain induced by

the anti cancer drug adriamycin: insight into chemobrain." Free Radic Res **39**(11): 1147-1154.

Jungsuwadee, P., M. P. Cole, R. Sultana, G. Joshi, J. Tangpong, D. A. Butterfield, D. K. St Clair and M. Vore (2006). "Increase in Mrp1 expression and 4-hydroxy-2-nonenal adduction in heart tissue of Adriamycin-treated C57BL/6 mice." Mol Cancer Ther **5**(11): 2851-2860.

Jungsuwadee, P., T. Zhao, E. I. Stolarczyk, C. M. Paumi, D. A. Butterfield, D. K. St Clair and M. Vore (2012). "The G671V variant of MRP1/ABCC1 links doxorubicin-induced acute cardiac toxicity to disposition of the glutathione conjugate of 4-hydroxy-2-trans-nonenal." Pharmacogenet Genomics **22**(4): 273-284.

Kang, S. W., H. Z. Chae, M. S. Seo, K. Kim, I. C. Baines and S. G. Rhee (1998). "Mammalian peroxiredoxin isoforms can reduce hydrogen peroxide generated in response to growth factors and tumor necrosis factor-alpha." The Journal of biological chemistry **273**(11): 6297-6302.

Keeney, J. T., S. Forster, R. Sultana, L. D. Brewer, C. S. Latimer, J. Cai, J. B. Klein, N. M. Porter and D. Allan Butterfield (2013). "Dietary vitamin D deficiency in rats from middle to old age leads to elevated tyrosine nitration and proteomics changes in levels of key proteins in brain: Implications for low vitamin D-dependent age-related cognitive decline." Free Radic Biol Med **65C**: 324-334.

Keeney, J. T., X. Ren, G. Warrier, T. Noel, D. K. Powell, J. M. Brelsfoard, K. E. Saatman, R. Sultana, D. K. St Clair and D. A. Butterfield (2014). "Doxorubicin-induced elevated oxidative stress in brain and cognitive decline: protection by MESNA and insights into mechanisms of chemotherapy-induced cognitive impairment ("chemobrain")." In Press.

Keeney, J. T., A. M. Swomley, S. Forster, J. L. Harris, R. Sultana and D. A. Butterfield (2013). "Apolipoprotein A-I: insights from redox proteomics for its role in neurodegeneration." Proteomics Clin Appl **7**(1-2): 109-122.

Kim, H. Y., K. A. Tallman, D. C. Liebler and N. A. Porter (2009). "An azido-biotin reagent for use in the isolation of protein adducts of lipid-derived electrophiles by streptavidin catch and photorelease." Molecular & cellular proteomics : MCP **8**(9): 2080-2089.

Kim, J. I., W. K. Ju, J. H. Choi, E. Choi, R. I. Carp, H. M. Wisniewski and Y. S. Kim (1999). "Expression of cytokine genes and increased nuclear factor-kappa B activity in the brains of scrapie-infected mice." Brain research. Molecular brain research **73**(1-2): 17-27.

Kim, S., R. Di Cosimo and J. San Filippo, J. (1979). "Spectrometric and chemical characterization of superoxide." Anal Chem **51**(6): 679-681.

Kinnunen, K. M., R. Greenwood, J. H. Powell, R. Leech, P. C. Hawkins, V. Bonnelle, M. C. Patel, S. J. Counsell and D. J. Sharp (2011). "White matter damage and cognitive impairment after traumatic brain injury." Brain **134**(Pt 2): 449-463.

Klamt, F., C. Gottfried, F. Tramontina, F. Dal-Pizzol, M. L. Da Frota, Jr., J. C. Moreira, R. D. Dias, E. Moriguchi, S. Wofchuk and D. O. Souza (2002). "Time-related increase in mitochondrial superoxide production, biomolecule damage and antioxidant enzyme activities in cortical astrocyte cultures." Neuroreport **13**(12): 1515-1518.

Kogo, J., Y. Takeba, T. Kumai, Y. Kitaoka, N. Matsumoto, S. Ueno and S. Kobayashi (2006). "Involvement of TNF-alpha in glutamate-induced apoptosis in a differentiated neuronal cell line." Brain Res **1122**(1): 201-208.

Konat, G. W., M. Kraszpulski, I. James, H. T. Zhang and J. Abraham (2008). "Cognitive dysfunction induced by chronic administration of common cancer chemotherapeutics in rats." Metab Brain Dis **23**(3): 325-333.

Koppal, T., J. Drake, S. Yatin, B. Jordan, S. Varadarajan, L. Bettenhausen and D. A. Butterfield (1999). "Peroxynitrite-induced alterations in synaptosomal membrane proteins: insight into oxidative stress in Alzheimer's disease." Journal of neurochemistry **72**(1): 310-317.

Labetoulle, M., C. Capelli, F. Dubreuil, O. Kirsch, G. Perlemuter, C. Buffet, J. Quillard, H. Offret and E. Frau (2001). "[Orbital metastasis of hepatocellular carcinoma]." Gastroenterol Clin Biol **25**(10): 914-915.

Lardinois, O. M. (1995). "Reactions of bovine liver catalase with superoxide radicals and hydrogen peroxide." Free Radic Res **22**(3): 251-274.

Lauderback, C. M., J. M. Hackett, F. F. Huang, J. N. Keller, L. I. Szweda, W. R. Markesbery and D. A. Butterfield (2001). "The glial glutamate transporter, GLT-1, is oxidatively modified by 4-hydroxy-2-nonenal in the Alzheimer's disease brain: the role of Abeta1-42." J Neurochem **78**(2): 413-416.

Lee, S. P., Y. S. Hwang, Y. J. Kim, K. S. Kwon, H. J. Kim, K. Kim and H. Z. Chae (2001). "Cyclophilin a binds to peroxiredoxins and activates its peroxidase activity." The Journal of biological chemistry **276**(32): 29826-29832.

Lefebvre d'Hellencourt, C., C. N. Montero-Menei, R. Bernard and D. Couez (2003). "Vitamin D3 inhibits proinflammatory cytokines and nitric oxide production by the EOC13 microglial cell line." Journal of neuroscience research **71**(4): 575-582.

Leibrock, C., T. F. Ackermann, M. Hierlmeier, F. Lang, S. Borgwardt and U. E. Lang (2013). "Akt2 Deficiency is Associated with Anxiety and Depressive Behavior in Mice." Cell Physiol Biochem **32**(3): 766-777.

Lemire, J. M. and D. C. Archer (1991). "1,25-dihydroxyvitamin D3 prevents the in vivo induction of murine experimental autoimmune encephalomyelitis." The Journal of clinical investigation **87**(3): 1103-1107.

Li, Q., S. Sanlioglu, S. Li, T. Ritchie, L. Oberley and J. F. Engelhardt (2001). "GPx-1 gene delivery modulates NFkappaB activation following diverse environmental injuries through a specific subunit of the IKK complex." Antioxidants & redox signaling **3**(3): 415-432.

Liebler, D. C. (2008). "Protein damage by reactive electrophiles: targets and consequences." Chemical research in toxicology **21**(1): 117-128.

Liochev, S. I. and I. Fridovich (2007). "The effects of superoxide dismutase on H2O2 formation." Free Radic Biol Med **42**(10): 1465-1469.

Liscum, L. and K. W. Underwood (1995). "Intracellular cholesterol transport and compartmentation." J Biol Chem **270**(26): 15443-15446.

Liu, Z. G., H. Hsu, D. V. Goeddel and M. Karin (1996). "Dissection of TNF receptor 1 effector functions: JNK activation is not linked to apoptosis while NF-kappaB activation prevents cell death." Cell **87**(3): 565-576.

Llewellyn, D. J., I. A. Lang, K. M. Langa and D. Melzer (2011). "Vitamin D and cognitive impairment in the elderly U.S. population." The journals of gerontology. Series A, Biological sciences and medical sciences **66**(1): 59-65.

Llewellyn, D. J., I. A. Lang, K. M. Langa, G. Muniz-Terrera, C. L. Phillips, A. Cherubini, L. Ferrucci and D. Melzer (2010). "Vitamin D and risk of cognitive decline in elderly persons." Archives of internal medicine **170**(13): 1135-1141.

Llewellyn, D. J., K. M. Langa and I. A. Lang (2009). "Serum 25-hydroxyvitamin D concentration and cognitive impairment." Journal of geriatric psychiatry and neurology **22**(3): 188-195.

Lovell, M. A. and W. R. Markesbery (2008). "Oxidatively modified RNA in mild cognitive impairment." Neurobiol Dis **29**(2): 169-175.

MacEwan, D. J. (2002). "TNF receptor subtype signalling: differences and cellular consequences." Cell Signal **14**(6): 477-492.

MacMillan-Crow, L. A., J. P. Crow and J. A. Thompson (1998). "Peroxynitrite-mediated inactivation of manganese superoxide dismutase involves nitration and oxidation of critical tyrosine residues." Biochemistry **37**(6): 1613-1622.

Mallampalli, R. K., A. J. Ryan, R. G. Salome and S. Jackowski (2000). "Tumor necrosis factor-alpha inhibits expression of CTP:phosphocholine cytidylyltransferase." J Biol Chem **275**(13): 9699-9708.

Mashiach, E., S. Sela, T. Weinstein, H. I. Cohen, S. M. Shasha and B. Kristal (2001). "Mesna: a novel renoprotective antioxidant in ischaemic acute renal failure." Nephrol Dial Transplant **16**(3): 542-551.

Matsunaga, T., Y. Hiasa, H. Yanagi, T. Maeda, N. Hattori, K. Yamakawa, Y. Yamanouchi, I. Tanaka, T. Obara and H. Hamaguchi (1991). "Apolipoprotein A-I deficiency due to a codon 84 nonsense mutation of the apolipoprotein A-I gene." Proc Natl Acad Sci U S A **88**(7): 2793-2797.

Mattiazzi, M., M. D'Aurelio, C. D. Gajewski, K. Martushova, M. Kiaei, M. F. Beal and G. Manfredi (2002). "Mutated human SOD1 causes dysfunction of oxidative phosphorylation in mitochondria of transgenic mice." J Biol Chem **277**(33): 29626-29633.

McCarty, M. F. (2006). "Down-regulation of microglial activation may represent a practical strategy for combating neurodegenerative disorders." Med Hypotheses **67**(2): 251-269.

McDonald, B. C. and A. J. Saykin (2013). "Alterations in brain structure related to breast cancer and its treatment: chemotherapy and other considerations." Brain Imaging Behav.

McPherson, D. B., R. P. Kilker and T. D. Foley (2002). "Superoxide activates constitutive nitric oxide synthase in a brain particulate fraction." Biochem Biophys Res Commun **296**(2): 413-418.

Meck, W. H., R. M. Church and M. S. Matell (2013). "Hippocampus, time, and memory-A retrospective analysis." Behav Neurosci **127**(5): 642-654.

Mendes, A. F., A. P. Carvalho, M. M. Caramona and M. C. Lopes (2002). "Role of nitric oxide in the activation of NF-kappaB, AP-1 and NOS II expression in articular chondrocytes." Inflamm Res **51**(7): 369-375.

Miller, A. F. (2003). Superoxide processing. Comprehensive Coordination Chemistry II. T. J. Meyer and J. A. McCleverty. Oxford, Elsevier Science**:** 479-506.

Minelli, A., S. Grottelli, A. Mierla, F. Pinnen, I. Cacciatore and I. Bellezza (2012). "Cyclo(His-Pro) exerts anti-inflammatory effects by modulating NF-kappaB and Nrf2 signalling." Int J Biochem Cell Biol **44**(3): 525-535.

Mitsumoto, A. and Y. Nakagawa (2001). "DJ-1 is an indicator for endogenous reactive oxygen species elicited by endotoxin." Free radical research **35**(6): 885-893.

Mitsumoto, A., Y. Nakagawa, A. Takeuchi, K. Okawa, A. Iwamatsu and Y. Takanezawa (2001). "Oxidized forms of peroxiredoxins and DJ-1 on two-dimensional gels increased in response to sublethal levels of paraquat." Free radical research **35**(3): 301-310.

Miyagi, M., H. Sakaguchi, R. M. Darrow, L. Yan, K. A. West, K. S. Aulak, D. J. Stuehr, J. G. Hollyfield, D. T. Organisciak and J. W. Crabb (2002). "Evidence that light modulates protein nitration in rat retina." Molecular & cellular proteomics : MCP **1**(4): 293-303.

Mizwicki, M. T., G. Liu, M. Fiala, L. Magpantay, J. Sayre, A. Siani, M. Mahanian, R. Weitzman, E. Y. Hayden, M. J. Rosenthal, I. Nemere, J. Ringman and D. B. Teplow (2013). "1alpha,25-Dihydroxyvitamin D3 and Resolvin D1 Retune the Balance between Amyloid-beta Phagocytosis and Inflammation in Alzheimer's Disease Patients." Journal of Alzheimer's disease : JAD **34**(1): 155-170.

Moreira, P. I., A. Nunomura, M. Nakamura, A. Takeda, J. C. Shenk, G. Aliev, M. A. Smith and G. Perry (2008). "Nucleic acid oxidation in Alzheimer disease." Free Radic Biol Med **44**(8): 1493-1505.

Mukhopadhyay, S. S., K. S. Leung, M. J. Hicks, P. J. Hastings, H. Youssoufian and S. E. Plon (2006). "Defective mitochondrial peroxiredoxin-3 results in sensitivity to oxidative stress in Fanconi anemia." The Journal of cell biology **175**(2): 225-235.

Muller, K., P. M. Haahr, M. Diamant, K. Rieneck, A. Kharazmi and K. Bendtzen (1992). "1,25-Dihydroxyvitamin D3 inhibits cytokine production by human blood monocytes at the post-transcriptional level." Cytokine **4**(6): 506-512.

Mumby, D. G. (2001). "Perspectives on object-recognition memory following hippocampal damage: lessons from studies in rats." Behav Brain Res **127**(1-2): 159-181.

Mumby, D. G., M. J. Glenn, C. Nesbitt and D. A. Kyriazis (2002). "Dissociation in retrograde memory for object discriminations and object recognition in rats with perirhinal cortex damage." Behav Brain Res **132**(2): 215-226.

Murray, P. J. (2006). "Understanding and exploiting the endogenous interleukin-10/STAT3-mediated anti-inflammatory response." Curr Opin Pharmacol **6**(4): 379-386.

Nakashima, S. and Y. Nozawa (1999). "Possible role of phospholipase D in cellular differentiation and apoptosis." Chem Phys Lipids **98**(1-2): 153-164.

Naressi, A., C. Couturier, I. Castang, R. de Beer and D. Graveron-Demilly (2001). "Java-based graphical user interface for MRUI, a software package for quantitation of in vivo/medical magnetic resonance spectroscopy signals." Comput Biol Med **31**(4): 269-286.

Netto, L. E. S., H. Z. Chae, S. W. Kang, S. G. Rhee and E. R. Stadtman (1996). "Removal of hydrogen peroxide by thiol-specific antioxidant enzyme (TSA) is involved with its antioxidant properties. TSA possesses thiol peroxidase activity." The Journal of biological chemistry **271**(26): 15315-15321.

Neveu, I., P. Naveilhan, C. Menaa, D. Wion, P. Brachet and M. Garabedian (1994). "Synthesis of 1,25-dihydroxyvitamin D3 by rat brain macrophages in vitro." Journal of neuroscience research **38**(2): 214-220.

Nezbedova, P. and J. Brtko (2004). "1alpha,25-dihydroxyvitamin D3 inducible transcription factor and its role in the vitamin D action." Endocr Regul **38**(1): 29-38.

Nishitoh, H., M. Saitoh, Y. Mochida, K. Takeda, H. Nakano, M. Rothe, K. Miyazono and H. Ichijo (1998). "ASK1 is essential for JNK/SAPK activation by TRAF2." Mol Cell **2**(3): 389-395.

Nithipongvanitch, R., W. Ittarat, J. M. Velez, R. Zhao, D. K. St Clair and T. D. Oberley (2007). "Evidence for p53 as guardian of the cardiomyocyte mitochondrial genome following acute adriamycin treatment." J Histochem Cytochem **55**(6): 629-639.

Nonn, L., M. Berggren and G. Powis (2003). "Increased expression of mitochondrial peroxiredoxin-3 (thioredoxin peroxidase-2) protects cancer cells against hypoxia and drug-induced hydrogen peroxide-dependent apoptosis." Mol Cancer Res **1**(9): 682-689.

Nozawa, Y. (2002). "Roles of phospholipase D in apoptosis and pro-survival." Biochim Biophys Acta **1585**(2-3): 77-86.

Nunomura, A., T. Hofer, P. I. Moreira, R. J. Castellani, M. A. Smith and G. Perry (2009). "RNA oxidation in Alzheimer disease and related neurodegenerative disorders." Acta Neuropathol **118**(1): 151-166.

Oh, H. Y., E. J. Lee, S. Yoon, B. H. Chung, K. S. Cho and S. J. Hong (2007). "Cholesterol level of lipid raft microdomains regulates apoptotic cell death in prostate cancer cells through EGFR-mediated Akt and ERK signal transduction." Prostate **67**(10): 1061-1069.

Old, L. J. (1976). "Tumor necrosis factor." Clin Bull **6**(3): 118-120.

Oliveira-Marques, V., H. S. Marinho, L. Cyrne and F. Antunes (2009). "Role of hydrogen peroxide in NF-kappaB activation: from inducer to modulator." Antioxidants & redox signaling **11**(9): 2223-2243.

Olojo, R. O., R. H. Xia and J. J. Abramson (2005). "Spectrophotometric and fluorometric assay of superoxide ion using 4-chloro-7-nitrobenzo-2-oxa-1,3-diazole." Anal Biochem **339**(2): 338-344.

Oprins, J. C., C. van der Burg, H. P. Meijer, T. Munnik and J. A. Groot (2002). "Tumour necrosis factor alpha potentiates ion secretion induced by histamine in a human intestinal epithelial cell line and in mouse colon: involvement of the phospholipase D pathway." Gut **50**(3): 314-321.

Osburg, B., C. Peiser, D. Domling, L. Schomburg, Y. T. Ko, K. Voigt and U. Bickel (2002). "Effect of endotoxin on expression of TNF receptors and transport of TNF-alpha at the blood-brain barrier of the rat." American journal of physiology. Endocrinology and metabolism **283**(5): E899-908.

Othman, A. I., M. A. El-Missiry, M. A. Amer and M. Arafa (2008). "Melatonin controls oxidative stress and modulates iron, ferritin, and transferrin levels in adriamycin treated rats." Life Sci **83**(15-16): 563-568.

Owen, J. B., F. Di Domenico, R. Sultana, M. Perluigi, C. Cini, W. M. Pierce and D. A. Butterfield (2009). "Proteomics-determined differences in the concanavalin-A-fractionated proteome of hippocampus and inferior parietal lobule in subjects with Alzheimer's disease and mild cognitive impairment: implications for progression of AD." J Proteome Res **8**(2): 471-482.

Perluigi, M. and D. A. Butterfield (2011). "The identification of protein biomarkers for oxidative stress in Down syndrome." Expert Rev Proteomics **8**(4): 427-429.

Perluigi, M., R. Coccia and D. A. Butterfield (2012). "4-Hydroxy-2-nonenal, a reactive product of lipid peroxidation, and neurodegenerative diseases: a toxic combination illuminated by redox proteomics studies." Antioxid Redox Signal **17**(11): 1590-1609.

Perluigi, M., F. Di Domenico, A. Giorgi, M. E. Schinina, R. Coccia, C. Cini, F. Bellia, M. T. Cambria, C. Cornelius, D. A. Butterfield and V. Calabrese (2010). "Redox proteomics in aging rat brain: involvement of mitochondrial reduced glutathione status and mitochondrial protein oxidation in the aging process." Journal of neuroscience research **88**(16): 3498-3507.

Perry, S. W., S. Dewhurst, M. J. Bellizzi and H. A. Gelbard (2002). "Tumor necrosis factor-alpha in normal and diseased brain: Conflicting effects via intraneuronal receptor crosstalk?" J Neurovirol **8**(6): 611-624.

Poly, C., J. M. Massaro, S. Seshadri, P. A. Wolf, E. Cho, E. Krall, P. F. Jacques and R. Au (2011). "The relation of dietary choline to cognitive performance and white-matter hyperintensity in the Framingham Offspring Cohort." Am J Clin Nutr **94**(6): 1584-1591.

Pomerantz, J. L. and D. Baltimore (2002). "Two pathways to NF-kappaB." Mol Cell **10**(4): 693-695.

Poon, H. F., H. M. Shepherd, T. T. Reed, V. Calabrese, A. M. Stella, G. Pennisi, J. Cai, W. M. Pierce, J. B. Klein and D. A. Butterfield (2006). "Proteomics analysis provides insight into caloric restriction mediated oxidation and expression of brain proteins associated with age-related impaired cellular processes: Mitochondrial dysfunction, glutamate dysregulation and impaired protein synthesis." Neurobiology of aging **27**(7): 1020-1034.

Porter, N. A., S. E. Caldwell and K. A. Mills (1995). "Mechanisms of free radical oxidation of unsaturated lipids." Lipids **30**(4): 277-290.

Pratt, D. A., K. A. Tallman and N. A. Porter (2011). "Free radical oxidation of polyunsaturated lipids: New mechanistic insights and the development of peroxyl radical clocks." Acc Chem Res **44**(6): 458-467.

Prentki, M. and F. M. Matschinsky (1987). "Ca2+, cAMP, and phospholipid-derived messengers in coupling mechanisms of insulin secretion." Physiol Rev **67**(4): 1185-1248.

Przybelski, R. J. and N. C. Binkley (2007). "Is vitamin D important for preserving cognition? A positive correlation of serum 25-hydroxyvitamin D concentration with cognitive function." Archives of biochemistry and biophysics **460**(2): 202-205.

Pun, P. B. and M. P. Murphy (2012). "Pathological significance of mitochondrial glycation." Int J Cell Biol **2012**: 843505.

Qin, S., J. Ding, T. Kurosaki and H. Yamamura (1998). "A deficiency in Syk enhances ceramide-induced apoptosis in DT40 lymphoma B cells." FEBS Lett **427**(1): 139-143.

Quazi, F. and R. S. Molday (2011). "Lipid transport by mammalian ABC proteins." Essays Biochem **50**(1): 265-290.

Rader, D. J. and A. Daugherty (2008). "Translating molecular discoveries into new therapies for atherosclerosis." Nature **451**(7181): 904-913.

Raffa, R. B. (2010). "Imaging as a means of studying chemotherapy-related cognitive impairment." Adv Exp Med Biol **678**: 70-76.

Raffa, R. B. (2010). "Is a picture worth a thousand (forgotten) words?: neuroimaging evidence for the cognitive deficits in 'chemo-fog'/'chemo-brain'." J Clin Pharm Ther **35**(1): 1-9.

Raffa, R. B. (2011). "A proposed mechanism for chemotherapy-related cognitive impairment ('chemo-fog')." J Clin Pharm Ther **36**(3): 257-259.

Raffa, R. B., P. V. Duong, J. Finney, D. A. Garber, L. M. Lam, S. S. Mathew, N. N. Patel, K. C. Plaskett, M. Shah and H. F. Jen Weng (2006). "Is 'chemo-fog'/'chemo-brain' caused by cancer chemotherapy?" Journal of clinical pharmacy and therapeutics **31**(2): 129-138.

Raffa, R. B. and R. J. Tallarida (2010). "Chemo fog: cancer chemotherapy-related cognitive impairment. Preface." Adv Exp Med Biol **678**: vii-viii.

Raha, S. and B. H. Robinson (2000). "Mitochondria, oxygen free radicals, disease and ageing." Trends Biochem Sci **25**(10): 502-508.

Ramachandran, S., A. Venugopal, S. K, R. G, S. Charles, D. G, N. S. Chandran, A. Mullassari, M. R. Pillai and C. C. Kartha (2012). "Proteomic profiling of high glucose primed monocytes identifies cyclophilin A as a potential secretory marker of inflammation in type 2 diabetes." Proteomics **12**(18): 2808-2821.

Rath, P. C. and B. B. Aggarwal (1999). "TNF-induced signaling in apoptosis." J Clin Immunol **19**(6): 350-364.

Reed, T., M. Perluigi, R. Sultana, W. M. Pierce, J. B. Klein, D. M. Turner, R. Coccia, W. R. Markesbery and D. A. Butterfield (2008). "Redox proteomic identification of 4-hydroxy-2-nonenal-modified brain proteins in amnestic mild cognitive impairment: insight into the role of lipid peroxidation in the progression and pathogenesis of Alzheimer's disease." Neurobiol Dis **30**(1): 107-120.

Reed, T. T., W. M. Pierce, Jr., D. M. Turner, W. R. Markesbery and D. A. Butterfield (2009). "Proteomic identification of nitrated brain proteins in early Alzheimer's disease inferior parietal lobule." Journal of cellular and molecular medicine **13**(8B): 2019-2029.

Reed, T. T., W. M. Pierce, W. R. Markesbery and D. A. Butterfield (2009). "Proteomic identification of HNE-bound proteins in early Alzheimer disease: Insights into the role of lipid peroxidation in the progression of AD." Brain Res **1274**: 66-76.

Regent, A., H. Dib, K. H. Ly, C. Agard, M. C. Tamby, N. Tamas, B. Weksler, C. Federici, C. Broussard, L. Guillevin and L. Mouthon (2011). "Identification of target antigens of anti-

endothelial cell and anti-vascular smooth muscle cell antibodies in patients with giant cell arteritis: a proteomic approach." Arthritis Res Ther **13**(3): R107.

Reich, S. D., F. Steinberg, N. R. Bachur, C. E. Riggs, Jr., R. Goebel and M. Berman (1979). "Mathematical model for adriamycin (doxorubicin) pharmacokinetics." Cancer Chemother Pharmacol **3**(2): 125-131.

Rhee, S. G., S. W. Kang, L. E. Netto, M. S. Seo and E. R. Stadtman (1999). "A family of novel peroxidases, peroxiredoxins." BioFactors **10**(2-3): 207-209.

Robinson, R. A., M. B. Lange, R. Sultana, V. Galvan, J. Fombonne, O. Gorostiza, J. Zhang, G. Warrier, J. Cai, W. M. Pierce, D. E. Bredesen and D. A. Butterfield (2011). "Differential expression and redox proteomics analyses of an Alzheimer disease transgenic mouse model: effects of the amyloid-beta peptide of amyloid precursor protein." Neuroscience **177**: 207-222.

Rubio-Perez, J. M. and J. M. Morillas-Ruiz (2012). "A review: inflammatory process in Alzheimer's disease, role of cytokines." ScientificWorldJournal **2012**: 756357.

Sadeghi, K., B. Wessner, U. Laggner, M. Ploder, D. Tamandl, J. Friedl, U. Zugel, A. Steinmeyer, A. Pollak, E. Roth, G. Boltz-Nitulescu and A. Spittler (2006). "Vitamin D3 down-regulates monocyte TLR expression and triggers hyporesponsiveness to pathogen-associated molecular patterns." Eur J Immunol **36**(2): 361-370.

Saito, K., M. Seishima, M. P. Heyes, H. Song, S. Fujigaki, S. Maeda, J. H. Vickers and A. Noma (1997). "Marked increases in concentrations of apolipoprotein in the cerebrospinal fluid of poliovirus-infected macaques: relations between apolipoprotein concentrations and severity of brain injury." The Biochemical journal **321 (Pt 1)**: 145-149.

Sanchez-Tillo, E., M. Wojciechowska, M. Comalada, C. Farrera, J. Lloberas and A. Celada (2006). "Cyclophilin A is required for M-CSF-dependent macrophage proliferation." Eur J Immunol **36**(9): 2515-2524.

Sarkar, P., C. Reichman, T. Saleh, R. B. Birge and C. G. Kalodimos (2007). "Proline cis-trans isomerization controls autoinhibition of a signaling protein." Mol Cell **25**(3): 413-426.

Sarkisyan, G. and P. B. Hedlund (2009). "The 5-HT7 receptor is involved in allocentric spatial memory information processing." Behav Brain Res **202**(1): 26-31.

Satoh, K., T. Matoba, J. Suzuki, M. R. O'Dell, P. Nigro, Z. Cui, A. Mohan, S. Pan, L. Li, Z. G. Jin, C. Yan, J. Abe and B. C. Berk (2008). "Cyclophilin A mediates vascular remodeling by promoting inflammation and vascular smooth muscle cell proliferation." Circulation **117**(24): 3088-3098.

Satoh, K., H. Shimokawa and B. C. Berk (2010). "Cyclophilin A: promising new target in cardiovascular therapy." Circ J **74**(11): 2249-2256.

Saykin, A. J., T. A. Ahles and B. C. McDonald (2003). "Mechanisms of chemotherapy-induced cognitive disorders: neuropsychological, pathophysiological, and neuroimaging perspectives." Semin Clin Neuropsychiatry **8**(4): 201-216.

Schneider-Brachert, W., V. Tchikov, J. Neumeyer, M. Jakob, S. Winoto-Morbach, J. Held-Feindt, M. Heinrich, O. Merkel, M. Ehrenschwender, D. Adam, R. Mentlein, D. Kabelitz and S. Schutze (2004). "Compartmentalization of TNF receptor 1 signaling: internalized TNF receptosomes as death signaling vesicles." Immunity **21**(3): 415-428.

Schoch, K. M., H. N. Evans, J. M. Brelsfoard, S. K. Madathil, J. Takano, T. C. Saido and K. E. Saatman (2012). "Calpastatin overexpression limits calpain-mediated proteolysis and behavioral deficits following traumatic brain injury." Exp Neurol **236**(2): 371-382.

Schreck, R., K. Albermann and P. A. Baeuerle (1992). "Nuclear factor kappa B: an oxidative stress-responsive transcription factor of eukaryotic cells (a review)." Free Radic Res Commun **17**(4): 221-237.

Schulz, E., P. Wenzel, T. Munzel and A. Daiber (2012). "Mitochondrial Redox Signaling: Interaction of Mitochondrial Reactive Oxygen Species with Other Sources of Oxidative Stress." Antioxid Redox Signal.

Scialo, F., V. Mallikarjun, R. Stefanatos and A. Sanz (2012). "Regulation of Lifespan by the Mitochondrial Electron Transport Chain: Reactive Oxygen Species-Dependent and Reactive Oxygen Species-Independent Mechanisms." Antioxid Redox Signal.

Seigers, R., S. B. Schagen, O. Van Tellingen and J. Dietrich (2013). "Chemotherapy-related cognitive dysfunction: current animal studies and future directions." Brain Imaging Behav.

Selmaj, K. W., M. Farooq, W. T. Norton, C. S. Raine and C. F. Brosnan (1990). "Proliferation of astrocytes in vitro in response to cytokines. A primary role for tumor necrosis factor." J Immunol **144**(1): 129-135.

Semba, R. D., D. K. Houston, L. Ferrucci, A. R. Cappola, K. Sun, J. M. Guralnik and L. P. Fried (2009). "Low serum 25-hydroxyvitamin D concentrations are associated with greater all-cause mortality in older community-dwelling women." Nutr Res **29**(8): 525-530.

Shadan, S., P. S. James, E. A. Howes and R. Jones (2004). "Cholesterol efflux alters lipid raft stability and distribution during capacitation of boar spermatozoa." Biol Reprod **71**(1): 253-265.

Shinde, U. A., A. A. Mehta and R. K. Goyal (2000). "Nitric oxide: a molecule of the millennium." Indian J Exp Biol **38**(3): 201-210.

Siegel, G. J. (2006). Basic neurochemistry : molecular, cellular, and medical aspects. Amsterdam ; Boston, Elsevier.

Sies, H. (1997). "Oxidative stress: oxidants and antioxidants." Exp Physiol **82**(2): 291-295.

Simo, M., X. Rifa-Ros, A. Rodriguez-Fornells and J. Bruna (2013). "Chemobrain: A systematic review of structural and functional neuroimaging studies." Neurosci Biobehav Rev **37**(8): 1311-1321.

Sitcheran, R., P. Gupta, P. B. Fisher and A. S. Baldwin (2005). "Positive and negative regulation of EAAT2 by NF-kappaB: a role for N-myc in TNFalpha-controlled repression." EMBO J **24**(3): 510-520.

Soares, D. P. and M. Law (2009). "Magnetic resonance spectroscopy of the brain: review of metabolites and clinical applications." Clin Radiol **64**(1): 12-21.

Song, H. Y., C. H. Regnier, C. J. Kirschning, D. V. Goeddel and M. Rothe (1997). "Tumor necrosis factor (TNF)-mediated kinase cascades: bifurcation of nuclear factor-kappaB and c-jun N-terminal kinase (JNK/SAPK) pathways at TNF receptor-associated factor 2." Proc Natl Acad Sci U S A **94**(18): 9792-9796.

Sotgia, F., U. E. Martinez-Outschoorn, A. Howell, R. G. Pestell, S. Pavlides and M. P. Lisanti (2012). "Caveolin-1 and cancer metabolism in the tumor microenvironment: markers, models, and mechanisms." Annu Rev Pathol **7**: 423-467.

Souza, J. M., Q. Chen, B. Blanchard-Fillion, S. A. Lorch, C. Hertkorn, R. Lightfoot, M. Weisse, T. Friel, E. Paxinou, M. Themistocleous, S. Chov and H. Ischiropoulos (2001). "Reactive nitrogen species and proteins: biological significance and clinical relevance." Advances in experimental medicine and biology **500**: 169-174.

Squadrito, G. L. and W. A. Pryor (1998). "Oxidative chemistry of nitric oxide: the roles of superoxide, peroxynitrite, and carbon dioxide." Free Radic Biol Med **25**(4-5): 392-403.

Stadtman, E. R. and B. S. Berlett (1991). "Fenton chemistry. Amino acid oxidation." J Biol Chem **266**(26): 17201-17211.

Stellwagen, D., E. C. Beattie, J. Y. Seo and R. C. Malenka (2005). "Differential regulation of AMPA receptor and GABA receptor trafficking by tumor necrosis factor-alpha." J Neurosci **25**(12): 3219-3228.

Sterrenberg, L., R. H. Julicher, A. Bast and J. Noordhoek (1984). "Adriamycin stimulates NADPH-dependent lipid peroxidation in liver microsomes not only by enhancing the production of O2 and H2O2, but also by potentiating the catalytic activity of ferrous ions." Toxicol Lett **22**(2): 153-159.

Subramaniam, R., F. Roediger, B. Jordan, M. P. Mattson, J. N. Keller, G. Waeg and D. A. Butterfield (1997). "The lipid peroxidation product, 4-hydroxy-2-trans-nonenal, alters the conformation of cortical synaptosomal membrane proteins." J Neurochem **69**(3): 1161-1169.

Sultana, R., M. Baglioni, R. Cecchetti, J. Cai, J. B. Klein, P. Bastiani, C. Ruggiero, P. Mecocci and D. A. Butterfield (2013). "Lymphocyte mitochondria: toward identification of peripheral biomarkers in the progression of Alzheimer disease." Free Radic Biol Med **65C**: 595-606.

Sultana, R., D. Boyd-Kimball, J. Cai, W. M. Pierce, J. B. Klein, M. Merchant and D. A. Butterfield (2007). "Proteomics analysis of the Alzheimer's disease hippocampal proteome." Journal of Alzheimer's disease : JAD **11**(2): 153-164.

Sultana, R. and D. A. Butterfield (2008). "Slot-blot analysis of 3-nitrotyrosine-modified brain proteins." Methods in enzymology **440**: 309-316.

Sultana, R. and D. A. Butterfield (2009). "Oxidatively modified, mitochondria-relevant brain proteins in subjects with Alzheimer disease and mild cognitive impairment." Journal of bioenergetics and biomembranes **41**(5): 441-446.

Sultana, R., M. Perluigi and D. Allan Butterfield (2013). "Lipid peroxidation triggers neurodegeneration: a redox proteomics view into the Alzheimer disease brain." Free Radic Biol Med **62**: 157-169.

Sultana, R., M. Perluigi and D. A. Butterfield (2009). "Oxidatively modified proteins in Alzheimer's disease (AD), mild cognitive impairment and animal models of AD: role of Abeta in pathogenesis." Acta Neuropathol **118**(1): 131-150.

Sultana, R., M. Perluigi, S. F. Newman, W. M. Pierce, C. Cini, R. Coccia and D. A. Butterfield (2010). "Redox proteomic analysis of carbonylated brain proteins in mild cognitive impairment and early Alzheimer's disease." Antioxid Redox Signal **12**(3): 327-336.

Sultana, R., H. F. Poon, J. Cai, W. M. Pierce, M. Merchant, J. B. Klein, W. R. Markesbery and D. A. Butterfield (2006). "Identification of nitrated proteins in Alzheimer's disease brain using a redox proteomics approach." Neurobiology of disease **22**(1): 76-87.

Surmeli, N. B., N. K. Litterman, A. F. Miller and J. T. Groves (2010). "Peroxynitrite mediates active site tyrosine nitration in manganese superoxide dismutase. Evidence of a role for the carbonate radical anion." J Am Chem Soc **132**(48): 17174-17185.

Szabo, C., H. Ischiropoulos and R. Radi (2007). "Peroxynitrite: biochemistry, pathophysiology and development of therapeutics." Nat Rev Drug Discov **6**(8): 662-680.

Szapacs, M. E., H. Y. Kim, N. A. Porter and D. C. Liebler (2008). "Identification of proteins adducted by lipid peroxidation products in plasma and modifications of apolipoprotein A1 with a novel biotinylated phospholipid probe." Journal of proteome research **7**(10): 4237-4246.

Takeuchi, H., S. Jin, J. Wang, G. Zhang, J. Kawanokuchi, R. Kuno, Y. Sonobe, T. Mizuno and A. Suzumura (2006). "Tumor necrosis factor-alpha induces neurotoxicity via glutamate release from hemichannels of activated microglia in an autocrine manner." J Biol Chem **281**(30): 21362-21368.

Tanaka, M. and S. Yoshida (1980). "Mechanism of the inhibition of calf thymus DNA polymerases alpha and beta by daunomycin and adriamycin." J Biochem **87**(3): 911-918.

Tang, C., Y. Liu, P. S. Kessler, A. M. Vaughan and J. F. Oram (2009). "The macrophage cholesterol exporter ABCA1 functions as an anti-inflammatory receptor." The Journal of biological chemistry **284**(47): 32336-32343.

Tang, C., A. M. Vaughan, G. M. Anantharamaiah and J. F. Oram (2006). "Janus kinase 2 modulates the lipid-removing but not protein-stabilizing interactions of amphipathic helices with ABCA1." J Lipid Res **47**(1): 107-114.

Tang, C., A. M. Vaughan and J. F. Oram (2004). "Janus kinase 2 modulates the apolipoprotein interactions with ABCA1 required for removing cellular cholesterol." J Biol Chem **279**(9): 7622-7628.

Tang, H., M. Lee, O. Sharpe, L. Salamone, E. J. Noonan, C. D. Hoang, S. Levine, W. H. Robinson and J. B. Shrager (2012). "Oxidative stress-responsive microRNA-320 regulates glycolysis in diverse biological systems." FASEB journal : official publication of the Federation of American Societies for Experimental Biology.

Tangpong, J., M. P. Cole, R. Sultana, S. Estus, M. Vore, W. St Clair, S. Ratanachaiyavong, D. K. St Clair and D. A. Butterfield (2007). "Adriamycin-mediated nitration of manganese superoxide dismutase in the central nervous system: insight into the mechanism of chemobrain." J Neurochem **100**(1): 191-201.

Tangpong, J., M. P. Cole, R. Sultana, G. Joshi, S. Estus, M. Vore, W. St Clair, S. Ratanachaiyavong, D. K. St Clair and D. A. Butterfield (2006). "Adriamycin-induced, TNF-alpha-mediated central nervous system toxicity." Neurobiol Dis **23**(1): 127-139.

Tangpong, J., P. Sompol, M. Vore, W. St Clair, D. A. Butterfield and D. K. St Clair (2008). "Tumor necrosis factor alpha-mediated nitric oxide production enhances manganese superoxide dismutase nitration and mitochondrial dysfunction in primary neurons: an insight into the role of glial cells." Neuroscience **151**(2): 622-629.

Tannock, I. F., T. A. Ahles, P. A. Ganz and F. S. Van Dam (2004). "Cognitive impairment associated with chemotherapy for cancer: report of a workshop." J Clin Oncol **22**(11): 2233-2239.

Tape, C. and R. Kisilevsky (1990). "Apolipoprotein A-I and apolipoprotein SAA half-lives during acute inflammation and amyloidogenesis." Biochimica et biophysica acta **1043**(3): 295-300.

Thayer, W. S. (1988). "Evaluation of tissue indicators of oxidative stress in rats treated chronically with adriamycin." Biochem Pharmacol **37**(11): 2189-2194.

Tsukamoto, K., K. Hirano, K. Tsujii, C. Ikegami, Z. Zhongyan, Y. Nishida, T. Ohama, F. Matsuura, S. Yamashita and Y. Matsuzawa (2001). "ATP-binding cassette transporter-1 induces rearrangement of actin cytoskeletons possibly through Cdc42/N-WASP." Biochem Biophys Res Commun **287**(3): 757-765.

Tukaj, S., P. Trzonkowski and C. Tukaj (2012). "Regulatory effects of 1,25-dihydroxyvitamin D(3) on vascular smooth muscle cells." Acta Biochim Pol **59**(3): 395-400.

Undurti, A., Y. Huang, J. A. Lupica, J. D. Smith, J. A. DiDonato and S. L. Hazen (2009). "Modification of high density lipoprotein by myeloperoxidase generates a pro-inflammatory particle." J Biol Chem **284**(45): 30825-30835.

Uttara, B., A. V. Singh, P. Zamboni and R. T. Mahajan (2009). "Oxidative stress and neurodegenerative diseases: a review of upstream and downstream antioxidant therapeutic options." Curr Neuropharmacol **7**(1): 65-74.

Valentine, J. S. and A. B. Curtis (1975). "A convenient preparation of solutions of superoxide aniom and the reaction of superoxide anion with a copper (II) complex." J Am Chem Soc **97**(1): 224-226.

Valko, M., D. Leibfritz, J. Moncol, M. T. Cronin, M. Mazur and J. Telser (2007). "Free radicals and antioxidants in normal physiological functions and human disease." Int J Biochem Cell Biol **39**(1): 44-84.

van Duijn, C. M., M. C. Dekker, V. Bonifati, R. J. Galjaard, J. J. Houwing-Duistermaat, P. J. Snijders, L. Testers, G. J. Breedveld, M. Horstink, L. A. Sandkuijl, J. C. van Swieten, B. A. Oostra and P. Heutink (2001). "Park7, a novel locus for autosomal recessive early-onset parkinsonism, on chromosome 1p36." Am J Hum Genet **69**(3): 629-634.

Vander Heiden, M. G., L. C. Cantley and C. B. Thompson (2009). "Understanding the Warburg effect: the metabolic requirements of cell proliferation." Science **324**(5930): 1029-1033.

Varadarajan, S., S. Yatin, M. Aksenova and D. A. Butterfield (2000). "Review: Alzheimer's amyloid beta-peptide-associated free radical oxidative stress and neurotoxicity." J Struct Biol **130**(2-3): 184-208.

Vaughan, A. M., C. Tang and J. F. Oram (2009). "ABCA1 mutants reveal an interdependency between lipid export function, apoA-I binding activity, and Janus kinase 2 activation." J Lipid Res **50**(2): 285-292.

Vergeer, M., A. G. Holleboom, J. J. Kastelein and J. A. Kuivenhoven (2010). "The HDL hypothesis: does high-density lipoprotein protect from atherosclerosis?" J Lipid Res **51**(8): 2058-2073.

Verstappen, C. C., J. J. Heimans, K. Hoekman and T. J. Postma (2003). "Neurotoxic complications of chemotherapy in patients with cancer: clinical signs and optimal management." Drugs **63**(15): 1549-1563.

Vieth, R., H. Bischoff-Ferrari, B. J. Boucher, B. Dawson-Hughes, C. F. Garland, R. P. Heaney, M. F. Holick, B. W. Hollis, C. Lamberg-Allardt, J. J. McGrath, A. W. Norman, R. Scragg, S. J. Whiting, W. C. Willett and A. Zittermann (2007). "The urgent need to recommend an intake of vitamin D that is effective." The American journal of clinical nutrition **85**(3): 649-650.

Waarts, B. L., R. Bittman and J. Wilschut (2002). "Sphingolipid and cholesterol dependence of alphavirus membrane fusion. Lack of correlation with lipid raft formation in target liposomes." J Biol Chem **277**(41): 38141-38147.

Wajant, H., K. Pfizenmaier and P. Scheurich (2003). "Tumor necrosis factor signaling." Cell Death Differ **10**(1): 45-65.

Wang, G., M. Dinkins, Q. He, G. Zhu, C. Poirier, A. Campbell, M. Mayer-Proschel and E. Bieberich (2012). "Astrocytes secrete exosomes enriched with proapoptotic ceramide and prostate apoptosis response 4 (PAR-4): potential mechanism of apoptosis induction in Alzheimer disease (AD)." J Biol Chem **287**(25): 21384-21395.

Wang, L. W., Y. F. Tu, C. C. Huang and C. J. Ho (2012). "JNK signaling is the shared pathway linking neuroinflammation, blood-brain barrier disruption, and oligodendroglial apoptosis in the white matter injury of the immature brain." Journal of neuroinflammation **9**(1): 175.

Wang, S., S. Kotamraju, E. Konorev, S. Kalivendi, J. Joseph and B. Kalyanaraman (2002). "Activation of nuclear factor-kappaB during doxorubicin-induced apoptosis in endothelial cells and myocytes is pro-apoptotic: the role of hydrogen peroxide." The Biochemical journal **367**(Pt 3): 729-740.

Warburg, O. (1930). The metabolism of tumours. London, Constable.

Warburg, O., K. Posener and E. Negelein (1924). "On the metabolism of carcinoma cells." Biochem Z **152**: 309-344.

Wardman, P. and L. P. Candeias (1996). "Fenton chemistry: an introduction." Radiat Res **145**(5): 523-531.

Weaver, C. M. and J. C. Fleet (2004). "Vitamin D requirements: current and future." The American journal of clinical nutrition **80**(6 Suppl): 1735S-1739S.

Weber, C. and H. Noels (2011). "Atherosclerosis: current pathogenesis and therapeutic options." Nat Med **17**(11): 1410-1422.

Weber, W. P. and G. W. Gokel (1977). Reactions of Superoxide Ions. Berlin Heidelberg, Springer Berlin Heidelberg.

Wonsey, D. R., K. I. Zeller and C. V. Dang (2002). "The c-Myc target gene PRDX3 is required for mitochondrial homeostasis and neoplastic transformation." Proceedings of the National Academy of Sciences of the United States of America **99**(10): 6649-6654.

Wu, Z., M. A. Wagner, L. Zheng, J. S. Parks, J. M. Shy, 3rd, J. D. Smith, V. Gogonea and S. L. Hazen (2007). "The refined structure of nascent HDL reveals a key functional domain for particle maturation and dysfunction." Nature structural & molecular biology **14**(9): 861-868.

Xu, W., I. G. Charles, S. Moncada, P. Gorman, D. Sheer, L. Liu and P. Emson (1994). "Mapping of the genes encoding human inducible and endothelial nitric oxide synthase (NOS2 and NOS3) to the pericentric region of chromosome 17 and to chromosome 7, respectively." Genomics **21**(2): 419-422.

Yamauchi, Y., C. C. Chang, M. Hayashi, S. Abe-Dohmae, P. C. Reid, T. Y. Chang and S. Yokoyama (2004). "Intracellular cholesterol mobilization involved in the ABCA1/apolipoprotein-mediated assembly of high density lipoprotein in fibroblasts." J Lipid Res **45**(10): 1943-1951.

Yamauchi, Y., M. Hayashi, S. Abe-Dohmae and S. Yokoyama (2003). "Apolipoprotein A-I activates protein kinase C alpha signaling to phosphorylate and stabilize ATP binding cassette transporter A1 for the high density lipoprotein assembly." J Biol Chem **278**(48): 47890-47897.

Yang, J. H., X. Y. Dai, X. Ou, X. R. Hao, D. L. Cao, Z. S. Jiang, L. S. Liu, Z. Wang, G. H. Yi, D. H. Wei, G. X. Wang and C. K. Tang (2007). "Effect of apolipoprotein A-I on expression and function of ATP-binding cassette transporter A1 through PKA signaling." Progress in Biochemistry and Biophysics **34**(6): 611-619.

Yang, R., L. Li, S. B. Seidelmann, G. Q. Shen, S. Sharma, S. Rao, K. G. Abdullah, K. G. Mackinlay, R. C. Elston, Q. Chen, E. J. Topol and Q. K. Wang (2010). "A genome-wide linkage scan identifies multiple quantitative trait loci for HDL-cholesterol levels in families with premature CAD and MI." J Lipid Res **51**(6): 1442-1451.

Yatin, S. M., S. Varadarajan and D. A. Butterfield (2000). "Vitamin E Prevents Alzheimer's Amyloid beta-Peptide (1-42)-Induced Neuronal Protein Oxidation and Reactive Oxygen Species Production." J Alzheimers Dis **2**(2): 123-131.

Yen, H. C., T. D. Oberley, S. Vichitbandha, Y. S. Ho and D. K. St Clair (1996). "The protective role of manganese superoxide dismutase against adriamycin-induced acute cardiac toxicity in transgenic mice." J Clin Invest **98**(5): 1253-1260.

Yin, K., X. Deng, Z. C. Mo, G. J. Zhao, J. Jiang, L. B. Cui, C. Z. Tan, G. B. Wen, Y. Fu and C. K. Tang (2011). "Tristetraprolin-dependent post-transcriptional regulation of inflammatory cytokine mRNA expression by apolipoprotein A-I: role of ATP-binding membrane cassette transporter A1 and signal transducer and activator of transcription 3." J Biol Chem **286**(16): 13834-13845.

Yu, X. P., T. Bellido and S. C. Manolagas (1995). "Down-regulation of NF-kappa B protein levels in activated human lymphocytes by 1,25-dihydroxyvitamin D3." Proceedings of the National Academy of Sciences of the United States of America **92**(24): 10990-10994.

Zhang, L. H., H. D. Youn and J. O. Liu (2001). "Inhibition of cell cycle progression by the novel cyclophilin ligand sanglifehrin A is mediated through the NFkappa B-dependent activation of p53." The Journal of biological chemistry **276**(47): 43534-43540.

Zhao, D., M. A. Frohman and J. K. Blusztajn (2001). "Generation of choline for acetylcholine synthesis by phospholipase D isoforms." BMC Neurosci **2**: 16.

Zhao, G. J., K. Yin, Y. C. Fu and C. K. Tang (2012). "The interaction of ApoA-I and ABCA1 triggers signal transduction pathways to mediate efflux of cellular lipids." Mol Med **18**(1): 149-158.

Zheng, L., B. Nukuna, M. L. Brennan, M. Sun, M. Goormastic, M. Settle, D. Schmitt, X. Fu, L. Thomson, P. L. Fox, H. Ischiropoulos, J. D. Smith, M. Kinter and S. L. Hazen (2004). "Apolipoprotein A-I is a selective target for myeloperoxidase-catalyzed oxidation and functional impairment in subjects with cardiovascular disease." The Journal of clinical investigation **114**(4): 529-541.

Zhu, Y., B. D. Mahon, M. Froicu and M. T. Cantorna (2005). "Calcium and 1 alpha,25-dihydroxyvitamin D3 target the TNF-alpha pathway to suppress experimental inflammatory bowel disease." Eur J Immunol **35**(1): 217-224.

Zittermann, A., J. F. Gummert and J. Borgermann (2009). "Vitamin D deficiency and mortality." Curr Opin Clin Nutr Metab Care **12**(6): 634-639.

Zou, J. Y. and F. T. Crews (2005). "TNF alpha potentiates glutamate neurotoxicity by inhibiting glutamate uptake in organotypic brain slice cultures: neuroprotection by NF kappa B inhibition." Brain Res **1034**(1-2): 11-24.

Zucchelli, S., S. Vilotti, R. Calligaris, Z. S. Lavina, M. Biagioli, R. Foti, L. De Maso, M. Pinto, M. Gorza, E. Speretta, C. Casseler, G. Tell, G. Del Sal and S. Gustincich (2009). "Aggresome-forming TTRAP mediates pro-apoptotic properties of Parkinson's disease-associated DJ-1 missense mutations." Cell death and differentiation **16**(3): 428-438.

VITA

Jeriel T. R. Keeney was born in Flint, MI. Jeriel attended Atherton High School in Burton, MI. Jeriel started college at the age of 17 at Mott Community College receiving three Associate degrees. At the age of 19, Jeriel went on to attend graduate school at the University of Michigan, College of Pharmacy in Ann Arbor, MI where he investigated the effect of experimental anti-cancer drugs on the enzyme systems . Following 12 years of teaching at both the college and high school levels, Jeriel returned to school receiving a Bachelor of Arts degree at the University of Michigan, Flint in 2008 with majors in chemistry, math, and biology. In 2009, Jeriel joined Dr. D. Allan Butterfield's laboratory at the University of Kentucky (UK), Department of Chemistry where he completed his Ph.D. with a focus in neurochemistry and chemotherapy-induced cognitive impairment. While at UK, Jeriel was inducted into the Delta Epsilon Iota (DEI) academic honor society, while also publishing in several peer-reviewed journals and receiving several fellowships.

SCIENTIFIC PUBLICATIONS

Keeney JT, Swomley AM, Harris JL, Fiorini A, Mitov MI, Perluigi M, Sultana R, Butterfield DA. “Cell cycle proteins in brain in mild cognitive impairment: insights into progression to Alzheimer disease.” Neurotox Res. 2012 Oct; 22(3):220-30. Epub 2011 Nov 15. (One of, if not the most downloaded articles in Neurotox Res according to several emails from the journal editor.)

Keeney JT, Swomley AM, Förster S, Harris JL, Sultana R, Butterfield DA. “Apolipoprotein A-I: Insights from redox proteomics for its role in neurodegeneration.” Proteomics Clin Appl. 2013 Jan;7(1-2):109-22. doi: 10.1002/prca.201200087. (Used for the cover image.)

Keeney JT, Förster S, Welleford AS, Sultana R, Brewer L, Latimer C, Cai J, Klein JB, Porter NM, Butterfield DA. **“**Dietary Vitamin D Deficiency in Rats from Middle- to Old-age Leads to Elevated Tyrosine Nitration and Proteomics Changes in Levels of Key Proteins in Brain: Implications for Low Vitamin D-dependent Age-Related Cognitive Decline.” Free Radic Biol Med. 2013 Jul 18;65C:324-334. doi: 10.1016/j.freeradbiomed.2013.07.019. [Epub ahead of print]

Swomley AM, Förster S, **Keeney JT**, Triplett J, Sultana R, Butterfield DA. “Aβ, Oxidative Stress in Alzheimer Disease: Evidence Based on Proteomics Studies.” Biochim Biophys Acta. 2013 Oct 9. doi:pii: S0925-4439(13)00297-4. 10.1016/j.bbadis.2013.09.015. [Epub ahead of print]

Keeney JT, Miriyala S, Ren X, Noel TJ, Powell DK, Sultana R, Moscow JA, Vore M, St. Clair DK, Butterfield DA. “Prevention of mitochondrial damage in brain and oxidative stress in plasma of TNF-α knockout mice treated with the anti-cancer drug doxorubicin: Implications for chemotherapy-induced cognitive impairment (“Chemobrain”).” Manuscript in preparation, 2013.

Keeney JT, Ren X, Warrier G, Noel TJ, Powell DK, Brelsfoard JM, Saatman KE, *S*ultana R, St. Clair DK, Butterfield DA. “Doxorubicin-induced elevated oxidative stress in brain and cognitive decline: protection by MESNA and insights into mechanisms of chemotherapy-induced cognitive impairment (“chemobrain”).” Manuscript in preparation, 2013.

Keeney JT, Miriyala S, *S*ultana R, St. Clair DK, Butterfield DA. “Superoxide induces protein oxidation in plasma and TNF- α elevation in macrophage culture: Insights into mechanisms of neurotoxicity caused by Doxorubicin.” Manuscript in preparation, 2013.

Keeney JT, Ren, X, Sultana R, Zhu H, Butterfield DA. “HNE binding on apolipoprotein A-I caused by the anti-cancer drug doxorubicin in plasma: Insights into structural and functional changes.” Manuscript in preparation, 2013.

Keeney JT, Miriyala S, Ren X, Noel TJ, Powell DK, Sultana R, Moscow JA, Vore M, St. Clair DK, Butterfield DA. “Insights into the mechanism of chemotherapy-induced cognitive impairment caused by the anti-cancer drug doxorubicin: Perspectives from a human clinical pilot study.” Manuscript in preparation.

Keeney JT, Swomley AM, Warrier G, Sultana R, Pearson KJ, Mattison J, Butterfield DA. “Dietary Modulation by Resveratrol of Oxidative Damage Caused by a Diabetic-Inducing Diet in Non-human Primate Brain.” Manuscript in preparation.